Out of equilibrium quantum dynamics and disordered systems in bosonic ultracold atoms

Bruno Sciolla

UNIVERSITÉ PARIS-SUD 11 - ORSAY

et

INSTITUT DE PHYSIQUE THÉORIQUE - CEA/SACLAY

École Doctorale de Physique de la Région Parisienne - ED 107

Thèse de doctorat

Spécialité : **Physique Théorique**

Sujet de la thèse :

Dynamique quantique hors-équilibre et systèmes désordonnés pour des atomes ultrafroids bosoniques

---

présentée par Bruno SCIOLLA

pour obtenir le grade de Docteur de l'Université Paris-sud 11

Directeur de thèse : Henri ORLAND

Thèse préparée sous la direction de Giulio BIROLI

Soutenue le jeudi 13 septembre 2012 devant le jury composé de :

Leticia CUGLIANDOLO	Rapporteur
Michele FABRIZIO	Rapporteur
Antoine GEORGES	Examinateur
Henk HILHORST	Examinateur
Corinna KOLLATH	Examinateur
Guilhem SEMERJIAN	Examinateur
Giulio BIROLI	Membre invité

Résumé :

Durant cette thèse, je me suis intéressé à deux thématiques générales qui peuvent être explorées dans des systèmes d'atomes froids : d'une part, la dynamique hors-équilibre d'un système quantique isolé, et d'autre part l'influence du désordre sur un système fortement corrélé à basse température.

Dans un premier temps, nous avons développé une méthode de champ moyen, qui permet de résoudre la dynamique unitaire dans un modèle à géométrie particulière, le réseau complètement connecté. Cette approche permet d'établir une correspondance entre la dynamique unitaire du système quantique et des équations du mouvement classique. Nous avons mis à profit cette méthode pour étudier le phénomène de transition dynamique qui se signale, dans des modèles de champ moyen, par une singularité des observables aux temps longs, en fonction des paramètres initiaux ou finaux de la trempe. Nous avons montré l'existence d'une transition dynamique quantique dans les modèle de Bose-Hubbard, d'Ising en champ transverse et le modèle de Jaynes-Cummings. Ces résultats confirment l'existence d'un lien fort entre la présence d'une transition de phase quantique et d'une transition dynamique.

Dans un second temps, nous avons étudié un modèle de théorie des champs relativiste avec symétrie O(N) afin de comprendre l'influence des fluctuations sur ces singularités. À l'ordre dominant en grand N, nous avons montré que la transition dynamique s'apparente à un phénomène critique. En effet, à la transition dynamique, les fonctions de corrélations suivent une loi d'échelle à temps égaux et à temps arbitraires. Il existe également une longueur caractéristique qui diverge à l'approche du point de transition. D'autre part, il apparaît que le point fixe admet une interprétation en terme de particules sans masse se propageant librement. Enfin, nous avons montré que la dynamique asymptotique au niveau du point fixe s'apparente à celle d'une trempe d'un état symétrique dans la phase de symétrie brisée.

Le troisième volet de cette thèse apporte des éléments nouveaux pour la compréhension du diagramme des phases du modèle de Bose-Hubbard en présence de désordre. Pour ce faire, nous avons utilisé et étendu la méthode de la cavité quantique en champ moyen de Ioffe et Mézard, qui doit être utilisée avec la méthode des répliques. De cette manière, il est possible d'obtenir des résultats analytiques pour les exposants des lois de probabilité de la susceptibilité. Nos résultats indiquent que dans les différents régimes de la transition de phase de superfluide vers isolant, les lois d'échelle conventionnelles sont tantôt applicables, tantôt remplacées par une loi d'activation. Enfin, les exposants critiques varient continûment à la transition conventionnelle.

Mots clefs : atomes froids, quench quantiques, systèmes fortement corrélés, Bose-Hubbard, transition de phase quantique, effet cône de lumière, systèmes désordonnés, méthode de la cavité, astuce des répliques, verre de Bose

Out of equilibrium quantum dynamics and disordered systems in bosonic ultracold atoms

Abstract:

This thesis deals with two general themes, both of which may be studied in ultracold atom systems: on the one hand, the out of equilibrium dynamics of closed quantum systems, and on the other hand the impact of disorder on a strongly correlated system at zero temperature.

The first part is focused on mean field completely connected models. We show that the dynamics can be solved and mapped onto classical equations of motion for collective coordinates. We applied this technique to address the problem of the dynamical transition. This phenomenon is signalled by singular behaviour of time averages of observables as a function of the parameters of the quench. We showed that the dynamical transition occurs in the Bose-Hubbard model, the Ising model in a transverse field and the Jaynes-Cummings model. These results hint for the existence of a strong link between the quantum phase transition at zero temperature and the dynamical transition.

In the second part, we studied the impact of fluctuations on the dynamical transition, using field theory techniques on a relativistic theory with O(N) symmetry. At leading order in N, the dynamical transition bear similarities with a critical phenomenon. At the transition, correlation functions have a two-time scaling law, and there is a diverging lengthscale as the transition is approached. Besides, the fixed point may be described in terms of a gas of massless effective particles, which is a peculiar case of the much more general light cone effect. Finally, we relate the fixed point dynamics to the quench dynamics from the symmetric to the broken symmetry phase.

The third part of this thesis is about the disordered Bose-Hubbard model and the nature of its phase transitions. We used and extended the quantum cavity method coupled with the replica trick, within the mean-field cavity approximation introduced by Ioffe, Mezard. This method provides analytical estimates for the phase diagram and about the nature of the quantum phase transition. We find that the conventional transition, with power law exponents, is changed into an activation-like transition in some regions. This effect is accompanied by continuously varying critical exponents at the conventional transition. The method also give access to the large tails of superfluid susceptibility, which allows to characterize the Bose glass phase.

Key words: cold atoms, quantum quenches, strongly correlated systems, Bose-Hubbard, quantum phase transitions, light cone effect, disordered systems, cavity method, replica trick, Bose glass

Articles de référence

Publiés dans des revues à comité de lecture

{**1**} *Quantum Quenches and Off-Equilibrium Dynamical Transition in the Infinite-Dimensional Bose-Hubbard Model*, B. Sciolla, G. Biroli, Physical Review Letters **105** 220401 (2010)

{**2**} *Dynamical transitions and quantum quenches in mean-field models*, B. Sciolla, G. Biroli, Journal of Statistical Mechanics : Theory and Experiment P11003 (2011)

En préparation

{**3**} *Quenches in the ϕ^4 model*, B. Sciolla, G. Biroli (2012)

{**4**} *Disordered Bose-Hubbard model, a cavity approach*, B. Sciolla, G. Biroli (2012)

Remerciements

Je tiens d'abord à remercier Giulio qui a très bien inspiré et dirigé mon travail de thèse. Faire de la physique avec lui est un plaisir, de par sa culture scientifique et son approche intuitive. D'autre part, il m'a beaucoup encouragé et soutenu tout au long de la thèse, et il m'a permis de voyager et de rencontrer des scientifiques de tous horizons, ce qui a été très enrichissant et stimulant.

Je veux aussi remercier Olivier Parcollet qui a généreusement partagé avec moi son expertise numérique mais aussi scientifique à de nombreuses reprises.

Je profite de l'occasion pour faire une petite apostrophe à tous les thésards de l'IPhT et d'autres laboratoires de la région parisienne avec qui j'ai passé de bons moments.

Enfin, cette thèse est dédiée à toute ma famille et à mes amis, qui comptent énormément pour moi.

Contents

Chapter 1

Ultracold atoms and nonequilibrium dynamics, a general perspective

1.1 Ultracold atoms as a playground for quantum many-body physics

1.1.1 A new born field with lots of perspectives

In 1995, evaporative cooling techniques allowed for the first experimental realization of Bose-Einstein condensation in dilute atomic gases [1]. Following this success, thanks to tremendous progress in techniques to cool, trap and manipulate atoms in a variety of ways, a new branch of physics called cold atoms emerged at the crossroads of atomic physics, mesoscopic physics, condensed matter and statistical physics. As we will see, there are plenty of ultracold atoms setups, but their common feature is to trap and cool down a controllable number of atoms so as to reach temperatures of quantum degeneracy.

After an early period in which weakly interacting bosons were the only focus, cold atoms systems soon showed up as unique among the host of physical systems in the quantum realm, in terms of controllability and versatility, as illustrated by the following list of achievements.

First, different atom species and reference energy levels are used, such that trapped atoms can be either bosons or fermions, or have different spin (0, 1/2 or 1). Several species can also be trapped in parallel. The trapping potential is made by using lasers or magnetic fields, and it is possible to implement various shapes, from smooth traps to hypercubic lattices, frustrated lattices, superlattices in one, two or three dimensions. Even quenched disorder can be introduced in these systems which are without defects otherwise.

The interactions between atoms are typically of s-wave type, the sign and strength of which may be tuned with Feshbach resonances. Some atoms or molecules have long range interactions, due to a large dipole electric or magnetic moment, like ^{52}Cr, molecules [2] or Rydberg atoms [3], which are strongly excited neutral gases for which the 100s Rydberg level is typi-

cally reached.

The ensemble of atoms is typically in almost complete isolation from its environment, a very peculiar property which makes it possible to access either the equilibrium or the off-equilibrium properties. Cold atom systems are ideal to study out of equilibrium physics thanks to the real time control over the trap and the interactions, which is discussed at length in the following. The atoms may also be coupled to lasers or ions to study dissipative dynamics in controlled conditions [4].

Beside the good controllability of cold atoms, these systems can also be probed easily, for example by using time of flight imaging. The above list, although impressive, is only partially representative of all accomplishments and projects currently under way. A more detailed description of the atomic physics needed to implement the Bose-Hubbard model is given in chapter 2.

1.1.2 A wealth of physics

Thanks to this vast range of experimental techniques, a lot of physical effects are accessible or will be in the near future. In the following, we review some achievements and perspectives with emphasis on strongly correlated systems, see [5] for a more exhaustive review.

Following the first Bose-Einstein condensation experiments [1], the coherent properties of a large assembly of atoms were directly demonstrated two years after [6], within a setup involving two originally isolated condensates, which were released and produced robust interference patterns as they overlap. Thereafter, quantized vortex formation [7] and spinor condensates [8] were observed in weakly interacting bosonic condensates.

Cold atom systems started drawing the attention of the whole condensed matter community when lattice systems in the regime of strong correlations were built. The original idea proposed by Jacksch et al. [9] was to simulate solid state compounds, with direct control over most physical parameters and without the defects inherent to standard condensed matter samples [1]. In the seminal experiment of Greiner et al. in 2002 [10], the quantum phase transition from superfluid to Mott insulator has been observed in the regime of strong correlations, as shown in figure 1.1. This paved the way to the observation of all sorts of many-body low temperature physics, especially quantum phase transitions. For example, the Tonks-Girardeau gas has been investigated two years later [11].

Some experimental groups then managed to trap fermions, to study a fermionic degenerate gas in quite different conditions from those in solid state materials. Reaching high degeneracy with ^{40}K atoms with attractive interactions allowed for the formation of molecules of fermions and further Bose-Einstein condensation thereof [12]. This experiment fostered thorough experimental and theoretical investigation of the transition between the Bose-Einstein condensate

1. The principle of the quantum simulator was actually suggested by Feynman a long time before it was experimentally feasible.

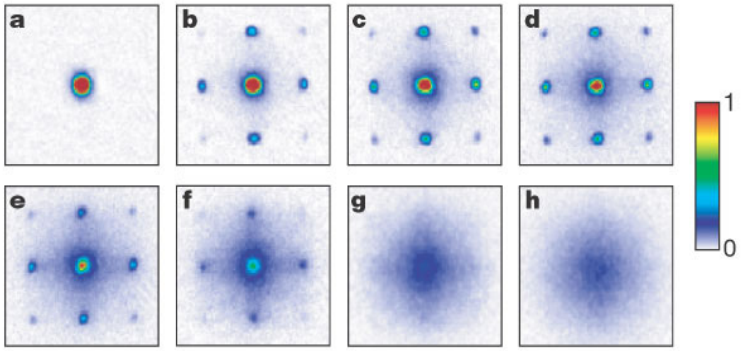

Figure 1.1: Momentum distribution from time of flight imaging in the experiment of Greiner et al. [10] with growing trapping potential V_0 (growing ratio U/J), showing the superfluid to Mott insulator transition (a→ h). See section 2.4 for the interpretation.

of molecules and the Bardeen-Cooper-Schrieffer pairing in a dilute Fermi gas, called the BEC-BCS crossover [13].

Combining these techniques gives in principle the opportunity to make experiments on the pure [2] Hubbard model, with the underlying problem of high-T_c superconductivity.

However, in the state of the art experiments [14, 15], the temperatures reached at present are too high, hence there is currently active research to find new methods to cool down fermions [16].

Other modern topics of condensed matter physics may also be "simulated", such as the quantum Hall effect and topological phases, with proposals involving dilute rotating Bose-Einstein condensates [17] with preliminary experimental results [18, 19].

Although the complete absence of impurities in cold atom systems is often an advantage, disordered quantum systems and the phenomenon of many-body localization can also be investigated with cold atoms. Indeed, a quenched random potential can be built using laser speckle, superimposed incommensurate periodic lattices or another trapped atom species. Current studies involve non interacting atoms [20, 21] and are therefore focused on traditional Anderson localization, but the regime of arbitrary interactions will probably be studied soon, to address the theoretical prediction of a finite temperature insulator to conductor transition [22].

Let us now briefly mention topics that are more distant from traditional condensed matter systems, but with promising new physics.

Cold atom systems are very well isolated from their environment, yet controlled dissipation can be introduced if needed. Hybrid systems of ultracold neutral atoms and a single trapped ion were devised [4], which allows to study the interplay between strong interactions and dissipation [23] or can serve as a probing device [24]. Bulk dissipation can also be achieved by

2. With cold atoms, it is possible to realize a single band Hubbard model, by contrast with solid state compounds where a lot of complications superimpose to the Hubbard model physics: there are several contributing orbitals, interactions are unknown parameters and samples always contain some degree of disorder.

coupling to phonons with the perspective of new out of equilibrium phases and phase transitions [25, 26]. There are also proposals to use a dissipative channel to reach low temperatures in fermionic lattice systems [27].

The debated question of the existence of a supersolid phase in ^{4}He [28] triggered questions about the existence of a supersolid phase in a different context, such as cold atoms. One should distinguish between a "supersolid phase" within an extended Bose-Hubbard model [3] [29], which is maybe a small abuse of terminology, and a genuine supersolid phase without any external potential, see [30] for a proposal using Rydberg atoms.

The above supersolid phase is just an example of exotic phases in systems with dipolar long-range interactions [2]. In one dimension, a Haldane Bose insulator has been predicted [31].

Some physical quantities may only be accessible in systems where direct time-dependent control is possible. The notion of entanglement entropy [32], which has occupied a growing place in low dimensional and zero temperature physics, was not considered to be observable until recent proposals involving local quenches [33].

Of course, while mentioning quantum information, it is necessary to recall that realizing the elusive quantum computer with cold atoms is a major goal for many research groups, with some progress like the realization of a controlled-NOT gate [3]. Recently, concepts from statistical physics of glassy systems have been applied to shed light on combinatorial optimization problems, in particular for constraint satisfaction solving [34, 35]. The quantum adiabatic algorithm has been proposed to solve hard problems on a quantum computer [36]. Yet this algorithm proved to be limited, due to the exponentially small gap at a first order quantum phase transition [37], which must be crossed adiabatically to solve a problem with a quantum computer. The study of mean-field models for the statics and dynamics [38] of disordered quantum systems is an important step towards understanding these aspects. Notice that the role of quantum fluctuations in structural glasses is a broad topic with various applications beyond quantum computation [39, 40].

Finally, cold atoms are a privileged setup to explore the realm of out of equilibrium physics, which is our main interest here and will be discussed in the following.

1.2 Out of equilibrium dynamics

1.2.1 Dynamics in isolated systems

Most of the many-body quantum systems under study up to the nineties, such as electrons in a solid, quantum dots, mesoscopic systems, etc. were coupled to external degrees of freedom (phonons, impurities or a contact reservoir) and were either at equilibrium or underwent dissipative dynamics. For the condensed matter community, cold atoms experiments were

3. A phase where both off-diagonal long range order $O = \lim_{|i-j|\to\infty} \langle \hat{b}_i^\dagger \hat{b}_j \rangle$ and checkerboard density wave order $C = \sum_i (-1)^{\delta_{x_i}+\delta_{y_i}} (\langle n_i \rangle - \rho)$ are present (δ_{x_i} is the parity of x_i and ρ is the average density).

the first example of systems which are effectively isolated from their environment on a large timescales [4]. Recently, the progress in femtosecond time-resolved pump and probe experiments on solid state compounds allowed to explore far from equilibrium regimes [41]. At present, the dynamics is accessible on timescales three orders of magnitude lower than the electron-phonon coupling times [42], such that the electron gas can be studied in quasi complete isolation from its environment.

Beside these few exceptions, cold atoms is the ideal framework to study out of equilibrium dynamics, because of the possibility to tune interactions at will and to do measurements at any times. This awakened a lot of fundamental questions which have been the subject of intense theoretical research in the past years and of some remarkable experiments.

The general out of equilibrium setup is as follows: the system is supposed to be in a known initial quantum state defined by a density matrix $\hat{\rho}_0$ at some remote time in the past, and to be driven out of equilibrium at will by the experimentalist, which formally amounts to a controlled time dependency of the Hamiltonian with some parameter $\hat{H}(\lambda(t))$.

The most common protocols are the ramp drive, where the parameter $\lambda(t)$ is linearly tuned in time, and the quantum quench. Although the later term has several different meanings depending on the context, we will use it to refer to protocols such that $\lambda(t)$ is changing until an intermediate time τ and left constant afterwards. As a consequence, the system state $\hat{\rho}(t)$ is out of equilibrium for $t > \tau$ but may be decomposed over an orthonormal basis $|\,\alpha\,\rangle$ of $\hat{H}(\lambda(\tau))$, with evolution

$$\hat{\rho}(t) = \sum_{\alpha,\alpha'} c_{\alpha,\alpha'} e^{i(E_\alpha - E_{\alpha'})(t-\tau)} |\,\alpha'\,\rangle\langle\,\alpha\,| \tag{1.1}$$

Of course, this result alone tells very little about the encapsulated physics.

In the next sections, we describe what we think are the most studied and relevant questions about quantum out of equilibrium physics in isolated systems, both from the theoretical and experimental point of view. We begin with the central question of thermalization of an isolated system left out of equilibrium after a quench, and mention the studies addressing the relaxation dynamics. After that, we turn to the universal properties inherited from quantum critical points during slow ramp protocols, in particular the production of topological defects and the Kibble-Zurek mechanism. Then, we address the typical physics after a quench, such as the light-cone effect of correlations or coherent properties due to the isolation of the system. We also highlight some topics which do not fall into the previous categories and which maybe deserve closer attention.

4. One can find few other examples of intrinsically isolated quantum system in cosmology, in the early times of the universe, and in heavy ions collisional physics as well. Interesting questions were already addressed which we shall refer to later on.

1.2.2 Thermalization and integrability

Generalities about thermalization

With the actual realization of isolated quantum systems, a quite old and natural question [43] reappeared: under which conditions and how does an isolated quantum system initially out of equilibrium relaxes to equilibrium? As of today, most of the progress made is towards asking more accurate questions: What occurs specifically in integrable models, in systems close to integrability? What is the link between quantum chaos and thermalization? Is there a parallel between localization and relaxation?

First, notice that the question of thermalization should not be asked on the level of the full density matrix, since it is clear that the condition on (1.1) $\hat{\rho}(t) = \hat{\rho}_{\text{eq}}$ will (for all purposes) never be satisfied after an arbitrary quench. As a consequence, the question of thermalization should be whether all observables of interest or a reduced density matrix relax to values similar to a reference ensemble. Also, due to the phenomenon of quantum recurrence [44], thermalization is conventionally considered only in the thermodynamic limit, although in reality recurrence times are huge even in small systems and do not exclude an effective thermal behavior for almost all times.

Chaotic systems

Chaotic quantum systems have very peculiar relaxational properties. The Eigenstate Thermalization Hypothesis (ETH) [45] states that thermalization is due to peculiar properties of individual eigenstates. According to it, for *almost all* ($\tilde{\forall}$) eigenstates $|\,\alpha\,\rangle$ which contribute to the ensemble [5], they resemble the equilibrium density matrix, in the sense that for almost all observables $\hat{A}$,

$$\tilde{\forall}\alpha, \quad \tilde{\forall}\hat{A}, \quad \left\langle \alpha \left| \hat{A} \right| \alpha \right\rangle = \text{Tr}\left(\hat{\rho}_{\text{eq}}\hat{A}\right) \tag{1.2}$$

If this property holds, it implies thermalization in the previous sense for the time averages

$$\overline{\text{Tr}\left(\hat{\rho}(t)\hat{A}\right)} = \lim_{T\to\infty}\frac{1}{T}\int_0^T \mathrm{d}t \sum_{\alpha,\alpha'} c_{\alpha,\alpha'} e^{i(E_\alpha - E_{\alpha'})(t-\tau)} \left\langle \alpha \left| \hat{A} \right| \alpha' \right\rangle \tag{1.3}$$

$$= \sum_{\alpha} c_{\alpha,\alpha} \left\langle \alpha \left| \hat{A} \right| \alpha \right\rangle \tag{1.4}$$

$$= \text{Tr}\left(\hat{\rho}_{\text{eq}}\hat{A}\right) \tag{1.5}$$

Surprisingly, the Eigenstate Thermalization Hypothesis has been found to hold in a non integrable system in some regimes [46], but why this is true is unclear. Actually, the eigenstate

5. In a macroscopic system, say in the canonical ensemble, due to the exponential number of states $\Omega(E) = e^{NS(E)}$ with $S(E)$ the entropy, only energy levels in a small window of energy $[E, E + \mathrm{d}E\,]$ contribute significantly to the density matrix averages $\hat{\rho}_{\text{eq}}$.

thermalization hypothesis does not necessarily implies thermalization [47]. Indeed, there are physical cases when the average of a relevant observable $\hat{A}$ or the exact projection of the initial density matrix $c_{\alpha,\alpha}$ have significant contributions from *atypical* states outside of the energy window of the ensemble, which do not satisfy the eigenstate thermalization hypothesis (1.2), and thermalization does not occur.

Integrable systems

Many studies about quantum quenches in one dimensional integrable systems have been carried out, for various reasons, ranging from the fact that exact computations are possible and challenging, or because the physics is expected to be peculiar, and of course because of their possible realization in experiments. Despite the fact that thermalization to standard canonical or microcanonical ensembles after a quench has soon been ruled out, a proposal was made for a thermalization to a Generalized Gibbs Ensemble [48] built with one parameter λ_n for each conserved quantity $\hat{I}_n$, chosen such that the constraint $\left\langle \hat{I}_n(t) \right\rangle = \mathrm{Tr}\left(\hat{\rho}_{\mathrm{GGE}}\hat{I}_n\right)$ is satisfied, where

$$\hat{\rho}_{\mathrm{GGE}} = e^{-\sum_n \beta_n \hat{I}_n} \tag{1.6}$$

Some restrictions on the applicability of these ensembles were derived in the case of free bosons or fermions [49], but we refer to [50] for a discussion of the scope and predictive power of such an approach. Note that trying to enforce Fluctuation-Dissipation Relations [51] leads to frequency and observable dependent temperatures $\beta^{\hat{A},\hat{B}}(\omega)$. On the whole, it seems fair to say that these ensembles are different from conventional ensembles.

Let us now turn to the famous experiment of the "quantum Newton's cradle" [52], which is described by the one dimensional Lieb-Liniger gas, i.e. a gas of bosonic atoms where the dominant interactions are two-body (elastic) repulsive interactions, which would be an integrable system were it not for the superimposed harmonic trap. In the experiment, two pulses are send onto the equilibrium system and give additional momentum $\pm 2\hbar k$ to the atoms. Due to the harmonic trap, two groups of atoms oscillate coherently for thousands of periods as shown in figure 1.2 (left panel), and the distribution $f(p)$ hardly evolves at all, producing the quantum analog of a classical Newton's cradle. Most of the heating and particle loss is shown to be caused by three-body collisions and spontaneous emission, i.e. by inherent limitations of the experimental setup and not by the many-body relaxation. It is also shown that the regime of strong interactions between the two packets was reached, since putting the system out of equilibrium under the same conditions in three dimensions resulted in a fast relaxation in less than twice the oscillation period τ.

This experiment is generally considered as the strongest experimental signature to date of the peculiar dynamics of integrable models. However, due to the breaking of integrability, this experiment rather stands for the quantum analog of the (classical) Fermi-Pasta-Ulam chain, where relaxation is not found in a full range of an integrability breaking parameter. This similarity is hinting for the existence of a quantum analog of the Kolmogorov-Arnold-Moser threshold for classical system [50], but this is still a completely open question.

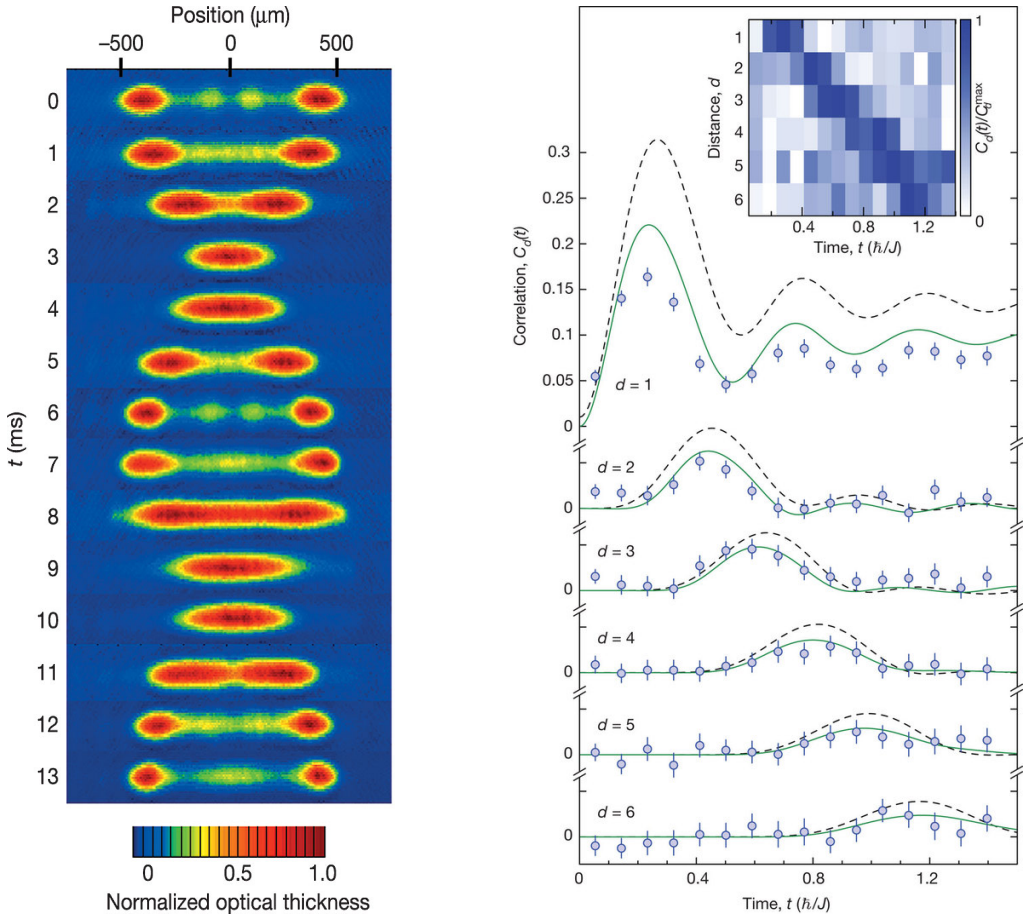

Figure 1.2: *Left panel:* Quantum Newton's cradle experiment of Kinoshita et al. [52]. Real space density plot along the x-axis of the two colliding packets, as a function of time (vertical axis). Each image is obtained by repeating the whole experiment and performing a direct imaging at a given time t after the quench.
Right panel: Light cone effect after a quench in the Bose-Hubbard model [53]. Main plot: correlations of the parity operator $C_d(t)$ (see in the text) as a function of time for distances $d = \{1, 6\}$. The light cone effect is manifest as a positive correlation, the maximum of which is propagating ballistically at some light cone speed. Inset: relative correlations of the parity operator $C_d(t)$ as a function of distance and time. The correlations reach a maximum at the propagating front, and are much smaller beyond.

Generic systems

The absence of thermalization in some regimes of quenches in a general system has been discovered in the one dimensional Bose-Hubbard model [54], and again came as a complete surprise. In this model, thermalization is found in the regime of intermediate interactions, close to the Mott transition, but not in the regime of large interactions where the off-diagonal correlations $\langle \hat{b}_0^\dagger \hat{b}_r \rangle$ reach an out of equilibrium steady value [54].

Further investigations [55] on the same system have confirmed this scenario for quenches from an inhomogeneous initial state and with varying final interactions U_f. The relaxation time τ seems to diverge with the system size L above a threshold $U_f > U_f^c$. This loss of ergodicity is interpreted in terms of a Lanczos basis $|n\rangle$ built from the initial state $|\Psi_0\rangle$ and the recursive application of the final Hamiltonian $\hat{H}$. The absence of thermalization is then related to localization in the $|n\rangle$ basis, drawing an intriguing parallel between nonergodicity and Anderson localization.

A natural idea is to relate this ergodicity/nonergodicity to the chaotic versus integrable nature of the system. The current consensus [6] is that the regularity of a quantum many-body problem is characterized by the level fluctuations statistics: a chaotic system has Gaussian Orthogonal, Unitary or Symplectic Ensemble (GOE/GUE/GSE) statistics, whereas an integrable system has Poissonian statistics [58]. In this respect, the level statistics of the Bose-Hubbard model is *mixed*, with Poisson statistics close to the integrable points $U = 0$, $U = \infty$ and Wigner statistics for intermediate U [59]. The exact nature of the spectrum statistics in the thermodynamic limit as a function of U (and of the energy scale E) is still an open question [60].

The general question of relaxation due to perturbations from integrability seems to be a key question, explored for example in [61]. It seems that depending on the amplitude of the integrability breaking term, there may be a smooth crossover from the integrable case with full memory of the initial conditions to the full quantum chaos regime where thermalization occurs.

Of course, thermalization is occasionally found in mixed systems, especially in dimension $d \geq 2$ as in the $d = 3$ Hubbard model using time dependent Dynamical Mean Field Theory (t-DMFT) [62], or with hard core bosons in $d = 2$ [46]. As of today, a general picture about thermalization (or its absence) in mixed systems is not available.

1.2.3 Relaxational dynamics

In some cases, the physical process responsible for relaxation towards equilibrium can be qualitatively and quantitatively understood. The three-dimensional Hubbard model has been realized in the group of Esslinger [63] to study the quench dynamics. The system is prepared with an initial excess of doublons (doubly occupied sites), and their relaxation rate is monitored

6. Quantum chaos is a huge field, where a system is often called chaotic if some underlying classical model is chaotic [56, 57]. Unlike the former definition, the broader, more general definition which we consider here applies to generic many-body systems.

for different interactions U and tunneling J. The relaxation rate observed in the experiment is $\tau \sim J^{-1}e^{\alpha U/J}$, and can be found analytically from high order scattering processes involving many background excitations [64].

On this question, let us mention that remarkable progress has been made in the high energy and cosmology communities on the nonequilibrium dynamics in quantum field theories. The breakthrough came from 1/N expansions within the Baym-Kadanoff/one particle irreducible formalism [65]. It allowed to observe thermalization in a non-linear O(N) field theory [66] in one dimension. The thermalization involves three different stages on completely different timescales: a first stage of onset of correlations, followed by a long stage of slow power law like drifting, and finally an exponential damping to a thermal state [67]. A similar scenario has been observed in the two dimensional model [68]. This line of research is currently very active due to potential applications to heavy ions collisions.

1.2.4 Kibble-Zurek mechanism

The previous questions about thermalization and of the mechanisms causing relaxation apply to a broad range of systems. In the quest for universal out of equilibrium phenomenon, one is naturally led to think about what happens during quenches across a critical point. Since a critical point is associated with a diverging timescale, it is natural to consider very slow ramps to access universal properties. In the limit of an arbitrarily slow ramp protocol $\lambda(t) = \lambda_0 + ut$, a system initially in the ground state stays in the ground state $|\Psi_0(\lambda)\rangle$ for all times (the "quantum adiabatic theorem"). A sufficient condition for a procedure to be adiabatic in a system with gap $\Delta(\lambda)$ is that the typical rate of evolution of the gap $\frac{\mathrm{d}\Delta}{\mathrm{d}t}$ satisfies

$$\frac{\mathrm{d}\Delta}{\mathrm{d}t} \ll \Delta^2 \tag{1.7}$$

This condition can not be satisfied for a quench across a quantum phase transition, where the gap closes as a power law in the system size $\Delta_c \sim L^{-a}$. For small deviations from adiabaticity, the dynamics of defect production is expected to inherit some universal properties of the critical point, as was first observed by Kibble and Zurek in the context of classical systems [69, 70].

Estimates of the number of defects produced may be obtained by simple scaling or adiabatic perturbation theory [71, 72], recalling that close to a critical point λ_c, the gap scales as $\Delta(\lambda) = (\lambda - \lambda_c)^{z\nu}$ with z the dynamical exponent and ν the correlation length exponent $\xi(\lambda) = (\lambda - \lambda_c)^{-\nu}$.

In the case of a linear ramp quench $\lambda(t) = \lambda_0 + ut$, according to (1.7), adiabaticity is broken at a coupling $\lambda^* - \lambda_c \lesssim u^{\frac{1}{z\nu+1}}$. This defines a typical lengthscale $\xi^* \sim u^{\frac{-\nu}{z\nu+1}}$ beyond which diabatic effect will occur, which is naively expected to result in the creation of topological defects, of density $n_{\mathrm{ex}} \sim (\xi^*)^d \sim u^{\frac{-d\nu}{z\nu+1}}$. This scaling has indeed been observed in many integrable quantum systems [50] and generalized to other quench procedures $\lambda(t) = \lambda_0 + ut^r$ [73, 74], in a disordered Ising chain [75], or in a quench through critical lines [76].

A direct experimental observation of this phenomenon is still lacking. Production of vortices during the formation of a Bose-Einstein condensate were observed [77], but the number

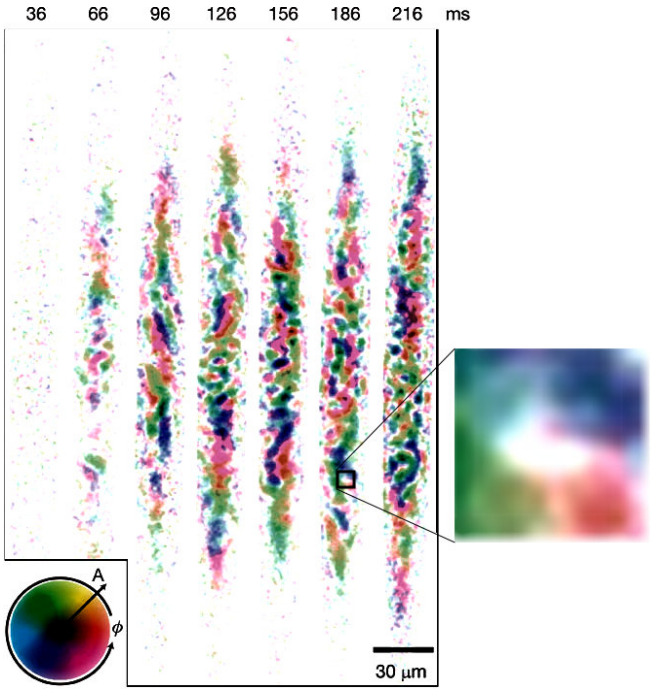

Figure 1.3: Adapted from Sadler et al. [78]: experiment on the formation of a spinor condensate after a quench. Snapshots of the formation of the condensate in the oval shaped trap as a function of time. The darker areas have higher magnetization density and the hue indicates spin orientation in the plane. Vortices and domain walls appear as bright regions with non zero Berry phase along a contour surrounding the defect ($\phi \to \phi + 2\pi n$ along the contour), the zoomed area clearly shows a $n = -1$ vortex.

of defects is too small to check the scaling behavior [7], because of the impossibility to cool the system fast enough.

A more promising experiment involves quenches in a spinor Bose-Einstein condensate [78], where an effective O(2) symmetry is broken after the quench, with production of domains walls and vortices, see figure 1.3. However, the scaling has not yet been observed, again for lack of sufficient statistics.

1.2.5 Quenches to the broken symmetry phase

We turn now to the rather overlooked question of the nature of the dynamics during a quench from the disordered phase to the ordered phase. At first sight, one could believe that the answer to this question is just the Kibble-Zurek mechanism. However, the Kibble-Zurek

7. The scaling behavior is expected to be the *classical* one (the original Kibble and Zurek mechanism), since in this case the condensation is a finite temperature transition.

mechanism is only concerned with the formation of topological defects as the system is getting close to the quantum critical point $\lambda(t) \sim \lambda_c$, and there is certainly some nontrivial subsequent dynamics which it does not describe, as was already remarked in the classical case [79].

To clarify this point, let us adopt the convention that the disordered phase is for $\lambda < \lambda_c$ (and respectively the ordered phase is for $\lambda > \lambda_c$). If we assume a slow ramp quench $\lambda(t) = \lambda_0 + ut$ starting from the disordered phase ($\lambda_0 < \lambda_c$), the different stages of evolution and the corresponding density of defects n_{ex} can be schematically summarized in table 1.1.

stage 1	stage 2	stage 3
$\lambda \ll \lambda_c - \lambda^*$	$\lvert\lambda - \lambda_c\rvert \lesssim \lambda^*$	$\lambda \gg \lambda_c + \lambda^*$
Adiabatic evolution	Kibble-Zurek mechanism	Defects dynamics
$n_{\text{ex}} \sim 0$	$n_{\text{ex}} \sim u^{\frac{-d\nu}{z\nu+1}}$	$n_{\text{ex}}(t)$ nontrivial !

Table 1.1: Three typical stages of the evolution during a sweep to the broken symmetry phase

After a quasi-adiabatic evolution (stage 1) and the onset of the initial density of defects predicted by the Kibble-Zurek mechanism (stage 2), the system is out of equilibrium: it contains defects such as domain walls and vortices, which we expect to move, interact, collide or spontaneously collapse, yielding nontrivial evolution of n_{ex} (stage 3). Moreover, very little is known of two-points correlation functions when crossing the critical point and in the long time evolution. It would be of great interest to understand if there is a quantum equivalent of the classical theory of phase ordering kinetics [80], describing the growth of a characteristic length, aging [81, 82], the associated scaling functions, and if there are quantum dynamical universal properties.

The above scenario is also relevant in the case of a sudden quench from the disordered phase to the ordered phase $\lambda_i \to \lambda_f$, as shown in table 1.2. Topological defects appear in on a small timescale τ (stage 1b) and have nontrivial subsequent dynamics on larger timescales (stage 2b is similar to stage 3 of table 1.1).

stage 1b	stage 2b
$t \sim \tau$	$t \gg \tau$
Fast defect formation	Defects dynamics
n_{ex} non universal	$n_{\text{ex}}(t)$ nontrivial !

Table 1.2: Two schematic stages of the evolution during a sudden quench to the broken symmetry phase

An example of such a scenario is given in [83], showing the dynamics of vortex formation in the Bose-Hubbard model after a quench.

Even in the case where topological defects are not stable, correlation functions may have a scaling regime, as is well known in quenched classical systems [80]. Notable results were obtained in relativistic field theories with large N expansions [84]. It has been demonstrated

analytically that there are nontrivial out of equilibrium stationary solutions, with a scaling for Keldysh correlation functions $G^K(p^0, \mathbf{p}) = s^{2+\kappa_s} G^K(s^z p^0, s\mathbf{p})$, where the dynamical exponent is $z = 1$. In the regime of high momentum, Kolmogorov or weak-wave turbulence scaling is found, with exponent $\kappa_s = d - 3/2$, whereas new fixed points are found in the low momentum regime with $\kappa_s = d + 1$, a scaling confirmed by simulations [85]. We examine this question in the ϕ^4 theory at leading order in N in section 4.6.9.

1.2.6 Light-cone effect

The physics of out of equilibrium two-point correlations is interesting beyond the restricted case of ordering dynamics. A salient feature observed in arbitrary quenches is the existence of bounds for the speed of propagation of information across a system, as has been known for a long time in spin systems as the Lieb-Robinson bound [86], and referred to as a light cone effect in the quench literature. This problem can be dealt with analytically in special cases, like free scalar field theories and one dimensional conformal theories [87].

The light-cone effect has recently been observed in a remarkable experiment [53] described by the Bose-Hubbard model, where the two-point equal time parity correlation functions $C_d(t)$ were measured after a sudden quench.

$$C_d(t) = \langle\, \hat{s}_0(t)\hat{s}_d(t)\,\rangle - \langle\, \hat{s}_0(t)\,\rangle \langle\, \hat{s}_d(t)\,\rangle \tag{1.8}$$

$$\hat{s}_i(t) = e^{i\pi(\hat{n}_i(t)-\rho)} \tag{1.9}$$

Correlations visibly reach a maximum on a propagating front as shown in figure 1.2 (left panel). If one has in mind the picture of quasiparticles propagating at maximum speed c and reaching the two points 0 and d at time t, one would expect a complete absence of correlations for large distances $d > 2ct$ and possibly non zero correlations for $d < 2ct$ as is found for example in conformal field theories [87]. A lot of questions need further attention: the velocity c may depend on which quasiparticles are excited after the quench, or one may ask how the velocity compares with other relevant quantities as the speed of sound [88]. We explore again this effect in section 4.6.5.

1.2.7 Quantum coherence

Most of the effects mentioned above are characteristic of the effectively irreversible dynamics occurring in a system out of equilibrium. Despite the unitary, strictly reversible evolution, correlations are building up in an intricate way, and the system may look irreversibly modified or even equilibrated in a coarse-grained picture. In this section, we mention a few effects which signal the fully coherent dynamics of an isolated system.

The effect known as Bloch oscillations has been observed in optical lattices [89]. These are oscillations of the mean velocity of single atoms, which occur when an external field is applied on top of a periodic potential. The phenomenon is irrelevant in solids due to the scattering

of electrons on lattice defects, but present in a perfect one dimensional lattice and in good agreement with theoretical estimates.

Another famous example of coherent dynamics is the experiment of Greiner on collapse and revival of the wavefunction [90], which we describe in section 2.4.

1.2.8 Quantum fluctuations relations

Finally, we turn to the issue of fluctuation relations, which opened a new branch of classical out of equilibrium physics with exact results for *arbitrarily out of equilibrium* processes. These theorems relate some nonequilibrium averages to equilibrium properties and have several variants: the Galavotti-Cohen, Jarzynski, Crooks, Hatano-Sasa, Evans-Searles relations. They are valid in Markovian, stochastic and Hamiltonian systems as well [91]. Some of these relations depend on the presence of a bath, whereas some others are valid in an isolated "quenched" system, i.e. driven out of equilibrium by an external force.

A quantum generalization of these results is not straightforward due to subtleties in the definition of the work in a quantum system [92], but is at present at least partially achieved [93]. This problem is still in its infancy, and applications have just been suggested [94, 95].

1.3 Analytical and numerical methods

To close this chapter, let us mention the various theoretical and computational methods devised to study out of equilibrium physics, most of which are extensions of equilibrium techniques.

The simplest techniques are mean-field like and rely only on local degrees of freedom: time-dependent Gutzwiller Ansatz, large spin limit [96] or other saddle point methods, which we review in section 3.6. These methods may be refined to account for spatial or temporal fluctuations, for example by systematic $1/z$ expansion [97], or using variational Ansatz with constraints on correlations [55] (Jastrow factors). In some physical systems, there are natural approximations such as the Gross-Pitaevskii equation for bosonic systems [98], or phase space methods [99] for the regime of weak interactions. However, in strongly correlated systems, good effective theories are lacking in most situations — or to phrase it more precisely, effective theories valid in all regimes are not believed to exist at all.

The exception to the above rule are one dimensional systems, where exact solutions of strongly interacting systems were found. There is an intense activity to derive analytical results about the quench dynamics using several methods: conformal field theory [87], the bosonization technique [100], the mapping to free fermions [101, 48, 102, 103, 104], or more recently Bethe Ansatz techniques [105].

In non-integrable models, one may want to fall back to perturbative expansions. To handle nonequilibrium field theory, the Keldysh formalism [106] is the most natural framework. The two-particle irreducible, or Baym-Kadanoff [107] formalism, has a broad range of application

and is purposely designed to conserve a given set of quantities such as energy, particle number, etc. It has been used extensively in the high-energy community [108], since unlike other approximation schemes, it prevents the occurrence of so-called secular diagrams, those diagrams which are diverging in time even in the weak coupling case [65]. The two-particle irreducible formalism has later been generalized to n-particle irreducible formalisms to include arbitrary n-point correlation functions [65]. In the future, developing renormalization schemes is a necessity to study multiscale or critical nonequilibrium properties, see for example [109, 110].

Although the above analytical and numerical techniques are powerful, they are not general and reliable enough to secure our knowledge of strongly correlated systems. Hence, powerful, first principles numerical techniques are needed to make progress. Of course, full diagonalization is always an option [111] but is restricted to extremely small systems, since studying the quench dynamics requires to compute *all* eigenstates of the Hamiltonian.

The reference method to study one dimensional systems is the Density Matrix Renormalization Group (DMRG) [112]. This method fostered a lot of research activity on quantum entanglement, with the introduction of concepts from the quantum information community. The original algorithm has been understood in terms of Matrix Product States, which led to new algorithms such as the Time Evolving Block Decimation (TEBD) algorithm [113].

For finite dimensional fermionic systems, the DMFT method [114] is currently the most advanced method capable of handling general Hamiltonian. It has recently been generalized to compute the real time evolution [62, 115]. The core of the method is to approximate the self-energy on the lattice by the one of an effective impurity, hence the bottleneck of the method is to solve an out of equilibrium impurity problem, which is now feasible by Continuous Time Quantum Monte Carlo (CTQMC) thanks to recent progress [116].

Chapter 2

The Bose-Hubbard model, a paradigmatic example of a strongly correlated system in cold atoms

2.1 From cold atoms to the Bose-Hubbard model

In this section, we describe the basic ingredients needed to understand the physics of bosons trapped in an optical lattice, and how the Bose-Hubbard model is derived from first principles.

2.1.1 Dipole trapping potential

Initially, atomic physics experiments were designed to create Bose-Einstein Condensates of weakly interacting particles. With recent progress, designing strongly interacting systems of bosonic or fermionic atoms has become possible. These experiments use optical lattices to create an effective periodic potential reminiscent of the ionic potential in conventional condensed matter compounds, which we present in this section.

Optical lattices are formed by superimposing two or three orthogonal standing wave laser fields, to trap the atoms in a periodic array of one, two or three dimensions [5] as depicted in figure 2.1. The physical origin [117] of the trapping potential is the polarization of atoms by the field, and the coupling of the resulting dipole to the field. For an oscillating electric field $\mathbf{E}(\mathbf{x})e^{i\omega t}$, the atom has an induced dipole, which close to a resonance is due to virtual transitions from the original state $|\, g \,\rangle$ to an excited state $|\, e \,\rangle$ of excess energy $\hbar\omega_e$.

The corresponding dipole energy is $\hat{H}_{\text{dip}} = -\hat{\boldsymbol{\mu}} \cdot \mathbf{E}$ where the dipole operator is $\hat{\boldsymbol{\mu}} = \sum_i q_i \hat{\mathbf{r}}_i$. The dipole Hamiltonian induces transitions from the original state to the excited state, and may be expressed as $\hat{H}_{\text{dip}} = \Omega(|\, e \,\rangle\langle\, g \,| + |\, g \,\rangle\langle\, e \,|)/2$ with the Rabi frequency $\Omega = -2\mathbf{E} \cdot \langle\, e \,|\hat{\boldsymbol{\mu}}|\, g \,\rangle$. Since only virtual transitions are expected to play a role, the excited state can be adiabatically eliminated provided $\delta = \omega - \omega_e \gg \Omega$, i.e. if the laser is far detuned with the transition. In these

conditions, the net result of the dipole interaction is in an effective potential $V(\mathbf{x}) = \frac{|\Omega(\mathbf{x})|^2}{4\delta}$.

The frequency of the laser is called blue detuned when $\delta > 0$, in which case the atoms are repelled from maxima of the field, and red detuned when $\delta < 0$ and atoms are attracted to them.

The above reasoning neglects the possibility of an excited state $|\, e \,\rangle$ to decay to a third state $|\, g^* \,\rangle$ by spontaneous emission. An atom which decays in this way is not subject to the dipole potential anymore, and is essentially lost for the experiment. However, this loss may be controlled since the scattering rate Γ_{sc} is proportional to the population of the excited state which can be computed and reads $\Gamma_{\text{sc}} \propto \frac{|\Omega(\mathbf{x})|^2}{4\delta^2}$. To reduce the loss rate, the laser field should be as strong as possible and the frequency far detuned, $|\delta| \gg \Omega$. Usually alkali-metal atoms are used in experiments for their large polarizability, allowing to go into regimes of negligible loss.

To build a three dimensional lattice, like in the pioneering experiment of Greiner et al. [10], three orthogonal lasers are focused on the trapping region using optical fibers. Their frequencies are slightly shifted using acousto-optical modulators and their polarization is chosen orthogonal to each other to avoid cross interferences [118]. The resulting dipole trapping potential is of the form

$$V(x, y, z) = V_0 \left(\cos^2(k_x x) + \cos^2(k_y y) + \cos^2(k_z z) \right) \tag{2.1}$$

Furthermore, the trap is of finite width because laser beams typically have a Gaussian intensity profile of width w in the transverse direction with respect to their propagation

$$V(x, y, z) = V_0 \left(\cos^2(k_x x) e^{-\frac{y^2+z^2}{2w^2}} + \dots \right) \tag{2.2}$$

This is an argument in favor of red detuned lasers, which can provide both the periodic potential and the trapping potential at the same time.

To study single particle eigenstates in the trapping potential [5], it is customary to consider an infinite lattice of period $d = \pi/k$ instead of the full trap. The eigenstates are Bloch functions $\psi_{n,\mathbf{q}+\mathbf{R}}(\mathbf{r})$ with band indices n and quasimomentum $\mathbf{q}$ in the Brillouin zone. The tight binding limit is characterized by a trapping energy V_0 large with respect to the recoil energy $E_r = k^2/2m$, the natural unit of kinetic energy [1]. In this limit, the basis of Wannier functions $w_{n,\mathbf{R}}(\mathbf{r})$ is the most natural. Wannier functions have a lattice site index $\mathbf{R} = dn_x\mathbf{i} + dn_y\mathbf{j} + dn_z\mathbf{k}$, d is the spatial period and n_x, n_y and n_z are integers. For the first lowest bands, Wannier eigenfunctions are localized around the site $\mathbf{R}$ and resemble the nth excited state of a harmonic oscillator in the limit $V_0 \gg E_r$. The Wannier states are not much modified when the smooth part of the trapping potential $V(\mathbf{x})$ is included.

1. The recoil energy is actually the kinetic energy acquired by a particle absorbing a photon of frequency $\nu = c/\lambda$, however no real transition of this sort occur since the atomic levels are far of resonance with the laser field frequency.

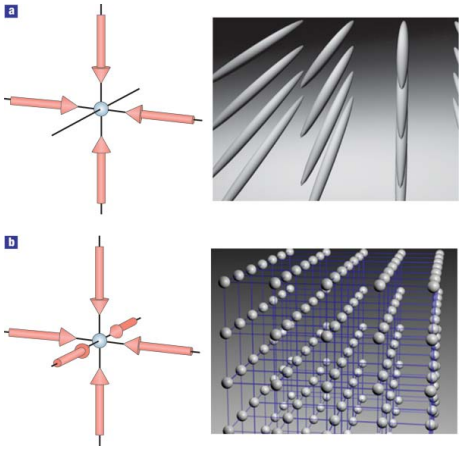

Figure 2.1: Optical lattice obtained by superimposition of two or three orthogonal lasers. **a)** Two superimposed laser form an array of one dimensional tubes. **b)** Three orthogonal lasers produce a cubic three-dimensional lattice.

In the following, we will consider the regime of temperatures, tunneling and interactions where only the first band is populated. Since the first gap is of the order of $\Delta = \sqrt{4V_0E_r}$ [117], even out of equilibrium a single band is involved in the dynamics provided all timescales of the quench are large compared to h/Δ.

2.1.2 Interactions and Feshbach resonance

The interactions between neutral atoms are dominated by van der Waals forces originating from dipole-dipole interactions. The scattering of two atoms, in relative motion, is described by a scattering eigenstate $\psi(\mathbf{r}) \sim e^{i\mathbf{k}.\mathbf{r}} + f(k,\theta)\frac{e^{ikr}}{r}$ where $f(k,\theta)$ is the scattering amplitude. For small temperatures in the sub-millikelvin regime, the scattering is dominated by low values of the relative angular momentum l. As a consequence, between identical atoms, s-wave scattering dominates for bosons. In this case, the scattering amplitude is a constant $f(k,\theta) \approx -a$. The scattering cross section is simply $\sigma = \int \frac{\mathrm{d}\sigma}{\mathrm{d}\Omega}\mathrm{d}\Omega = \int |f(k,\theta) + f(k,\pi-\theta)|^2\mathrm{d}\Omega = 8\pi a^2$. In this limit, interactions are completely characterized by the scattering length a and may be represented by an effective potential $V(\mathbf{x}) = \frac{4\pi\hbar^2 a}{m}\delta(\mathbf{x})$. As a consequence, the potential may be either attractive for $a < 0$ or repulsive otherwise.

To simulate condensed matter systems, it is crucial to reach the regime of strong interactions and to tune them at will. The phenomenon of Feshbach resonance fulfills this goal, allowing to tune the scattering length a of two-body collisions with a magnetic field. To describe it, it is necessary to include the internal states of the atoms in the description, i.e. their spin, excitation or species [119]. For definiteness we consider the case of alkali atoms, for which the internal variables are the electronic spin $S = 1/2$ and the nuclear spin I, and the

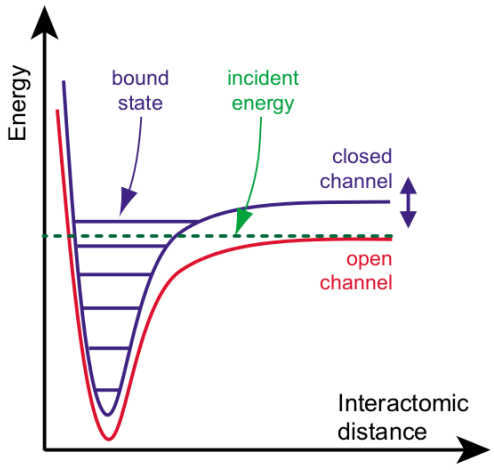

Figure 2.2: The interaction potential for atoms in their original state before the collision (open channel) and with different quantum numbers (closed channel), the picture is from [5]. The Feshbach resonance occurs due to the small energy difference between the energy of the incident state and of a bound state with different quantum numbers.

dominant couplings are the hyperfine coupling $a_{\text{hf}}\hat{\mathbf{S}}\cdot\hat{\mathbf{I}}$ and Zeeman coupling [2] $(2\mu_B\hat{S}_z - \mu_n\hat{I}_z)B$. In a strong magnetic field this Hamiltonian is almost diagonal in the $|S_z, I_z\rangle$ basis, and the Feshbach resonance can be qualitatively understood in perturbation theory in a_{hf}. The following analysis is the simplest description of the Feshbach resonance, an exhaustive review can be found in [120]. A Feshbach resonance occurs, as shown in figure 2.2, when the energy E_0 of the free colliding atoms $|\alpha,\beta\rangle = |S_z^\alpha, I_z^\alpha, S_z^\beta, I_z^\beta\rangle$ (the open channel) is very close to the unperturbed energy E_0^c of a bound state of the two atoms with different quantum numbers $|\alpha',\beta'\rangle$ (the closed channel). This situation arises since the effective potential governing the two-body collision depends on the internal state of the two atoms.

The scattering length is altered by the resonance due to the additional phase shift $\delta = \delta_0(k) + \delta(k)$, where $\delta_k = -\arctan\frac{\Gamma(k)}{2(E_0 - E_0^c)}$ related to the scattering amplitude by $f(k) = \frac{1}{k\cot\delta(k) - ik}$, where the width of the resonance is $\Gamma(k) = 2\pi\left|\langle\alpha',\beta'|a_{\text{hf}}\hat{\mathbf{S}}\cdot\hat{\mathbf{I}}|\alpha,\beta\rangle\right|^2$. In s-wave scattering, the width $\Gamma(k)$ is linear for small k and we can parametrize it as $\Gamma(k) \sim \frac{\hbar^2 k}{Mr^*}$. Then, the scattering length is $a = -\lim_{k\to 0} f(k) = a_0 + \frac{\hbar^2}{Mr^*(E_0 - E_0^c)}$. In practice, a magnetic field B allows to tune the Zeeman shift of levels to change $E_0 - E_0^c \sim (\mu - \mu_c)(B - B_0)$ and the scattering length at will.

The energy levels E_0, E_0^c and the width of the resonance $\Gamma(k)$ are generally not calculated from first principles, since they depend on fine properties of the interaction potential. As a consequence, scattering lengths are measured experimentally to determine the resonance field B_0, the non-resonant scattering length a_0 and the width parameter ΔB.

2. μ_B denotes the magnetic moment of the electron, the Bohr magneton, and μ_n the magnetic moment of the nucleus.

In the regime of strong interactions, three body inelastic collisions are not negligible anymore. They cause recombination processes, in which two atoms form a bound state while a third atom carries aways the resulting excess energy [121]. This effect is desirable to produce molecules, but is the main cause of loss of particles when single alkali atoms are studied and places limitations on the densities and scattering lengths a that one can use.

2.1.3 Bose-Hubbard model

Let us combine all previous elements to describe the effective Hamiltonian of bosons loaded in an optical lattice and subject to two-body s-wave elastic scattering interactions. Recall that we made the assumption that only the lowest band is populated. In addition, we suppose that the Wannier functions overlap is negligible beyond the first neighbors of a lattice site, which is true for large enough trapping potential V_0. Under these approximations it is possible to derive [117] the standard Bose-Hubbard Hamiltonian with nearest neighbor hopping

$$\hat{H} = -\sum_{\langle ij \rangle} J_{ij} \left(\hat{b}_i^\dagger \hat{b}_j + \text{h.c.} \right) + \sum_i \frac{U_i}{2} \hat{n}_i (\hat{n}_i - 1) + \sum_i \epsilon_i \hat{n}_i \tag{2.3}$$

where the hopping amplitude J_{ij} between site i and j and the two-body on site repulsion U are expressed in terms of Wannier functions [9]

$$J_{ij} = \int \mathrm{d}^3\mathbf{x} \;\; w^*(\mathbf{x} - \mathbf{x_i}) \left(-\frac{\hbar}{2m} \nabla^2 + V(\mathbf{x}) \right) w(\mathbf{x} - \mathbf{x_j}) \tag{2.4}$$

$$U_i = 4\pi \frac{a\hbar^2}{m} \int \mathrm{d}^3\mathbf{x} \;\; |w(\mathbf{x})^4| \tag{2.5}$$

$$\epsilon_i = \int \mathrm{d}^3\mathbf{x} \;\; V(\mathbf{x}) \; |w(\mathbf{x})|^2 \tag{2.6}$$

2.1.4 Experimental probes

In the following, we make a short review of available experimental probes and the physical quantities that they monitor. As theorists, we are primarily interested in a few quantities which are the key to understand many-body physics. The Green's functions $G(r, r', t)$ and the one particle spectral density $\rho(\omega)$ are defined as

$$G(r, r', t) = \langle T_t \hat{b}_r(t) \hat{b}_{r'}^\dagger \rangle \tag{2.7}$$

$$\rho(\omega) = -\frac{1}{\pi \mathrm{Vol}} \int \mathrm{d}r \, \mathrm{Im} G(r, r, \omega) \tag{2.8}$$

They allow to identify quasiparticle excitations and their spectral properties, to monitor gaps, etc. It is also of interest to detect directly the various order parameters characteristic of phase transitions, such as the off-diagonal long-range order (2.11). Finally, many "observables" often

make the link between theory and experiment, such as local density $\langle \hat{n} \rangle$, the compressibility $\kappa = \frac{\partial \langle \hat{n} \rangle}{\partial \mu}$, susceptibility, etc.

Developing powerful probing methods for cold atoms is a mandatory step to put these "quantum simulators" to work. Most present methods are destructive, which is not too much of a problem since all experiments can be repeated. The most popular methods are described below.

- *Time of flight absorption imaging* is certainly the most widespread method. In this destructive measurement, the trap is suddenly released, atoms propagate and fall freely for a chosen time of flight t and the resulting cloud is detected using absorption imaging [5]. To be able to detect atoms at such a low densities, a laser beam resonant with an atomic transition is sent through the cloud, and the shadow image is recorded on a standard CCD camera.

  After the sudden release of the trap, atoms which were in a Bloch state with quasimomentum $\mathbf{q}$ are a in superposition of plane waves of momentum $\mathbf{q_n} = \mathbf{q} + 2k\mathbf{n}$ with $\mathbf{n} = n_x\mathbf{i} + n_y\mathbf{j} + n_z\mathbf{k}$ spanning all integers. The density of atoms in space $n(\mathbf{x})$ measured by the absorption imaging after time t is related to the one particle density matrix in momentum space $G(\mathbf{k}) = \sum_{\mathbf{R},\mathbf{R}'} \langle \hat{b}^\dagger_{\mathbf{R}} \hat{b}_{\mathbf{R}'} \rangle e^{i\mathbf{k}(\mathbf{R}-\mathbf{R}')}$ (recall that $\mathbf{R}$ spans the lattice sites)

$$n(\mathbf{x}) = \left(\frac{M}{\hbar t}\right)^3 |w(\mathbf{k})|^2 G(\mathbf{k}) \qquad \mathbf{k} = \frac{M\mathbf{x}}{\hbar t} \tag{2.9}$$

  This expression is obtained assuming that the atoms are propagating ballistically, without interactions, after the release of the trap, and that the original spatial extension of the trap is small compared to the final size of the cloud. According to (2.9), the real space imaging directly yields the original one particle density matrix in momentum space.

  The time of flight measurement allows one to identify the onset of coherence in the many-body system. For example, the superfluid phase is characterized by the off-diagonal long-range order $n_0 = \lim_{|\mathbf{R}-\mathbf{R}'|\to\infty} \langle \hat{b}^\dagger_{\mathbf{R}} \hat{b}_{\mathbf{R}'} \rangle$. When long-range order is present, the time of flight imaging is formally equivalent to Bragg scattering in solid state materials with the coherent matter-wave playing the role of light, and a diffraction pattern characteristic of the geometry of the optical trap is obtained.

- *Shot-noise correlations* also contain valuable informations [122]. One measure of the quantum operator $\hat{n}(\mathbf{x})$ is not sufficient to characterize its full distribution, and each measure will exhibit shot-noise fluctuations, typically of the order of $\sqrt{N}$ for a Gaussian distribution where N is, for example, the number of atoms measured in a unique camera cell. The study of density-density correlations $\langle \hat{n}(\mathbf{x})\hat{n}(\mathbf{x}') \rangle$, an analog of the Hanbury-Brown-Twiss interferometry in optics [123], allows to trace back four-point correlation functions $\langle \hat{b}^\dagger(\mathbf{k})\hat{b}^\dagger(\mathbf{k}')\hat{b}(\mathbf{k}')\hat{b}(\mathbf{k}) \rangle$. This is useful, for example, to reveal coherent properties of the Mott insulating phase [124], which are invisible at the level of two-point correlations unlike in the superfluid phase. Another application is the distinction of Mott and glassy phases in disordered systems [125].

- *Bragg scattering* (with light) is another tool to probe periodic cold atom systems. It allows to measure the dynamical structure factor $S(\omega, \mathbf{k})$ which is the Fourier transform of density-density correlation functions $\langle\, \hat{n}(\mathbf{x}, t)\hat{n}(0,0)\,\rangle$. This technique is a good complement to the time of flight imaging. It could also be a tool for thermometry with fermions [126], a central issue with the current difficulties to reach degeneracy, and it allows to address the spin degrees of freedom with light polarization [127].
- *Momentum-resolved photoemission spectroscopy* is another famous method of condensed matter physics [128] which has been transposed to cold atoms [129]. A radio frequency photon induces a spin-flip on one atom, effectively ejecting it from the system, allowing to measure directly the single particle density of states $\rho(\mathbf{k}, \omega) = -\frac{1}{\pi}\mathrm{Im}G(\mathbf{k}, \omega)$. This technique allowed for the direct demonstration of strong correlations in a fermionic lattice system [130].
- *Single site resolution imaging* [131, 132] is one of the last major achievement to this date, it allows to measure directly the density (or rather its parity) at each individual site. The method has been used to measure correlated particle-hole pairs and string order [133].

2.2 Phase diagram of the Bose-Hubbard model

2.2.1 Generic features

After this digression about measurement techniques, we describe the zero temperature phase diagram of the Bose-Hubbard model. Original studies date back to the nineties [134], motivated by experiments involving supercooled ^{4}He absorbed in a porous medium and by granular superconductors. The general underlying question was the interplay between coherent and insulating properties, a problem which drew a lot of interests in fermionic systems. The famous phase diagram of the Bose-Hubbard model has first been derived in [134], along with the critical behavior, the multicritical points and the impact of disorder on the phase transitions.

In the following, we will consider the infinite, translation invariant model (2.3) with constant chemical potential $\epsilon_i = -\mu$ in the grand canonical ensemble,

$$\hat{H} = -J \sum_{\langle ij \rangle} \left(\hat{b}_i^\dagger \hat{b}_j + \text{h.c.} \right) + \frac{U}{2} \sum_i \hat{n}_i(\hat{n}_i - 1) - \mu \sum_i \hat{n}_i \tag{2.10}$$

For convenience, we set $U = 1$ and we measure energies in units of U. The phase diagram is the result of the competition between local interaction and kinetic energy. For small U, the system is in the *Mott insulator* phase, where the density is commensurate $n = \langle \hat{n} \rangle \in \mathbb{N}$. This phase is gapped and incompressible, $\kappa = \frac{\partial n}{\partial \mu} = 0$. This is a consequence of the fact that introducing excess particles in the system costs interaction energy U and that the kinetic energy gained from delocalization is not strong enough to overcome it.

For large enough $J > J_c(\mu)$, there is a quantum phase transition to a *superfluid* phase. It is indeed expected that as interactions become less relevant with respect to the kinetic energy, the

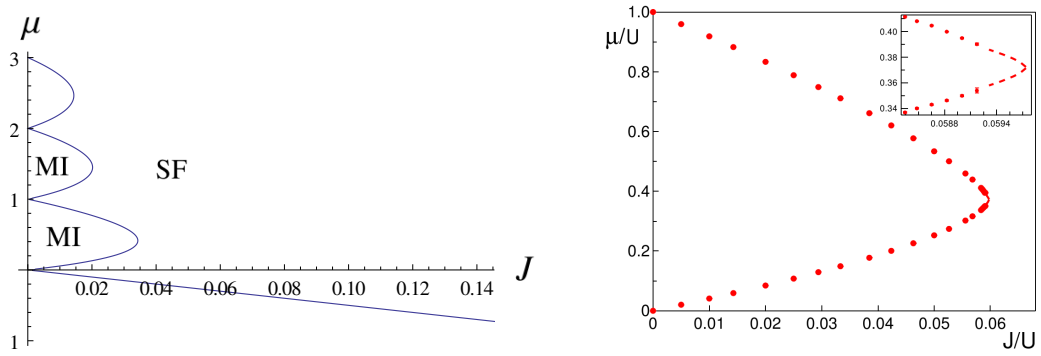

Figure 2.3: Left panel: Mean-field phase diagram as obtained from the cavity method in $d = 3$, as a function of J/U, μ/U (derived in section 2.2.2). Right panel: Close view of the first insulating lobe for $d = 2$ from Monte Carlo simulations [135].

most favored state for a bosonic system is coherent and undergoes Bose Einstein condensation. The order parameter characteristic of coherence is the *off-diagonal long range order*

$$n_0 = \lim_{r\to\infty} \langle \hat{b}_i^\dagger \hat{b}_{i+r} \rangle \tag{2.11}$$

In the Mott insulating phase, the strong interaction U disfavors number fluctuations and superfluid order. Notice that the original Hamiltonian is invariant under the global U(1) symmetry $\hat{b}_i \to \hat{b}_i e^{i\phi}$. This symmetry is spontaneously broken in the superfluid phase, and phase twists give rise to soft modes, the phonons, so that the superfluid phase is gapless.

The phase diagram is shown in figure 2.3. One of its striking features is that the Mott insulator regions have a lobe shape. Each different lobe has a different integer density, as can be seen in the atomic limit $J = 0$. It is rather easy to understand in a perturbative expansion in J that the Mott insulator is more easily destabilized near integer values of μ, where the gap is smallest, which explains the lobe shape.

2.2.2 Mean-field phase diagram

A qualitative phase diagram can be obtained with a simple mean-field argument [136]: consider a single site i, and approximate the action of all neighbors by an effective field Ψ

$$\hat{H}_i = -J(\hat{b}_i^\dagger \Psi + \hat{b}_i \Psi^\dagger) + \frac{U}{2}\hat{n}_i(\hat{n}_i - 1) - \mu \hat{n}_i \tag{2.12}$$

A naive and plausible estimate of the field Ψ is to replace it by the average over the neighbors j of i: $\Psi = \sum_j \langle \hat{b}_j \rangle$ where the average is taken on each effective single sites j with Hamiltonian $\hat{H}_j$. The self-consistent value of Ψ is evaluated numerically for all (J, μ) for lack of a convenient analytical expression [3]. The phase diagram at zero temperature is shown in figure 2.3.

3. The single site averages in the infinite dimensional Fock space $\{|0_i\rangle, |1_i\rangle, \ldots\}$ gives rise to infinite series, see for example [137].

Let us show some simple properties of the Mott insulator phase. The model is trivial to solve at $J = 0$ where the ground state is a pure Fock state $|\Psi_0\rangle = \otimes|n(\mu)\rangle$ where [4] $n(\mu) = [\mu]$. Since for $J = 0$ there is a gap between the ground state and the first excited state $|\Psi_1\rangle = \otimes|n(\mu) \pm 1\rangle$, by continuity, this gap is present in the whole Mott phase and the closure of the gap signals the phase transition.

Another remarkable property is that the ground state (all eigenstates) has integer, constant number of bosons $\langle E_0|\hat{N}|E_0\rangle = L^d n(\mu)$, where $\hat{N} = \sum_i \hat{n}_i$, because $\hat{N}$ is conserved by $\hat{H}$ and in particular by the kinetic term $\hat{K} = -J\sum_{\langle ij\rangle}\left(\hat{b}_i^\dagger \hat{b}_j + \text{h.c.}\right)$. In perturbation theory in $\hat{K}$, only terms with the same total number of bosons are generated at arbitrary order. This argument again breaks down when the gap closes at the phase transition $J = J_c$ where the perturbation series diverges. Hence the compressibility $\kappa = \frac{\partial\langle\hat{N}\rangle}{\partial\mu}$ is zero in all the Mott insulating phase.

As a final remark, this mean-field approximation is actually equivalent to the variational Gutzwiller Ansatz, where one chooses a factorized wavefunction as a variational Ansatz

$$|\psi\rangle = \bigotimes_j \sum_{n=0}^{\infty} \psi_n^j |n_j\rangle \qquad \psi_n^j = \psi_n \tag{2.13}$$

where all coefficients ψ_n^j are independent of the site j because of translation invariance.

At finite temperature, the superfluid order is destroyed above a critical temperature $T_c(J,\mu)$ and the Mott insulating phase is replaced by a strongly correlated gas of bosons with small compressibility $\chi \sim e^{-(E_1-E_0)/kT}$ at low temperature, because of Arrhenius activation.

2.2.3 Critical points

Let us now show that the quantum phase transition from Mott insulator to superfluid belong to two different universality classes at different points of the μ, J, U phase diagram. To do so, we use the bosonic path integral at finite temperature [138], using the coherent state representation in a Suzuki-Trotter decomposition, or equivalently the Euclidean continuation $t \to -i\tau$ of the unitary evolution, which reads

$$Z = \text{Tr}\, e^{-\beta H} = \int \mathcal{D}\psi_i \mathcal{D}\psi_i^* e^{-S[\psi]} \tag{2.14}$$

$$S = \int_0^\beta \mathrm{d}\tau \left(\sum_i \left(\psi_i^*(\partial_\tau - \mu)\psi_i + \frac{U}{2}\psi_i^*\psi_i^*\psi_i\psi_i \right) - J\sum_{\langle ij\rangle}\left(\psi_i^*\psi_j + \psi_j^*\psi_i\right)\right) \tag{2.15}$$

Notice that the particle-hole asymmetry is visible in the $\psi \leftrightarrow \psi^*$ asymmetry of the $\psi_i^*\partial_\tau\psi_i$ term [139]. It is possible to decouple the hopping term, performing a Hubbard-Stratonovich

4. $[x]$ is the integer part of x

transformation with auxiliary fields Ψ_i and using the inverse matrix $(J^{-1})_{ij}$

$$Z = \int \mathcal{D}\psi_i \mathcal{D}\psi_i^* \mathcal{D}\Psi_i \mathcal{D}\Psi_i^* e^{-S[\psi,\Psi]} \tag{2.16}$$

$$S = \int_0^\beta \mathrm{d}\tau \left(\sum_i \left(\psi_i^*(\partial_\tau - \mu)\psi_i + \frac{U}{2}\psi_i^*\psi_i^*\psi_i\psi_i \right) - \sum_{ij} \left(\Psi_i^*(J^{-1})_{ij}\Psi_j \right) \right) \tag{2.17}$$

Notice that this Hubbard-Stratonovich transformation is exact and generalizes the previous mean-field approximation. The next step is to integrate over the fields ψ_i. Actually, this manipulation is useful [140] because it singles out the slow modes of the order parameter field Ψ_i, which we will see are responsible for the phase transition. Thus to characterize the quantum phase transition, a gradient expansion in time and space derivatives of Ψ is sufficient, and the following result is obtained [134] in the continuum limit

$$Z = \int \mathcal{D}\Psi_i \mathcal{D}\Psi_i^* e^{-S[\Psi]} \tag{2.18}$$

$$S = \int_0^\beta \mathrm{d}\tau \int \mathrm{d}^d x \left(a_1\, \Psi^* \partial_\tau \Psi + a_2\, \partial_\tau \Psi^* \partial_\tau \Psi + \frac{1}{2}|\vec{\nabla}\Psi|^2 + r|\Psi|^2 + \frac{u}{2}|\Psi|^4 \right) \tag{2.19}$$

In principle, one needs to perform a renormalization group study of this action, the phase transition corresponding to fixed points. The second derivative $\partial_\tau \Psi^* \partial_\tau \Psi$ term, which was not present in the action (2.17), is generated under the renormalization group flow but is not relevant unless the first term $a_1\, \Psi^* \partial_\tau \Psi$ flows to zero.

The generic quantum phase transition [136] is characterized by nonzero a_1 and occurs almost everywhere on the transition lines. In this case, the coupling in $\partial_\tau \Psi^* \partial_\tau \Psi$ is irrelevant. It is a transition from zero density of hole excitations $Q = \langle |\Psi_r|^2 \rangle = \langle \hat{b}_i^\dagger \hat{b}_i \rangle - n(\mu)$ to a nonzero density in the superfluid phase. Its lower and upper critical dimensions are $d_l = 0$ and $d_u = 2$.

The multicritical point occurs when a_1 flows to zero under the renormalization group, in which case the particle-hole symmetry is dynamically restored, since $\Psi^* \partial_\tau \Psi$ is the only symmetry breaking term. The next relevant term is $\partial_\tau \Psi^* \partial_\tau \Psi$, and in the limit of zero temperature, the factor a_2 may be rescaled to $1/2$ and the transition in characterized by the rotational invariance in $(\tau, \mathbf{x})$. Hence, this quantum phase transition belongs to the universality class of the classical XY model in d+1 dimensions. This dynamical restoration of the particle-hole symmetry only occurs at the tips of the Mott lobe, since it can be shown [141] that a_1 vanishes when $\frac{\mathrm{d}\langle \hat{N} \rangle}{\mathrm{d}\mu} = 0$. Finally, the lower and upper critical dimension of the classical XY model are $d_l = 2$ and $d_u = 4$, therefore the multicritical point exists for $d > 1$.

Notice that as usual, the finite temperature transition is given by an action in a slab geometry of size (β, ∞) in the variables $(\tau, \mathbf{x})$, which is in the universality class of the classical XY model in d dimensions on all points of the superfluid-gas transition, because the finite size imaginary time direction is reduced to arbitrary small length under the flow of the renormalization group.

2.2.4 Theoretical and numerical methods

A quite complete review of the various methods that have been employed to analyze the model can be found in [8]. Here, we only mention a few studies which use various representative techniques. The only analytical techniques available are perturbative expansions, which can not describe the whole phase diagram. For example, the strong coupling limit expansion, even at high orders [142], is limited to the Mott insulator phase.

Nevertheless, there are several efficient numerical methods which are reliable in the entire phase diagram. The Density Matrix Renormalization Group is generally applicable to any one dimensional system. The Bose-Hubbard model and a generalized version with nearest neighbors interactions has been studied in [143].

Monte Carlo simulations is a first principles way of simulating bosonic systems, applicable in any dimensions. For example, in [144], the three-dimensional phase diagram has been computed using the worm algorithm.

Another remarkable approach is the lattice non-perturbative renormalization group (NPRG). In general, renormalization group techniques allow to determinate universal quantities only, such as the critical exponents and scaling functions. The recently developed lattice NPRG technique [145] gives access to *non-universal* quantities, like the phase diagram or the equation of state [141]. This method allowed for a direct check of the generic and multicritical point scaling [134] and of many other subtle infrared properties of the superfluid phase [146].

2.3 Experiments: Equilibrium physics

The successive realization of three dimensional [10], one dimensional [147] and two dimensional [148] optical lattices in the strong correlation regime allowed for the exploration of the Mott insulator to superfluid transition.

The first evidence of this transition is the Greiner et al. experiment [10] ; the absorption images are shown in figure 1.1. As we have shown above in section 2.1.4, the absorption image is a direct picture of the single particle Green's function $G(\mathrm{k})$ in momentum space. With vanishing periodic potential $V_0 = 0$ (panel (a)), the bosons form a simple Bose-Einstein Condensate and the distribution has a single peak centered around $\mathrm{k} = 0$. In the superfluid phase with nonzero $V_0 > 0$, a diffraction pattern is visible, since $G(\mathbf{R}) \overset{|\mathbf{R}|\to\infty}{\to} n_0$ and according to (2.9)

$$n(\mathbf{x}) = N\left(\frac{M}{\hbar t}\right)^3 \left| w\left(\frac{M\mathbf{x}}{\hbar t}\right)\right|^2 \sum_{\mathbf{R}} G(\mathbf{R}) e^{i\frac{M}{\hbar t}\mathbf{x}\cdot\mathbf{R}} \tag{2.20}$$

The diffraction pattern is visible in the superfluid phase (panel (b), (c), (d)) with a factor of attenuation $w(\frac{M\mathbf{x}}{\hbar t})$. On the other hand, the diffraction pattern is lost in the Insulator phase, where $G(\mathbf{R})$ decays exponentially, and only the smooth Wannier profile is visible (panel (h)). Yet, the presence of sharp peaks in time of flight measurements is not sufficient to characterize the

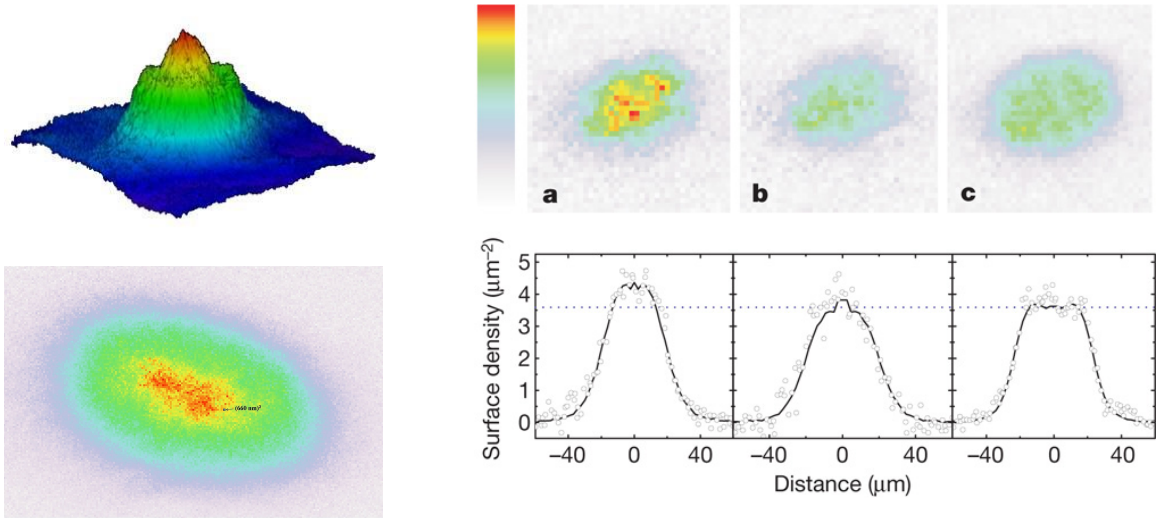

Figure 2.4: Density profile of cold bosons in a two-dimensional lattice at strong interactions in the experiment of the Chicago group [150]. Right upper panel: Color plot of the density in real space. Right lower panel: Cut of the density plot along the major axis. The dashed horizontal line denotes unit filling. From a) to c): Growing interaction $U = 2.4E_R$, $U = 9.4E_R$ and $U = 22E_R$ in units of the recoil energy E_R. At the center of the trap, the systems goes from superfluid to Mott insulator. The Mott insulator phase is characterized by a flat density profile despite the varying potential $V(x)$, characteristic of its incompressibility.

superfluid phase. A precise analysis shows that coherence peaks remain in the Mott phase, as long as significant correlations remain on lengthscales of several lattice spacings, for example due to coherent particle-hole pair excitations [5].

This discussion is further complicated due to the trapping potential, producing very inhomogeneous systems. Nevertheless, to a good approximation, a given small region of the lattice may be thought as a patch of an infinite system with a slowly varying chemical potential $\mu(\mathbf{x})$. This local density approximation has been checked by exact numerical simulations [149].

The coexistence of superfluid and Mott insulating regions in the trap produces the "wedding cake" structure of figure 2.4. Indeed, in superfluid regions, the density varies continuously with the chemical potential $\mu(\mathbf{x})$. On the contrary, the Mott insulating phase is incompressible, hence the density has characteristic plateaus which allow to detect the Mott state without ambiguity.

As a side remark, let us mention that from the theorist point of view, a refined analysis of correlations and phase transitions requires systems as close as possible to the thermodynamic limit, i.e. large, translation invariant systems. This is even more crucial to study quenches, since the dynamics is dominated by transport properties in inhomogeneous systems [151], which is certainly a problem of interest, but is not the archetypal quench.

There is certainly room for improvement in this direction, for instance using blue-detuned light sheets to ensure confinement [152]. A Bose-Einstein condensate in a two-dimensional

box has already been realized [153], which we hope will help design homogeneous optical lattices.

2.4 Out of equilibrium physics, experiments

After the realization of low temperature equilibrium samples, experiments on quenches were the next step to take. The out of equilibrium dynamics after a quench from the superfluid to deep into the Mott phase has been investigated in [90]. The authors coined the term *collapse and revival of the matter wavefunction* to describe the oscillations of the fraction of coherent atoms, shown in figure 2.5. The global coherence of the system is periodically lost and restored on short times, until the oscillations are damped. In the experiment, the damping is mainly due to dephasing between sites of different chemical potential and is an effect of the inhomogeneous trap.

Early analysis of the phenomenon relied on the fact that the initial state is in the limit of the weakly interacting condensate, yielding a quasi coherent initial state, and that the final interaction are strong enough to neglect $J \ll U$ such that the evolution is essentially a non linear evolution of a single coherent state with local Hamiltonian $U\hat{n}_i(\hat{n}_i - 1)/2$, yielding a period of $\tau = h/U$. The authors have also studied the impact of larger interactions in the initial state, leading to diminished initial number fluctuations $\sigma_n^2 = \langle\, \hat{n}^2(t=0)\,\rangle - \langle\, \hat{n}(t=0)\,\rangle^2$, referred as "squeezing" of the local coherent state. The damping rate of the coherent oscillations is found, in this regime, to be proportional to σ_n. It should be emphasized that although this analysis is certainly appealing to the quantum optics and atomic physics community, it leaves untouched many questions. For example, the mean-field calculation predicts that such oscillations are not particular to the regime of low final J/U but occur everywhere in the Mott phase, with a non trivial period $\tau(U, J) \neq h/U$, which is computed in section 3.4.2. Understanding the damping rate in an homogeneous system is of particular interest. It originates from emission of pairs of "phasons" [154].

The same superfluid to Mott quench [131] has been studied with single-site imaging. However, due to large gradients of the potential, the width of Mott insulating regions is of a few lattice sites only, a case in which fast thermalization occurs with superfluid regions playing the role of a bath. As a consequence, the occupation number statistics relaxes exponentially to the equilibrium value in the Mott insulating regions.

The reverse Mott to superfluid ramping quench has been realized in [155]. The resulting state has vortices and other type of excitations, but again the inhomogeneity of the trap does not allow for quantitative measurements. The predicted oscillations in the superfluid fraction [154] were not found, but we hope that these preliminary results will foster new experiments.

Quenches within the superfluid phase, from the strongly to the weakly interacting regime, have been studied in a one-dimensional lattice system [156]. Due to the large filling number $n \sim 100$, the system is well described by the Gross-Pitaevskii equation, provided some quantum fluctuations are included using the Truncated Wigner Approximation. The observed phase

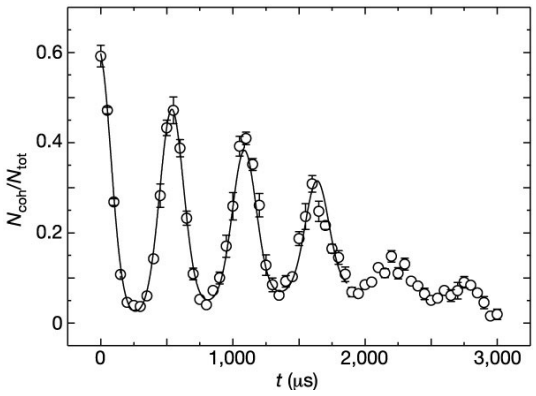

Figure 2.5: Time-dependent collapse and revival of the fraction of coherent atoms $N_{\rm coh}/N_{\rm tot}$ after a quench, from [90]. The fast relaxation is essentially due to the inhomogeneity of the trap.

coherence dynamics is in agreement with the model.

Let us finally mention that in the experiments on the light cone effect [53], already mentioned in section 1.2.6, two-point correlations were measured on distances up to 6 lattice sites in a one-dimensional system, demonstrating the fast progress of experimental techniques.

2.5 Out of equilibrium physics, theory

Many theoretical and numerical studies of the out of equilibrium Bose-Hubbard model have been carried out to address a large variety of physical effects.

Let us mention again that the Bose-Hubbard model is a good example of a mixed system and was often chosen to study thermalization [54, 46, 55], as described in section 1.2.2.

An interesting case of out of equilibrium processes, which we have not discussed so far, is when the system is originally inhomogeneous. For example, the dynamics of a small density wave has been studied in the one dimensional lattice [157] using t-DMRG, allowing to measure the decay of the excitation, the sound velocity, and to assess the regime of validity of analytical predictions.

The quenches from the Mott phase to the superfluid phase in two dimensions has been considered in [154], using a coherent state path integral which describes the soft "phasons" modes of the strongly correlated superfluid. The authors find an oscillating superfluid order parameter, and compute its damping rate by phason pair emission.

The same quench has been analyzed again in a $1/z$ (z is the coordination number) expansion in [97], from a different perspective. A light-cone effect is found close to the critical point, visible in two-point correlations $\langle\, \hat{b}_0^\dagger(t)\hat{b}_{\mathbf{r}}(t)\,\rangle \sim \exp(\gamma\sqrt{t^2 - \mathbf{r}c^2})$, with an effective limiting propagation speed $c = 3J(U-J)/m^*$. The growth rate $\gamma^2 = J - J_c$ is vanishing at the critical point, and governs the small-range condensed fraction $n_L = \sum_{|\mathbf{r}-\mathbf{r}|<L}\langle\, \hat{b}_{\mathbf{r}}^\dagger(t)\hat{b}_{\mathbf{r}'}(t)\,\rangle/L^2$ which

grows like $n_L \sim e^{\gamma t}$ for $L \ll ct$. The condensate fraction is present on a scale $L_{\text{typ}} = ct$ since n_L saturates at $n_L \sim 1/L^2$ for $L \gg L_{\text{typ}}$. The quenches to deep into the superfluid phase revealed a diffusive, instead of ballistic, propagation of correlations. An interesting extension of this work would be to understand the role and dynamics of topological defects during such a quench.

Some studies are more closely related to the present experimental setups and include the harmonic trapping potential, with quite different physics. Time dependent Gutzwiller Ansatz have been often used as simple approach to inhomogeneous systems, and the method easily generalizes to different conditions, such as a two-species system [158]. The superfluid to Mott quenches and the reverse quenches are studied within t-DMRG in [151]. The transport of energy and particles turns out to play a crucial role in the dynamics. The formation of Mott domains, splitting superfluid regions, is found to impair transport and to prevent thermalization on long times.

Chapter 3

Quantum dynamics in completely connected models

3.1 Introduction

In physics, mean-field analysis often proved to be a good starting point to study new problems. Out of equilibrium quantum dynamics is no exception to this rule. There are several variants of mean-field like methods: the large spin limit in the Ising model [96], and the Gutzwiller Ansatz, applied to the Hubbard model [159], a variant of the Dicke model [160], the Bose-Hubbard model with an external trapping potential in [161, 162, 158, 163] and superlattice models [164]. A saddle-point method specific to the Bose-Hubbard model has been developed in [110]. The slow annealing through first order phase transitions has been studied in [38].

In the first part of this chapter, we review a related approach introduced in [165, 166], allowing to describe quenches in completely connected models, and apply it to the Bose-Hubbard model. Systems defined on completely connected graphs may, to some extent, be good descriptions of some experimental systems as for instance in cavity quantum electrodynamics experiments [160, 167]. However, their dynamics is also the same as that of lattice systems, in the limit where the number of dimensions goes to infinity, thus we may use them as mean-field solutions for lattice systems with finite dimension. It is worth comparing this idea to the Gutzwiller Ansatz method mentioned above. When applied to a homogeneous finite dimensional lattice of coordination number z with hopping term J', it yields the *same dynamics* as the exact solution of the completely connected model with hopping $J/V = J'z'/V$ [166]. The solution to completely connected models is thus closely related to standard mean-field approximations, and analytical results can be derived naturally in this framework.

As we shall show, the quantum dynamics in a completely connected system can be solved by mapping the unitary evolution onto an effective classical model undergoing Newtonian dynamics. This drastic simplification originates from the symmetry of the completely connected

Hamiltonian under any permutation of sites. We restrict our analysis to cases where the system is in the ground state before the quench, in which case the wavefunction is symmetric under permutation of sites at all times. In this subspace, the states are parametrized using a few local macroscopic observables, which, in the thermodynamic limit, are governed by an effective classical Hamiltonian evolution.

In a second part, we apply this approach to sudden quenches in the Bose-Hubbard model, a relevant scenario for cold atom experiments. Actually, the sudden quench is an idealization of the ramping quench performed in experiments to prevent transition to higher bands, as discussed in section 2.1.1.

Under a generic quench within the superfluid phase, we find that the superfluid order is oscillating on short times, but surprisingly the average superfluid order after the quench is a non-monotonous function of $|U_f - U_i|$. Moreover, it decays logarithmically to zero on a special line of parameters (U_i, U_f). For these special quenches, the superfluid order relaxes exponentially to zero. We refer to this peculiar feature as a dynamical transition. Strikingly, the microcanonical equilibrium ensemble towards which the system would relax on large times, if it were able to thermalize, has non-zero superfluid order. Thus, this transition is a purely *dynamical* phenomenon, unrelated to the melting of superfluid order under heating.

Finally, we discuss the limitations of mean-field methods as well as what is expected to hold true in finite dimensional lattice models. The discussion of the generic features of the dynamical transition is postponed to chapter 4.7.

3.2 Generic symmetric formalism

3.2.1 Site permutation symmetry

We consider a generic Hamiltonian on a completely connected lattice of V sites [1], i.e. where all pairs of sites (i, j) are connected, which we suppose to be symmetric under permutation of sites. The Hilbert space may have any local degrees of freedom: 1/2-spins, bosons, fermions with or without spin, etc. For definiteness, we choose bosons and call $|\{n_i\}\rangle$ the Fock basis. We suppose that the Hamiltonian is the sum of a local energy term $\hat{U}$ and of two-site couplings $\hat{K}$. It is always possible to work in the basis where $\hat{U}$ is diagonal, here for simplicity we choose $\hat{U}$ to be diagonal in the Fock basis.

$$\hat{U} = \sum_i \mathcal{F}(\hat{n}_i) \tag{3.1}$$

$$\hat{K} = \frac{1}{V} \sum_{ij} \mathcal{G}(\hat{b}_i^\dagger, \hat{b}_j^\dagger, \hat{b}_i, \hat{b}_j) \tag{3.2}$$

All Hamiltonians of this class are symmetric under any permutation of site indices. In full generality, the theory of representations allows to decompose the Hilbert space into symmetry

1. V stands for volume.

sectors, classified using Young tableaux. For example, in the familiar case of N spin 1/2 degrees of freedom, these symmetry sectors under permutation coincide with eigenspaces of $\hat{S}^2$ of total spin $S = N/2 - K$. The maximal spin subspace $S = N/2$ is completely symmetric under permutation of spins, the minimal spin subspace $S = 0$ (if N is even) is completely antisymmetric and all intermediate values of S have nontrivial symmetry properties. Although these symmetry properties may be put to work in the general case, as has been done for spins in [168], we will consider here situations where the initial state is permutation symmetric.

Such an assumption is naturally satisfied when one considers quenches starting from the ground state of the system [2]. Since the site permutation symmetry is conserved by the unitary evolution, the dynamics takes place into the subspace of symmetric wave functions. This is a drastic simplification, because instead of computing the dynamics in a Hilbert space of dimension $\sim e^V$, the number of accessible states will be polynomial in the system size and easy to parametrize.

3.2.2 Effective Schrödinger equation

We now derive the effective Schrödinger equation in the symmetric sector. To illustrate the method, we consider the completely connected Bose-Hubbard Hamiltonian

$$\hat{H}_{\mathrm{BH}} = -\frac{J}{V}\sum_{i\neq j}\hat{b}_j^\dagger\hat{b}_i + \frac{U}{2}\sum_i \hat{n}_i(\hat{n}_i - 1) \tag{3.3}$$

$$\hat{U} = \frac{U}{2}\sum_i \hat{n}_i(\hat{n}_i - 1) \qquad \hat{K} = -\frac{J}{V}\sum_{i\neq j}\hat{b}_j^\dagger\hat{b}_i \tag{3.4}$$

To simplify the derivation, one can study a truncated model where the number of bosons per site is between zero and $n_b^{\max} = 2$, although we will consider less stringent truncations up to $n_b^{\max} = 5$ later. To build all symmetric states, one can apply the symmetrization operator $\hat{\mathcal{S}}$, whose action on any particular Fock state $|\{n_i\}\rangle$ is to yield the linear combination of every possible site-permuted Fock state:

$$\hat{\mathcal{S}}|\{n_i\}\rangle = \sum_\sigma |\{n_{\sigma(i)}\}\rangle \tag{3.5}$$

Any symmetric state is completely characterized by the fraction of sites with 0, 1 and 2 bosons $x_0 = \sum_i \langle\, \delta_{\hat{n}_i,0}\,\rangle / V$, $x_1 = \sum_i \langle\, \delta_{\hat{n}_i,1}\,\rangle / V$, $x_2 = \sum_i \langle\, \delta_{\hat{n}_i,2}\,\rangle / V$, thus can be referred as $|x_0, x_1, x_2\rangle = |\mathbf{x}\rangle$ where $\mathbf{x}$ is a shorthand for all variables. Since the Fock states form a basis of generic states, the $\{|\mathbf{x}\rangle\}$ states form a basis of the symmetric sector. In order to express the Schrödinger

2. The ground state is generally invariant under permutation symmetry, but there are exceptions like systems with attractive interactions, or frustrated systems, which we do not consider here.

evolution in this basis, we have to compute the transition elements $\langle \mathbf{x}'|\hat{H}|\mathbf{x}\rangle$. With our previous parametrization of $\hat{H}$, there are diagonal and non-diagonal terms that we call for convenience:

$$\langle \mathbf{x}|\hat{U}|\mathbf{x}\rangle = D(\mathbf{x})V \tag{3.6}$$

$$\langle \mathbf{x} + \mathbf{m}/V|\hat{K}|\mathbf{x}\rangle = -W_m(\mathbf{x})V \tag{3.7}$$

Notice that only few off-diagonal transitions are allowed [3], characterized by a vector of integers $\mathbf{m} = \{m_0, m_1, \ldots\}$. For example, in the Bose-Hubbard model (3.3), $\hat{K}$ links states which differ by one boson jump. Thus x_0, x_1 and x_2 can only differ by $1/V$ or $2/V$. For example, after a jump $|2_i \ldots 0_j \ldots\rangle \to |1_i \ldots 1_j \ldots\rangle$, $x_1' = x_1 + 2/V$, $x_0' = x_0 - 1/V$ and $x_2' = x_2 - 1/V$. This transition is labeled $\mathbf{m} = \{m_0 = -1, m_1 = 2, m_2 = -1\}$. Moreover, the reverse move is a transition characterized by $-\mathbf{m}$, with same amplitude $W_{-\mathbf{m}}(x) = W_{\mathbf{m}}(x)$ at leading order in V.

Thanks to the "locality" of transition elements between symmetric states, the Schrödinger equation in the symmetric basis $|\psi\rangle = \sum_{\mathbf{x}} \psi_{\mathbf{x}}(t)|\mathbf{x}\rangle$ takes a simple form. The Schrödinger equation projected on $\langle \mathbf{x}|$ reads $\langle \mathbf{x}|i\partial_t|\psi\rangle = \langle \mathbf{x}|\hat{H}|\psi\rangle$:

$$i\partial_t \psi_{\mathbf{x}} = VD(\mathbf{x})\psi_{\mathbf{x}} - V\sum_{\mathbf{m}} W_{\mathbf{m}}(\mathbf{x})\Big(\psi_{\mathbf{x}+\mathbf{m}} + \psi_{\mathbf{x}-\mathbf{m}}\Big) \tag{3.8}$$

$$= V\Big(D(\mathbf{x}) - 2\sum_{\mathbf{m}} W_{\mathbf{m}}(\mathbf{x})\cosh(\mathbf{m}\cdot\partial_{\mathbf{x}}/V)\Big)\psi_{\mathbf{x}} \tag{3.9}$$

where we used $\psi_{\mathbf{x}+\mathbf{m}/V} = \exp(\mathbf{m}\cdot\partial_{\mathbf{x}}/V)\psi_{\mathbf{x}}$. Remarkably, the Schrödinger equation (3.9) involves an effective $\hbar = 1/V$, thus the regime of interest $V \to \infty$ corresponds to the *classical regime*. Furthermore, for the ground state, the initial wave function is a narrow wave packet of width $1/\sqrt{V}$. To see that it is so, one can look for the lowest eigenstate of the Schrödinger equation (3.9) and recognize that for low energy eigenstates, only the zeroth and second order in $\partial_{\mathbf{x}}$ contribute, and that for a smooth potential the limit $\hbar \to 0$ always leads to a nearly Gaussian ground state of width $\sqrt{\hbar} = 1/\sqrt{V}$ in both space and momentum variables. Therefore at small times the wavefunction is a narrow wave-packet, fully described by its average (or center) $\mathbf{x}(t) = \langle \hat{\mathbf{x}}\rangle$ and average momentum $\mathbf{p}(t) = \langle \hat{\mathbf{p}}\rangle$. Both quantities evolve following a classical Hamiltonian dynamics obtained from the quantum one by replacing $\hat{\mathbf{p}} = \frac{i}{V}\partial_{\mathbf{x}} \to \mathbf{p}(t)$ and $\hat{\mathbf{x}} \to \mathbf{x}(t)$:

$$H[\mathbf{x}, \mathbf{p}] = D(\mathbf{x}) - 2\sum_{\mathbf{m}} W_{\mathbf{m}}(\mathbf{x})\cos(\mathbf{m}\cdot\mathbf{p}) \tag{3.10}$$

The classical Hamiltonian evolution of the variables $\dot{\mathbf{x}}(t) = \partial H/\partial \mathbf{p}$ and $\dot{\mathbf{p}}(t) = -\partial H/\partial \mathbf{x}$ yields the evolution of the wave packet after the quantum quench, and give access to all observables as a function of time. The previous statements about the wave-packet evolution are confirmed by a careful expansion of the wavefunction as $\psi_{\mathbf{x},t} \sim e^{V\mathcal{J}(\mathbf{x},t)}$ in [166].

3. The minus sign in the definition of $W_{\mathbf{m}}(\mathbf{x})$ is for later convenience.

We conclude that the quench dynamics in connected models takes the form of an effective classical Hamiltonian evolution. To compute physical observables after an arbitrary quench quench starting from the ground state at time $t = t_i$, one must determine the initial conditions $\{\mathbf{x}_i, \mathbf{p}_i\}$ minimizing $H[\mathbf{x}, \mathbf{p}](t_i)$ and compute the classical dynamics of $\{\mathbf{x}(t), \mathbf{p}(t)\}$ induced by the effective Hamiltonian $H(t)$ for $t > t_i$.

3.3 Bose-Hubbard model with strong truncation

In the following, we apply the previous method to study sudden quenches in the truncated Bose-Hubbard model with $n_b^{\max} = 2$. The effective classical Hamiltonian is derived first and detailed properties of the phase space of effective trajectories are given. Then, we turn to quench dynamics and characterize the peculiar physics at the dynamical transition.

3.3.1 Schrödinger equation and effective Hamiltonian

As shown previously, symmetric states of the truncated Bose-Hubbard model are called $|x_0, x_1, x_2\rangle$. Since the total number of sites $V = V(x_0 + x_1 + x_2)$ is fixed, and the overall density of bosons $n = N/V = x_1 + 2x_2$ is conserved by the dynamics, the symmetric states can be labeled by one variable only, which we choose to be x_1 that we call x from now on. The state $|x\rangle$ is by definition $|x\rangle = |x_0 = 1 - x_1 - x_2, x_1 = x, x_2 = (n - x_1)/2\rangle$.
To compute the transition rates, we proceed as follows. The tunneling term $-1/V \sum_{i \neq j} \hat{b}_j^\dagger \hat{b}_i$ gives rise to transitions from $|N_0/V, N_1/V, N_2/V\rangle$ to three states, $|(N_0 - 1)/V, (N_1 + 2)/V, (N_2 - 1)/V\rangle$, $|(N_0+1)/V, (N_1-2)/V, (N_2+1)/V\rangle$ and $|N_0/V, N_1/V, N_2/V\rangle$. Using the previous notations, the only possible transitions correspond to $m = 2$, $m = -2$, $m = 0$, the last one is of course a diagonal contribution. On the other hand, the repulsion term $1/2 \sum_i \hat{n}_i(\hat{n}_i - 1)$ is diagonal in the $|x\rangle$ basis, and after inspection, the transition rates are at leading V order:

$$W_x = x[(2 - x - n)(n - x)/2]^{1/2} \tag{3.11}$$

$$D_x = U(n - x)/2 - x(2 + n - 3x)/2 \tag{3.12}$$

In the same lines as above, the wave-packet in the x space is governed by an effective classical Hamiltonian

$$H[x, p] = D_x - 2W_x \cos(2p) \tag{3.13}$$

Note that the dimension of the Hilbert space has been reduced from e^V to V in this case. The case $n_b^{\max} = 2$ is especially convenient because the Hamiltonian is one dimensional thus integrable, and what differs and what is essentially similar for weaker truncations will be discussed in section 3.5.

3.3.2 Phase space properties

The simplest physical quantities to compute with the Hamiltonian derived above are the ground state properties. The ground state corresponds to the trajectory of lowest energy, which has constant zero momentum $p(t) = 0$ and constant coordinate $x(t) = x_0$ such that $\frac{\partial H[x,p]}{\partial x}\Big|_{x=x_0} = 0$. One finds that x_0 is

$$x_0 = \begin{cases} 1 & \text{if } U \geq U_c, \quad \text{Mott insulator} \\ \dfrac{U/U_c + 1}{2} < 1 & \text{if } U < U_c, \quad \text{Superfluid} \end{cases} \tag{3.14}$$

We recover the quantum phase transition from superfluid to Mott insulator at $U_c = 3 + 2\sqrt{2} \simeq 5.82$.

In the thermodynamic limit, the Mott insulator ground state is $|x = 1\rangle$ i.e. a pure Fock state $|1, 1, \ldots\rangle$. On the other hand, the superfluid ground state $|x = x_0\rangle$ is not a pure Fock state, with $1/2 < x_0 < 1$. The equivalent of the off-diagonal long range order $|\Psi_0|^2 = \lim_{|i-j|\to\infty} \langle \hat{b}_i^\dagger \hat{b}_j \rangle$ is $|\Psi_0|^2 = \frac{1}{V^2} \langle \sum_{ij} \hat{b}_i^\dagger \hat{b}_j \rangle$ since all sites are neighbors. In the ground state,

$$|\Psi_0|^2 = \begin{cases} 0 & \text{if } U \geq U_c, \quad \text{Mott insulator} \\ \dfrac{x_0(1-x_0)U_c}{2} > 0 & \text{if } U < U_c, \quad \text{Superfluid} \end{cases} \tag{3.15}$$

The typical phase portraits for trajectories of higher energies are depicted in figure 3.1 for U smaller and larger than U_c. All trajectories are periodic in time. Their main features as a function of U are the following:

- For $U < U_c$ the Mott ground state is at $x_0 = 1$. All trajectories of higher energy have unbounded momentum p.
- For $U > U_c$ the superfluid ground state is at $x_0 < 1$ of equation (3.14), and surrounding trajectories close in energy have bounded momentum p. For higher energies, there is a region of unbounded momentum, and a separatrix between the two regions, on which the trajectory is singular. While all other trajectories are periodic, on the separatrix trajectory position and momentum converge exponentially in time to $x(t) \to 1$ and $p(t) \to p_0$, a nontrivial constant.

3.4 Sudden quenches

We now discuss the dynamics following a sudden quantum quench $U(t) = U_i + \theta(t)(U_f - U_i)$ and its dependence on the final and initial value of U. In the following we call a quench "from superfluid" when $U_i < U_c$ and "from Mott" when $U_i > U_c$, and "to superfluid" or "to Mott" when $U_f > U_c$ and $U_f < U_c$.

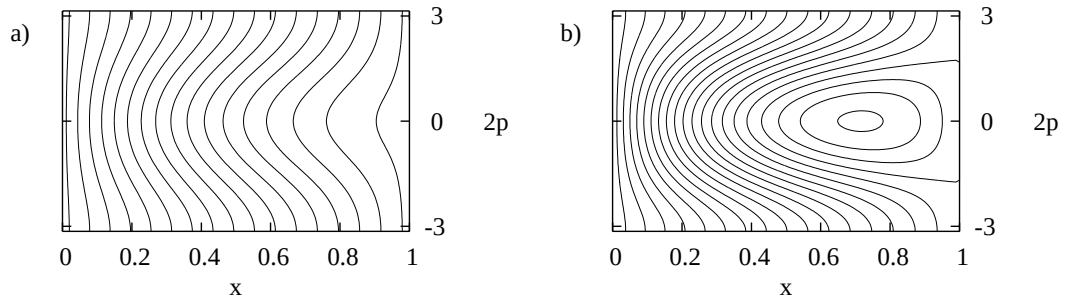

Figure 3.1: Phase portraits $(x, 2p)$ of trajectories for (a) $U = 6.6$ and (b) $U = 2.5$. The Hamiltonian is periodic in $p \to p + \pi/2$.

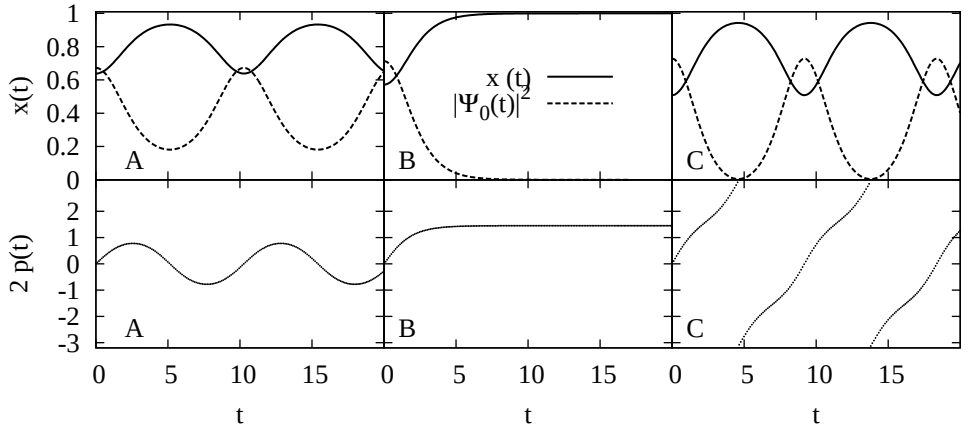

Figure 3.2: Position $x(t)$, momentum $p(t)$ and superfluid order $|\Psi_0^2|$ as a function of time t, for three trajectories A, B and C, for $U = 3.33 < U_c$. The scale is the same for all graphs.

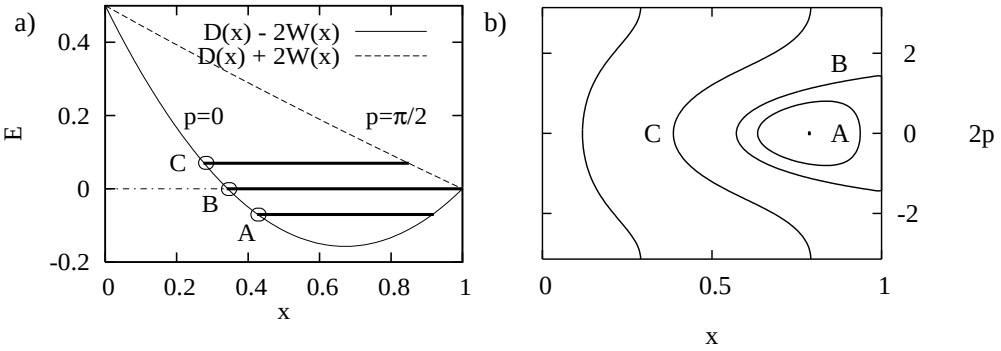

Figure 3.3: a) Potential energy landscape for $U = 3.33 < U_c$, with the energy E of trajectories A, B and C. Due to the momentum dependency of the Hamiltonian (3.13), the position $x(t)$ is restricted to the interval $D_x - 2W_x < x(t) < D_x + 2W_x$. b) The same trajectories in phase space $(x, 2p)$.

3.4.1 Mott to superfluid quench

Starting from the Mott ground state $x_0 = 1$, the trajectory is stuck at $x(t) \sim 1$ even for large times. In order to check this, let us linearize the equation of motion around $x = 1$. From (3.13) we find $\dot{x} = \partial H/\partial p = 4W_x \sin(2p)$, and $\sin(2p)$ can be extracted from $E = D_x - 2W_x \cos(2p)$ to obtain $\dot{x} = -\sqrt{4W_x^2 - D_x^2}$. Thus, for a small deviation from the fixed point $\epsilon(t) = 1 - x(t) \ll 1$,

$$\dot{\epsilon} = \epsilon/\tau, \quad \tau = 2/\sqrt{(U_c - U)(U - U_d)} \tag{3.16}$$

The trajectory $\epsilon(t) = 0$ is unstable, and since the wave function has a width $1/\sqrt{V}$, its typical evolution is given by $\epsilon(t) = 1/\sqrt{V}e^{t/\tau}$. Therefore, in the effective picture, the trajectory is stuck at the Mott ground state on times of the order of $\ln V$. A sheer analysis of this regime of quenches within the completely connected model has been carried out in [169], however we believe that this stationary state is a peculiarity of mean field models. Indeed, in a finite dimensional system, the situation is an example of a quench towards the broken symmetry phase, in which spatial fluctuations play a key role, to be discussed in section 4.6.9.

3.4.2 Superfluid to Mott quench

In a superfluid to Mott quench, the initial condition is given by the ground state packet characterized by $\{x = \frac{U/U_c+1}{2}, p = 0\}$. The trajectory after the quench is of the type (C) of figure 3.2 and the superfluid order parameter $|\Psi_0^2|$ oscillates. This sort of quench has been performed in the seminal experiment of collapse and revival of the matter wavefunction [90]. Unlike in the lattice model, in the completely connected model the coherent oscillations of the superfluid order are not damped, because of the lack of spatial fluctuations. It is noteworthy that the period of oscillations T is predicted by the mean-field argument to depend on the final couplings U_f and J_f in a nontrivial way:

$$T = \int \mathrm{d}x \left(2\sqrt{4W_x^2 - (E - D_x)^2}\right)^{-1} \tag{3.17}$$

In the original experiment, only the trivial limit $J_f/U_f \to 0$ of almost independent sites has been considered, with a period equal to $T = h/U$. The previous result generalizes this result for arbitrary (J_f, U_f) and the coherent oscillations are a genuine feature of a strongly coupled system on a lattice. Unfortunately, the regime of finite J_f/U_f has not been explored in the original experiment.

3.4.3 Superfluid to superfluid quench and the dynamical transition

In this section, we show simplified results from [166], neglecting some features that turn out to be irrelevant for higher truncations $n_b^{\max} > 2$. In this regime of parameters, depending on the relative values of U_i and U_f, there are different regimes of the quench dynamics. For $U_f < U_i$

or $U_f > U_i$ but below a threshold U_f^d , the superfluid order is oscillating after the quench as in trajectory (A) of figure 3.2, with bounded momentum. For $U_f > U_f^d$ the superfluid order is oscillating again but with unbounded momentum as in trajectory (C). For the special value $U_f = U_f^d$, the quench trajectory is the separatrix (B), the superfluid order relaxes exponentially to zero, and concomitantly the wave-packet relaxes exponentially to the *Mott insulator ground state* $|x = 1\rangle$ with relaxation time τ of equation (3.16).

For quenches close to the dynamical transition, $U_f \sim U_f^d$, oscillations take place on a time scale that diverges as $-\tau \ln(|U_f^d - U_f|)$. This dynamical singularity, or dynamical transition, takes place on a line $U_f^d = (U_c + U_i^d)/2$ in the (U_i, U_f) plane.

To illustrate the physical consequences of the transition, in figure 3.4 (right panel) we show the *time average* of the superfluid order $\overline{|\Psi_0|^2(t)}$ as a function of U_f for quenches starting from $U_i = 0$. The superfluid order is vanishing with a logarithmic singularity $\overline{|\Psi_0|^2(t)} \sim -1/\ln(|U_f^d - U_f|)$ at the dynamical transition. In the Hubbard model, a similar phenomenon has been uncovered with t-DMFT [62], but in this case, the system thermalizes to an equilibrium state after the quench at the transition, with respect to the canonical ensemble of the same energy. Specifically, the authors compared averages in the final state to those at equilibrium at an effective temperature $T = 1/\beta$ such that the energy was the same:

$$\mathrm{Tr}\ (e^{-\beta \hat{H}} \hat{H})/Z(\beta) = \langle\, \hat{H}(t)\, \rangle_{\mathrm{quench}} \tag{3.18}$$

In our case, we compared the time average of the superfluid order after the quench $\overline{|\Psi_0|^2(t)}$ to its value in the canonical ensemble at the same energy [4] as in equation (3.18), as shown in figure 3.4 (right panel). Exactly at the dynamical transition point $U_f = U_f^d$, the superfluid order vanishes after the quench (full line). However, in the equilibrium system of the same energy, the superfluid order is nonzero (dashed line). As a consequence, the system is out of equilibrium after the quench and would thermalize, if it were to relax, to a state with finite superfluid order. Thus, the exponential relaxation of the superfluid order is a purely *dynamical effect*.

All the different regimes described above are summarized in the quench phase diagram of figure 3.4 (left panel). Notice that the dynamical transition occurs in the regime of superfluid to superfluid quenches, where no special features are expected. This is one of the reasons why this phenomenon has been overlooked, despite the many studies of quenches using Gutzwiller Ansatz [161, 162, 158, 163]. The other reason is that by just implementing the Gutzwiller equations, such singularities may be left unnoticed. The regimes of quenches from the Mott insulator to the superfluid phase, indicated by (M), is expected to be very different in finite dimensional lattices than in the mean-field approximation as discussed in section 3.4.1.

4. We considered the canonical ensemble within the Gutzwiller Ansatz.

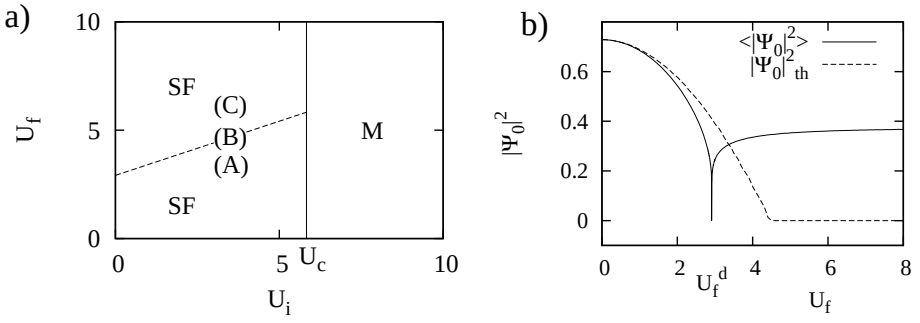

Figure 3.4: a) Dynamical phase diagram for the Bose-Hubbard model with $n_b^{\max} = 2$. In the M area, within mean field, the system remains stuck to the Mott insulator ground state after the quench. Quenches from the superfluid phase are oscillating and similar to (A) or (C). The dynamical transition (B) separating the two is displayed as a dashed line, it meets the Mott phase at $U_f = U_c$. b) Superfluid order $\langle|\Psi_0|^2\rangle$ as a function of U_f. Continuous line: time average after a quench. Dashed line: microcanonical average at the corresponding energy after the quench. The initial coupling is $U_i = 0$, but the evolution is qualitatively similar for all U_i with a dynamical transition.

3.5 Bose-Hubbard model with weaker truncation

3.5.1 Effective Hamiltonian

As previously mentioned, it is of interest to relax the truncation to allow for up to $n_b^{\max} > 2$ bosons per site and to consider the qualitative and quantitative differences with respect to the case $n_b^{\max} = 2$. Of course, the standard Bose-Hubbard model is expected to be recovered when $n_b^{\max}$ is sufficiently high compared to the average density, $n_b^{\max} \gg n$.

In the general case, any symmetric wave function can be parametrized by the fractions x_i of sites with i bosons per site, $i \in [0, n_b^{\max}]$. Since the x_i are fractions, they satisfy $\sum_i x_i = 1$. Moreover the density $n = \sum_i i x_i$ is fixed, thus there are only $n_b^{\max} - 1$ free variables left. The wave function is expanded in the symmetric basis like $|\psi\rangle = \sum_{\mathbf{x}} \psi_{\mathbf{x}}(t)|\mathbf{x}\rangle$ and the transition elements $D(\mathbf{x})$ and $W_{\mathbf{m}}(\mathbf{x})$ can be computed as done previously. For instance, there are 3 different types of transitions $\mathbf{m}$ when $n_b^{\max} = 3$ and 6 when $n_b^{\max} = 4$. Taking the classical equivalence for packet states, the resulting Hamiltonian can be put in the form (3.10):

$$H(\mathbf{x}, \mathbf{p}) = D(\mathbf{x}) - 2 \sum_{\mathbf{m}} W_{\mathbf{m}}(\mathbf{x}) \cos(\mathbf{m} \cdot \mathbf{p}) \tag{3.19}$$

Specifically, when $n_b^{\max} = 3$, if one chooses x_1 and x_2 as free variables, the Hamiltonian is

$$H(x_1, x_2, p_1, p_2) = D - 2W_1 \cos(p_1 + p_2) - 2W_2 \cos(2p_1 - p_2) - 2W_3 \cos(p_1 - 2p_2) \quad (3.20)$$

$$W_1 = J(3x_0x_1x_2x_3)^{1/2} \quad W_2 = Jx_1(2x_0x_2)^{1/2} \quad W_3 = Jx_2(6x_1x_3)^{1/2} \quad (3.21)$$

$$D = x_2 + 3x_3 - J(x_0x_1 + 2x_1x_2 + 3x_2x_3) \quad (3.22)$$

$$x_0 = 1 - x_1 - x_2 - x_3 \qquad x_3 = \frac{1}{3}(n - x_1 - 2x_2) \quad (3.23)$$

Notice that because $0 < x_i < 1$, there are constraints on the possible values of x_i, such as $x_2 < (n - x_1)/2$. For all $n_b^{\max}$, there is a Mott insulator to superfluid quantum phase transition at some coupling U_c if the density n is an integer. Notice that the critical coupling U_c for $n_b^{\max} > 2$ is exactly identical to its $n_b^{\max} = 2$ value. Above the critical coupling $U > U_c$ the ground state is a Mott insulator $x_n = 1, x_{i\neq n} = 0$ (all sites have n bosons), and below $U < U_c$ the ground state is superfluid with all $x_i \neq 0$.

3.5.2 Regularity of trajectories after a quench

In the previous case $n_b^{\max} = 2$, the effective dynamics was one-dimensional, and thus integrable. For $n_b^{\max} > 2$, the phase space is of dimension $2(n_b^{\max} - 1)$, and the trajectories may be either regular or chaotic. In order to characterize them, their regularity properties should be measured. For chaotic trajectories, neighboring trajectories separate exponentially in time in the phase space $y = \{x_i, p_i\}$, like $\delta y(t) \sim \exp(\lambda t)\delta y(0)$ with typical rate of separation λ called Lyapunov exponent [170]. The Lyapunov exponents [5] for several trajectories with different initial conditions $\{x_1^i, x_2^i, p_1 = p_2 = 0\}$ are plotted in figure 3.5 (left panel) in the superfluid phase $U = 2.86 < U_c$, with $n_b^{\max} = 3$ and density $n = 1$. The phase space is characteristic of mixed systems, where regular regions with $\lambda = 0$ (within the error bars) and fully chaotic regions $\lambda > 0$ coexist in an intricated way [6]. In regular trajectories, the fractions $x_i(t)$ are oscillating in a quasi-periodic way without definite period. The quench at the dynamical transition is at $E = 0$, and the corresponding trajectory is apparently chaotic.

For $U > U_c$, when the ground state is a Mott insulator, all trajectories are regular. We notice that the regularity of a trajectory affects the time of spreading of the packet (determined by the time of separation of two neighboring trajectories). Actually, the time of separation is typically a power law $t \sim V^\alpha$ for regular trajectories but only $t \sim \ln V$ for chaotic ones.

3.5.3 Dynamical transition

The most pressing question is the existence of a dynamical transition for $n_b^{\max} > 2$. Since separatrices are not easy to identify formally, our best indication is to look at the time averaged

5. Lyapunov exponents are determined using a simplified version of the usual Gram-Schmidt orthonormalization of the Lyapunov vectors.

6. This was expected since fully integrable or chaotic systems in $d > 1$ are "special" (of zero measure) among Hamiltonian systems, most of which are mixed in the previous sense.

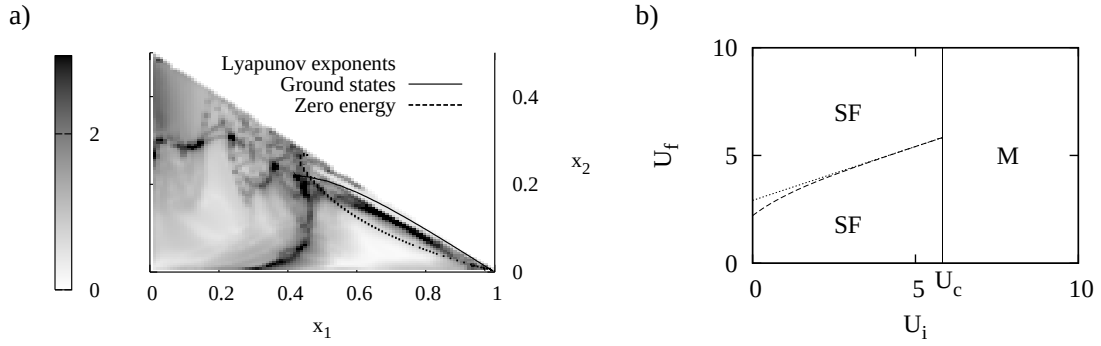

Figure 3.5: a) Lyapunov exponents of the trajectories with initial conditions $\{x_1, x_2, p_1 = p_2 = 0\}$, for $U = 2.86$ plotted in levels of gray. The bright zone is regular (numerically $\lambda \lesssim 0.05$), the dark zones are chaotic. The Lyapunov exponents corresponding to initial conditions given by ground states obtained varying U_i are indicated by a continuous line. The dashed line indicates initial conditions with zero energy. The dynamical transition corresponds to their intersection. b) Dynamical phase diagram for $n_b^{\max} = 4$. The dynamical transition is at the dashed line. The dotted line is the dynamical transition when $n_b^{\max} = 2$, for comparison.

superfluid order $|\Psi_0|^2$ as a function of U_f for a given U_i in figure 3.6 (right panel). It shows that the singularity occurs for $n_b^{\max} = \{2, 3, 4, 5\}$ and that the dependence in $n_b^{\max}$ of the divergence is very weak beyond $n_b^{\max} = 4$, since the two set of values for $n_b^{\max} = 4$ and $n_b^{\max} = 5$ are identical up to 0.01%. Some features of the case $n_b^{\max} = 2$ persist ; for example, at the dynamical transition, the momentum $2p_1 - p_2$ becomes unbounded, see figure 3.6 (left panel). As before, the dynamical transition still occurs at the special coupling U_f^d where the final energy equals the energy $E = 0$ of the unstable Mott trajectory $x_n = 1, x_{i\neq n} = 0$.

The quench phase diagram is shown in figure 3.5 (right panel) for $n_b^{\max} = 4$ and unit filling factor $\langle \hat{n} \rangle = 1$. We observe that the transition line is very similar to the transition line for $n_b^{\max} = 2$ except for low U_i, and that they are asymptotically equal around $U_i = U_c$. Since the probability of having more than 4 bosons on the same site is extremely small, of the order of 0.01% when $n_b^{\max} \gg 4$, we can safely assume that this phase diagram is quantitatively representative of the phase diagram *without truncation*.

Even though the existence of the dynamical transition for any $n_b^{\max}$ is beyond doubt, its origin in terms of the Hamiltonian system is hard to identify. Unlike in the one dimensional case, it is hard to establish numerically whether or not the trajectory goes arbitrarily close to the point $x_1 = 1$ (ground state of the Mott insulator) at the dynamical transition, a point where the trajectory is exponentially slowed down. If it was the case, the logarithmic divergence would follow. One could imagine that the trajectory at $E = 0$ is an unstable manifold (the equivalent of the separatrix in one dimension), which would support the existence of a singularity for a trajectory arbitrarily close to it. A possible scenario, in which the surface $E = 0$ is ergodic, does not seem to be validated by numerical integration of trajectories.

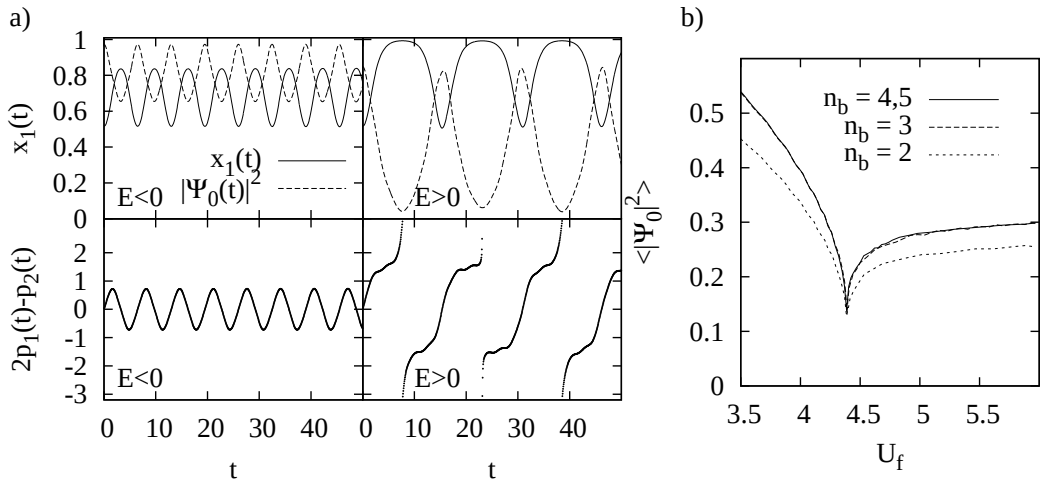

Figure 3.6: a) Evolution of $x(t)$ and $p(t)$ with time, $n_b^{\max} = 3$, $n = 1$ and $U_i = 1$. Left panel, $U_f = 2.5$, and right panel, $U_f = 3.29$, respectively below ($E < 0$) and above ($E > 0$) the dynamical transition at $U_f^d = 3.21$. b) Superfluid order parameter $\langle|\Psi_0|^2\rangle$ as a function of U_f for $n = 1$, $U_i = 3$, with $n_b^{\max} = 2, 3, 4$ and 5. The curve $n_b^{\max} = 2$ is shifted of 0.025 along the U_f axis for comparison.

To conclude, despite the difficulty to analyze analytically the dynamical transition when $n_b^{\max} > 2$, the evidence presented above is quite conclusive about its existence in the non truncated Bose-Hubbard model.

3.6 Discussion: the dynamical transition in mean-field models

The mean-field dynamics of several other models has been studied: the Hubbard model in [159], the generalized Jaynes-Cummings model and of the Ising model in a transverse field [166] and superlattice models [7] with similar conclusions. A dynamical transition has been found for quenches within the *broken symmetry* phase, with logarithmic singularity of averages around the dynamical transition point. Notice that these singular quenches always occur far from the critical coupling $U_f^d \neq U_c$.

It is worth emphasizing that the existence of a dynamical transition seems to be conditioned by the existence of the static quantum phase transition. To support this statement, one can study the completely connected Bose-Hubbard model away from integer densities, where there is no *equilibrium* quantum phase transition, then one finds that there is no dynamical transition either. This property is valid in all models we studied and also in the Hubbard model [159].

7. Private communication of F. Wolf and M. Rigol, based on [164].

For completeness, let us mention a formal argument [166] to understand why the singular trajectory, which is responsible for singularities around the dynamical transition, should be related to the existence of a quantum phase transition. Let us consider a quench from the unbroken symmetry phase to the broken symmetry phase in a completely connected model, where the dynamical evolution is expected to be exponentially slow, see equation (3.16). The reason is that the symmetry must break up and the order must develop in the whole system at once, and the typical time scale to depart from a tiny initial distance $\Delta x(t = 0) \ll 1$ from the symmetric phase (Mott insulator, etc.) is of the order of $\ln V$. The point is that this slow trajectory is precisely the *time reversal* of the singular trajectory that is responsible for the dynamical transition. Therefore, and this will conclude the argument, the existence of a quantum phase transition implies the existence of two slow trajectories [8], one corresponding to the quenches from the symmetric state to the symmetry breaking phase, and its time reversal, responsible for the dynamical transition.

3.7 Utility and restrictions of the mean-field approach

The general purpose of this work was twofold. First, we described a method to study the quantum quench dynamics of generic completely connected models, providing a mapping to effective classical dynamics. There are two reasons for considering completely connected models. In some cases, such as in the generalized Jaynes-Cummings model, and the Dicke model, they provide the correct physical description. In others, such as the transverse field Ising model or the Bose-Hubbard model, they lead to an approximative treatment of finite dimensional systems. In the latter case, the range of validity of the approximation is possibly limited to short times only.

Our analysis may prove useful to understand other unrelated problems. For example, it has been extended in [38] to study the slow annealing through a first order phase transition, showing how the excess energy scales when the annealing time is finite or exponentially large. These analytical results yield quantitative estimates of the limits of the quantum adiabatic procedure, which is a recently developed route to help solving constrained problems.

Our second aim was to study and to reveal the existence of out of equilibrium dynamical transitions induced by quantum quenches. In agreement with other studies [159, 171], we showed that within the mean-field approximation, the dynamical transitions occur in quenches from the broken symmetry phase to other regions of the broken symmetry phase, and that this is a quite general phenomenon for systems with a quantum phase transition at equilibrium. Notice that the dynamical transition is not restricted to sudden quenches, and is shown to occur with a ramp quench too [172]. Actually, the dynamics (3.10) directly extends to arbitrary quench protocols. Another interesting protocol is to use an oscillating parameter, a problem which is studied in the Ising model [96], yet the authors find no signature of a dynamical transition.

8. Rigorously, there is a full class of symmetry breaking trajectories depending on the initial conditions $\Delta \mathbf{x}(t = 0)$ if the classical Hamiltonian is not one dimensional.

Let us discuss briefly the range of applicability and limitations of the approach. Clearly, the mean-field approximation misses several essential physical effects. Relaxation and thermalization, for which spatial and temporal fluctuations must be taken into account, are not present.

From this point of view, it is a much cruder mean-field approximation than t-DMFT, which captures some dynamical fluctuations. Furthermore, the dynamics of a quench from the unbroken symmetry phase to the broken symmetry phase is not properly described for the reasons mentioned above. Inhomogeneities, topological defects or domain growth are out of reach. Notice that schemes to include the phonon coupling have been devised in the Hubbard model, to study the dynamical transition, ramp quenches [172] and intriguing surface effects [173].

On the contrary, our mean field approximation is expected to capture well the evolution of local quantities on short times, since it does not require any perturbative expansion in parameters (U, $J\ldots$) of the Hamiltonian. For example, in a U/J expansion around the non-interacting limit, neither the static superfluid to Mott insulator transition nor the out of equilibrium dynamical transition would be correctly described, despite the fact that some spatial fluctuations could be included in the formalism. As a consequence, one should use expansions that are "non-perturbative" to some degree. In section 4.6.4, we study a case where this can be achieved in a archetypal field theory.

Let us finally mention some possible extensions of the mean-field analysis. The truncated Wigner approximation allows to include first order corrections to the classical limit (3.10) and has been applied to the Dicke model in [160]. A more elaborate, exact description of the Dicke model using Glauber's Q-function or the Husumi function relates the relaxation dynamics to quantum diffusion [174]. This approach describes the impact of chaos in the underlying classical model on relaxation in the original quantum problem.

Chapter 4

Quenches in the ϕ^4 model

4.1 Perspectives on the dynamical transition

In the previous chapter, we described the dynamical transition at the mean-field level and found it to be ubiquitous in models with a static quantum phase transition. To motivate our next study, let us first give a short overview of the current knowledge of the dynamical transition.

The dynamical transition has first been observed in the Hubbard model within time dependent DMFT [62]. The authors find that during quenches from a non interacting state $U = 0$, the dynamics has a qualitatively different nature as a function of the final interaction U_f. For quenches below a threshold $U_f < U_f^d$, observables such as the double occupancy or the discontinuity of the Green's function at zero momentum relax to a steady nonequilibrium value on short times. For large values of the coupling $U_f > U_f^d$, these observables have an oscillatory behavior. These two regions are separated by a sharp crossover regime at $U_f \sim U_f^d$, where a fast thermalization to the canonical ensemble occurs within t-DMFT.

This study motivated the development of out of equilibrium Gutzwiller Ansatz approximation to identify the phenomenon within mean-field [159]. Within this approximation, the two different regimes separated by a dynamical transition are recovered. The dynamical transition is identified as a very sharp, logarithmic singularity in the dependency of time averaged observables as a function of the final quench value $\overline{\langle \hat{O} \rangle} = 1/|\ln\left(|U_f^d - U_f|\right)|$. The crucial role of half filling is also observed, any deviation from it turns the transition into a smooth crossover. As we have shown in the previous chapter, this observation is valid in general: a dynamical phase transition can only occur whenever an underlying equilibrium quantum phase transition is present in the system. Several other questions have also been addressed with this method, for example it has been shown that although most of studies focus on sudden quenches, the dynamical transition occurs for ramp quenches too.

A conformal field approach has been devised in [171] to relate the dynamics of a ϕ^4 theory to a classical critical film [171], but the results of this approach are also technically mean-field. Due to the absence of any relaxation process in the mean-field approaches, a very natural

question is to understand the impact of fluctuations on the dynamical transition.

To fulfill this goal, an approach supplementing mean-field with additional fluctuations has been developed, using a slave spin formalism [175]. It allows to explore the interplay between local evolution and correlation functions. In the first formulation of the problem, the dynamical transition was accompanied by an instability. The formalism has been made self-consistent in [172], allowing to show that the logarithmic divergences at the dynamical transition are indeed smoothed out by correlations. However, a clear separation of two regimes is still present.

There are many unresolved questions about the dynamical transition, which motivated our next study. For example, it is unclear whether the transition is a crossover or if has features of critical phenomenon. We also would like to have a more clear understanding of the two regimes below and above the transition. Moreover, there is a lot to understand about the dynamics of correlations: what is the meaning of the instability at low momentum, when and how fast does the system thermalizes, is there a diverging length if the system is "critical" in any sense... These considerations were the incentive to look for a formalism where this program could be pursued, even at the expense of the model not being directly applicable to an experimental system. We were naturally lead to study the ϕ^n model because of the intense research activity that it fosters. Besides, this model is almost directly relevant for the Bose-Hubbard model, since the particle-hole symmetric transition is of the relativistic O(2) symmetry class. Indeed, it is known that the large N approximations are predictive even at relatively small $N \gtrsim 4$.

4.2 Out of equilibrium ϕ^4

Before we proceed to the core of the subject, let us give a short summary of the long history of the methods which we are going to use. Indeed, the methods to explore the physics of many-body systems (isolated or open) out of equilibrium within quantum field theory have undergone a steady development these last decades. The Baym-Kadanoff or two-particle irreducible formalism is used is various domains of physics, such as heavy ions collisions, the formation of structures in the early universe [176], molecular electronics and plasma physics [177]. There are also numerous condensed-matter applications such transport in mesoscale and nanoscale structures [178], Bose-Einstein condensates of weakly interacting particles [176], pump-probe experiments in strongly correlated materials [41] and of course cold atoms.

The Baym-Kadanoff formalism [107] is the most widespread scheme, because of its ability to respect conservation laws such as energy conservation. In the high energy physics community, the Baym-Kadanoff equations has been extensively compared to other approximation schemes [108]. In particular, they pointed out that unlike many other approximations, at any finite order of perturbative expansion, physical quantities do not diverge with time. For example, a naive expansion of the self-energy in terms of the *bare* propagator (like in the one particle irreducible approximation) yields an expansion which is divergent at any order in perturbation theory.

Recently, numerous studies about ϕ^4 theories made significant progress on the nonequilibrium dynamics, in particular for isolated systems, which have already been alluded to in section 1.2.3 and 1.2.5. For example, the difference between the quantum Boltzmann equation and the second order expansion in $\lambda\phi^4$ has been explored in [179]. A very remarkable breakthrough was the observation of thermalization [66] in the ϕ^4 model in one dimension, which also demonstrated that the thermalization does not look like a simple exponential relaxation but instead involves several nontrivial stages on timescales which cover many orders of magnitude. Finally, nonequilibrium fixed points with scaling laws for correlations have been found at next-leading order [84, 85].

In the following, we describe the quantum phase transition from a symmetric to the broken symmetry phase and find the expected massless Goldstone modes associated with spontaneous symmetry breaking in section 4.3.

After that, we review the standard Keldysh technique and we show how it is generalized to finite temperature initial conditions. We also introduce the Baym-Kadanoff formalism and show how to express the conserved energy in full generality in section 4.4 and we derive the next-leading order equations in section 4.5.

We find that the dynamical transition is still present with fluctuations at leading order in N, and that it has the characteristic features of a *critical phenomenon* in section 4.6: the propagator has scaling properties and there is a diverging lengthscale. We also find that beside the normal light-cone effect, which we find for arbitrary quenches, there is a light cone effect with scaling at the transition. Finally, we compare the dynamical transition to a very different class of quenches, i. e. quenches from the symmetric phase to the broken symmetry phase, and we show that, surprisingly, they share the same dynamics.

4.3 Description and equilibrium properties of the model

4.3.1 Description of the model

We consider a relativistic theory of real vector fields $\hat{\phi}^n(\mathbf{x}, t)$, where the local rotational degrees of freedom is of dimension N, $\vec{\phi} \in \mathbb{R}^N$, and the fields are defined on a three dimensional space $\mathbf{x} \in \mathbb{R}^3$, or rather, since this model is relativistic, in Minkovskian geometry $x = (\mathbf{x}, t) \in \mathbb{M}$. We assume that the internal degree of freedom have rotational symmetry O(N), and that the action is non linear due to a quartic interaction term. The real-time action of such a model reads, with implicit summation over vector indices n

$$S[\phi] = \int \mathrm{d}^3x\, \mathrm{d}t \left(\frac{1}{2}\phi_x^n(\Box_x + m_0^2)\phi_x^n + \frac{\lambda}{4!N}(\phi_x^n\phi_x^n)^2 \right) = \int \mathrm{d}t\, \mathcal{L}[\phi](t) \tag{4.1}$$

where $\Box = \partial_\mu \partial^\mu = \partial_t^2 - \nabla^2$, and we use natural units $c = \hbar = 1$. The quantum operator fields $\hat{\phi}_x^n$ and its canonical conjugate $\partial_t \hat{\phi}_x^n$ obey the following commutation relations at equal times

$$[\partial_t \hat{\phi}_x^n, \hat{\phi}_{x'}^m] = \delta^d(\mathbf{x} - \mathbf{x}')\delta_{nm} \text{ if } t = t' \tag{4.2}$$

$$[\hat{\phi}_x^n, \hat{\phi}_{x'}^m] = 0 \text{ if } t = t \tag{4.3}$$

$$[\partial_t \hat{\phi}_x^n, \partial_{t'} \hat{\phi}_{x'}^m] = 0 \text{ if } t = t' \tag{4.4}$$

This model has a quantum phase transition at a critical mass $(m_0^c)^2 < 0$, between a phase with spontaneous symmetry breaking $\langle \hat{\phi} \rangle > 0$ for $(m_0)^2 < (m_0^c)^2$ and a paramagnetic phase $\langle \hat{\phi} \rangle = 0$ for $(m_0)^2 > (m_0^c)^2$.

In the following, we will make extensive use of expansions in the large N limit, which is a classical limit of a sort. We consider the equilibrium system in section 4.3.2 and the quench dynamics after a sudden change of the bare mass $(m_0^i)^2 \to (m_0^f)^2$ in section 4.6.

The quantities of interest [1] are the average field $\phi_{\mathbf{x}t}^n = \langle \hat{\phi}_{\mathbf{x},t}^n \rangle$, which we take to be along the axis $n = 1$, the connected Keldysh correlation functions $G^{nm}_{tt'\mathbf{x}\mathbf{x}'} = \langle \{\hat{\phi}_{\mathbf{x},t}^n, \hat{\phi}_{\mathbf{x}',t'}^m\} \rangle - \phi_{\mathbf{x}t}^n \phi_{\mathbf{x}'t'}^m$ and the retarded correlation functions $G^{\mathrm{R}\,nm}_{tt'\mathbf{x}\mathbf{x}'} = \theta(t-t')\langle [\hat{\phi}_{\mathbf{x},t}^n, \hat{\phi}_{\mathbf{x}',t'}^m] \rangle$. Because of the planar symmetries in the initial state, all quenched correlations are diagonal in field indices $G^{nm} = \delta_{nm} G^{nn}$ at all times. The relevant correlations are the longitudinal $G^{11} = G^{/\!/}$ mode and $N-1$ transverse modes $G^{ii} = G^{\perp}$, $i \neq 1$.

Notice that the action (4.1) may also be regarded as the continuum limit of a three dimensional lattice with N harmonic oscillators per site, with nearest neighbors quadratic coupling and an additional quartic local potential.

4.3.2 Finite temperature physics at leading order

Our first goal is to show the finite temperature equations at leading order in N and derive the phase diagram. All details of the derivation are in section 4.5 where the more general next-leading order case will be treated.

To compute finite temperature averages $\langle \hat{A} \rangle = \mathrm{Tr}\left(\hat{A} e^{-\beta \hat{H}}\right)$, one can use the Matsubara formalism [180] which boils down to replacing $e^{-\beta \hat{H}}$ by a unitary evolution in imaginary time $e^{-i\int_0^\beta \mathrm{d}t\, \hat{H}}$ with $t = -i\tau$. Correlation functions $G(\tau, 0, \mathbf{x}, 0)$ are functions of the imaginary time τ. Due to translation invariance and periodicity in τ, the Keldysh propagator may be Fourier

1. Our convention is to use Heisenberg operators $\hat{A}(t) = \hat{U}_{0\leftarrow t} \hat{A} \hat{U}_{t\leftarrow 0}$, and that all averages $\langle \hat{A}(t) \rangle = \langle \Psi | \hat{A}(t) | \Psi \rangle$ are with respect to the physical state $|\Psi\rangle$ at the time of the quench $t = 0$. The unitary evolution operator is $\hat{U}_{b\leftarrow a} = \hat{T} \exp\left(-i \int_a^b \mathrm{d}t\, \hat{H}(t)\right)$. The time ordered product $\hat{T}$ is defined with two bosonic operators $\hat{A}$, $\hat{B}$ as

$$\left\langle \hat{T} \hat{A}(\mathbf{x}, t) \hat{B}(\mathbf{x}', t') \right\rangle = \Theta(t - t') \left\langle \hat{A}(\mathbf{x}, t) \hat{B}(\mathbf{x}', t') \right\rangle + \Theta(t' - t) \left\langle \hat{B}(\mathbf{x}', t') \hat{A}(\mathbf{x}, t) \right\rangle \tag{4.5}$$

With n bosonic operators $\hat{A}_1(t_1), \ldots, \hat{A}_n(t_n)$, the time ordered product selects the ordering of operators for which the times t_n grows from the right to the left.

Figure 4.1: "Tadpole" self-energy diagram contributing to the leading-order equations.

transformed into $G(\omega, \mathbf{p}) = \int_0^\beta \mathrm{d}\tau \int \mathrm{d}^3\mathbf{x}\, e^{i\omega\tau} e^{i\mathbf{p}\cdot\mathbf{x}} G(\tau, 0, \mathbf{x}, 0)$ with Matsubara frequencies $\omega_n = \frac{2\pi n}{\beta}$. For convenience we use the shorthand $\int_{\omega,\mathbf{p}} = \int \frac{\mathrm{d}^3p}{(2\pi)^3} \frac{1}{\beta} \sum_\omega$. The presence of a nonzero field $\phi^n = \langle\, \hat{\phi}^n \,\rangle$ may be handled, changing variables to $\phi^n(\tau, \mathbf{x}) \to \phi^n + \delta\phi^n(\tau, \mathbf{x})$ in the path integral. Then, one can use standard perturbation theory to compute the self-energy as the sum over all one-particle irreducible diagrams. The leading contribution in the large N limit is the tadpole or "Hartree-Fock" diagram of figure 4.1.

The self-consistent equations on ϕ, $G^\perp(\omega, \mathbf{p})$ and $G^{/\!/}(\omega, \mathbf{p})$ are

$$\left(m_0^2 + \chi + \frac{\lambda}{6N} \int_{\omega,\mathbf{p}} G^{/\!/}(\omega, \mathbf{p})\right)\phi = 0 \tag{4.6}$$

$$\chi = \frac{\lambda}{6N}\left(\phi^2 + \frac{1}{2}\sum_n \int_{\omega,\mathbf{p}} G^{nn}(\omega, \mathbf{p})\right) \tag{4.7}$$

$$G^{/\!/}(\omega, \mathbf{p}) = \frac{1}{2}\frac{1}{\omega^2 + \mathbf{p}^2 + m_0^2 + \chi + \frac{\lambda}{3N}\phi^2} \tag{4.8}$$

$$G^\perp(\omega, \mathbf{p}) = \frac{1}{2}\frac{1}{\omega^2 + \mathbf{p}^2 + m_0^2 + \chi} \tag{4.9}$$

The equation (4.6) is equivalent to the minimization of an effective potential $V(\phi)$

$$\frac{\partial V(\phi)}{\partial \phi} = 0 \tag{4.10}$$

$$V(\phi) = \frac{1}{2}\phi^2\left(m_0^2 + \frac{\lambda}{12N}\sum_n \int_{\omega,\mathbf{p}} G^{nn}(\omega, \mathbf{p}) + \frac{\lambda}{6N}\int_{\omega,\mathbf{p}} G^{/\!/}(\omega, \mathbf{p})\right) + \frac{\lambda}{4!N}\phi^4 \tag{4.11}$$

which is satisfied if $\phi = 0$ or if

$$\phi^2 = -\frac{6N}{\lambda}m_0^2 - \frac{1}{2}\int_{\omega,\mathbf{p}} \left(3G^{/\!/}(\omega, \mathbf{p}) + (N-1)G^\perp(\omega, \mathbf{p})\right) \tag{4.12}$$

At zero temperature, the equal time correlations are obtained from $G(\tau \to 0^+, 0, \mathbf{x}, 0)$, with the inverse Fourier transform $G(\tau, 0, \mathbf{x}, 0) = \int_{\omega,\mathbf{p}} e^{-i\omega t} e^{-i\mathbf{p}\cdot\mathbf{x}} G(\omega, \mathbf{p})$, which yields

$$G^{/\!/}(\mathbf{p}) = \frac{1}{4\sqrt{\mathbf{p}^2 + m_0^2 + \chi + \frac{\lambda}{3N}\phi^2}} \qquad G^\perp(\mathbf{p}) = \frac{1}{4\sqrt{\mathbf{p}^2 + m_0^2 + \chi}} \tag{4.13}$$

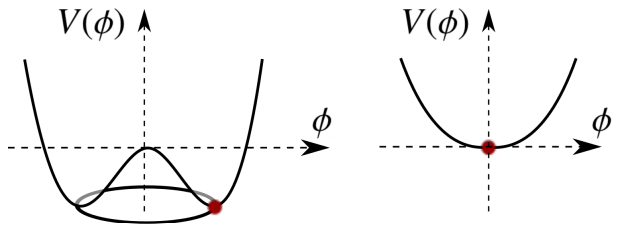

Figure 4.2: Effective potential $V(\phi)$ in the symmetry breaking phase (left panel) and in the symmetric phase (right panel). The red dot denotes the equilibrium value of ϕ, a minimum of $V(\phi)$.

The self-consistent values of ϕ, $G^{/\!/}(\mathbf{p})$ and $G^{\perp}(\mathbf{p})$ are easy to obtain numerically by iteration of equations (4.12) and (4.13). Let us now describe the zero temperature phase diagram, with the effective potential of figure 4.2:

- In the symmetric phase with $(m_0)^2 > (m_0^c)^2$, even though the mass $(m_0)^2$ may be negative, the global contribution of the quadratic ϕ^2 factor of (4.11) is positive and $\phi = 0$ is the only solution. The O(N) symmetry is preserved, $G^{\perp} = G^{/\!/}$ and the propagators (4.9) are those of a free theory with augmented effective mass $m_{\text{eff}}^2 = m_0^2 + \chi$. The fact that the symmetry is not broken despite a negative bare square mass $m_0^2 < 0$ is due to fluctuations, one can also refer to it as the shift of the bare critical point due to one loop corrections.
- In the phase with spontaneous symmetry breaking, $(m_0)^2 < (m_0^c)^2$, the average field ϕ is nonzero. The effective mass on the transverse directions is expected to be zero, because these are Goldstone modes. It is indeed zero at leading order because of equation (4.6): $\chi = -m_0^2$ plus a term $\frac{\lambda}{3N}\int_{\omega,\mathbf{p}} G^{/\!/}(\omega,\mathbf{p})$ of order $1/N$. We can neglect this subleading correction, which amounts to throw a term of subleading order in the self-energy [2], and obtain

$$G^{/\!/}(\mathbf{p}) = \frac{1}{4\sqrt{\mathbf{p}^2 + \frac{\lambda}{3N}\phi^2}} \qquad G^{\perp}(\mathbf{p}) = \frac{1}{4|\mathbf{p}|} \tag{4.14}$$

After this basic presentation of the model, we turn to techniques needed to handle field theory out of equilibrium.

2. Presumably, this feature would be absent, or rejected to the next order in N if the self-energy was expanded at the next order.

4.4 Out of equilibrium formalism: Keldysh and 2-PI formalism

4.4.1 Short introduction to Keldysh techniques

In this section, we give a brief introduction to the Keldysh formalism, a method to generalize perturbative field theory to out of equilibrium problems [181, 180, 178]. The path integral formalism with action (4.1) is, by definition, designed to compute transition elements of the unitary evolution operator

$$\left\langle \phi_f(\mathbf{x}) \left| \hat{U}_{t'\leftarrow t} \right| \phi_i(\mathbf{x}) \right\rangle = \left\langle \phi_f(\mathbf{x}) \left| \hat{T} \exp\left\{ -i \int_t^{t'} \mathrm{d}t'' \, \hat{H}(t'') \right\} \right| \phi_i(\mathbf{x}) \right\rangle \tag{4.15}$$

$$= \int_{\phi(\mathbf{x},t)=\phi_i(\mathbf{x})}^{\phi(\mathbf{x},t')=\phi_f(\mathbf{x})} \mathcal{D}\phi(\mathbf{x},t)\, e^{iS[\phi(\mathbf{x},t)]} \tag{4.16}$$

Starting from an initial density matrix $\hat{\rho}_0$, any out of equilibrium quantity of interest is of the form

$$\left\langle \hat{A}(t)\hat{B}(t')\dots \right\rangle = \mathrm{Tr}\left(\hat{\rho}_0 \hat{U}_{0\leftarrow t} \hat{A} \hat{U}_{t\leftarrow 0} \hat{U}_{0\leftarrow t'} \hat{B} \hat{U}_{t\leftarrow 0'} \dots \right) \tag{4.17}$$

$$= \mathrm{Tr}\left(\hat{\rho}_0 \hat{U}_{0\leftarrow t} \hat{A} \hat{U}_{t\leftarrow t'} \hat{B} \hat{U}_{t'\leftarrow 0} \dots \right) \tag{4.18}$$

We assume that there are only two operators $\hat{A}$ and $\hat{B}$ for simplicity and that they are diagonal in the $|\phi\rangle$ basis. Inserting the identity $\hat{\mathbb{I}} = \int \mathcal{D}\phi(\mathbf{x}) \; |\phi(\mathbf{x})\rangle\langle\phi(\mathbf{x})|$ and expressing all amplitudes using (4.16), for $t > t'$

$$Z = \int_{\mathrm{c}} \mathcal{D}\phi_t^+ \, \mathcal{D}\phi_t^- \; \langle \phi_0^- | \hat{\rho}_0 | \phi_0^+ \rangle \, e^{iS[\phi^+]-iS[\phi^-]} \tag{4.19}$$

$$\left\langle \hat{A}(t)\hat{B}(t') \right\rangle = \int_{\mathrm{c}} \mathcal{D}\phi_t^+ \, \mathcal{D}\phi_t^- \; \langle \phi_0^- | \hat{\rho}_0 | \phi_0^+ \rangle \, A(\phi_t^+) \, B(\phi_{t'}^+) \, e^{iS[\phi^+]-iS[\phi^-]} \tag{4.20}$$

$$S[\phi^+] = \int_0^t \mathrm{d}t \, \mathcal{L}[\phi^+](t) \qquad S[\phi^-] = \int_0^t \mathrm{d}t \, \mathcal{L}[\phi^-](t) \tag{4.21}$$

where we have called ϕ^+ fields from the operator $U_{t\leftarrow 0}$ and ϕ^- fields from $U_{0\leftarrow t}$. These field are defined on times in $t' \in [0, t]$ and back in $t' \in [t, 0]$, which defines the Keldysh contour. Due to the trace, there is periodicity $\phi^+(t = 0) = \phi^-(t = 0)$ indicated by the notation c. Since $Z = \langle 1 \rangle$ according to (4.20), then $Z = 1$.

The propagators on the contour $G^{jj'}(x, x')$ have Keldysh indices $\{j, j'\} = \pm$ (using the shorthand $x = (\mathbf{x}, t)$) and are defined as

$$G^{jj'}(x, x') = \int \mathcal{D}\phi_t^+ \, \mathcal{D}\phi_t^- \; \langle \phi_0^- | \hat{\rho}_0 | \phi_0^+ \rangle \, \phi^j(x) \, \phi^{j'}(x') \, e^{iS[\phi^+]-iS[\phi^-]} \tag{4.22}$$

Since the path integral yields time-ordered averages along the contour, the contour propagators are related to the original propagators as

$$G^{++}(x,x') = \left\langle T\hat{\phi}(x)\hat{\phi}(x')\right\rangle \qquad G^{--}(x,x') = \left\langle \check{T}\hat{\phi}(x)\hat{\phi}(x')\right\rangle \tag{4.23}$$

$$G^{+-}(x,x') = \left\langle \hat{\phi}(x')\hat{\phi}(x)\right\rangle = G^{<}(x,x') \qquad G^{-+}(x,x') = \left\langle \hat{\phi}(x)\hat{\phi}(x')\right\rangle = G^{>}(x,x') \tag{4.24}$$

The contour propagators are redundant and obey

$$G^{++}(x,x') + G^{--}(x,x') = G^{+-}(x,x') + G^{-+}(x,x') \tag{4.25}$$

$$G^{++}(x,x') - G^{--}(x,x') = \mathrm{sgn}(t-t')\left(G^{-+}(x,x') - G^{+-}(x,x')\right) \tag{4.26}$$

To emphasize the causal structure, get rid of this redundancy and make connexion with the usual propagators, it is customary to do a Keldysh rotation in the indices, which amounts to define new fields of a time $t' \in [0,t]$

$$\phi^{\mathrm{cl}} = \frac{1}{\sqrt{2}}\left(\phi^{+} + \phi^{-}\right) \qquad \phi^{\mathrm{q}} = \frac{1}{\sqrt{2}}\left(\phi^{+} - \phi^{-}\right) \tag{4.27}$$

and express propagators along the Keldysh contour $G^{jj'}(x,x')$ in terms of all $G^{\alpha\beta}(x,x')$ in the "classical-quantum" basis (see the review [106] for an explanation of this terminology).

$$\begin{pmatrix} G^{\mathrm{cl\,cl}}(x,x') & G^{\mathrm{cl\,q}}(x,x') \\ G^{\mathrm{q\,cl}}(x,x') & G^{\mathrm{q\,q}}(x,x') \end{pmatrix} = \begin{pmatrix} G^{K}(x,x') & G^{R}(x,x') \\ G^{A}(x,x') & 0 \end{pmatrix} \tag{4.28}$$

$$G^{K}(x,x') = G^{>}(x,x') + G^{<}(x,x') \tag{4.29}$$

$$G^{R}(x,x') = \theta(t-t')(G^{>}(x,x') - G^{<}(x,x')) \tag{4.30}$$

$$G^{A}(x,x') = \theta(t'-t)(G^{<}(x,x') - G^{>}(x,x')) \tag{4.31}$$

By definition $G^{K}(x,x') = G^{K}(x',x)$ and $G^{R}(x,x') = G^{A}(x',x)$. For real fields (i.e. $\hat{\phi}_x^{\dagger} = \hat{\phi}_x$) the propagators have the additional symmetry $G^{>}(x,x')^{*} = G^{<}(x,x')$, thus $G^{K}(x,x')^{*} = G^{K}(x,x')$ and $G^{R/A}(x,x')^{*} = -G^{R/A}(x,x')$. The action may then be expressed in terms of the new fields as

$$iS[\phi^{+}] - iS[\phi^{-}] = i\int \mathrm{d}^3x \int_0^t \mathrm{d}t \left(\frac{1}{2}\vec{\phi}_x^{\mathrm{cl}}(\Box_x + m_0^2)\vec{\phi}_x^{\mathrm{q}} + \frac{1}{2}\vec{\phi}_x^{\mathrm{q}}(\Box_x + m_0^2)\vec{\phi}_x^{\mathrm{cl}}\right. \tag{4.32}$$

$$\left. + \frac{2\lambda}{4!N}(\vec{\phi}_x^{\mathrm{cl}}\cdot\vec{\phi}_x^{\mathrm{cl}} + \vec{\phi}_x^{\mathrm{q}}\cdot\vec{\phi}_x^{\mathrm{q}})(\vec{\phi}_x^{\mathrm{cl}}\cdot\vec{\phi}_x^{\mathrm{q}})\right) \tag{4.33}$$

The free propagator of the action is off-diagonal in the R/A/K basis

$$G_0^{-1}(x,x') = \begin{pmatrix} 0 & i(\Box_x + m_0^2)\delta(x-x') \\ i(\Box_x + m_0^2)\delta(x-x') & 0 \end{pmatrix} \tag{4.34}$$

Including interactions within a perturbative expansion yields a dressed propagator $G(x,x')$. The inverse of G is defined as $GG^{-1}|x,x'' = \int \mathrm{d}x'\, G(x,x')\cdot G^{-1}(x',x'') = \delta(x-x'')$ where the

dot means matrix product in R/A/K basis. It is expressed in terms of the inverse of the R/A/K propagators as

$$G^{-1}(x,x') = \begin{pmatrix} 0 & (G^A)^{-1}(x,x') \\ (G^R)^{-1}(x,x') & (G^K)^{-1}(x,x') \end{pmatrix} \tag{4.35}$$

The perturbative expansion is conventionally written under the form of a Dyson expansion using the self-energy $\Sigma(x,x')$ which is the sum over all one-particle irreducible diagrams, and has the following causal structure

$$\Sigma(x,x') = \begin{pmatrix} 0 & \Sigma^A(x,x') \\ \Sigma^R(x,x') & \Sigma^K(x,x') \end{pmatrix} \tag{4.36}$$

The Dyson series can formally be resummed to yield the Schwinger-Dyson equation

$$G_{xy} = G_{0xy} + G_0 \Sigma G|_{xy} \tag{4.37}$$

$$G_0{}^{-1} G|_{xy} = \delta_{xy} + \Sigma G|_{xy} \tag{4.38}$$

which in turns yields the Kadanoff-Baym equations, after explicit computation in the R/A/K basis

$$i(\Box_x + m_0^2) G^A_{xy} = \delta_{xy} + \int_z \Sigma^A_{xz} G^A_{zy} \tag{4.39}$$

$$i(\Box_x + m_0^2) G^R_{xy} = \delta_{xy} + \int_z \Sigma^R_{xz} G^R_{zy} \tag{4.40}$$

$$i(\Box_x + m_0^2) G^K_{xy} = \int_z \Sigma^R_{xz} G^K_{zy} + \int_z \Sigma^K_{xz} G^A_{zy} \tag{4.41}$$

This is the usual starting point to evaluate the self-energy directly from the free propagator (4.34) in a perturbative expansion in λ with vertices inherited from (4.32). However, the initial conditions are still hidden in the boundary conditions $\langle\, \phi_0^- \,|\, \hat{\rho}_0 \,|\, \phi_0^+ \,\rangle$ for which we have no recipe. A common practice is to start from Gaussian initial conditions and to focus on properties that are robust with respect to the initial state [108]. To improve on this, the most natural route to follow is to try to include any thermal initial conditions.

4.4.2 Contour path integral with thermal initial conditions

We turn now to the formal way of including thermal initial conditions in the Keldysh formalism. This endeavor is by no means original and although it is difficult to track back the first attempt along these lines, it was already in the air in 1988 [179]. In the following, we choose to postpone any Keldysh rotation and matrix notation as far as possible and stick to generic contour integral integration. This procedure is very effective and allows to deal with the Baym-Kadanoff formalism with light notations.

To include thermal conditions, we replace the density matrix $\hat{\rho}_0 = e^{-\beta\hat{H}}/Z(\beta)$ by a path integral on an imaginary portion of the time contour

$$\langle \phi_0^- | \hat{\rho}_0 | \phi_0^+ \rangle = Z(\beta)^{-1} \left\langle \phi_0^- \left| T \exp\left\{ -i \int_0^{-i\beta} \mathrm{d}t'' \, \hat{H}(t'') \right\} \right| \phi_0^+ \right\rangle \tag{4.42}$$

$$= Z(\beta)^{-1} \int_{\phi^0(t=0)=\phi^+(t=0)}^{\phi^0(t=-i\beta)=\phi^-(t=0)} \mathcal{D}\phi^0(\mathbf{x}, t)\, e^{iS[\phi(\mathbf{x},t)]} \tag{4.43}$$

These fields belong to a new branch that we call 0, which complements the branches $+, -$ defined for the time evolution.

The resulting closed time path (CPT) has three branches, one from $t = 0$ to $t = -i\beta$ (branch 0), then to $t = -i\beta + \infty$ (branch 1) and finally back to $t = -i\beta$ (branch 2) with periodic boundary conditions. For convenience, we call the fields on the different branches $\phi^{\{0,1,2\}}$. Imposing periodic boundary $\phi^0(t = 0) = \phi^2(t = -i\beta)$, the path integral defined on this contour yields the dynamics of a system with thermal initial conditions. A perturbative expansion involves integrals over the contour c, which we write using a factor $f^{0,1,2} = \{-i, 1, -1\}$ to parameterize the contour time with a *real* variable t on the three branches

$$\int_{\mathrm{c}} \mathrm{d}t = \int_0^{\beta} (-i\mathrm{d}t) + \int_0^{\infty} \mathrm{d}t + \int_0^{\infty} (-\mathrm{d}t) \tag{4.44}$$

$$= \int f^t \mathrm{d}t \tag{4.45}$$

The partition function (4.19) reads

$$Z = Z(\beta)^{-1} \int_{\mathrm{c}} \mathcal{D}\phi^{\{0,1,2\}} \; e^{i\int_{\mathrm{c}} S[\phi]} = 1 \tag{4.46}$$

The inverse of propagators are defined, calling the complete integral $\int \mathrm{d}x \overset{\text{def}}{=} \int \mathrm{d}^3\mathbf{x} \int \mathrm{d}t$ (without the f^x factor, that we include explicitly below)

$$\int f^y G_{xy} G^{-1}_{yz} \mathrm{d}y = \int f^y G^{-1}_{xy} G_{yz} \mathrm{d}y = \delta^{\mathrm{c}}_{xz} = \frac{1}{f^z}\delta(x - z) \tag{4.47}$$

$$\int f^y G_{xy} \delta^{\mathrm{c}}_{yz} \mathrm{d}y = G_{xz} \tag{4.48}$$

The delta function δ^{c} is defined such that the second equality is fulfilled. In the following, we avoid the use of δ^{c} and prefer the explicit f^x factors. Using a dot to refer to the full integral $G \cdot H|_{xy} = \int \mathrm{d}z \, f^z G_{xz} H_{zy}$, the Schwinger-Dyson equation reads once again

$$G_{xy} = G_{0xy} + G_0 \cdot \Sigma \cdot G|_{xy} \tag{4.49}$$

$$G^{-1}_{0xz} \cdot G_{zy} = \frac{\delta_{xy}}{f^y} + \Sigma \cdot G|_{xy} \tag{4.50}$$

For definiteness, let us write the free propagator corresponding to the contour action of the partition function (4.46)

$$G_{0\,xy}^{-1\,nn} = \frac{-i}{(f^x)^2}\frac{\delta^2 S[\phi]}{\delta\phi_x\delta\phi_y} \tag{4.51}$$

$$= \frac{i}{f^x}\delta_{x-y}\left(\left(\Box_x + m^2 + \frac{\lambda}{6N}\phi_x^2\right) + \frac{\lambda}{3N}\phi_x^2\delta_{n1}\right) \tag{4.52}$$

4.4.3 Baym-Kadanoff expansion

An efficient rationale to derive approximations for the self-energy, which ensures energy conservation, is the two particle irreducible (2-PI) or Baym-Kadanoff formalism. It is based on the effective action $\Gamma[\phi, G]$, a functional of the field and correlations, which is related to the generating functional $Z[J, K]$ as follows

$$Z[J,K] = \int D\phi\; e^{i\left(S[\phi_x] + \int_c \phi_x J_x + \frac{1}{2}\int_c \phi_x K_{xy}\phi_y\right)} \tag{4.53}$$

$$W[J,K] = -i\ln Z[J,K] \tag{4.54}$$

$$G_{xy}^{ab} = \langle\, T_c\, \phi_x^a\phi_y^b \,\rangle - \langle\, \phi_x^a \,\rangle\langle\, \phi_y^b \,\rangle \tag{4.55}$$

$$\Gamma[\phi,G] = W[J,K] - \int_c \phi J - \frac{1}{2}\int\int_c (\phi K\phi + GK) \tag{4.56}$$

The 2-PI effective action can be expressed [182] in terms of the bare and dressed propagator G_0 and G and the field ϕ as

$$\Gamma[\phi,G] = S[\phi] + \frac{i}{2}\mathrm{Tr}\;\ln G^{-1} + \frac{i}{2}\mathrm{Tr}\; G_0^{-1}\cdot G + \Gamma^{(2)}[\phi,G] \tag{4.57}$$

Where G_0 is defined as in (4.51) and the trace and the logarithm are defined as series expansions with a product replaced by the $\cdot$ operation. In (4.57), $\Gamma^{(2)}[\phi, G]$ is the sum of 2-PI vacuum diagrams (times a factor $-i$), computed with the dressed propagators G, with vertices extracted from the translated action $S[\phi + \Phi]$, where the vertices are terms of order three or more in the fluctuating field Φ.

The physical fields ϕ and propagators G are extrema of the effective action,

$$\frac{\delta\Gamma}{\delta\phi_x} = 0 \qquad \text{and} \qquad \frac{\delta\Gamma}{\delta G_{xy}} = 0 \tag{4.58}$$

The equations of evolution for the fields ϕ read

$$\frac{\delta S}{\delta\phi_x} + \frac{i}{2}\frac{\delta G_0^{-1}}{\delta\phi_x}G_{xx} + \frac{\delta\Gamma^{(2)}}{\delta\phi_x} = 0 \tag{4.59}$$

This equation is valid on the three parts of the contour $\{0, 1, 2\}$. The extremum principle on propagators yields once again the Dyson equation, with the explicit expression for the self-energy

$$f^x f^y \left(-\frac{i}{2} G^{-1}_{xy} + \frac{i}{2} G^{-1}_{0\,xy} \right) + \frac{\delta \Gamma^{(2)}}{\delta G_{xy}} = 0 \tag{4.60}$$

$$G^{-1}_{xy} = G^{-1}_{0\,xy} - \Sigma_{xy} \tag{4.61}$$

$$\Sigma_{xy} = \frac{2i}{f^x f^y} \frac{\delta \Gamma^{(2)}}{\delta G_{xy}} \tag{4.62}$$

Unlike the previous Dyson equation (4.50), (4.61) provides a systematic procedure to express the self-energy Σ: it is obtained from the sum of all two-particle irreducible diagrams with one line cut, built from the *dressed* propagator, since $\Gamma^{(2)}$ is a functional of G only in (4.57). Moreover, in any approximation scheme based on a truncation of $\Gamma^{(2)}$, *energy is conserved* as time evolves, a we prove in the next section.

In section 4.4.1, because we ignored initial conditions, the R/A/K basis was the most natural set of Green function to keep track of. To include thermal initial conditions, the Green function matrix clearly has three indices $G^{\{0,1,2\}}$. The Keldysh rotation may be still performed on indices $\{0, 1\} \to \{\mathrm{cl}, \mathrm{q}\}$ to get rid of the redundancy (4.25). Beside, G^{00} are well-known Matsubara propagators which are routinely evaluated. However, solving the differential equations of evolution for the physical Keldysh, advanced or retarded functions G^K requires to evaluate mixed correlations such as $G^{0\mathrm{cl}}$ and $G^{0\mathrm{q}}$. A convenient scheme to compute these, which takes the appropriate symmetries into account to minimize computational effort, has very recently been devised in the atoms and molecules community [183].

4.4.4 Energy conservation

As emphasized above, the energy (or any other conserved quantities preserved by the Hamiltonian) is conserved within the Baym-Kadanoff scheme. Yet we still need to give its explicit expression. In a relativistic theory, the energy is not a Lorentz invariant quantity. The natural, Lorentz-invariant structure is the energy momentum tensor $\theta^{\mu\nu}(x)$, which is the Noether current associated with space-time translations, and has zero divergence $\partial_\mu \theta^{\mu\nu}(x) = 0$. In a given reference frame, this implies for $\nu = 0$ that $\partial_t \theta^{00}(x,t) - \partial_{x_i} \theta^{i\,0}(x,t) = 0$. Integrating over the space variables, we find that the total energy $E(t) = \int \mathrm{d}^3x\, \theta^{00}(x,t)$ is conserved (assuming, as always, that boundary contributions vanish). The general expression of the momentum-

tensor in a field theory [184] is

$$\theta^{\mu\nu}(x) = -\frac{1}{4}\left(-\frac{\partial}{\partial x_\nu}+\frac{\partial}{\partial y_\nu}\right)\left(-\frac{\partial}{\partial x_\mu}+\frac{\partial}{\partial y_\mu}\right)\Big(\phi_x\phi_y+G_{xy}\Big)\Big|_{y=x} \tag{4.63}$$

$$+\, g^{\mu\nu}\Big(E_{\rm int}(x)+E_{\rm pot}(x)\Big) \tag{4.64}$$

$$E_{\rm int}(x) = -\frac{1}{f^x}\frac{\partial\Gamma^{(2)}}{\partial\lambda(x)}\lambda(x)\Big|_{\lambda(x)=\lambda} \tag{4.65}$$

$$E_{\rm pot}(x) = -\frac{i}{2}J(x)\phi(x) - \frac{i}{4}\int \mathrm{d}z\, f^z\left(\Sigma_{xz}G_{zx}+G_{xz}\Sigma_{zx}\right) \tag{4.66}$$

In the above expression, we define the kernel $J_x = \frac{i}{f^x}\frac{\delta\Gamma}{\delta\phi_x}$ and the self-energy Σ is defined in (4.62). With this notation, (4.59) reads

$$\partial_t^2\phi = -(m^2+p^2)\phi - iJ_x \tag{4.67}$$

In the following, we prove that $\theta^{\mu\nu}$ satisfies $\frac{\partial}{\partial x^\mu}\theta^{\mu\nu}(x)=0$. We first observe that the derivative $\frac{\partial}{\partial x_\nu}E_{\rm int}(x)$ can be put in a simple form, because only ϕ_x and G_{xz} are x-dependent

$$\frac{\partial}{\partial x_\nu}E_{\rm int}(x) = -\frac{1}{f^x}\left(\frac{\delta\Gamma^{(2)}}{\delta\phi_x}\frac{\partial}{\partial x_\nu}\phi_x + \int \mathrm{d}z\left(\frac{\delta\Gamma^{(2)}}{\delta G_{zx}}\frac{\partial}{\partial x_\nu}G_{xz}+\frac{\delta\Gamma^{(2)}}{\delta G_{xz}}\frac{\partial}{\partial x_\nu}G_{zx}\right)\right) \tag{4.68}$$

$$= iJ(x)\frac{\partial}{\partial x_\nu}\phi(x) + \frac{i}{2}\int \mathrm{d}z\, f^z\left(\frac{\partial}{\partial x_\nu}G_{xz}\Sigma_{zx}+\Sigma_{xz}\frac{\partial}{\partial x_\nu}G_{zx}\right) \tag{4.69}$$

This identity can also be derived as a Ward identity, from the invariance of the action under small translations $x_\nu \to x_\nu+\xi_\nu$. Now, let us prove that $\frac{\partial}{\partial x^\mu}\theta^{\mu\nu}(x)=0$, taking the derivative of the first term only

$$-\frac{1}{4}\frac{\partial}{\partial x^\mu}\left(\left(-\frac{\partial}{\partial x_\nu}+\frac{\partial}{\partial y_\nu}\right)\left(-\frac{\partial}{\partial x_\mu}+\frac{\partial}{\partial y_\mu}\right)\Big(\phi_x\phi_y+G_{xy}\Big)\Big|_{y=x}\right) \tag{4.70}$$

$$= -\frac{1}{4}\left(-\frac{\partial}{\partial x_\nu}+\frac{\partial}{\partial y_\nu}\right)\left(\frac{\partial}{\partial x^\mu}+\frac{\partial}{\partial y^\mu}\right)\left(-\frac{\partial}{\partial x_\mu}+\frac{\partial}{\partial y_\mu}\right)\Big(\phi_x\phi_y+G_{xy}\Big)\Big|_{y=x} \tag{4.71}$$

Then, using the equation of motion of ϕ and G, one can see that the terms in $\delta(x-y)$ all vanish, and that

$$= -\frac{1}{4}\left(-\frac{\partial}{\partial x_\nu}+\frac{\partial}{\partial y_\nu}\right)\Big(i\Big(J_x\phi_y-J_y\phi_x\Big)+i\int \mathrm{d}z\, f^z\Big(G_{xz}\Sigma_{zy}-\Sigma_{xz}G_{zy}\Big)\Big)\Big|_{y=x} \tag{4.72}$$

$$= -iJ(x)\frac{\partial}{\partial x_\nu}\phi(x) - \frac{i}{2}\int \mathrm{d}z\, f^z\left(\frac{\partial}{\partial x_\nu}G_{xz}\Sigma_{zx}+\Sigma_{xz}\frac{\partial}{\partial x_\nu}G_{zx}\right) - \frac{\partial}{\partial x_\nu}E_{\rm pot}(x) \tag{4.73}$$

$$= g^{\mu\nu}\frac{\partial}{\partial x^\mu}\Big(-E_{\rm int}(x)-E_{\rm pot}(x)\Big) \tag{4.74}$$

Which proves that $\frac{\partial}{\partial x^\mu}\theta^{\mu\nu}(x)=0$. Within the ϕ^4 theory or whenever there is only one vertex with 4 legs, the two energies are related by $E_{\rm pot}(x) = -2E_{\rm int}(x)$.

4.5 Next leading order equations

We focus now on deriving the next leading order equations of motion in the O(N) model within the formalism developed above. It is convenient to introduce an auxiliary field description to account for the broken symmetry field. To do so, we perform a Hubbard-Stratonovich transform to eliminate the quartic term of (4.46), with an auxiliary field χ, to get an action on the closed contour

$$Z = Z(\beta)^{-1} \int D\phi^{\{0,1,2\}} \quad \exp\left\{ i \int_0^{\infty,\beta} \mathrm{d}t\, f^t \int_x -\left(\frac{1}{2}\phi_x^a(\Box + m^2)\phi_x^a - \frac{3N}{2\lambda}(\chi^a)^2 + \frac{1}{2}\chi^a\phi^a\phi^a \right) \right\} \tag{4.75}$$

We use the following notations for correlations of the auxiliary field $K_{xy}^{ab} = \langle\, T_c \chi_x^a \phi_y^b \,\rangle_c$ and $\bar{K}_{xy}^{ab} = \langle\, T_c \phi_x^a \chi_y^b \,\rangle_c$ and $D_{xy}^{ab} = \langle\, T_c \chi_x^a \chi_y^b \,\rangle_c$. The free propagators are

$$G_0^{-1}{}_{xy}^{ab} = \frac{i}{f^x}\delta^{ab}(\Box_x + m^2 + \chi^a)\delta(x-y) \tag{4.76}$$

$$K_0^{-1}{}_{xy}^{ab} = \frac{i}{f^x}\delta^{ab}\phi^a\delta(x-y) \tag{4.77}$$

$$D_0^{-1}{}_{xy}^{ab} = -\frac{i}{f^x}\delta^{ab}\frac{3N}{\lambda}\delta(x-y) \tag{4.78}$$

In the following it will be temporarily convenient to introduce a matrix notation in $\{\phi, \chi\}$, to define the self-energies $\Sigma, \bar{\Xi}, \Xi, D$. Each propagator carries the following dependencies: two space-time indices (x, y), two contour indices (a, b), the fields involved ($\chi\chi$, $\phi\chi$ or $\phi\phi$) and the O(N) index, yet only the field ϕ carries a field index.

$$\mathbf{G} = \begin{pmatrix} G & \bar{K} \\ K & D \end{pmatrix} \qquad \mathbf{\Sigma} = 2i\frac{\delta\Gamma^(2)}{\delta\mathbf{G}} = \begin{pmatrix} \Sigma & \bar{\Xi} \\ \Xi & \Pi \end{pmatrix} \tag{4.79}$$

The equations of evolution of the fields ϕ are given by the stationarity condition $\frac{\delta\Gamma}{\delta\phi} = 0$, and $\frac{\delta\Gamma}{\delta\chi} = 0$, and read

$$-(\Box_x + m^2 + \chi_x^a)\phi_x^a = (K_{xx}^a + \bar{K}_{xx}^a)/2 = K_{xx}^a \tag{4.80}$$

$$\chi_x^a = \frac{\lambda}{6N}\left(\phi_x^a\phi_x^a + G_{xx}^{aa}\right) \tag{4.81}$$

The evolution of propagators is governed by the matricial Schwinger-Dyson equation $\mathbf{G}_{xy}^{-1} = \mathbf{G}_0^{-1}{}_{xy} - \mathbf{\Sigma}_{xy}$. The upper right and lower left matrix elements are redundant equations on Ξ and

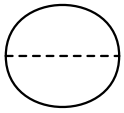

Figure 4.3: The only NLO diagram for $\Gamma^{(2)}$. Full lines are G propagators, the dashed line is the D propagator.

$\bar{\Xi}$, because $\Xi_{xy} = \bar{\Xi}_{yx}$. The three remaining equation are

$$i(\Box_x + m^2 + \chi_x^a)G_{xy}^{ab} = -iK_{xy}\phi_x^a + \frac{\delta^{ab}}{f^x}\delta_{xy} + \int_z f^z \mathrm{d}^{d+1}z\, \Sigma_{xz}^{ac} G_{zy}^{cb} \tag{4.82}$$

$$iK_{xy}^a = \frac{\lambda}{3N}\left(i\phi_x^a G_{xy}^{aa} - \int_z \mathrm{d}^{d+1}z\, f^z \Pi_{xz}^{ac} K_{zy}^{cb}\right) \tag{4.83}$$

$$iD_{xy} = \frac{\lambda}{3N}\left(-\frac{1}{f^a}\delta_{xy} + i\phi_x^a \bar{K}_{xy} - \int_z \mathrm{d}^{d+1}z\, f^z \Pi_{xz}^{ac} D_{zy}^{cb}\right) \tag{4.84}$$

The self-energy is the functional derivative $\Sigma_{xy} = \frac{2i}{f^x f^y}\frac{\delta\Gamma}{\delta G_{xy}}$, where $\Gamma^{(2)}$ is the sum of 2-PI vacuum diagrams (times a factor $-i$), computed with the vertex with two ϕ and one χ branches, which comes with a factor $\frac{i}{2}f^x$. At next leading order in $1/N$, there is only one diagram $\Gamma^{(2)} = -\frac{i}{2}\int_{xy} G_{xy}^{ab} G_{xy}^{ab} D_{xy}$ shown in figure 4.3.

With this effective action, the components of the self-energy $\mathbf{\Sigma}$ are

$$\Sigma_{xy}^{ab} = -iD_{xy}G_{xy}^{ab} \tag{4.85}$$

$$\Xi = 0, \quad \bar{\Xi} = 0 \tag{4.86}$$

$$\Pi_{xy} = -\frac{i}{2}G_{xy}^{ab}G_{xy}^{ab} \tag{4.87}$$

From there on, the derivation of next leading order equations is quite straightforward. We recover as special cases the finite temperature equations [185] and real-time equations without initial conditions [186]. It is also easy to derive the leading order finite temperature equations of section 4.3.2. In the following, we study quenches at leading order only for the sake of simplicity. Computing the next-leading order corrections to the real time evolution is sometimes very important to resolve some pathologies of the leading order equations, such as the absence of thermalization.

4.6 Dynamical transition at leading order

In the following, we fall back to the leading order equations of motion and study the dynamical transition and quenches of symmetry breaking.

4.6.1 Leading order equations out of equilibrium

At leading N order, the equations are drastically simplified. The self-energy is given by the tadpole contribution, which is local in space and time $\Sigma_{xy} \sim \delta(x-y)$. For this reason, the convolutions between the self-energy and the propagator (4.39) are trivial and the tadpole contribution is a dynamical correction to the mass. The equation of motion are

$$\partial_t^2 \phi_t = -\left(m^2(t) + \frac{\lambda}{3N}\int_p G^{/\!/}_{ptt}\right)\phi_t \tag{4.88}$$

$$\partial_t^2 G^{\perp}_{ptt'} = -\left(p^2 + m^2(t)\right) G^{\perp}_{ptt'} \tag{4.89}$$

$$\partial_t^2 G^{/\!/}_{ptt'} = -\left(p^2 + m^2(t) + \frac{\lambda}{3N}\phi_t^2\right) G^{/\!/}_{ptt'} \tag{4.90}$$

$$m^2(t) = \frac{\lambda}{6N}\left(\phi_t^2 + \int_p G^{/\!/}_{ptt} + (N-1)\int_p G^{\perp}_{ptt}\right) \tag{4.91}$$

The conserved intensive energy is

$$E_t = E_t^K + E_t^{\text{int}} \tag{4.92}$$

$$E_t^K = \frac{1}{2}\left(\partial_t\phi|_t \partial_t\phi|_t + \int_p \partial_t\partial_{t'} G^{aa}_{tt'}|_{t'=t} + \int_p (m_0^2 + p^2) G^{aa}_{ptt} + m_0^2\phi^2_{x_0}\right) \tag{4.93}$$

$$E_t^{\text{int}} = \frac{\lambda}{4!N}\phi_t^4 + \frac{\lambda}{12N}\int_p \phi_t^2 G^{aa}_{ptt} + \frac{\lambda}{6N}\int_p \phi_t^2 G^{/\!/}_{ptt} + \frac{\lambda}{4!N}\int_p G^{aa}_{ptt}\int_{p'} G^{bb}_{p'tt} \tag{4.94}$$

It is even possible and useful to avoid the subleading order N discrepancy of section 4.3.2 by introducing simplified equations of motion that are equivalent at leading order, where the $1/N$ contribution from the longitudinal mode is neglected and all correlations $G^{nn} = G$ are equal

$$\partial_t^2 \phi_t = -m^2(t)\ \phi_t \tag{4.95}$$

$$\partial_t^2 G_{ptt'} = -\left(p^2 + m^2(t)\right) G_{ptt'} \tag{4.96}$$

$$\partial_{t'}^2 G_{ptt'} = -\left(p^2 + m^2(t')\right) G_{ptt'} \tag{4.97}$$

$$m_t^2 = m_0^2 + \frac{\lambda}{6N}\left(\phi_t^2 + \frac{N}{2}\int \frac{\mathrm{d}^3 p}{(2\pi)^3} G_{ptt'}\right) \tag{4.98}$$

The conserved intensive energy becomes

$$E_t = E_t^K + E_t^{\text{int}} \tag{4.99}$$

$$E_t^K = \frac{1}{2}\left(\partial_t\phi|_t \partial_t\phi|_t + N\int_p \partial_t\partial_{t'} G_{tt'}|_{t'=t} + N\int_p (m_0^2 + p^2) G_{ptt} + m_0^2\phi^2_{x_0}\right) \tag{4.100}$$

$$E_t^{\text{int}} = \frac{\lambda}{4!N}\phi_t^4 + \frac{\lambda}{12}\int_p \phi_t^2 G_{ptt} + \frac{\lambda N}{4!}\int_p G_{ptt}\int_{p'} G_{p'tt} \tag{4.101}$$

Notice that the field dynamics (4.95) can be written as a classical motion in a potential

$$\partial_t^2 \phi_t = -\frac{\partial V(\phi)}{\partial \phi} \tag{4.102}$$

$$V(\phi) = \left(m_0^2 + \sum_n \frac{1}{2} \int \frac{\mathrm{d}^3 p}{(2\pi)^3} G^{nn}_{ptt'} \right) \frac{\phi^2}{2} + \frac{\lambda}{4!N} \phi_t^4 \tag{4.103}$$

$$V(\phi) = m_\phi^2 \frac{\phi^2}{2} + \frac{\lambda}{4!N} \phi^4 \tag{4.104}$$

Where we defined yet another mass $m_\phi^2(t)$ which shapes the potential $V(\phi)$.

The dynamics of the field ϕ_t (4.95) and correlations $G_{tt'p}$ (4.96) looks superficially similar to a free field evolution, except for the time dependency of the effective mass $m^2(t)$, which has dramatic effects. This set of equations is not exactly solvable and we have recourse to numerical integration [3].

At leading order, there are a large number of spurious conserved quantities

$$n_p(t) + \frac{1}{2} = N \left(G_{ptt'} \partial^2_{tt'} G_{ptt'} - (\partial_t G_{ptt'})^2 \right)^{1/2} \Big|_{t=t'} = \text{cste}$$

which excludes relaxation to equilibrium. On the other hand, the next leading order contribution allows for thermalization on large times [66], but the effect we are interested in is already visible at leading order.

As a final remark, we use thermal initial conditions, but due to the locality of the self-energy, there is no need to compute mixed G^{q0} correlations 4.4.3. Actually, the retarded and advanced propagators are also decoupled from the equations on the Keldysh propagator and the field. The initial conditions on the Keldysh propagator are obtained from the analytic continuation of the imaginary time propagators, obtained from (4.8) and (4.9)

$$G^{nn}(p, t = 0, t' = 0) = \frac{1}{2} \frac{1}{\sqrt{\mathbf{p}^2 + m^2_{(n)}}} \left(\frac{1}{2} + n_p(\beta) \right) \tag{4.105}$$

$$\partial_t G^{nn}(p, t = 0, t' = 0) = 0 \tag{4.106}$$

$$\partial_t \partial_{t'} G^{nn}(p, t = 0, t' = 0) = \frac{1}{2} \sqrt{\mathbf{p}^2 + m^2_{(n)}} \left(\frac{1}{2} + n_p(\beta) \right) \tag{4.107}$$

$$n_p(\beta) = \frac{1}{e^{\beta \sqrt{\mathbf{p}^2 + m^2_{(n)}}} - 1} \tag{4.108}$$

$$m^2_{(n)} = \begin{cases} \mathbf{p}^2 + m_0^2 + \chi + \frac{\lambda}{3N} \phi^2 & \text{if } n = 1 \\ \mathbf{p}^2 + m_0^2 + \chi & \text{if } n \neq 1 \end{cases} \tag{4.109}$$

3. We simulated three dimensional systems using a discretization in absolute momentum space, akin to a three dimensional discrete system of size between 500^3 and 2000^3 depending on the run.

4.6.2 Quantum quenches

In the typical cold atoms experiment, the system under study can be put out of equilibrium by tuning the strength of an interaction parameter. Here, we consider similar sudden quantum quenches, where the squared mass $(m_0)^2$ is suddenly switched from a value $(m_0^i)^2$ to $(m_0^f)^2$ at fixed interaction strength λ. The quench dynamics in the $\vec{\phi}^4$ model at leading order has been studied in [187], where it is found that the mass $m^2(t)$ typically relaxes to a constant after a transient regime, as shown in figure 4.5 (left panel), whenever both $(m_0^i)^2$ and $(m_0^f)^2$ are positive, i.e. quenches are within the symmetric phase $\phi = 0$. It turns out that in other regimes of quenches, a completely different scenario occurs. Indeed, we find that there is a dynamical transition which occurs for quenches within the symmetry breaking regime $(m_0^i)^2 < 0 \rightarrow (m_0^{f(d)})^2 < 0$ with nonzero initial field $\phi_{t=0}$.

4.6.3 Dynamical transition in the mean-field approximation

We first describe the dynamical transition within the mean-field approximation, to contrast it with the richer leading order approximation. The mean-field approximation has been studied within a conformal field theory approach, based on a mapping from the imaginary time evolution to a classical critical film and the analytical continuation to real times [171]. It neglects all corrections due to fluctuations and the field dynamics is given by a simplified version of (4.102) and (4.103) :

$$\frac{\mathrm{d}\phi}{\mathrm{d}t} = -\frac{\partial V(\phi)}{\partial \phi} \tag{4.110}$$

$$V(\phi) = \frac{1}{2}m_0^2\phi^2 + \frac{\lambda}{4!N}\phi^4 \tag{4.111}$$

Unlike in the leading order equations, the effective potential $V(\phi)$ is *static* and the field evolution $\phi(t)$ is exactly solvable [171]. The motion of the field is qualitatively represented in figure 4.4 (left panel), where various quenches with different initial mass $(m_0^i)^2$ and with same final mass $(m_0^f)^2$ are depicted [4]:

- Below the transition (b), the field oscillates around one minimum of the potential.
- Above the transition (a), the field oscillates symmetrically around zero.
- At the transition (t), the field relaxes exponentially to zero, to the maximum of the potential at $\phi = 0$.

The phenomenology of this mean-field transition is the same as the one found in mean-field models of chapter 3. For example, the long time average of an observable such as $\phi(t)$ has a

4. The dynamical transition is accessible either by tuning $(m_0^f)^2$ at constant $(m_0^i)^2$ or conversely.

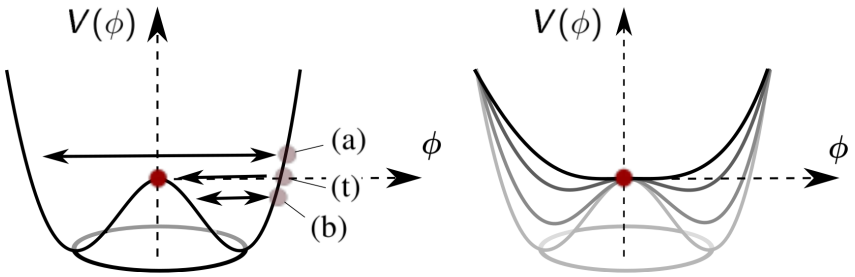

Figure 4.4: Left panel: Effective potential driving the dynamics of ϕ_t. From top to bottom: quench above (a), at (t) and below (b) the dynamical transition. The potential $V(\phi)$ is static in the mean-field approximation, but is time-dependent at leading order in N. Right panel: Long time evolution of the potential $V(\phi)$ at the dynamical transition. The effective mass goes to zero as $m^2(t) \sim 1/t$ (oscillations are not shown for clarity) such that the asymptotic potential $V(\phi) \sim \frac{\lambda}{4!N}\phi^4$ is critical.

logarithmic singularity around the dynamical transition

$$\overline{\phi} \overset{\text{def}}{=} \lim_{T\to\infty} \frac{1}{T}\int_0^T \mathrm{d}t\ \phi_t \sim \frac{cste}{\left|\ln\left((m_0^f)^2 - (m_0^{f(d)})^2\right)\right|} \tag{4.112}$$

Our goal is to determine the impact of fluctuations on this simple scenario.

4.6.4 Dynamical transition at leading order

We find that the dynamical transition is still present when fluctuations are included at leading order in N, as given by equations (4.95) and (4.96). Unlike in the mean-field case, the field dynamics is modified by correlations, and it relaxes to a constant on large times after the quench.

As a signature of the transition, we show asymptotic value of the field $\overline{\phi} = (1/T)\int_0^T \mathrm{d}t\ \phi_t$ and of the mass $\overline{m^2(t)}$ in figure 4.5 (right panel), as a function of the relative distance to the dynamical critical point:

$$\Delta = \left[(m_0^{f(d)})^2 - (m_0^f)^2\right]/(m_0^{f(d)})^2 \tag{4.113}$$

The transition is characterized by the following properties:

- Below the transition, the field relaxes to a nonzero asymptotic value $\phi_t \to \overline{\phi}$. The mass $m^2(t)$ of equation (4.98) relaxes to zero, which is a necessary condition for a stationary nonzero ϕ (4.95). In equilibrium, zero mass was associated with a diverging transverse propagator (4.14). However, the propagator G_{ptt} has no such simple analytical expression after the quench, and is actually characterized by a finite lengthscale r_b^* which we define later.

- Above the transition, the field relaxes to zero. The mass relaxes to a positive value $m^2(t) \sim \Delta$ shown in figure 4.5, which in turns defines a natural lengthscale $r_a^*(\Delta) \sim \Delta^{-1/2}$.

These features are compatible with the early time dynamics of the field depicted in figure 4.4 (left panel). Below the transition, the field oscillates around a single minimum, whereas above it oscillates symmetrically and relaxes to zero on large times.

Some aspects of this transition had already been discovered in [188]. Our contribution is to study in detail the critical regime where a scaling law for correlations emerges, and to show the existence of a diverging lengthscale around the transition. These features are decisive to assert the critical nature of the dynamical transition.

4.6.5 Critical quench

Let us now describe the dynamics of the critical quench. The quench at $(m_0^f)^2 = (m_0^{f(d)})^2$ is a singular quench, for which the fields evolves towards the unstable point $\phi = 0$, and decays exponentially to zero as depicted in figure 4.4. It becomes negligible in for all purposes in a finite time T, as for example in equation (4.98). For larger times $t > T$ the field is on an unstable point of equation (4.95), at the top of the potential $V(\phi)$. This dynamical erasure of the order parameter is the crucial feature of the critical point, with drastic consequences on the evolution of correlations and of the effective mass.

The subsequent dynamics for $t > T$ is divided into two stages. At first, the effective mass $m^2(t)$ is negative, and long range correlations build up exponentially like

$$G_{ptt} \sim G_{p00} \exp\left(2\sqrt{-p^2 - m^2(t)}\ \ t\right) \tag{4.114}$$

for all momenta below a cutoff $\Lambda^2 = |m^2(t = 0)|$. As a consequence, the mass $m^2(t)$ grows exponentially.

In a second stage, the effective mass $m^2(t)$ reach positive values due to the previous growth of correlations (4.98), and then stabilizes and decreases with a slow, oscillating, power law decay $m^2(t) \lesssim m_i \cos(2\Lambda t)/t$ shown in figure 4.5 (left panel) and figure 4.4 (right panel). The drop of the effective mass drives the system to a massless, critical state.

Strikingly, on late times, the low momentum modes enter a *two-times scaling regime*:

$$G_{ptt'} \sim \frac{1}{p^2}\mathcal{F}\left(pt^z, \frac{t}{t'}\right) \tag{4.115}$$

$$\mathcal{F}\left(pt, \frac{t}{t'}\right) \sim \cos\left(pt\left(1 - \frac{t'}{t}\right)\right) - \cos\left(pt\left(1 + \frac{t'}{t}\right)\right) \tag{4.116}$$

with a dynamical exponent $z = 1$. The agreement between numerical simulations and this scaling form for equal-time correlations is excellent, as shown in figure 4.6. The real space

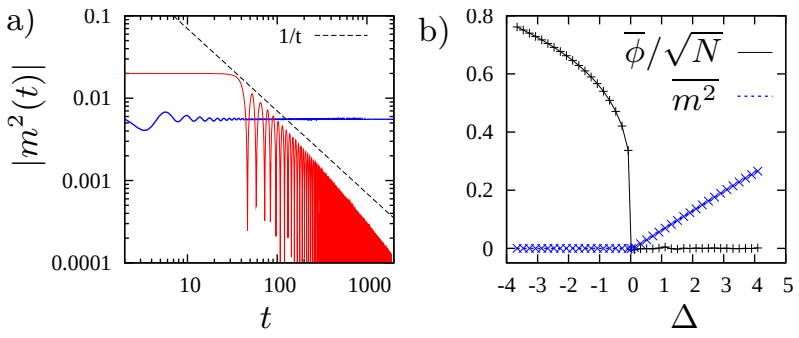

Figure 4.5: a) $|m^2(t)|$ for a quench within the unbroken symmetry phase – thick line – and at the dynamical transition – thin line. In the second case, m^2 decays faster than $1/t$. b) Dynamical transition: Large times average of $\overline{\phi_t}/\sqrt{N}$ and $\overline{m^2(t)}$ (the later is rescaled by a factor 10^4) as a function of the relative distance to the critical point Δ (in %).

counterpart of this scaling reads:

$$G_{rtt'} \sim \frac{1}{r}\mathcal{H}\left(\frac{r}{t},\frac{t}{t'}\right) \tag{4.117}$$

$$\mathcal{H}\left(\frac{r}{t},\frac{t}{t'}\right) = \Theta\left(\frac{r}{t}-1+\frac{t'}{t}\right)\Theta\left(1+\frac{t'}{t}-\frac{r}{t}\right) \tag{4.118}$$

The numerical scaling for $t = t'$ is shown in figure 4.7 (right panel) and for $t \neq t'$ in figure 4.8. Remarkably, this expression for correlations is the same as for quenches in a *free* field theory where the final mass is $(m_0^f)^2 = 0$ [87], but the huge difference is that in the present case the vanishing mass is *dynamically* generated in a non trivial interacting theory.

The two-times scaling in real space may be interpreted qualitatively from the fact that $m^2(t)$ vanishes. On large times, the effective physics is a massless free theory, where excitations are effective bosons [87] which propagate at celerity c. In the limit of a large number of bosons, the fields are classical. According to the Huygens-Fresnel principle, plane wave propagation can be interpreted, in three dimensions, in terms of a continuum of virtual emitters. This interpretation is illustrated in figure 4.9: between the origin and a point at a distance r, correlations $G_{rtt'}$ at successive times t' and t are nonzero only provided there exist a virtual emitter in the past, susceptible to reach the two points at times t' and t respectively.

4.6.6 Light-cone effect

Let us now discuss the difference between the usual light-cone effect and the critical light-cone effect that we obtain.

The light-cone effect is a property expected to apply to any quantum system with short range interactions, as a consequence of the (generalization of) Lieb-Robinson bounds on the

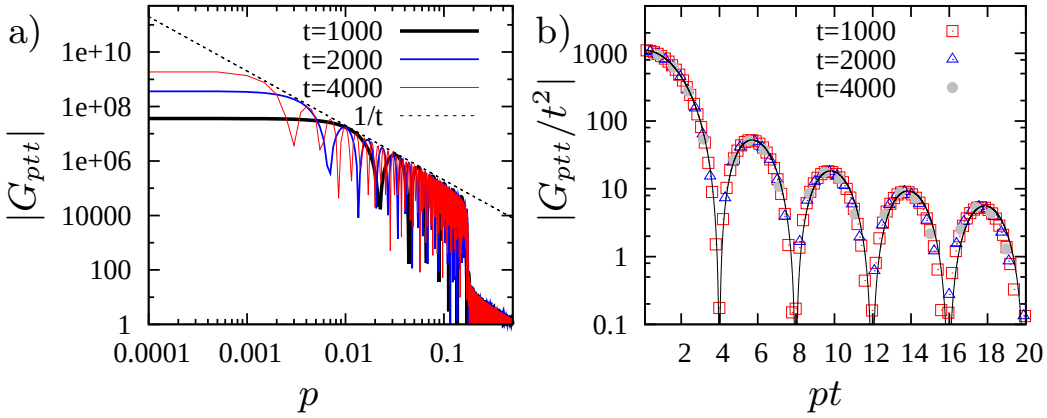

Figure 4.6: a) Equal-time correlations $|G_{ptt}|$ as a function of p for $t = \{1000, 2000, 4000\}$, log-log scale. Notice the divergence of correlations below a cutoff scale $p < \Lambda \approx 0.2$. b) Rescaled equal-time correlations $|G_{ptt}/t^2|$ as a function of pt for the same data, y-axis in log scale. All data collapse on the scaling law (4.116) drawn in black.

speed of propagation of information under a local perturbation. The light-cone effect has recently been observed in an experimental realization of the Bose-Hubbard model, and found to be in good agreement with numerical estimates of the velocity of information [53]. It is signaled by a jump in equal time correlations G_{rtt} at a distance $r = vt$. The velocity of the correlation front v may depend on both the initial state of the system and on the interactions after the quench. In our model, relativistic invariance guarantees that there is a bound on the speed of propagation of correlations with constant celerity c, as we observe in a generic quench in figure 4.10. There is a jump of correlations on distances below $r < 2ct$, above the constant background for $r > 2ct$. The figure also shows that the scaling (4.117) is not valid after an arbitrary quench 4.10 (right panel).

In the critical quench, the light cone effect is still present as shown in figure 4.7 where correlations are enhanced below $r < 2ct$. Furthermore, the scaling (4.117) of *two-times* correlations $G_{rtt'} = r^{-1}\mathcal{H}(r/t, t/t')$ holds, as shown in figure 4.8, a feature characteristic of a massless theory where effective particles propagate at a constant velocity c. In an arbitrary quench, two-times correlations do not have any specific properties, due to the complex dispersion relation of quasiparticles which propagate at celerity c *and* at lower speed as well.

4.6.7 Self-consistency

The above scaling holds in the regime $p \ll \Lambda$ at times $t/t' \sim 1$ and $t \sim 1/p$. We would like to check now the self-consistency between the scaling form of the propagator and the dynamics of the residual mass $m^2(t) \lesssim m_i \cos(2\Lambda t)/t$, related by (4.96) and (4.98).

To show that the scaling of correlations is compatible with the nonzero effective mass $m^2(t)$,

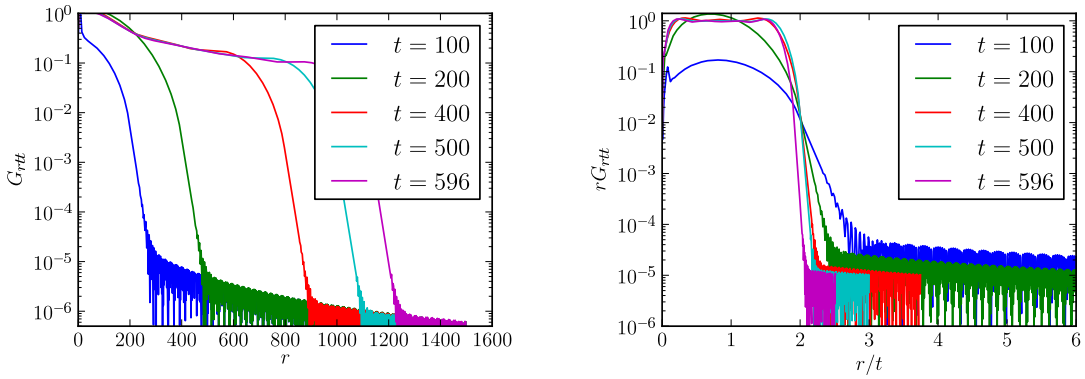

Figure 4.7: Left panel: Light cone effect after a quench at the dynamical transition. Right panel: Scaling of rG_{rtt} as a function of (r/t). The data collapses on the step function (4.117).

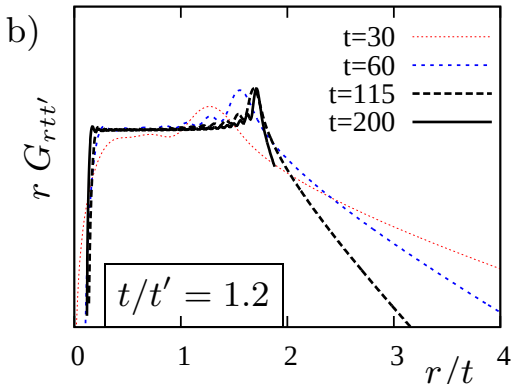

Figure 4.8: Rescaled two-times correlation function $r\ G_{rtt'}$ as a function of r/t for $t/t' = 1.2$. The data collapses on the rectangle step function (4.117) as t increases, with finite size effects at a scale Λ^{-1} which become smaller as t increases.

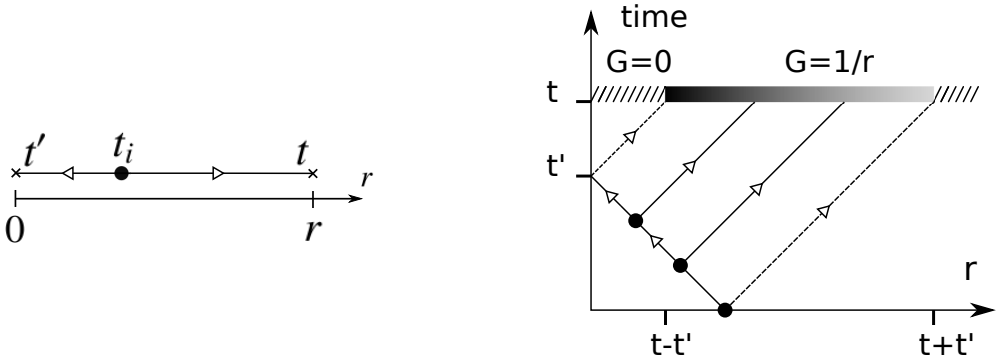

Figure 4.9: Left panel: Qualitative interpretation of the correlations in real space in terms of a common virtual emitter in the past. A pair of particles is emitted at time $t_i > 0$, the two particles propagate towards a point at $r = 0$ and another point at r respectively. The first reaches $r = 0$ at time t' and the second reaches r at time t. If such a process is possible, the two points correlation function $G_{rtt'}$ is non zero. Right panel: For given r and $t' > t$, $G_{rtt'}$ vanishes in the dashed areas, where it is out of causal reach of virtual emitters. For large r, no particles can reach r and 0 since the time to propagate is insufficient. For small r, during the lapse of time between t' and t, the second particle has gone too far to reach r at time t.

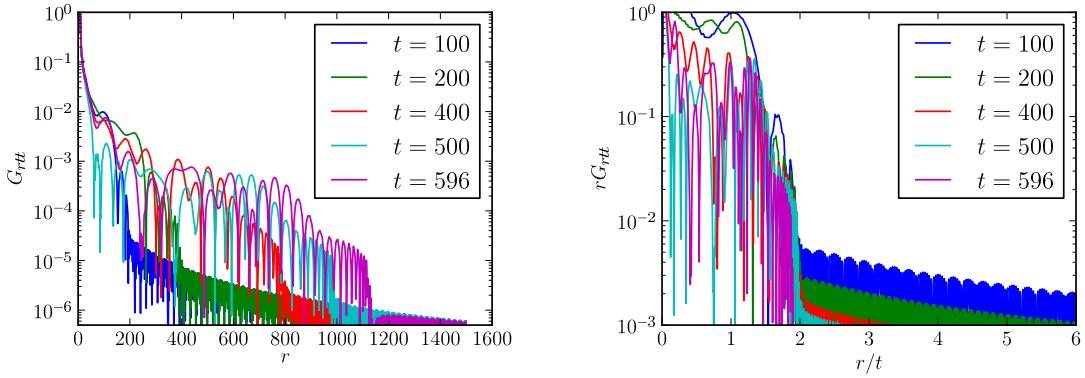

Figure 4.10: Left panel: Light cone effect after an arbitrary quench, visible as a bump over the constant correlation background in $G_{rtt}(r)$ at distances $r < 2t$. Right panel: Absence of scaling in the $rG_{rtt}(r/t)$ variables, although visibly correlation have a propagating front at $r/t = 2$.

we generalize to real space two-times correlations the result of [87] for a sudden quenches from $(m_0^i)^2$ to $(m_0^f)^2$ in a *free* field theory, taking the continuum limit:

$$G_{rtt'} = m_0^i \int \frac{\mathrm{d}^3 p}{(2\pi)^3} \frac{e^{i\vec{p}\cdot\vec{r}}}{\omega_p^2} \Big(\cos(\omega_p (t-t')) - \cos(\omega_p (t+t')) \Big) \tag{4.119}$$

with $\omega_p^2 = p^2 + (m_0^f)^2$. It is easy to see that for $(m_0^f)^2 = 0$ we obtain (4.115) and (4.116). The key observation to prove self-consistency is that even for $|(m_0^f)^2| > 0$, these correlations are asymptotically equal to those with $(m_0^f)^2 = 0$, on distances and times

$$x, t, t' \lesssim 1/|(m_0^f)^2|^{1/2} = r_* \tag{4.120}$$

with r_* the typical lengthscale of deviation from massless correlations.

Coming back to the interacting model, supposing that the scaling is valid below the scale x, we ask whether the massless scaling is spoiled on times $t, t' \sim x$ by the remaining mass $m^2(t) < (m_0^i)^2 \cos(2\Lambda t)/t$. According to the above criterion, correlations are massless-like on scales $x, t, t' \lesssim 1/|(m_0^f)^2|^{1/2}$ by hypothesis, and the mass is $1/|(m_0^f)^2|^{1/2} > t$, which shows that the scaling is valid on larger length scales, and by iteration of this reasoning to larger lengths and times the full scaling is obtained.

Reciprocally, assuming that the propagator $G_{ptt'}$ obeys scaling on scales $L^{-1} < p < \Lambda$, the contribution of correlations to $m^2(t)$ in (4.98) is, calling Λ' the high momentum physical cutoff:

$$\int_{1/L}^{\Lambda'} \frac{\mathrm{d}^3 p}{(2\pi)^3} G_{ptt} = \int_{1/L}^{\Lambda} \frac{\mathrm{d}p\, A p^2}{2\pi^2} \frac{1-\cos(2pt)}{p^2} + \int_{\Lambda}^{\Lambda'} \frac{\mathrm{d}^3 p}{(2\pi)^3} G_{ptt} \tag{4.121}$$

$$\sim \frac{A}{2\pi^2} \left(\Lambda - \frac{\sin(2t\Lambda)}{2t} \right) + C \tag{4.122}$$

Contributions from the two constant terms vanish, and accordingly the mass is vanishing like $m^2(t) \sim (m_0^i)^2 \cos(2\Lambda t)/t$. The decay of the mass has been evaluated more rigorously in [189, 188], where it is shown that it decays either like $m^2(t) \sim \cos\left(\Lambda t + \ln(t/t_1) + \theta\right)/t$ or faster, as shown in figure 4.5, which is enough to ensure self-consistency.

4.6.8 Critical properties

In this section, we analyze in detail critical properties around the critical point, at small relative distance $\Delta = \left[(m_0^f)^2 - (m_0^{f(d)})^2\right]/(m_0^{f(d)})^2 \lesssim 1$. Unlike in the critical quench $(m_0^f)^2 = (m_0^{f(d)})^2$, the field ϕ_t misses the unstable point at time T. From the first section, we recall that the field reaches a nonzero constant, which actually scales like $\overline{\phi} \sim |\Delta|^{1/4}$ below the transition, as shown in figure 4.11. Above the transition, the field decays to zero and the asymptotic square mass is positive, with scaling $m^2(t \to \infty) \sim \Delta$.

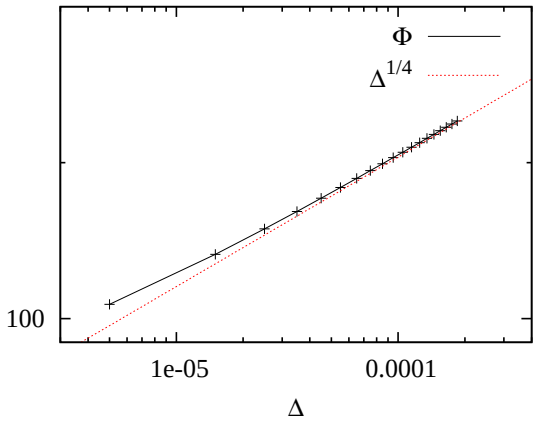

Figure 4.11: Logarithmic plot of $\overline{\Phi}(\Delta)$. The scaling law $\overline{\Phi} \sim \Delta^{1/4}$ is clearly satisfied, except very close to $\Delta = 0$ where subleading N and finite time effects alter it.

The scaling of correlations (4.115) is inherited on both sides of the transition for $|\Delta| \ll 1$. It is valid in a range of momenta $p^* < p < \Lambda$ and times $r^* > t > \Lambda^{-1}$ with p^* an additional lower bound, defining a lengthscale $r^* = (p^*)^{-1}$ which diverges at the critical point.

Above the transition, the scale p_a^* is naturally defined in terms of the additional mass $m^2(\infty)$ as $p_a^* = m(\infty)$ so that $r_a^* \sim 1/\Delta^{1/2}$. Below the transition, despite the fact that $m^2(\infty) = 0$, a numerical analysis of G_{ptt} reveals that there is a scale $r_b^* \sim 1/\Delta^{1/2}$ below which scaling is broken. Specifically, $G_{p,t=\infty,t=\infty}$ is scaling like $1/p^2$ only for $p > 1/r_b^*$, which defines another sort of effective mass with scaling $\Delta^{1/2}$.

The diverging length is shown in figure 4.12 (right panel) with a good fit to $r^*(\Delta) \sim 1/\Delta^{1/2}$, although r^* is defined differently on both sides. The logarithmic plot (left panel) confirms the power law scaling.

4.6.9 Quenches to the symmetry breaking phase

Let us now turn to an apparently unrelated problem, the question of how order develops after a quench from the symmetric phase $(m_0^i)^2 > (m_0^c)^2$ to the broken symmetry phase $(m_0^i)^2 < (m_0^c)^2$. Notice that this question is not answered by the Kibble-Zurek analysis, which only describes the early production of defects and does not describe the long time dynamics of the field and correlations. This problem has instead been studied in a different context and is referred to as spinodal decomposition [190].

The order dynamics after the quench is actually trivial, because the average field is rigorously $\phi_t = 0$ if it was zero in the initial state (as is the case whether the initial state is the ground state or a thermal state in the symmetric phase). The growth of order is only visible at the level of *correlations*. Contrary to the common intuition, a small perturbation of the initial conditions $\phi_{x,t=0} \neq 0$ does not the affect the dynamics very much [190], thus we only consider

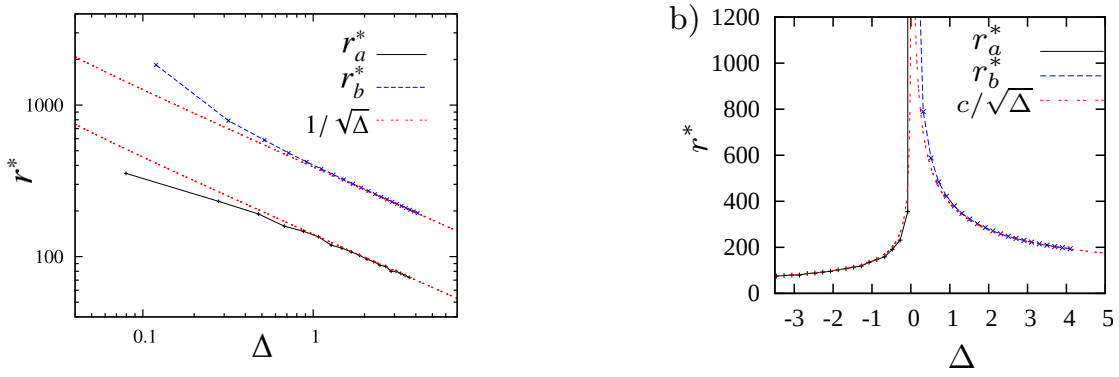

Figure 4.12: Left panel: Scaling of the diverging lengths $r_a^* \sim r_b^* \sim 1/\sqrt{\Delta}$ with Δ the relative distance to the critical point (in %). Once again the scaling is good not too close to the transition as in figure 4.11. Right panel: Diverging length r^* on both sides of the transition. Below the transition it is defined from the cutoff $r_b^* = 1/\Lambda^*$ in the scaling of correlations, whereas above the transition it is defined from the effective mass as $r_a^* = 1/|m_{t\to\infty}|$.

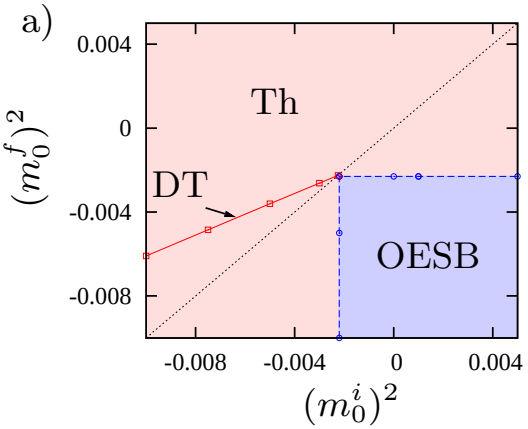

Figure 4.13: Quench phase diagram: Dynamics on large times after a quench from $(m_0^i)^2 \to (m_0^f)^2$ for $\lambda = 1$. *DT:* Dynamical transition line, *OESB:* Off equilibrium symmetry breaking, *Th:* Relaxation (thermalization at next leading order) on large times. Error bars are smaller than item size. The position of the transition lines depends on non-universal features, such as the interaction strength λ and the cutoff Λ'.

the perfectly symmetric scenario $\phi_{x,t=0} = 0$.

The dynamics of symmetry breaking goes as follows: at time $t = 0$, the system is in a physical state very similar to a system quenched at the dynamical transition after the time T defined above, i.e. $\phi = 0$ and $m^2(t) < 0$, as depicted in figure 4.4 (right panel). Therefore the dynamics is exactly the same as the one of the dynamical transition discussed above, with a decaying effective mass $m^2(t) \lesssim m_i \cos(2\Lambda t)/t$ and a scaling regime for correlations (4.116). Notice that such scaling relations have been studied extensively in classical systems [80]. In this context, two times scaling correlations are very often encountered and go under the name of aging. This term is not really appropriate for the ballistic effects which we obtain here.

As another side remark, let us mention that if there is a small homogeneous initial perturbation $\phi_{x,t=0} = \phi_0 \neq 0$, it is exponentially growing in early stages of the dynamics. However, if its impact is small before the time when $m^2(t)$ is negligible is reached, then the initial nonzero field is irrelevant for all times, since the effective potential for the field (4.95) is flat afterwards.

The purpose of this digression about the dynamical breaking of symmetry was to show that a common scaling regime occurs under two different classes of quenches: the dynamical transition quench and the quenches of symmetry breaking. The divergence of a correlation length together with the scaling regime of correlations is a strong hint of out of equilibrium quantum criticality. A complete quench phase diagram is shown in figure 4.13, summarizing all possible quenches $(m_0^i)^2 \to (m_0^f)^2$. There is a large regime of quenches where the mass and field relax to a finite value at leading order, and where thermalization is obtained at next-leading order [66] (Thermalization). Quenches were the symmetry is dynamically broken (Off-Equilibrium Symmetry Breaking) were not correctly described in the mean-field analysis of section 3.4.3, but are accessible within the current approach. Finally, the line of the dynamical transition is indicated (Dynamical Transition). Notice that these the two classes of quenches with equivalent dynamics — the dynamical transition and the symmetry breaking quenches — belong to completely different regimes.

4.6.10 Summary of the results

In the ϕ^4 model, the $1/N$ expansion allows to analyze the dynamical transition and quenches from the symmetric to the broken symmetry phase.

We showed that at the transition, instead of relaxing after the quench, the system settles in an out of equilibrium state, with a vanishing effective mass. In this nonequilibrium state, the correlations exhibit a light-cone effect, but additionally assume a two-times scaling form, understood in terms of effective massless particles. The same scaling limit is also found for symmetry breaking quenches, hinting for the existence of a corresponding universality class.

Clearly, it would be interesting to extend our analysis to the next leading order contribution, where *equal-time* scaling fixed points were found [85] with quite different scaling exponent. However, it seems that the effects that we obtain here occur on much faster times than the onset of these non-thermal fixed points. Understanding the dynamics of the dynamical transition and of the symmetry breaking in more realistic models is of prime importance. Clearly, in different

models, such a in the Bose-Hubbard model, the existence of topological defects should play a role. Finally, it is worth pointing out that the present and previously known results only address a few aspects of symmetry breaking, which needs a lot more investigations [190, 97].

4.6.11 Generic argument about the dynamical transition

In this section, we present speculations about a generic scenario for the dynamical transition in the ϕ^4 field theory and try to pin down what could be different in higher orders in perturbation theory. Indeed, it is always possible to write the field dynamics in a ϕ^4 theory, at any order in perturbation theory or even in a non-perturbative expansion scheme, by a generalization of equation (4.67):

$$\partial_t^2 \phi = -(m^2 + p^2)\phi - iJ[\phi, G] \tag{4.123}$$

where the kernel $J_x[\phi, G] = \frac{i}{f^x} \frac{\delta \Gamma}{\delta \phi_x}$ is an arbitrary complex function of the propagator G. In principle, one can even devise an *exact* scheme where arbitrary high correlations $\Delta^n(x_a, x_b, x_c, \ldots) = \langle \hat{\phi}_{x_a} \hat{\phi}_{x_b} \hat{\phi}_{x_c} \ldots \rangle$ would be accounted for, but in any case the kernel would be an odd function [5] of ϕ

$$J[\phi, G, \Delta^3, \ldots] = \mathcal{G}_1[G, \Delta^3, \ldots]\, \phi + \mathcal{G}_3[G, \Delta^3, \ldots]\, \phi^3 + \ldots \tag{4.124}$$

where the first (functional, self-consistent) coefficient $\mathcal{G}_1[G, \Delta^3, \ldots]$ would drive the transition from the symmetric phase to the symmetry breaking phase. Clearly, under a quench, there is no fundamental reason why it would be impossible to approach or reach "the top of the potential" $\phi = 0$ under peculiar quenches, especially when $\mathcal{G}_1$ is initially negative, although all coefficients $\mathcal{G}_1, \mathcal{G}_3, \ldots$ have their own time dependency. The *contrary* would be quite astonishing, requiring some conspiracy of higher correlation functions to repel the field from this unstable attractor.

Actually, once the field ends up close enough to $\phi = 0$, it is stabilized as shown in section 4.6.9, at least in the leading order approximation. It not yet possible to be sure that this stabilization, which is crucial for the argument to hold, still occurs in better approximation schemes. In a sense, we can conclude that the fate of the dynamical transition is related to the physics of symmetry breaking with an infinitesimal initial field $\phi \ll 1$.

Moreover, the previous argument relies on the fact that the initial correlations do not affect the large time dynamics in case of a symmetry breaking quench. assumption that initial conditions for propagators and for higher correlations are not very important (and thus that the dynamical critical quench and the symmetry breaking quench are alike) also relies on the universal features of the symmetry breaking quench.

5. By symmetry $\phi \to -\phi$, J is odd, and non analytic terms are not expected to occur even in a non perturbative scheme (for example, in non perturbative renormalization group).

4.7 Discussion of the dynamical transition

After this discussion of the dynamical transition in the ϕ^4 theory, I would like to comment on how our results compare with those obtained from other approaches.

- First of all, in many cases the dynamical transition is accompanied by a dynamical vanishing of the order parameter, or at least non monotonous average as a function of the final parameter U_f. Actually, the former feature has not been observed in all different approaches. In mean-field, as shown in the Hubbard model [159], in the ϕ^4 model at the mean-field level [171] and in the Bose-Hubbard model (in section 3.6), the order parameter always vanishes with a logarithm singularity. On the contrary, t-DMFT in the Hubbard model [62] predicts a fast thermalization with nonzero order parameter at the dynamical transition. Likewise, the vanishing of the order parameter has not been observed in the approach supplementing mean-field with additional fluctuations, using a slave spin formalism [175], and in another study using Ansatz wavefunctions with Jastrow factor corrections [191]. This is in contrast with what occurs in the ϕ^4 theory at leading order, where the order parameter vanishes as shown in section 4.6.3.
- Another major difference is the nature of the two regimes on both sides of the transition. Indeed, in the ϕ^4 model at large N, the two regions respectively have symmetry and break symmetry on large times. On the other hand, in the Hubbard model, the asymptotic state after the quench is probably in the metallic phase on both sides of the transition [159, 172, 62]. The transition rather separates two regimes of different *dynamics*. Below the transition, the dynamics is relaxational, with a prethermalization plateau [62], whereas above there are oscillations of the double occupancy, as expected in the strong coupling regime [159]. Regarding this discrepancy, one can wonder whether the dynamical transition in the ϕ^4 model and in the Hubbard model are qualitatively different phenomenon.
- The dynamics of correlations at the dynamical transition is a key element to decide whether the dynamical transition is a critical phenomenon. To decide if it is, we need a non-perturbative scheme that is capable of a good description of the equilibrium phase transition, *including critical exponents*, and which generalizes out of equilibrium, which is currently somewhat out of reach.

  Up to date, two different studies handle correlations: a slave boson inclusion of fluctuations in the Hubbard model [175] later made self-consistent in [172], and the present analysis of the ϕ^4 model. In both cases, low momentum modes correlations diverge on short times. In our case, we have described a critical scaling regime of two times correlations with simple exponents. It would be of prime interest to know whether this occurs too in the Hubbard model. On the other hand, t-DMFT predicts fast thermalization at the dynamical transition [62], but perhaps cannot be relied on too much in this regime, since it is not fit to describe long range correlations.
- In both of our takes on the problem, we suggested that there is a link between the dynamical transition and quenches of symmetry breaking. In mean-field, the two quench trajectories

are actually the time reversal of one another as described in section 3.6. On the other hand, including fluctuations, one is rather lead to think that the dynamics of the order parameter is indeed the time reverse of one another, but that the dynamics of correlations is actually the *same* (section 4.6.9).

- As a side remark, the above scenario of a dynamical transition is specific of $d \geq 2$ models. Indeed, in a one dimensional system, the order never persists at positive temperature and typically decays exponentially for any quench. Nevertheless, a different sort of dynamical transition with a non analytic behavior as a function of *time* has been uncovered recently in one dimensional systems [192, 193]. The link between the one dimensional case and the dynamical transition as we describe is not clear at present.
- Finally, it is worth mentioning that there is a classical analog to quenches to the unstable point [194]. In the Ising model, applying a pulsed magnetic field which favors a reversed magnetization, the system undergoes an out of equilibrium transition as a function of the pulse duration. This transition is also characterized by a diverging lengthscale and timescale, and is probably related to the dynamical transition observed with an alternative applied magnetic field.

Chapter 5

Disordered Bose-Hubbard model

5.1 Disordered Bose-Hubbard model

5.1.1 Short survey of the disordered Bose-Hubbard model

The general issue of the impact of quenched disorder in a quantum system was first studied by Anderson in fermionic systems [195]. The phenomenon of Anderson localization is a one body effect, occurring in the absence of interactions, in which electrons eigenstates are localized in space within a finite region instead of being spread as in a Bloch state. This exceptional phenomenon has become a milestone of condensed matter physics [196], understood thanks to the large effort to develop and adapt to the context techniques such as scaling arguments [197], diagrammatics and the mapping to the non-linear σ model [198], the replica trick [199, 200], and supersymmetry [140], which revealed a strong link to random matrix theory.

Understanding the further impact of electron-electron interactions in a disordered system is a long standing problem, intrinsically of many-body nature. Recently, many-body localization has been found to occur at finite temperature [201] in a system decoupled from a phonon bath.

The same question was addressed in parallel for interacting *bosons* with disorder, by Giamarchi and Schultz [202]. Soon after, Fisher et al. [134] studied the same problem with an additional periodic trapping potential, the disordered Bose-Hubbard model. At that time, the motivation was to understand Helium adsorbed on Vycor, but also to try to explore with bosons the general problem of strong correlations and the effect of disorder. Today, disordered non-interacting systems have been studied in cold atoms [20, 21]. All the techniques necessary to study experimentally strongly interacting disordered bosons are currently available, and it is merely a question of time before experimental groups realize these systems.

The standard Bose-Hubbard Hamiltonian has random random chemical potential and is defined as follows:

$$\hat{H} = \sum_i -\mu\hat{n}_i + \epsilon_i\hat{n}_i + \frac{U}{2}\hat{n}_i(\hat{n}_i - 1) - J\sum_{\langle i\,j\rangle}\left(\hat{b}_i^\dagger\hat{b}_j + \hat{b}_j^\dagger\hat{b}_i\right) \tag{5.1}$$

As in section 2.2, there is a hopping term of amplitude J, on-site two-body repulsion U due to s-wave scattering, a chemical potential μ in the grand-canonical ensemble and random on-site energy ϵ_i, typically introduced using laser speckle or incommensurate lattices. The early analysis [134] already provided countless insights and heuristic arguments about the low temperature phases of this model, most of which have been proved right. If the disorder distribution $P(\epsilon)$ is bounded, the model (5.1) gives rise to three phases: the superfluid phase, the Mott insulator phase, both already present in the pure case, and an additional *Bose glass* phase. For the sake of completeness, we recall the zero temperature properties of the superfluid and Mott phase, and then describe the Bose glass.

- The superfluid phase is gapless and has superfluid long range order.

$$n_0 = \lim_{|i-j|\to\infty} \langle \hat{b}_j^\dagger \hat{b}_i \rangle > 0 \tag{5.2}$$

  The uniform superfluid susceptibility χ is defined in the following as the local order $\langle \hat{b}_i \rangle$ induced by a small perturbation $\hat{H}' = \sum_i \hat{b}_i^\dagger \Psi + \text{h.c.}$:

$$\chi = \frac{\partial \langle \hat{b}_i \rangle}{\partial \Psi} \tag{5.3}$$

  The susceptibility is finite in the superfluid phase due to the linear single particle density of state $\rho(\omega) \sim \alpha\omega$. We show why this is the case later, but we recall that $\rho(\omega) = -\frac{1}{\pi \text{Vol}} \int \mathrm{d}r \, \text{Im} G(r, r, \omega)$ and that $G(r, r, \omega)$ is the Fourier transform of $G(r, r', t) = \langle T_t \hat{b}_r(t) \hat{b}_{r'}^\dagger \rangle$. The linearity of $\rho(\omega)$ is a well-known consequence of the Bogoliubov dispersion relation in the dilute gas regime $E_p = \left(\frac{p^2}{2m} (\frac{p^2}{2m} + 2Un_0) \right)^{1/2}$ where $n_0 = \langle \hat{b}_i \rangle$ is the condensate fraction [203]. The linear dispersion relation is also found in the strongly correlated case within non-perturbative renormalization group [146](without disorder).

- The Mott insulator phase is characterized by a gap and zero compressibility $\frac{\partial n}{\partial \mu}$. The density is commensurate $\langle \hat{n}_i \rangle \in \mathbb{N}$, and usually the Mott phase occurs in different regions of the phase diagram, the "lobes", each one having a different density. The superfluid order n_0 is zero in the Mott phase.

- The Bose-glass has no superfluid long range order, unlike the superfluid phase,

$$n_0 = \lim_{|i-j|\to\infty} \langle \hat{b}_j^\dagger \hat{b}_i \rangle = 0 \tag{5.4}$$

  It is gapless and compressible, unlike the Mott phase. The uniform superfluid susceptibility χ is infinite. This is the consequence of a finite single-particle density of state $\rho(\omega) = c$ at low energy. The argument of Fisher et al. [134] is that χ may be written $\chi = \int \mathrm{d}r \, \mathrm{d}\tau \, \overline{G(r, \tau)}$, which is infinite because around $r = 0$, $\overline{G(r = 0, \tau)} = \int_0^\infty \mathrm{d}\epsilon \, e^{-\epsilon|\tau|} \rho(\text{sgn}(\tau)\omega) \sim c/\tau$, yielding $\chi = \infty$ by integration over τ. Reciprocally, χ is finite in the superfluid phase where $\rho(\omega) \sim \alpha\omega$.

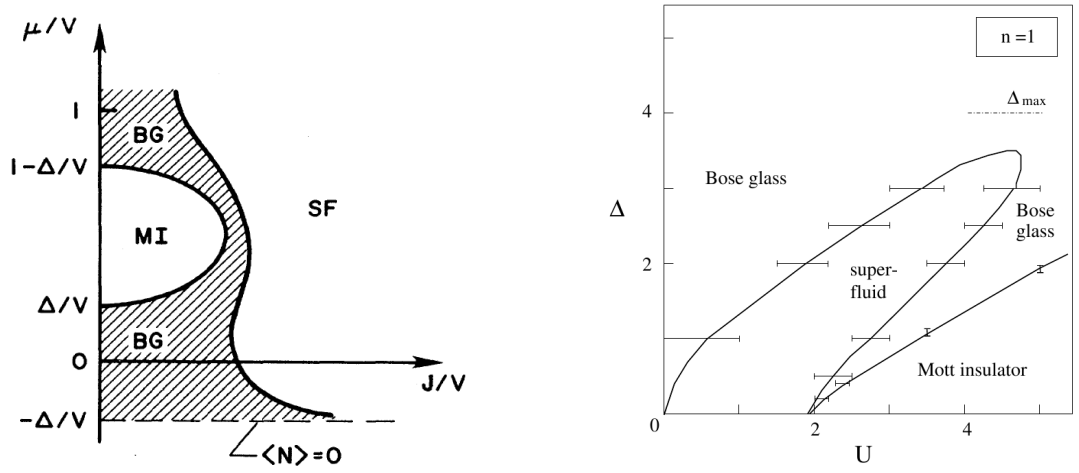

Figure 5.1: Left panel: Phase diagram of the disordered Bose-Hubbard model as understood by Fisher et al. [134] for small disorder $\Delta < 1/2$ in $\{\mu, J\}$. SF: superfluid, MI: Mott insulator, BG: Bose glass. Right panel: Phase diagram in $d = 1$ from DMRG [205] in the U, Δ variables at fixed $J = 1$ and commensurate filling $n = 1$.

There is a consensus about the qualitative shape of the phase diagram [134], after early observations of the Bose glass phase [204] and confirmations of the phase diagram by DMRG studies [205] shown in figure 5.1. More recently, Monte Carlo simulations showed that the Bose glass phase always intervenes between the Mott insulator and the superfluid phase [206] at commensurate filling, which was a debated issue. However, a correct identification of the different phases in a finite size system is still a challenge. As suggested in [207], the probability distribution of the energy gap allows to distinguish between the three phases.

A droplets argument has been argued to describe the Mott insulator to superfluid phase boundary [208]. According to it, the closure of the Mott insulator gap at $J > J_c$ is due to extremely rare realizations of the disorder, in arbitrary large regions, which allows for inclusions of a superfluid droplet. These droplets have arbitrary low energy excitations, such that the resulting density of states at small frequencies is exponentially small. This induces a transition of Griffiths type, and is really a peculiarity of bounded distributions of disorder ϵ. Yet, no direct evidence of this plausible scenario is known.

Additional phases are expected when the particle-hole symmetry is exactly conserved. This symmetry, which was responsible for the special Mott to superfluid transition at the tip of the lobes, is always broken by disorder on the chemical potential [139]. One must consider different models, such as the random Josephson junction model, or the Bose-Hubbard model with random couplings J_{ij}, to recover a particle-hole symmetric transition at commensurate fillings, which gives rise to a new *Mott glass* phase [209].

As of today, if there is some agreement about the nature of the phase diagram, very little

is known about the phase transitions. Most studies take for granted that the transition from superfluid to Mott insulator is conventional in $d \geq 2$. Basically, a conventional second order phase transitions is characterized by the usual scaling relations. Calling $\delta \sim \mu - \mu_c$ or $\delta \sim J - J_c$ the distance to the critical point, the correlation length, energy and order parameter scale like $\xi \sim \delta^{-\nu}$, $\omega \sim \xi^{-z}$ and $\langle \hat{b} \rangle \sim \delta^{\beta}$. The two-point correlations [1] $G(r,t) = \langle \hat{T} \hat{b}_r(\tau) \hat{b}_0^{\dagger}(0) \rangle_c$ scale as $G(r,\tau) \sim r^{-(d+z-2+\eta)} g(r/\xi, \tau/\xi^z)$ with a new critical exponent η. As a side remark, a disordered phase transition must satisfy the Harris criterion [210] $d\nu > 2$.

However, two major classes of disordered quantum phase transitions are known [211]: conventional phase transitions with power law critical properties, and infinite disorder fixed points, where the critical timescale scales exponentially with the distance δ to the critical point $\tau \sim e^{1/\delta^{\theta}}$ (the dynamical exponent z is "infinite").

In real space renormalization group (RG), a conventional fixed point (by contrast with an infinite disorder fixed point) is characterized by the convergence of the finite average disorder strength under the RG flow. Implementations of RG in $d = 2$ [212] indicate a conventional transition and shares features of a percolation transition, yet with nontrivial exponents unlike quantum models on dilute lattices [213]. The percolating nature of the Bose glass to superfluid transition was also found within a variational approach [214], which also allows to use other criterions for superfluidity than the superfluid stiffness. Notice that estimates of z have a long history: it was argued that $z = d$ in [134], measured in $d = 2$ to be $z = 2 \pm 0.1$ in early Monte Carlo at integer filling [215], in strong coupling expansion $z = 1.93$ has been computed [216] and more careful Monte Carlo analysis find $z = 1.4$ [217].

In one dimension, the renormalization group again leads to a finite disorder fixed point, yet with a Kosterlitz-Thouless transition where the typical length and time diverge as $\xi, \tau \sim e^{\alpha/\sqrt{\Delta}}$ [218]. The Luttinger parameter, characterizing the transition, goes from a weak randomness transition $K = 3/2$ found in [202] to a large randomness regime with continuously varying $K > 3/2$ [219, 220].

In the following, we apply the cavity method to this problem with methods inspired from [221], and study the phase diagram, the nature of the superfluid to insulator transition and the large tails of the superfluid distribution. This contribution is a substantial extension of previous mean-field type analysis of [222]. Indeed, their method is akin to the numerical population dynamics study of equation (5.11), whereas we derive a analytical expression for the phase boundary. Furthermore, the method we use allows to show analytically that the superfluid to insulator transition is of infinite disorder type on part of the transition line, a rather surprising feature which was not expected or even suspected. We also evaluate various critical exponents and relate them to the large tails of the susceptibility distribution.

1. The average is the connected correlation $\langle AB \rangle_c = \langle AB \rangle - \langle A \rangle \langle B \rangle$

5.1.2 From the quantum cavity method to the cavity mean-field equations

Studying problems on the Bethe lattice is a standard, recent way to provide advanced mean-field theory approximations. The Bethe lattice is a tree with constant branching ratio K, depicted in figure 5.2, generally constructed such that each site has the same number of neighbors as in a hypercubic lattice of dimension d, so that $K = d - 1$. In the tree geometry, many exact or approximate solutions have been developed. For a classical system without disorder, the Bethe-Peierls method [223] solves the model on a tree. It is also called the *cavity* approach and has been used to solve the spin glass on the Bethe lattice [224], a model for which a one step replica symmetry breaking solution was lacking. The cavity method has then been extended to the quantum case [225, 226] and applied to the Bose-Hubbard model [227]. The quantum cavity method requires Monte Carlo techniques to sample configurations. Approximate techniques were devised to study disordered supraconductors [228] and obtain analytical results, in a problem where direct numerical simulations would be close to impossible. Our goal is to understand the consequences of such an approach in the Bose-Hubbard model with disorder on a Bethe lattice. The Hamiltonian we consider is:

$$\hat{H} = \sum_i -\mu\hat{n}_i + \epsilon_i\hat{n}_i + \frac{U}{2}\hat{n}_i(\hat{n}_i - 1) - J\sum_{\langle ij\rangle}\left(\hat{b}_i^\dagger\hat{b}_j + \hat{b}_j^\dagger\hat{b}_i\right) \tag{5.5}$$

The energy is measured in units of U (we set $U = 1$), and the site-dependent noise ϵ_i has a flat distribution $P(\epsilon) = \Theta(|\epsilon| - \Delta/2)/\Delta$.

In the quantum cavity method, in the Fock representation [227], the basic variable is the history of the occupation numbers of a site $n_i(\tau)$ as a function of imaginary time $\tau \in [0, \beta[$. Any observable of interest is obtained from the probability distribution over histories $\eta[n_i(\tau)]$ on each site.

The distribution functions $\eta[n_i(\tau)]$ are computed by recursion along the branches of the tree, starting from the leafs and going up to the root. A step of the recursion is shown in figure 5.3. The cavity mapping relates $\eta[n_0(\tau)]$ on site 0 to the distribution of lower neighbors on the tree $i \in 1 \dots K$ through a functional equation which include sums over paths $\mathbf{n}_i = n_i(\tau)$:

$$\eta[\mathbf{n}_0] = \sum_{\mathbf{n}_1,\dots,\mathbf{n}_K} \eta[\mathbf{n}_1]\dots\eta[\mathbf{n}_K]w(\mathbf{n}_0, \mathbf{n}_1, \dots, \mathbf{n}_K) \tag{5.6}$$

This functional equation can only be solved using Monte-Carlo sampling. In the pure Bose-Hubbard model, it has been demonstrated that this approach allows to compute all quantities on the Bethe lattice with arbitrary precision [227].

However, the full cavity method would be very heavy in a disordered model, requiring to handle a distribution of the distributions $P(\eta[n_i])$ for reasons that will be clear later. Instead of the full cavity recursion, following the steps of Ioffe, Mézard [228], we use an approximation scheme based on a single, time independent variable Ψ_i representing a superfluid coupling

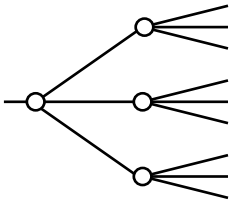

Figure 5.2: A part of the Bethe lattice with connectivity $K = 3$.

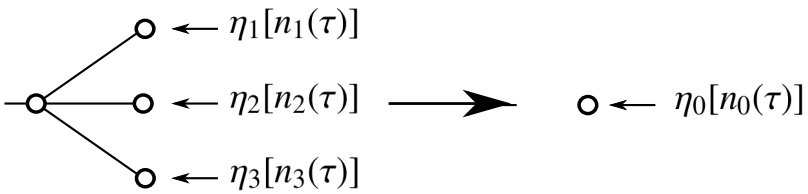

Figure 5.3: Representation of the quantum cavity recursion. The functional $\eta_0[n_0(\tau)]$ on site 0 is obtained from the functional $\eta_i[n_i(\tau)]$ of branches 1,2,3 further in the tree.

$-\hat{b}_i\Psi_i^\dagger$ + h.c.. This choice is sensible since the superfluid order is the physical quantity which we are most interested in. Although approximate, this same simplification yields good results in the quantum Ising model with random fields [221], and captures the essence of the effect of disorder.

The cavity recursion is defined in the following way. The effective cavity Hamiltonian for the vertex 0 is the one with the root link cut and nearest neighbors with field Ψ_i, as depicted in figure 5.4:

$$\begin{aligned}\hat{H}_{\text{full cav}} = &\sum_{i=0,1,\ldots,K}\left(-(\mu+\epsilon_i)\hat{n}_i + \frac{U}{2}\hat{n}_i(\hat{n}_i-1)\right)\\ &- J\sum_{i=1,\ldots,K}\left(\hat{b}_i\hat{b}_0^\dagger + \hat{b}_i^\dagger\hat{b}_0\right) - J\sum_{i=1,\ldots,K}(\Psi_i\hat{b}_i^\dagger + \text{h.c.})\end{aligned} \tag{5.7}$$

The recursion consists in integrating out the sites $1\ldots K$ neighboring 0, and to account for their influence on site 0 by an effective field Ψ_0:

$$\hat{H}_{\text{cav }0} = -(\mu+\epsilon_0)\hat{n}_0 + \frac{U}{2}\hat{n}_0(\hat{n}_0-1) - J\left(\Psi_0\hat{b}_0^\dagger + \Psi_0^\dagger\hat{b}_0\right) \tag{5.8}$$

A natural way to fix the recursion between Ψ_0 and the Ψ_i's is to impose

$$\langle\hat{b}_0\rangle_{\text{cav }0}(\Psi_0) = \langle\hat{b}_0\rangle_{\text{full cav}}(\{\Psi_i\}) \tag{5.9}$$

where we emphasize the dependencies on Ψ_i's. This relation being still too complicated for an analytical evaluation, we use a further approximation called the cavity mean-field approximation [221]. The average over the full Hamiltonian in the recursion (5.9) is replaced by the

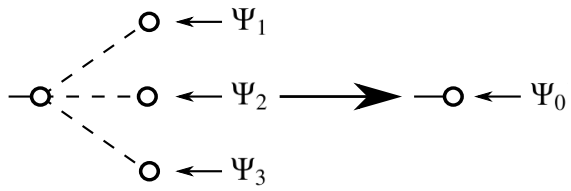

Figure 5.4: Pictorial representation of the cavity mean-field recursion. On the left-hand, the effective Hamiltonian is $\hat{H}_{\text{full cav}}$ from equation (5.7) for the full cavity recursion (5.9) (and $\hat{H}_{\text{m.f. cav}}$ from (5.10) for the mean-field cavity recursion (5.11)). On the right-hand side, after the mapping, the Hamiltonian is $\hat{H}_{\text{cav 0}}$ from (5.8).

average over:

$$\hat{H}_{\text{m.f. cav}} = -(\mu + \epsilon_0)\hat{n}_0 + \frac{U}{2}\hat{n}_0(\hat{n}_0 - 1) - J \sum_{i=1,\dots,K} \left(\langle \hat{b}_i \rangle_{\text{cav i}} \hat{b}_0^\dagger + \langle \hat{b}_i^\dagger \rangle_{\text{cav i}} \hat{b}_0 \right) \tag{5.10}$$

where the link between 0 and its neighbors was cut, and accounted for by its average effect on site 0 through $\hat{b}_i \to \langle \hat{b}_i \rangle_{\text{cav i}}$. The self-consistent equation (5.9) implies, comparing (5.8) and (5.10):

$$\Psi_0 = \sum_i \langle \hat{b}_i \rangle_{\text{cav i}}(\epsilon_i, \Psi_i) \tag{5.11}$$

The recursion cavity mean-field recursion (5.11) is of stochastic nature, and defines a stationary distribution of fields $P(\Psi)$ which satisfies:

$$P(\Psi) = \int \prod_i \mathrm{d}\epsilon_i \mathrm{d}\Psi_i P(\Psi_i)\, \delta\left(\Psi - \sum_i \langle \hat{b}_i \rangle_{\text{cav i}}(\epsilon_i, \Psi_i) \right) \tag{5.12}$$

Since the recursion (5.11) is real, the common complex argument of all Ψ's can be chosen real positive.

The mean-field recursion (5.11) and the self-consistent probability distribution (5.12) will be our main tools to study the phase diagram and critical properties. For instance, the superfluid phase will be characterized by nonzero Ψ's distribution $P(\Psi) \neq \delta(\Psi)$.

As we will see, despite the numerous simplifications needed to arrive at (5.11), it yields almost the same physics as the full recursion (5.9), as it has been found in the Ising model [229]. A less drastic approximation is studied in section 5.2 and confirms that the cavity mean field gives a good description of the superfluid to insulator transition on the Bethe lattice.

Notice that the naive mean-field consists in taking Ψ as a number and to neglect its distribution. The limit of infinite dimension of Fisher [134] or the finite-temperature analysis [230] are approximations of this type. In those cases, the Bose glass phase is not found at all, and the formalism only reproduces our results in the replica symmetric regime.

Besides, the full recursion on the probability distribution (5.12) has already been studied [222] by population dynamics, which the authors called the stochastic mean-field. As a consequence, the phase diagram that they obtain is the same as ours [2]. However, our analysis of (5.9) sheds light on the nature of the problem with the identification of a replica symmetry breaking regime, and allows to derive analytical results on the critical behavior and the large tails of the distribution. Moreover, we test the robustness of the method by studying the cavity recursion beyond cavity mean-field.

5.1.3 Mapping to directed polymers

In this section, we show how to cast the problem of studying the onset of superfluidity from equation (5.11) upon the computation of a classical partition function of polymers, a method introduced in [228].

At the onset of superfluidity, the fields Ψ are small and first order perturbation theory is sufficient. The recursion (5.11) reads:

$$\Psi_0 = \sum_i JG(U, \epsilon_i, \mu)\Psi_i \tag{5.13}$$

where $G(U, \epsilon, \mu)$ is shown in section 5.1.5.

To distinguish between the superfluid and insulating phases, it is convenient to look at the response of the system to a small superfluid field. For a Bethe lattice geometry, after applying a small superfluid field Ψ_b at the boundary, the field Ψ_0 at the root can be computed by recursive application of (5.13):

$$\Psi_0 = \sum_P \prod_{i \in P} JG(U, \epsilon_i, \mu)\Psi_b \tag{5.14}$$

where P denotes paths along the tree from the boundary b to the root 0. It turns out that this expression is formally equal to the partition function of a directed polymer with Boltzmann factors [3] $e^{-\beta E_i} = JG(\epsilon_i, U, \mu)$.

$$Z = \frac{\Psi_0}{\Psi_b} = \sum_P \prod_{i \in P} e^{-\beta E_i} \tag{5.15}$$

Following Cook, Derrida [231] the logarithm of the partition function is self-averaging and is easily computed using the replica trick. We prove a more general version of this result later in

2. Actually, it is not since the cavity method sets $K = d - 1$ whereas the recursion in mean-field is the same as (5.12) but with $K = d$.

3. The temperature β of the Boltzmann factor is not related to the temperature of the system.

section 5.2.2. For the time being we just state it and comment it:

$$\frac{1}{L}\overline{\ln\left(\frac{\Psi_0}{\Psi_b}\right)} = \frac{1}{L}\overline{\ln Z} = \min_{x\in[0,1]} f(x) = -\xi^{-1} \tag{5.16}$$

$$f(x) = \frac{1}{x}\ln\left(K\overline{G(U,\epsilon,\mu)^x}\right) + \ln J \tag{5.17}$$

The above equation should be understood as follows. The typical length of decay/increase of superfluidity is determined by the amplitude and sign of ξ:

$$\frac{\Psi_0}{\Psi_b} \overset{\text{typ}}{\sim} e^{-L/\xi} \tag{5.18}$$

A positive ξ is found in the insulating phase, where superfluidity cannot propagate into the system, and reciprocally $\xi < 0$ is an indicator of the superfluid phase. The superfluid order is predicted to diverge exponentially with distance by the result (5.16), however nonlinear corrections to (5.13) stabilize the average Ψ to a finite, positive value.

In the language of the replica method, the partition function is replica symmetric if the minimum of equation (5.16) is obtained for $x_{\min} = 1$ (when $f'(1) < 0$). Alternatively, the solution breaks replica symmetry for $x_{\min} < 1$.

The physics of this replica symmetry breaking may be understood as follows. On the one hand, when replica symmetry is preserved, most of the paths contribute to the quenched average of the partition function (5.16). On the other hand, when replica symmetry is broken, the quenched average is dominated by a few rare paths. In terms of the bosonic system, close to the phase boundary, one can say that superfluidity is established through most of the paths at the replica symmetric (RS) transition, whereas a few paths contribute to the onset of superfluidity at the replica symmetry breaking (RSB) transition.

This qualitative picture is supported by the properties of the partition function. In the replica symmetric phase, one can show that Z, which is a random variable, has a trivial distribution in the thermodynamic limit $P(Z) = \delta(Z - Z_0)$ (a consequence of the fact that all paths contribute roughly equally) such that the annealed $L^{-1}\ln\overline{Z}$ and quenched $L^{-1}\overline{\ln Z}$ averages are equal. It means that the typical realizations of the disorder yield the dominant contributions. Alternatively, in the replica symmetry breaking phase, $P(Z)$ is wide (since only a few paths contribute) but $L^{-1}\ln Z$ is self-averaging [4]. In this case, annealed and quenched averages are different, which indicates that rare realizations of the disorder have significant contributions.

5.1.4 Superfluid to insulator transition

We can now study the insulator to superfluid transition from the typical propagation in the system of an applied superfluid field given by (5.16). One can actually find an explicit equation

4. We recall for definiteness that a stochastic quantity x is called self-averaging if it has a deterministic, unique value $P(x) = \delta(x - x_0)$ in some limit.

for $J_c(\mu, U)$. Indeed, the criterion for replica symmetry breaking is $f'(1) = 0$, which yields:

$$f'(x) = -\frac{1}{x^2} \ln\left(K\overline{G^x}\right) + \frac{1}{x} \frac{\overline{(\ln G) G^x}}{\overline{G^x}} = 0 \tag{5.19}$$

Notice that $f'(x)$ is independent of J. As a consequence, $x_{\min}$ and thus the RS/RSB nature of the solution are independent of J [5]. As a consequence, an analytical expression can be obtained for the insulator to superfluid boundary $J_c(T, \mu, U)$, characterized by $\xi^{-1} = 0$. It is expressed in terms of $x_{\min}$ as:

$$J_c = \exp\left[-\frac{1}{x} \ln\left(K\overline{G(U, \epsilon, \mu)^x}\right)\right]_{x=x_{\min}} \tag{5.20}$$

This expression yields the exact phase boundary within the cavity approximation, since the linearization in Ψ from (5.11) to (5.13) is exact at the transition where $\Psi \ll 1$.

Notice that we do not yet specify the nature of the insulating phase for $J < J_c$, because the only stationary point for the distribution of fields in the insulating phase is the trivial distribution $P(\Psi) = \delta(\Psi)$, as has been remarked in a numerical study [222] of the recursion (5.13). Hence we postpone the discussion of the nature of insulating phases to section 5.6.1.

5.1.5 Zero temperature phase diagram

Given the explicit expression for the critical coupling J_c (5.20), all that is left to obtain the superfluid to insulator phase boundary is to compute the function $G(y = \mu - \epsilon)$ from (5.11) at linear order in perturbation theory. At zero temperature, one finds

$$G(y = \mu - \epsilon) = \frac{1 + y}{(p - y)(y - (p - 1))} \tag{5.21}$$

where $p = \lfloor y \rfloor + 1$ is [6] the filling number on site i of the ground state in the atomic limit. Let us now describe the phase diagram obtained from (5.20) and (5.21) for various disorder amplitude. We choose $K = 5$ to aim at describing three-dimensional lattices, where the mean-field cavity method results apply up to 10 to 20% [227] and always overestimate superfluidity.

- In the pure Bose-Hubbard model at $\Delta = 0$, the replica symmetry is preserved and (5.20) yields the familiar (cavity) mean-field phase boundary of figure 5.5, which is closely related to standard mean-field calculations of the phase diagram [134] except that the connectivity z entering the mean-field equation is replaced by $K = z - 1$, which arguably yields a better approximation [229].

5. The J-dependency is restored beyond the linearization (5.13), but these corrections are negligible at the transition where $\Psi \ll 1$.

6. $\lfloor x \rfloor$ is the integer part of x.

- At intermediate values of the disorder as in figure 5.6, the insulating lobes are significantly reduced, hence superfluidity is actually favored by disorder in these regions. On the contrary, we see that the low J regions between the lobes is insulating, i.e. superfluidity in these regions is quickly destabilized by disorder.

  This nontrivial dependency is a result of the interplay of two phenomenon: one consequence of the disorder is to tend to localize bosons and thus deplete superfluidity. Yet it also reduces the effect of strong interactions, allowing for resonant tunneling between neighboring sites and thus depleting the Mott insulator phase and favoring the onset of superfluidity. This nontrivial interplay is manifest in the multiple re-entrances of the superfluid as a function of Δ at fixed μ, shown in figure 5.7 (right panel).

  With respect to the stochastic mean-field where the same phase diagram is obtained [222], the new feature that we obtain is the RS nature of the transition, which is replica symmetric on the lobes and replica symmetry breaking in the inter-lobes regions, as shown in figure 5.6. The replica symmetry parameter $x_{\min}(\mu)$ of figure 5.7 (left panel) changes quite fast at the RS to RSB transition, but it is continuous [7].

  Let us recall that the physical meaning of the RSB transition is that superfluidity flows through a few paths with atypical realization of disorder, unlike at the RS transition. As we shall see in the following, this has consequences on the critical properties of the respective transitions.

- At large disorder $\Delta \gtrsim 1$, the insulating lobes and the replica symmetric phase shrink with growing Δ until they disappear completely, like for $\Delta = 1.2$ in figure 5.8, where the phase transition is always RSB. Notice that the insulator to superfluid transition occurs at a scale $J \sim 0.005$, one order of magnitude smaller than at small disorder in figure 5.6. The replica parameter $x(\mu)$ and of the critical coupling $J_c(\mu)$ still have sudden jumps as a function of μ. These jumps are similar to those at small disorder, which we discuss in the following section.

5.1.6 RS/RSB transitions

After this global, qualitative description of the phase diagram, we study in more detail the RS to RSB transition at intermediate disorder $\Delta \lesssim 1$. It is the point where both the replica parameter $x_{\min}$ drops and where the critical hopping J_c stabilizes suddenly with μ, a striking feature of the phase diagram.

For definiteness, we focus on the range $1/2 < \mu < 1$ where $p = 1$, the upper part of the first lobe of figure 5.6. The condition for replica symmetry breaking is that the minimum of $f(x)$ should be less than one, with $f(x)$ is obtained from (5.21) and (5.17):

$$f(x) = \frac{1}{x} \ln \left(K \int_{-\Delta/2}^{\Delta/2} \frac{\mathrm{d}\epsilon}{\Delta} \left(\frac{1+\mu-\epsilon}{(1-\mu+\epsilon)(\mu-\epsilon)} \right)^x \right) + \ln J \tag{5.22}$$

7. The minimum $x_{\min}(\mu)$ from (5.16) can not be discontinuous with μ when $f(x)$ is convex, which is the case here.

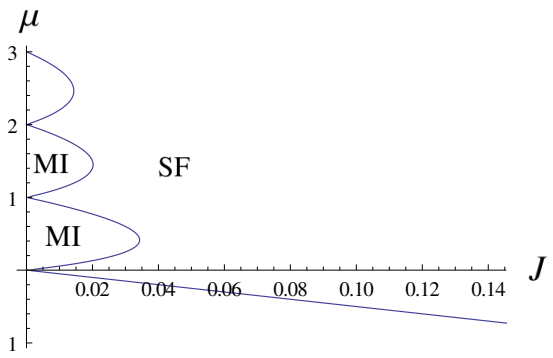

Figure 5.5: Phase diagram for $\Delta = 0$, $K = 5$. For large J, superfluid phase (SF). For low J, lobes of Mott insulating phase (MI) with density $n = 0, 1, 2, 3, \ldots$ from the bottom to the top.

Equation (5.22) has a singularity of the form $1/(1-\mu+\epsilon)^x$ causing $f(x = 1)$ to diverge whenever $\epsilon_0 = \mu - 1$ is within the integration range $[-\Delta/2, \Delta/2]$, i.e. when $\mu > \mu_* = 1-\Delta/2$. The physical origin of this divergence is the resonance between energy levels of two neighboring sites of different filling number, in perturbation theory in J.

In the regime $\mu > \mu_* = 1 - \Delta/2$, both $f(0)$ and $f(1)$ are infinite and $f(x)$ is finite for $0 < x < 1$, hence there is necessarily replica symmetry breaking. Actually, the RS/RSB transition occurs before $f(1)$ is infinite, at some transition point $\mu_{\mathrm{RS/RSB}} = \mu_* - \delta_s$. For $\Delta = 0.5$, we have computed $\delta_c = 0.0002684$ from numerical minimization of 5.22. This δ_c is much smaller than all other scales of the problem $\Delta = 1/2$, $\mu_* = 3/4$ and $J_c \sim 0.05$. A direct estimation of $f(x)$ is given in appendix 5.A.1 and the phase diagram in this region is shown in figure 5.14.

As we already pointed out above, the point μ_* where $f(1)$ diverges corresponds to a resonance in perturbation theory in J (or in Ψ) between neighboring sites of same energy but distinct filling. This only occur when there are two degenerate ground states in the unperturbed $J = 0$ Hamiltonian.

It is indeed clear that the ground state, in the atomic limit, is $|\psi\rangle = \otimes_i |n_i = p\rangle$ for $\mu < \mu_*$ and a mixture of $|n_i = p\rangle$ and $|n_i = p+1\rangle$ for $\mu > \mu_*$. This is actually the trivial Mott insulator to Bose glass transition at $J = 0$.

Let us emphasize though that the RS/RSB transition is a characteristic of the *superfluid to insulator* transition.

5.1.7 Finite temperature

The occurrence of RSB transition at zero temperature raises the question of its existence at finite temperature. This question is rather easy to answer, since the recursion (5.14) is the

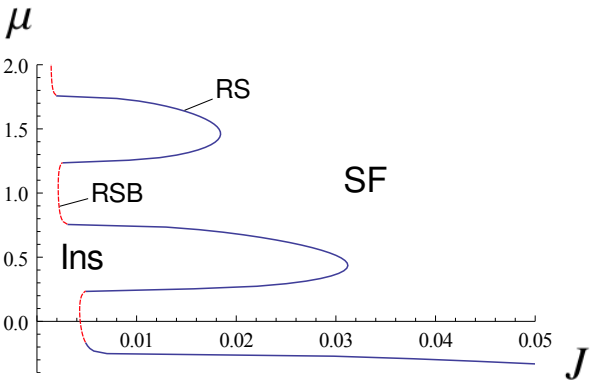

Figure 5.6: Phase diagram for $\Delta = 0.5$, $K = 5$: The blue line is the transition from a superfluid (SF) to insulating phases (Ins). The nature of the insulating phase is not determined by the recursion (5.16). The replica symmetric (RS) or replica symmetry breaking (RSB) nature of the transition is also indicated, the former occurring on the lobes, the later in the inter-lobes region.

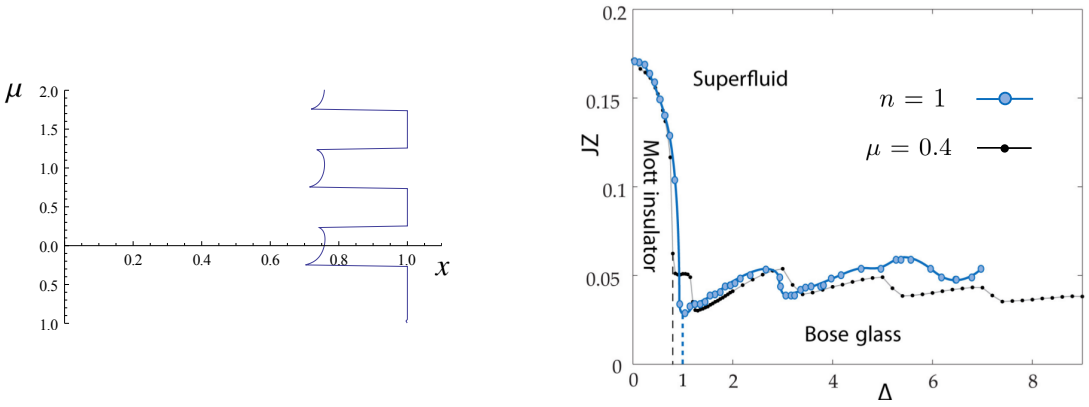

Figure 5.7: Left panel: RSB parameter x as a function of μ for $\Delta = 0.5$, $K = 5$. The RS (resp. RSB) transition is characterized by $x = 1$ (resp. $x < 1$). Notice the fast jumps of x at the RS/RSB transition, explained in section 5.1.6. Right panel: Adapted from [222], $\{\Delta, J\}$ phase diagram at fixed density $n = 1$ and fixed $\mu = 0.4$. The reentrance of the superfluid phase with growing Δ is characteristic of the nontrivial interplay between disorder and superfluidity.

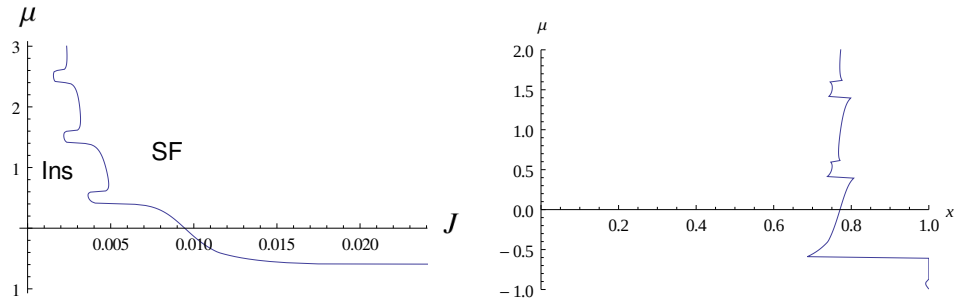

Figure 5.8: Left panel: phase diagram for $\Delta = 1, 2$, $K = 5$. Phase transition from superfluid (SF) to insulating phase (Ins). The order of magnitude of J_c is smaller than in figure 5.6. The remaining structure of lobes is obtained after complete "melting" of the lobes of figure 5.6. Right panel: RSB parameter x as a function of μ. Observe that the transition is RSB ($x < 1$) for all μ, but that $x(\mu)$ still has fast jumps of the type described in section 5.1.6.

same as before with a new $G(\epsilon, \mu, \beta)$ computed in the same way:

$$G(\epsilon, \mu, \beta) = \frac{1}{\sum_n e^{-\beta E_n}} \sum_n n \frac{e^{-\beta E_{n-1}} - e^{-\beta E_n}}{E_n - E_{n-1}} \tag{5.23}$$

where $E_n = -\mu n + \epsilon n + \frac{1}{2} n(n-1)$ is the atomic limit energy. Without disorder, the phase diagram has two phases, a correlated gas phase corresponding to the Mott insulating phase at $T = 0$, and a superfluid phase which undergoes a finite-T transition to correlated gas at some critical temperature $T_c(U, J)$. We will not analyze the finite temperature phase diagram thoroughly. It is clear that the RSB transition is still present at least at very small temperatures $T \lesssim \delta_c$, a result shown in appendix 5.A.2.

5.2 Beyond the cavity mean-field approximation

5.2.1 Effective cavity mapping

The mean-field cavity is very convenient to obtain analytical results, but one can question whether it is very representative of the physics of the full cavity recursion (5.7).

To improve on the previous approximation, we devise a new, more accurate approximation for (5.7). The most simple approximation beyond cavity mean-field is to make the approximation $\hat{b}_i \to \langle \hat{b}_i \rangle_{\text{cav i}}$ on neighbors $2 \dots K$ of 0 but the site 1, which we treat exactly. The effective Hamiltonian is:

$$\begin{aligned} \hat{H}_{\text{eff cav}} = &- (\mu + \epsilon_0)\hat{n}_0 + \frac{U}{2}\hat{n}_0(\hat{n}_0 - 1) - (\mu + \epsilon_1)\hat{n}_1 + \frac{U}{2}\hat{n}_1(\hat{n}_1 - 1) - J\left(\hat{b}_1 \hat{b}_0^\dagger + \hat{b}_1^\dagger \hat{b}_0\right) \\ &- J\left(\hat{b}_1 \Psi_1^\dagger + \hat{b}_1^\dagger \Psi_1\right) - J \sum_{i=2,\dots,K} \left(\langle \hat{b}_i \rangle_{\text{cav i}} \hat{b}_0^\dagger + \langle \hat{b}_i^\dagger \rangle_{\text{cav i}} \hat{b}_0\right) \end{aligned} \tag{5.24}$$

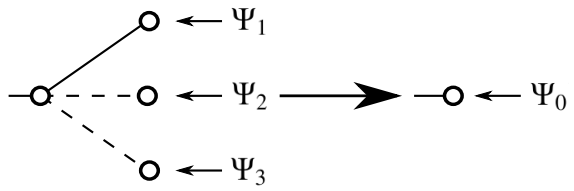

Figure 5.9: Pictorial representation of the partial cavity effective recursion. Unlike in figure 5.4, on the left-hand part, the bond between site 0 and 1 is full, meaning that the bond is included in the effective Hamiltonian $\hat{H}_{\text{cav eff}}$ of (5.24). On the right-hand side, the Hamiltonian is $\hat{H}_{\text{cav }0}$.

and is shown pictorially in figure 5.9. The effective recursion is again

$$\langle \hat{b}_0 \rangle_{\text{cav }0}(\Psi_0) = \langle \hat{b}_0 \rangle_{\text{eff cav}}(\{\Psi_i\}) \tag{5.25}$$

Notice that the choice of the site 1 to treat exactly is a priori arbitrary, but we can optimize it on physical grounds. Indeed, we noticed that the RSB transition is related to resonances between two sites with neighboring energies. These divergences being the result of first order perturbation theory, one may question the validity of the results. To address this concern, with the Hamiltonian (5.24), we will be able to treat two resonating site exactly (by diagonalization), i.e. at all orders in J. Thus, we chose the vertex 1, for a given realization of disorder, as the vertex of smallest $|\epsilon_i - \epsilon_0|$ among the K neighbors of 0.

We now wish to extend the express the recursion relation (5.25) on fields at linear order in Ψ. This can not be done analytically, since it involves a solution of the two-site Hamiltonian (5.24) without fields. This is instead done by diagonalization, and the recursion may be put under the general form:

$$\Psi_0 = \sum_{i \neq 1} H^{(a)}(\epsilon_0, \epsilon_1, \epsilon_i)\Psi_i + H^{(b)}(\epsilon_0, \epsilon_1)\Psi_1 \tag{5.26}$$

where there are two recursion functions $H^{(a/b)}$ because of the different treatment of site 1 and sites $2 \dots K$. The expression of $H^{(a/b)}$ in terms of eigenstates of (5.24) are derived in appendix 5.A.3.

5.2.2 Replica matrix formulation

As we will see, solving the recursion relation is more involved than what we have done in section 5.1.3.

As previously, we add a small boundary field Ψ_b, and see how superfluidity propagates to the root of the tree under recursion (5.26). For convenience, we label the sites with the distance to the root, going from L on leaves of the tree to 0 at the root. For a given path P, we call i a

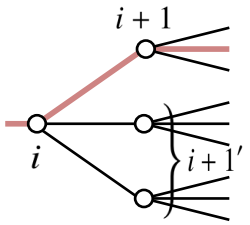

Figure 5.10: Labels of the sites on the tree. The red, thick links denote the considered path P.

site along the path, $i+1$ the next site on the path, and $i'+1$ *all* neighbors of i which are at a distance $i+1$ on the tree as in figure 5.10. With these notations,

$$\frac{\Psi_0}{\Psi_L} = \sum_P \prod_{i\in P} \exp\left\{-\beta E^{(i)}(\epsilon_i, \epsilon_{i+1}, \{\epsilon_{i'+1}\})\right\} \tag{5.27}$$

$$E^{(i)}(\epsilon_i, \epsilon_{i+1}, \{\epsilon_{i'+1}\}) = -\ln\left(H^{(a \text{ or } b)}(\epsilon_i, \epsilon_{i+1}, \{\epsilon_{i'+1}\})\right) \tag{5.28}$$

The energy distribution at site i is drawn from the distribution (b) (resp. (a)) if the disorder on the site $i+1$ of the chain is (resp. is *not*) the closest in energy to ϵ_i among all other neighbors $i'+1$.

The following complications appear, with respect to the cavity mean-field (5.14):

- There are two possible distributions (a/b) of energies on the tree.
- The local energies depend of disorder on site i *and* on its neighboring sites $i+1$ and $\{i'+1\}$.

Let us now try to evaluate the quenched averaged superfluid susceptibility using the replica trick:

$$\overline{\ln\left(\frac{\Psi_0}{\Psi_L}\right)} = \lim_{n\to 0} \frac{\overline{\left(\sum_P \prod_{i\in P} \exp\left\{-\beta E^{(i)}(\epsilon_i, \epsilon_{i+1}, \{\epsilon_{i'+1}\})\right\}\right)^n} - 1}{n} \tag{5.29}$$

Assuming that one-step replica symmetry breaking yields the exact solution [8], the dominant contribution comes from n/m groups of size m among the n replicas, using the abbreviation $\epsilon_i \to i$, $\epsilon_{i+1} \to i+1$ and $\{\epsilon_{i'+1}\} \to i'+1$:

$$\overline{\left(\frac{\Psi_0}{\Psi_L}\right)^n} \sim K^{nL/m} \overline{(H_{0,1,1'} H_{1,2,2'} \dots H_{L-1,L,L'})^m}^{n/m} \tag{5.30}$$

The above expression is best understood, if one writes averages over disorder explicitly:

$$\overline{(H_{0,1,1'} H_{1,2,2'} \dots H_{L-1,L,L'})^m} = \int \frac{\mathrm{d}0\mathrm{d}1\mathrm{d}1' \dots \mathrm{d}L\mathrm{d}L'}{\Delta\Delta^K \dots \Delta^K} H^m_{0,1,1'} H^m_{1,2,2'} \dots H^m_{L-1,L,L'} \tag{5.31}$$

8. In the previous case, the one step replica symmetry breaking solution (5.16) is exact [231].

One can realize that this may be solved by a recursion, going towards the root of the Bethe lattice, calling the partial integral on sites at distance equal or larger than $i+1$:

$$J_i(\epsilon_i) = \int \frac{\mathrm{d}(i+1)\mathrm{d}(i'+1)\dots\mathrm{d}L\mathrm{d}L'}{\Delta\Delta^K\dots\Delta^K} H^m_{i,i+1,i'+1}\dots H^m_{L-1,L,L'} \tag{5.32}$$

and remarking that J_i obeys a recursion equation:

$$J_i(\epsilon_i) = \Delta^{-K}\int \mathrm{d}(i+1)\mathrm{d}(i+1)' H^m_{i,i+1,i'+1} J_{i+1}(\epsilon_{i+1}) \tag{5.33}$$

$$= \int \mathrm{d}(i+1) M_{\epsilon_i,\epsilon_{i+1}} J_{i+1}(\epsilon_{i+1}) \tag{5.34}$$

The problem is now cast upon an eigenvalue problem, because this recursion is essentially a matrix product (in the continuous space of ϵ_i's) with matrix elements

$$M_{\epsilon_i,\epsilon_{i+1}} = \Delta^{-K}\int \mathrm{d}(i+1)' H^m_{i,i+1,i'+1} \tag{5.35}$$

The replica average is dominated by its largest eigenvalue [9] $\lambda(m)$ (a function of m)

$$\overline{\left(\frac{\Psi_0}{\Psi_L}\right)^n} \sim K^{nL/m}(M_{\epsilon_0,\epsilon_1}\dots M_{\epsilon_{L-1},\epsilon_L})^{nL/m} \tag{5.36}$$

$$\sim K^{nL/m}\lambda(m)^{nL/m} \tag{5.37}$$

and within the replica trick, the limit $n\to 0$, turns the $m\in[1,n]$ dependency into a minimizing parameter $x=m$ of range $x\in[0,1]$:

$$\frac{1}{L}\overline{\ln\left(\frac{\Psi_0}{\Psi_L}\right)} = \min_{x\in[0,1]}\lim_{n\to 0}\frac{1}{L}\frac{K^{nL/x}\lambda(x)^{nL/x}-1}{n} = \min_{x\in[0,1]}\frac{1}{x}\ln(K\lambda(x)) \tag{5.38}$$

Let us briefly summarize what the above formulation accomplishes.

- First, it is capable of solving a polymer partition function with several distribution of energies on different branches. This problem has been solved in [231] by a more direct approach, their proof is sketched in appendix 5.A.4. It can be directly shown that both solutions agree.
- Second, it allows to express the polymer partition function in cases where the energy depends on all neighboring energies.
- Last, the formulation still fits in the framework of replicas, preserving the intuitive physics of replica symmetry breaking.

9. In the large L limit, the boundary effects at sites 0 and L are largely irrelevant.

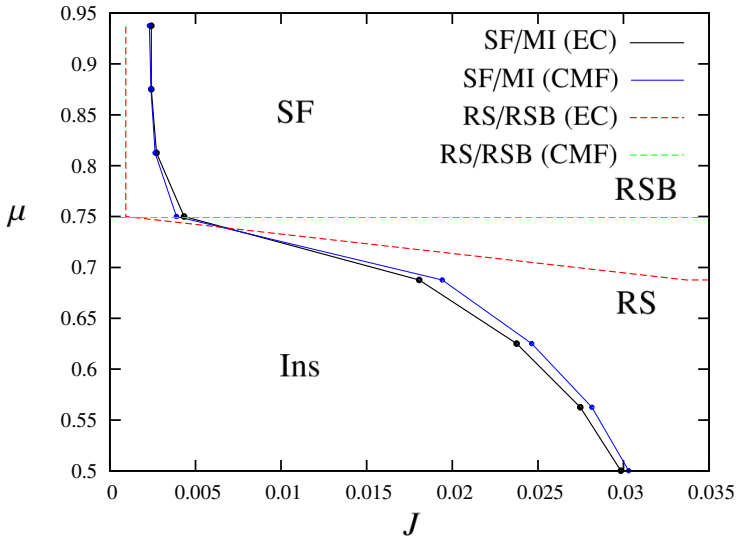

Figure 5.11: Phase diagram for the effective cavity mapping (5.25) at $K = 5$, $\Delta = 1/2$. The superfluid to insulator SF/MI transition is indicated, both within the effective cavity (EC) and cavity mean-field (CMF). Likewise, the RS/RSB transition is shown for both EC and CMF.

5.2.3 Phase diagram beyond cavity mean-field

The details of the numerical implementation of (5.38) are left to the appendix 5.A.5. For each x in the minimization of (5.38), the matrix $M_{\epsilon_n,\epsilon_{n+1}}$ is discretized, each element is computed and the discrete matrix is diagonalized. This is much more numerically involved compared to the cavity mean-field. Besides, the convergence with respect to the discretization step $\delta\epsilon \to 0$ is extremely impaired by singularities in $M_{\epsilon_n,\epsilon_{n+1}}$ — indeed, the same $1/(\epsilon_i - \epsilon_0)^x$ singularities seen in section 5.1.6 occur in the matrix.

Nevertheless, although good convergence is hard to reach, there are strong indications that the phase diagram is not very different from the cavity mean-field one, as shown in figure 5.11. The superfluid to insulator phase boundary is the same within a few percent, and the RS to RSB transition occurs at the same point.

These results are good indicators of the quality of the cavity mean-field approximation. A good agreement between cavity and cavity mean-field has also been found previously in the Ising model [229]. The new result is that there is a RS/RSB transition at small J in the inter-lobes regions.

In the following, we use again the cavity mean-field to have a closer look at critical properties, and how they are affected by the RS or RSB nature of the transition in section 5.3. Then, we study the superfluid susceptibility in the insulating phase to distinguish the Mott insulator from the Bose glass 5.4. Finally, we study critical properties of the susceptibility 5.5 and gather all the results to discuss the issue that they raise 5.6.1.

5.3 Critical superfluidity

In the previous sections, we have shown the phase diagram in cavity mean-field and beyond, and stressed that the superfluid to insulator transition was either of RS or RSB nature. Our next goal is to show how critical properties may be extracted from the cavity mean-field recursion, following the pioneering analysis [221]. We first focus on the growth of superfluid order at the transition.

5.3.1 Large tails of the field distribution

Before going into critical properties, we need to discuss properties of the field distribution at the transition, which will play an important role. As we shall see, the large tails of the probability distribution of the field are of power-law type [10] $P(\Psi) \sim 1/\Psi^{1+\mu}$ for $\Psi \gg 1$. We start from (5.12) and write the self-consistent relation on the distribution $P(\Psi)$ at linear order in Ψ:

$$P(\Psi) = \int \prod_i \mathrm{d}\epsilon_i \mathrm{d}\Psi_i P(\Psi_i)\ \delta\left(\Psi - \sum_i JG(\epsilon_i)\Psi_i\right) \tag{5.39}$$

Following [228], it is convenient to use the Laplace transform the probability distribution, to substitute :

$$\tilde{P}(s) = \int_0^\infty \mathrm{d}\Psi e^{-s\Psi} P(\Psi) \tag{5.40}$$

$$= \int \mathrm{d}\Psi \int \prod_i \mathrm{d}\epsilon_i \mathrm{d}\Psi_i P(\Psi_i)\ e^{-s\Psi}\ \delta\left(\Psi - \sum JG(\epsilon_i)\Psi_i\right) \tag{5.41}$$

$$\tilde{P}(s) = \left(\overline{\tilde{P}(JG(\epsilon)s)}\right)^K \tag{5.42}$$

To characterize the probability law for large fields, one must recall the expression of the Laplace transform in terms of moments of the distribution at small s:

$$\tilde{P}(s) = 1 - \langle\Psi\rangle s - \frac{1}{2}\langle\Psi^2\rangle s^2 + \dots \tag{5.43}$$

For a distribution with a power-law tail $P(\Psi) \sim 1/\Psi^{1+\mu}$ for large Ψ's, a non-analytic term $-as^\mu$ closes the expansion (all following terms with infinite moments $\langle\Psi^m\rangle$ with $m > \mu$ are absent). In the small s expansion, identifying order by order both sides of equation (5.42), the term of order s^μ yields:

$$1 = KJ^\mu \overline{G(\epsilon)^\mu} \tag{5.44}$$

$$\Leftrightarrow \mu f(\mu) = 0 \Leftrightarrow f(\mu) = 0 \tag{5.45}$$

10. The definition of the exponent μ is adopted for later convenience. Of course it is unrelated to the chemical potential, but this should not lead to confusion.

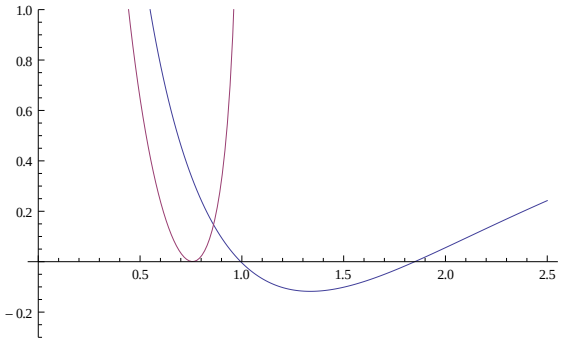

Figure 5.12: Shape of $f(x)$ at the phase transition in the RS and RSB regime. Blue curve: At the RS transition $\mu = 0.747$, $J_c = 0.0091$, $f(x = 1) = 0$ and $f(\mu_2) = 0$ with $\mu_2 > 1$. Red curve: At the RSB transition with $\mu = 1$ and $J_c = 0.00218$. $x_{\min} = 0.7577$ is the only zero of $f(x)$.

where $f(x)$ in (5.45) is defined in (5.17). Let us now comment on the value of μ at the transition. We recall that the critical condition is $f(x_{\min}) = 0$ on the RSB transition line, thus $\mu = x_{\min} < 1$. In the RS phase, the critical condition is $f(1) = 0$, thus $\mu_1 = 1$ is a solution, but there is a second solution $\mu_2 > 1$ as shown in figure 5.12 (indeed, $f'(1) < 0$, $f(1) = 0$ and $f(\infty) = \infty$). As we shall see in section 5.4, the tail of the distribution is actually governed by $\mu_2 > 1$.

5.3.2 Replica symmetric phase transition

After this preliminary analysis, the first critical property we want to understand is how the superfluid order parameter scales close to the quantum phase transition. In a conventional quantum phase transition, the typical field grows like a power law $\Psi_0 \sim (J - J_c(\mu))^\beta$.

For future reference, we write the general recursion (5.11) with a function $g(\epsilon_i, \Psi_i)$:

$$\Psi_0 = \sum_i g(\epsilon_i, \Psi_i) \tag{5.46}$$

As we will see, the exponent β has different values at the RS transition depending on whether $\mu > 3$ or $\mu < 3$. We consider the two cases separately.

- For $\mu > 3$, we first expand the general recursion relation on fields (5.11) at third order in the Ψ's, noticing that all even order contributions vanish because the bare Hamiltonian preserves the number of particles, and that the cubic contribution should be negative (to stabilize the exponential divergence in equation (5.18) for small fields):

$$\Psi_0 = \sum_i JG(\epsilon_i)\Psi_i - G_3(\epsilon_i)\Psi_i^3 \tag{5.47}$$

  The distribution of large fields at small distance from the critical point $\delta J = J - J_c << J_c$ inherit the property of the critical distribution, that is $P(\Psi) \sim \Psi_0^{-1}\Phi(\Psi/\Psi_0)$ where $\Psi_0(\delta J)$ is the typical field and $\Phi(X) \sim 1/X^{1+\mu}$ for large X, with the previous definition of μ (5.45).

In the replica symmetric phase, the typical field reads

$$\langle\Psi\rangle = \int \mathrm{d}\Psi\Psi P(\Psi) = \Psi_0 \int \mathrm{d}XX\Phi(X) \tag{5.48}$$

provided the first moment $\int dXX\Phi(X)$ is finite. The critical exponent β is found, averaging (5.47) and using (5.48) :

$$\langle\Psi\rangle = \Psi_0 \int \mathrm{d}XX\Phi(X) \tag{5.49}$$

$$= JK\overline{G(\epsilon)} \int \mathrm{d}\Psi P(\Psi)\Psi - K\overline{G_3(\epsilon)} \int \mathrm{d}\Psi P(\Psi)\Psi_j^3 \tag{5.50}$$

$$= JK\overline{G(\epsilon)}\Psi_0 \int dXX\Phi(X) - K\overline{G_3(\epsilon)}\Psi_0^3 \int dXX^3\Phi(X) \tag{5.51}$$

and using the critical replica symmetric condition from (5.20) $1 = J_c K\overline{G(\epsilon)}$ one obtains:

$$\left(1 - \frac{J}{J_c}\right)\Psi_0 \int \mathrm{d}XX\Phi(X) = -K\overline{G_3(\epsilon)}\Psi_0^3 \int dXX^3\Phi(X) \tag{5.52}$$

$$\Psi_0 = \left(\frac{\int \mathrm{d}XX\Phi(X)}{\overline{G_3(\epsilon)} \int dXX^3\Phi(X)}\right)^{1/2} \left(\frac{\delta J}{J_c}\right)^{1/2} \tag{5.53}$$

yielding the mean field exponent $\beta = 1/2$ as long as $\int dXX^3\Phi(X)$ is finite. This condition is not satisfied for $1 < \mu < 3$, which is still a RS transition.

- In the case $1 < \mu < 3$, the critical exponent is derived using the complete recursion (5.46) and the fact that only the tail of $P(\Psi) \sim \Psi_0^{-1}\Phi(\Psi/\Psi_0) \sim \Psi_0^{\mu}\Psi^{-1-\mu}$ contributes when $\Psi_0 \ll \Psi$:

$$\langle\Psi\rangle = \Psi_0 \int \mathrm{d}XX\Phi(X) = K \int \mathrm{d}\Psi P(\Psi)\overline{g(\epsilon,\Psi)} \tag{5.54}$$

$$\left(1 - \frac{J}{J_c}\right)\Psi_0 \int \mathrm{d}XX\Phi(X) = K \int \mathrm{d}\Psi P(\Psi)\overline{g(\epsilon,\Psi) - JG(\epsilon)\Psi} \tag{5.55}$$

$$= K\Psi_0^{\mu} \int \mathrm{d}\Psi\Psi^{-\mu-1}\overline{g(\epsilon,\Psi) - JG(\epsilon)\Psi} \tag{5.56}$$

Since the average $\langle\Psi\rangle$ is finite, so is the right-hand side of (5.56). Furthermore, all its Ψ_0 dependency is factorized, thus

$$\Psi_0 \sim \delta J^{\frac{1}{\mu-1}} \qquad \beta = \frac{1}{\mu - 1} \tag{5.57}$$

This scaling law holds as long as the average $\langle\Psi\rangle$ is finite, which is always true in the RS phase where $\mu > 1$. In the limit $\mu \to 1^+$, β diverges, indicating a drastic change of the nature of the phase transition. Indeed, we are going to show that the scaling is broken as we go into the RSB phase, and that the field develops exponentially slowly with δJ.

5.3.3 RSB Phase transition

As we have seen in section 5.3.1, the RSB phase is characterized by a heavy tail of the field distribution $P(\Psi) \sim 1/\Psi^{1+\mu}$ where $\mu = x_{\min} < 1$. Were the previous expression of $P(\Psi)$ exact for all Ψ, the average field $\langle\Psi\rangle$ would be infinite, which is an unphysical result. However, since (5.45) was obtained from a first order expansion in Ψ, we can assume that on the one hand, the heavy tail is indeed an important property of the system, but that on the other hand it is only valid below some cutoff scale [11] $\Psi \ll \Psi_m$. In the following, we make the hypothesis that the physics is driven by this low fields regime and not by extremely rare, large values of the field $\Psi \gtrsim \Psi_m$, and we simply set $P(\Psi > \Psi_m) = 0$.

As a consequence, the average field is [12]

$$\langle\Psi\rangle = \int_{\Psi_0}^{\Psi_m} \Psi \frac{\Psi_0^\mu}{\Psi^{1+\mu}} = \frac{1}{1-\mu}\left(\Psi_m^{1-\mu}\Psi_0^\mu - \Psi_0\right) \sim \frac{1}{1-\mu}\Psi_m^{1-\mu}\Psi_0^\mu \tag{5.58}$$

On the other hand, the marginally divergent average is

$$\langle\Psi^\mu\rangle = \int_{\Psi_0}^{\Psi_m} \Psi^\mu \frac{\Psi_0^\mu}{\Psi^{1+\mu}} = \Psi_0^\mu \ln(\frac{\Psi_m}{\Psi_0}) \tag{5.59}$$

In the following, we are going to evaluate the field Ψ_0 by an argument similar to the previous ones, but on the recursion equation for Ψ^μ, obtained from (5.46),

$$\langle\Psi^\mu\rangle = \left\langle\left(\sum_i g(\epsilon_i, \Psi_i)\right)^\mu\right\rangle \sim K\langle g(\epsilon,\Psi)^\mu\rangle \tag{5.60}$$

where we made the hypothesis that the dominant contribution to (5.60) comes from the largest term, which is true in the limit of large K due to the large tails of the distribution. To proceed, we need the following equality which holds trivially with the definition of J_c (5.20):

$$KJ^\mu\overline{G(\epsilon)^\mu}\int \mathrm{d}\Psi\Psi^\mu P(\Psi) = \left(\frac{J}{J_c}\right)^\mu \langle\Psi^\mu\rangle \tag{5.61}$$

Then, we use the previous expression for the recursion on Ψ^μ (5.60) and subtract (5.61):

$$\langle\Psi^\mu\rangle\left(1 - \left(\frac{J}{J_c}\right)^\mu\right) = K\int \mathrm{d}\Psi\Psi^\mu P(\Psi)\int \mathrm{d}\epsilon\left(\frac{g(\epsilon,\Psi)^\mu}{\Psi^\mu} - J^\mu G(\epsilon)^\mu\right) \tag{5.62}$$

11. In the Ising model [228], such a bound is already present at the level of the Hamiltonian. Here, there is no such natural bound. As a last resort, we can argue that large field values Ψ are present only at large filling numbers n which are not expected to alter the physics if truncated (one could say that at high filling number the Bose-Hubbard model is not valid anymore, e.g. because of three body collisions).

12. Since $\mu > 0$ is always positive (5.45), $\langle\,\Psi\,\rangle$ is always finite. The contrary would be surprising.

Then, we change make the change of variable $\epsilon = X\Psi$, $X \in [0, \infty[$, and write explicitly the singularities of G seen in section 5.1.6 as $G(\epsilon) = g(\epsilon)/(\epsilon - \epsilon_0)$.

$$\langle \Psi^\mu \rangle \left(1 - \left(\frac{J}{J_c}\right)^\mu\right) = K \int \mathrm{d}\Psi \Psi P(\Psi) \int \mathrm{d}X \left(\frac{g(X\Psi, \Psi)^\mu}{X^\mu} - J^\mu \frac{g(X\Psi)^\mu}{(X - \epsilon_0/\Psi)^\mu} \right) \tag{5.63}$$

The term on the right-hand side converges to a finite negative [13] value $-K\kappa(\mu)$ for small Ψ and thus using (5.58) and (5.59),

$$\Psi_0^\mu \ln(\frac{\Psi_m}{\Psi_0}) \left(1 - \left(\frac{J}{J_c}\right)^\mu\right) \sim -K\kappa(\mu) \frac{1}{1-\mu} \Psi_m^{1-\mu} \Psi_0^\mu \tag{5.64}$$

$$\Psi_0 \sim \Psi_m \exp\left(-\frac{J_c}{\delta J} \frac{K\kappa(\mu)}{\mu(1-\mu)} \right) \tag{5.65}$$

The growth of superfluidity at the transition is not a power-law as in a conventional phase transition. Instead, it has an essential singularity $\Psi^0 \sim \exp(-\frac{C}{\delta J})$ and grows slower than any power-law. This result valid at the RSB transition is in perfect agreement with the divergence of the exponent $\beta = \frac{1}{\mu - 1} \overset{\mu \to 1^+}{\to} \infty$ at the RS to RSB transition. This result has also been found and confirmed numerically by population dynamics [221] on the equivalent of our full recursion (5.46) in the Ising model.

5.4 Susceptibility in the insulating phases

In the insulating phase(s), the susceptibility under a small external superfluid field h may be computed along the same line as the fields in section 5.3.1. The linearized recursion relation (5.13) in presence of the external field reads:

$$\Psi_0 = \sum_i JG(\epsilon_i)\Psi_i + h \tag{5.66}$$

Calling the linear response $\chi = \Psi/h$, we use introduce the Laplace transform of its probability distribution, which satisfies the self-consistent equation:

$$\tilde{P}(s) = \int_0^\infty \mathrm{d}\chi e^{-s\chi} P(\chi) \tag{5.67}$$

$$= \int \mathrm{d}\chi \int \prod_i \mathrm{d}\chi_i \mathrm{d}\epsilon_i P(\chi_i)\, e^{-s\chi}\, \delta\left(\chi - \sum_i JG(\epsilon_i)\chi_i - 1\right) \tag{5.68}$$

$$= e^{-s} \left(\overline{\tilde{P}(JG(\epsilon)s)} \right)^K \tag{5.69}$$

13. The value is certainly negative, because the left-hand side of (5.63) is negative.

Again, the self-consistent equation (5.69) is expanded at small s: $\tilde{P}(s) = 1 - \langle\chi\rangle s - \ldots - as^{\mu}$. If $\mu > 1$, the average of χ is well defined, and identifying both sides of (5.69) at order s gives the value of $\langle\chi\rangle$:

$$\overset{\text{order } s}{\Rightarrow} \langle\chi\rangle = \frac{1}{1 - KJ\overline{G(\epsilon)}} = \frac{1}{1 - J/J_c} \tag{5.70}$$

We find that the average susceptibility $\langle\chi\rangle$ is divergent at the insulator to superfluid replica symmetric transition. Furthermore, the susceptibility is *not always finite* within the insulating phase and diverges for $J > J_\chi$ defined as:

$$J_\chi(\mu) = \left(K\overline{G(\epsilon)}\right)^{-1} \tag{5.71}$$

The line J_χ is shown in figure 5.14. It coincides with the RS superfluid boundary, but is distinct from the RSB superfluid boundary. As a consequence, the insulating region contains two phases, one with finite susceptibility which is the Mott insulator phase, and one with infinite susceptibility, the Bose glass phase.

The second information that we extract from equation (5.69) at order s^{μ} is valid in the whole insulating phase. It yields the exponent of the large tail of the probability distribution of susceptibilities $P(\chi) \sim 1/\chi^{1+\mu}$, which obeys:

$$1 = KJ^{\mu}\overline{G(\epsilon)^{\mu}} \Leftrightarrow f(\mu) = 0 \tag{5.72}$$

Notice μ obeys the same equation as (5.45). Therefore the solution μ of (5.72) yields the tails of the susceptibility distribution $P(\chi)$ in the insulating phase and at the transition, whereas it yields the tails of the field distribution $P(\Psi)$ in the superfluid phase close to the transition.

Equation (5.72) has several solutions both in the Bose glass phase and in the Mott insulator phase, as shown in figure 5.13. In the RS phase, the first solution is smaller than one, $\mu_1 < 1$, and the second is larger $\mu_2 > 1$. But the solution $\mu = \mu_1$ is not compatible with a finite average susceptibility found in (5.70), thus $\mu = \mu_2$ is the correct exponent [14]. By continuity, μ_2 is also governing the tail of $P(\chi)$ in the Bose glass phase.

The exponent μ governing the tails of the susceptibility is a function of the chemical potential μ and J. One can identify the "m-regions" in the insulating phase, where all moments $\langle\chi^{m'}\rangle$ with $m' \geq m$ are finite. In principle, m need not be an integer.

A particularly relevant region is the ∞-region, where all $\langle\chi^{m}\rangle$ are finite and where the distribution is not heavy-tailed. We call J_∞ the boundary of this region, defined as:

$$\lim_{\mu\to\infty} f_{J=J_\infty}(\mu) = 0 \tag{5.73}$$

14. A careful reader might argue that this argument is circular. A physical argument is that the exponent μ_1 predicts a diverging susceptibility in the whole insulating region even for arbitrary small disorder $\Delta \ll 1$, which is clearly unphysical since we expect most of the insulating phase to be a Mott insulator in this limit.

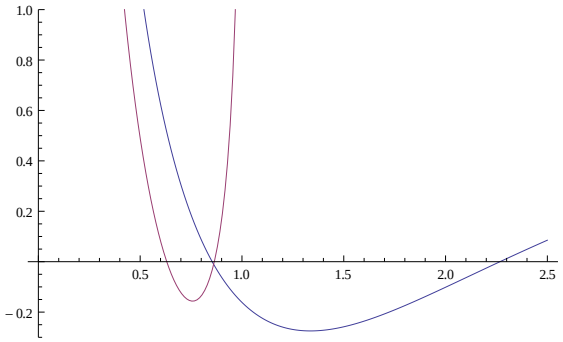

Figure 5.13: Shape of $f(x)$ at the phase transition in the RS and RSB regime. Blue curve: In the Mott insulator ($\mu = 0.747$, $J = 0.00778$) $f(\mu) = 0$ has two solutions $\mu_1 < 1$ and $\mu_2 > 1$. Red curve: In the Bose glass ($\mu = 1$, $J = 0.00186$), $f(\mu) = 0$ also has two solutions μ_1 and μ_2, both being less than 1. As explained in the text, in both cases the exponent governing the tails of susceptibility is the largest $\mu = \mu_2 > \mu_1$.

The integral in (5.17) is dominated by the maximum of the integrand $\max_\epsilon G(U, \epsilon, \mu)$, and one can show that J_∞ is:

$$J_\infty = \frac{1}{\max_\epsilon G(U, \epsilon, \mu)} \tag{5.74}$$

Another relevant region is the "3-region" where $\mu > 3$, since we have seen that this is a condition to have mean-field exponents at the superfluid transition in section 5.3.2. Again, this defines a transition line J_3 which we show in figure 5.15. This figure will be commented in detail in section 5.6.1.

After this description of the susceptibility in the insulating phase, we turn to its critical behavior when approaching the superfluid transition from the insulator side.

5.5 Critical susceptibility

5.5.1 Susceptibility around the transition

We now want to obtain the critical exponent which rules the divergence of the superfluid susceptibility around the critical point from the insulating side $\chi \sim \delta J^{-\gamma}$. In principle, we could use equation (5.70), but we want to check it using arguments of section 5.3.2. To determine the critical exponent γ, we use again the cubic recursion on fields (5.47), and suppose that the probability distribution for Ψ satisfies $P(\Psi) = h^{-1}\Phi(\Psi/h)$ (in other words, $P(\chi)$ has a well-

defined $h \to 0$ limit). The average value of fields is

$$\langle \Psi \rangle = h \int \mathrm{d}XX\Phi(X) = h\chi \tag{5.75}$$

$$= JK\overline{G(\epsilon)} \int \mathrm{d}\Psi P(\Psi)\Psi - K\overline{G_3(\epsilon)} \int \mathrm{d}\Psi P(\Psi)\Psi_j^3 + h \tag{5.76}$$

$$= JK\overline{G(\epsilon)}h \int dXX\Phi(X) - K\overline{G_3(\epsilon)}h^3 \int dXX^3\Phi(X) + h \tag{5.77}$$

$$\chi = JK\overline{G(\epsilon)}\chi + 1 \tag{5.78}$$

This yields the average susceptibility as found above, provided the third moment $\int dXX^3\Phi(X)$ is finite, which is true for $\mu > 3$. On the other hand, if the third moment diverges, we can write

$$\langle \Psi \rangle = \chi h = K \int \mathrm{d}\Psi P(\Psi)\overline{g(\epsilon, \Psi)} + h \tag{5.79}$$

$$\left(1 - \frac{J}{J_c}\right)\chi h = K \int \mathrm{d}\Psi P(\Psi)\overline{g(\epsilon, \Psi) - JG(\epsilon)\Psi} + h \tag{5.80}$$

$$= Kh^\mu \int \mathrm{d}\Psi \Psi^{-\mu-1}\overline{g(\epsilon, \Psi) - JG(\epsilon)\Psi} + h \tag{5.81}$$

We immediately see that the full h dependency of the first term in the last expression is $h^\mu \ll h$ for $\mu > 1$ and thus $\chi = 1/(1 - J/J_c)$ everywhere on the replica symmetric insulator to superfluid transition, which is the same as (5.70). As a conclusion, $\gamma = 1$ on the whole RS transition line. This is in contrast to the order parameter exponent β which varies when $1 < \mu < 3$.

5.5.2 Susceptibility at the replica symmetric transition

We derive the last exponent associated with susceptibility, governing the divergence of the induced field Ψ under a small perturbation h at the critical point, $\langle \Psi \rangle \sim h^{1/\delta}$. The probability distribution of fields follows a new scaling form $P(\Psi) = h^{-1/\delta}\Phi(\Psi/h^{1/\delta})$. In a first step, we assume that $\int \mathrm{d}XX^3\Phi(X)$ is finite, and we conclude from the cubic expansion in Ψ (5.48) that:

$$\langle \Psi \rangle = h^{1/\delta} \int \mathrm{d}XX\Phi(X) \tag{5.82}$$

$$= JK\overline{G(\epsilon)}^{1/\delta} \int dXX\Phi(X) - K\overline{G_3(\epsilon)}h^{3/\delta} \int dXX^3\Phi(X) + h \tag{5.83}$$

$$\tag{5.84}$$

On the critical line, the terms in $\int \mathrm{d}XX\Phi(X)$ compensate, and the remaining equation is consistent if and only if $\delta = 3$.

Following the same line of reasoning applied to the full recursion (5.46) when $1 < \mu < 3$ implies:

$$\langle \Psi \rangle = K \int \mathrm{d}\Psi P(\Psi) \overline{g(\epsilon, \Psi)} + h \tag{5.85}$$

$$\left(1 - \frac{J}{J_c}\right) \int \mathrm{d}X X \Phi(X) h^{1/\delta} = K h^{\mu/\delta} \int \mathrm{d}\Psi \Psi^{-1-\mu} \overline{g(\epsilon, \Psi) - JG(\epsilon)\Psi} + h \tag{5.86}$$

which is consistent for $\delta = \mu$ since the left-hand side vanishes at the critical point.

Notice that the three previously found critical exponent satisfy the conventional scaling relation $\beta = \gamma/(\delta - 1)$ on the whole replica symmetric transition line. The previous argument does not apply on the RSB transition line where $\mu < 1$, since the average of the field Ψ is infinite.

5.5.3 Susceptibility at the replica symmetry breaking transition

To compute the superfluid susceptibility on the RSB critical line, we adapt to our case an argument from [221]. As we have seen before, the probability distribution for the susceptibility in the insulating phase is $P(\chi) \sim a/\chi^{1+\mu}$ for large χ, with a constant a. This distribution is equivalent to a distribution of fields $P(\Psi) = P(\chi)/h = a h^\mu / \Psi^{1+\mu}$. This probability distribution is not valid beyond a cutoff Ψ_m defined in section 5.3.3. As a consequence, the average $\langle \Psi^m \rangle$ is roughly equal to:

$$\langle \Psi^m \rangle \sim \int_h^{\Psi_m} \mathrm{d}\Psi \, \frac{a h^\mu B^m}{B^{1+\mu}} = \frac{a h^\mu}{m - \mu} \left(\Psi_m^{m-\mu} - h^{m-\mu} \right) \tag{5.87}$$

$$\langle \Psi^m \rangle \sim \begin{cases} \dfrac{\Psi_m^{m-\mu} a}{B^{1+\mu}} \, h^\mu & \text{if } m > \mu \\ \dfrac{a}{B^{1+\mu}} \, h^m & \text{if } m < \mu \end{cases} \tag{5.88}$$

The average of the field $m = 1$ is larger than μ on the RSB transition. As a consequence, the field scales like $\Psi \sim h^\mu$. We immediately recover the fact that the susceptibility $\lim_{h \to 0} \Psi/h$ is infinite, both in the Bose glass phase and at the RSB transition.

Comparing the scaling of the field with h along the transition may be very confusing. Our results are:

$$\langle \Psi \rangle \sim h^{1/\delta} \tag{5.89}$$

$$\delta = \begin{cases} \min(\mu, 3) & \text{at RS transition} \\ \dfrac{1}{\mu} & \text{at RSB transition} \end{cases} \tag{5.90}$$

The dependency of δ on μ is literally inversed at $\mu = 1$. Actually, the divergence of the field is of completely different nature in the RS and RSB regions.

Indeed, the susceptibility is infinite only strictly at the transition in the RS regime where the quantum phase transition is conventional. On the other hand, the scaling law $\Psi \sim h^{\mu}$ is valid in the whole Bose glass phase and at the transition. This is in perfect agreement with the results in the Ising model [221, 229] where the response has been computed in the RSB phase only. On the other hand, we remark that $\delta \geq 1$ as expected, since the response can only be stronger than linear at a critical point. Of course the mean-field value $\delta = 3$ was expected in the mean-field regime. Finally, we notice that the hyperscaling relation $\beta = \gamma/(\delta - 1)$ makes no sense at the RSB transition where $\beta = \infty$, δ is finite and γ has no satisfying definition at all.

5.6 Conclusion

5.6.1 Augmented phase diagram

In this section, we give a description of the phase diagram including the properties of the insulating phases found in the previous sections. We postpone to section 5.6.3 the discussion of which of these results are not in accordance with current knowledge of the phase diagram on finite dimensional lattices.

In the insulating phase, there are three regions:

- A phase with divergent susceptibility, the Bose glass
- A phase with finite susceptibility and heavy-tailed susceptibility distribution, the "Mott insulator I"
- A phase with finite susceptibility and well-behaved susceptibility distribution, the "Mott insulator II"

The nature of the transition between the two last "phases" is yet to be determined, but certainly not second order. Whether this property of regularity of the susceptibility distribution is really relevant is not clear at the moment.

The respective location of these phases is depicted in figure 5.14 very close to the RS/RSB transition. Although it is quite expected that a Bose glass phase is found in the inter-lobes region, there is a direct superfluid to Mott insulator transition on the lobes, which is clearly not the case in a finite dimensional lattice. This direct transition is also present beyond cavity mean-field in the effective cavity approximation of section 5.2. At this stage, we are not able to decide whether this feature is due to the static approximation $\eta[n(\tau)] \to \Psi$ of section 5.1.2, or if it is a property of the phase diagram on a Bethe lattice.

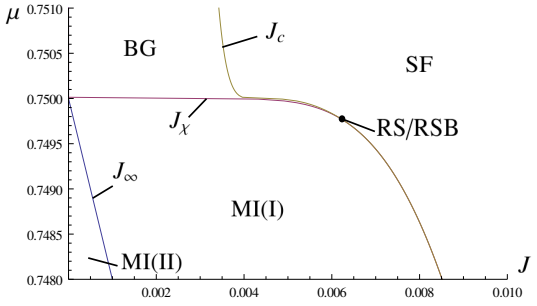

Figure 5.14: Close view of the top of the insulating lobe for $\Delta = 1/2$, $K = 6$. Yellow line J_c: Superfluid to insulator transition. Red line J_χ: Finite to infinite susceptibility transition. Blue line J_∞: Transition to a well behaved distribution of susceptibilities with all moments $\langle \chi^n \rangle$ defined. The four regions of the phase diagram are the superfluid (SF), Bose glass (BG), Mott insulator I (MI(I)) and the Mott Insulator (II). The black dot (RS/RSB) is the line of transition from RS ($\mu < \mu_* - \delta_c = 0.7498$ of section 5.1.6) to RSB transition.

5.6.2 Summary of critical properties

Let us now recall the result of section 5.3.2 and 5.3.3 and put them in perspective with the properties of susceptibility. The field Ψ_0 scales at the superfluid-insulator transition as:

$$\Psi_0 \overset{\text{RS}}{\sim} (\delta J)^\beta \quad \begin{cases} \beta = \frac{1}{2} & \text{if} \quad \mu > 3 \qquad (\text{RS}_\text{a}) \\ \beta = \frac{1}{\mu - 1} & \text{if} \quad 1 < \mu < 3 \qquad (\text{RS}_\text{b}) \end{cases} \tag{5.91}$$

$$\Psi_0 \overset{\text{RSB}}{\sim} \Psi_m \exp\left(-\frac{\mathcal{J}(\mu)}{\delta J}\right) \quad \text{if} \quad \mu < 1 \qquad (\text{RSB}) \tag{5.92}$$

The respective position of these regimes on the critical line is shown in figure 5.15. The mean-field exponent $\beta = 1/2$ is obtained when $\mu > 3$ as shown in section 5.3.2. The transition from $\mu < 3$ to $\mu > 3$ is called J_3. The line J_∞ of equation (5.74) defines a region of the transition line where not only β has its mean field value, but also where the distribution $P(\Psi)$ has no more heavy tails, a transition that we call (RS_∞). On the phase diagram, from the tip of the lobe and with growing chemical potential μ, the transition is of (RS_∞) type, then (RS_a), (RS_b) and finally (RSB) type in this order. The exponent μ keeps decreasing from a finite value at the (RS_a) transition to less than one in the (RSB) phase.

5.6.3 Discussion

Among the previous results, some are clearly new: the existence of a formal replica symmetry breaking for the superfluid propagation across the system, the strong tails of the superfluid field and superfluid susceptibility, the continuously varying critical exponents at the superfluid to insulator transition and a phenomenology reminiscent of an infinite disorder transition in the

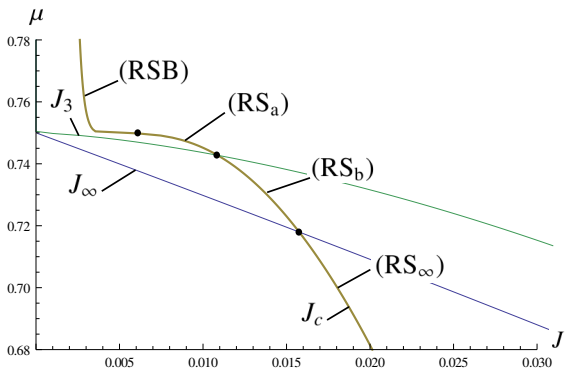

Figure 5.15: Larger view of the upper lobe for $1/2 < \mu < 1$. Yellow line J_c: Superfluid to insulator transition. Blue line J_∞: Transition to a well behaved distribution of susceptibilities with all moments $\langle \chi^n \rangle$ defined. Green line J_3: Transition from diverging $\mu > 3$ to $\mu < 3$. The superfluid to insulator transition is either of (RSB), (RS_a), (RS_b) or (RS_∞) type defined in the text.

inter-lobes regions. It is difficult to decipher which of these features are correct for the Bethe lattice, and even harder to speculate about their validity in lattice systems.

The exponential scaling of the field at the RSB transition may raise some doubt. In the disordered Ising chain, the transition is an infinite disorder fixed point with essential singularity [232]. Yet, the spontaneous magnetization is still a power law $M \sim \delta^\beta$, $\beta = \frac{3-\sqrt{5}}{2}$, with δ the distance to the critical point. This result is not reproduced by the mean-field cavity analysis [229] which yields an essential singularity $M \sim e^{-\alpha/\delta}$. On the other hand, the singular susceptibility $\chi \sim h^\mu$ similar to our result (5.89) and (5.90) obtained in the cavity method is in good agreement with the renormalization group result. As a consequence, in the Ising model, the RSB transition in cavity mean-field is a signature of the infinite disorder fixed point. In the Bose-Hubbard model, the crucial question is whether the superfluid to Bose glass phase is really of infinite disorder in the *inter-lobes* regions. It seems that none of previous studies really address this issue. First, most are focused on the commensurate transition, at the tip of the insulating lobe [206, 217]. Second, such an RSB transition is driven by rare realizations of disorder and is probably much harder to capture than a conventional transition.

Another remarkable prediction of the cavity method is that even at the conventional disordered transition, critical exponents vary continuously along the critical line, and are not universal. Continuously varying exponents are already known in the Griffiths region surrounding infinite disordered fixed points [233], but seems to be a new feature at conventional random quantum phase transitions.

After this conclusion on static effects, in the following section, the cavity is generalized to time dependent fields, and is used to compute the retarded propagator at leading order in J on large distances. This part is purposely left apart of the rest of the chapter because it does not provide further understanding of the physics as it stands. Nevertheless, there are good reasons

to believe that these results could be put to work. This section essentially deals with the strong coupling expansion of the retarded Green's function on a lattice many-body system.

5.7 Dynamical response

5.7.1 Cavity mean-field dynamical response

In this section, we derive a very natural extension of the static cavity method to a dynamical cavity method, extending fields Ψ to time dependent fields $\Psi(t)$. We will see that this method allows for a direct computation of retarded Green's functions in the forward scattering approximation. To do so, we will make the link with an approximation used to show that positive magnetoresistance occurs in bosonic systems [234] by contrast with Fermions.

As a starting point, we extend the cavity mean-field recursion (5.11) between a site i and its neighbors j to time dependent effective fields $\Psi_j(t)$:

$$\Psi_i(t) = \sum_j \langle \hat{b}_j(t) \rangle_{\text{cav j}}(\epsilon_j, \Psi_j(t)) \tag{5.93}$$

The average is computed on a the single disconnected site j, with time dependent field $\Psi_j(t)$. At first order in Ψ, the Kubo relation yields

$$\langle \hat{b}_j(t) \rangle_{\text{cav j}} = -i \int_{-\infty}^{t} \mathrm{d}t' \langle \left[\hat{b}_j(t), -J\Psi_j(t') \hat{b}_j^\dagger(t') \right] \rangle_0 \tag{5.94}$$

$$= J \int \frac{\mathrm{d}\omega}{2\pi} e^{-i\omega t} \left(\frac{n_j}{E_j^- - E_j + \omega} - \frac{n_j + 1}{E_j - E_j^+ + \omega} \right) \Psi_j(\omega) \tag{5.95}$$

where n_j, E_j, $E_j^\pm$ are the filling number, ground state and first excited states energy in the atomic limit $J = 0$. The cavity dynamical response is the transform $\Psi(\omega) = \int \mathrm{d}t\, e^{i\omega t} \Psi(t)$ and equation (5.95) becomes:

$$\Psi_i(\omega) = J \sum_j \left(\frac{n_j}{E_j^- - E_j + \omega} + \frac{n_j + 1}{E_j^+ - E_j - \omega} \right) \Psi_j(\omega) \tag{5.96}$$

Notice that the static limit $\omega \to 0$ reproduces the result (5.13), (5.21). We will show that this recursion relation is the same as the recursion relation on the retarded propagator $G_{i0}^R(t) = -i\Theta(t)\langle [b_i(t), b_0^\dagger] \rangle$, i.e. that:

$$G_{i0}^R(t) = J \sum_j \left(\frac{n_j}{E_j^- - E_j + \omega} + \frac{n_j + 1}{E_j^+ - E_j - \omega} \right) G_{j0}^R(t) \tag{5.97}$$

We claim that this expression is exact in the forward scattering approximation, which is the leading J contribution to the propagator in perturbation theory around the atomic limit. Since

the incoming boson at site 0 must reach site L to be destroyed [15], $G^R_{L0}(t)$ is of order J^L at leading order. A proof a this statement is postponed to section 5.7.3 and appendix 5.B.

5.7.2 Comparison with the hard-core case

Assuming that the expression (5.97) for the propagator is correct, we can analyze the case of hard-core bosons for a direct comparison with [234]. With hard core bosons, either $n_j = 1$ and the second term is zero (the transition to the filled state with 2 bosons is impossible) or $n_j = 0$ and only the second term contribute. Calling ϵ_j the on-site disorder (μ=0 in this paragraph),

$$G^R_{i,0}(\omega) = J \sum_j \left(\frac{\Theta(-\epsilon_j)}{-\epsilon_j + \omega} - \frac{\Theta(\epsilon_j)}{-\epsilon_j + \omega} \right) G^R_{j,0}(\omega) \tag{5.98}$$

$$= J \sum_j \left(\frac{\mathrm{sgn}(\epsilon_j)}{\epsilon_j - \omega} \right) G^R_{j,0}(\omega) \tag{5.99}$$

This formula is just exactly the same as the one found in [234] using an approximation on the exact recursion on propagators. Presumably, to obtain the retarded propagator in the forward scattering approximation, the cavity Ansatz is simpler to handle. Indeed, we were not able to derive formula (5.97) using a method similar to [234] (although this might be feasible). On the contrary, the dynamical cavity Ansatz is easily extended to any model.

5.7.3 Comparison with exact order J^i computation

Let us now do the most naive check, to understand whether (5.97) yields the forward scattering approximation, which is to compute $G^R_{i0}(\omega)$ explicitly in perturbation theory for a small distance i.

Using the unitary evolution operator $\hat{U}_{b\leftarrow a} = \hat{T} e^{-i\int_a^b dt \hat{H}(t)}$, the first part of the commutator in $G^R_{i0}(t) = -i\Theta(t)\langle[\hat{b}_i(t), \hat{b}_0^\dagger]\rangle$ reads:

$$\langle\, \hat{b}_i(t)\hat{b}_0^\dagger \,\rangle = \langle\, \hat{U}_{-\infty\leftarrow t}\, \hat{b}_i\, \hat{U}_{t\leftarrow 0}\, \hat{b}_0^\dagger\, \hat{U}_{0\leftarrow -\infty} \,\rangle \tag{5.100}$$

the operator $\hat{U}_{b\leftarrow a}$ is then expanded in the interaction representation around the atomic limit, up to a total order J^i. For definiteness, we call $\hat{H}_0 = \sum_i \frac{U}{2}\hat{n}_i(\hat{n}_i - 1) + (\epsilon_i - \mu)\hat{n}_i$, E_i its ground state energy on site i and $E_i^\pm$ the energy with one more/one less boson. For a chain with two

15. The description of perturbation theory in terms of bosons jumps is detailed later on.

sites ($i = 1$), the exact amplitude $G^R_{10}(\omega)$ contains six terms,

$$-J\frac{(n_1+1)(n_0+1)}{(E_0-E_0^+ +\omega)(E_1-E_1^+ +\omega)} \quad -J\frac{n_1 n_0}{(E_0-E_0^- -\omega)(E_1-E_1^- -\omega)} \tag{5.101}$$

$$-J\frac{n_1(n_0+1)}{(E_0-E_0^+ +\omega)(E_0^+-E_0+E_1^- -E_1)} \quad -J\frac{n_1(n_0+1)}{(E_1-E_1^- -\omega)(E_0^+-E_0+E_1^- -E_1)} \tag{5.102}$$

$$-J\frac{(n_1+1)n_0}{(E_1-E_1^+ +\omega)(E_0-E_0^- +E_1-E_1^+)} \quad -J\frac{(n_1+1)n_0}{(E_0-E_0^- -\omega)(E_0-E_0^- +E_1-E_1^+)} \tag{5.103}$$

Notice that this computation includes both corrections to the *ground state* and transition elements, up to order J. The four last contributions remarkably simplify to give the same result as (5.97). As one goes to higher i orders, more and more nontrivial resummations occur before the result (5.97) is finally confirmed. In this way, one cannot really prove that it is correct. That was the incentive to prove it by recursion, a quite cumbersome and not so enlightening discussion that is left to appendix 5.B. However, one could seriously consider extending the method beyond the forward scattering approximation, to produce approximate or exact resummed propagators at larger, possibly infinite J order.

5.7.4 Replica computation of the dynamical response

Using the recursion (5.97), one can compute large distance correlations $G^R_{L0}(\omega)$ on the tree as

$$\xi^{-1}(\omega) = \frac{1}{L}\overline{\ln\left(\frac{G^R_{L0}(\omega)}{G^R_{00}(\omega)}\right)} \tag{5.104}$$

The recursion relation is logarithmically self-averaging and the problem may be mapped, as before, to the computation of the logarithm of a partition function of directed polymers. However, the polymer weights is a product of factors which may be positive *or negative*. The problem of polymers with random sign and energy has been solved by Cook and Derrida [235] in the case where energy and signs were uncorrelated. As they conjectured, their result is certainly valid when this constraint is relaxed, i.e. when sign and energy are correlated like here. Their result is that there is an additional phase along with RS and RSB phases:

$$\xi_I(\omega)^{-1} = \ln \int \mathrm{d}\epsilon\ KJG(\omega,\epsilon) \tag{5.105}$$

$$\xi_{II}(\omega)^{-1} = \min_{x\in[0,2]} \frac{1}{x}\ln \int \mathrm{d}\epsilon\ KJ^x|G(\omega,\epsilon)|^x \tag{5.106}$$

$$\xi_{III}(\omega)^{-1} = \frac{1}{2}\ln \int \mathrm{d}\epsilon\ KJ^2|G(\omega,\epsilon)|^2 \tag{5.107}$$

$$G(\omega,\epsilon) = \left(\frac{n_j}{E_j^- - E_j + \omega} - \frac{n_j+1}{E_j - E_j^+ + \omega}\right) \tag{5.108}$$

Let us call x the minimum of ξ_{II} for x in $[0, \infty[$. The partition function 5.104 is then equal to:

$$\xi^{-1}(\omega) = \begin{cases} \xi_I^{-1}(\omega) & \text{if } x < 1 \\ \max\left(\xi_I^{-1}(\omega), \xi_{II}^{-1}(\omega)\right) & \text{if } 1 < x < 2 \\ \max\left(\xi_I^{-1}(\omega), \xi_{III}^{-1}(\omega)\right) & \text{if } x > 2 \end{cases} \tag{5.109}$$

This calculation is not so useful as such. Indeed, the correlations are always exponentially decaying at large distances in the insulating phases, both in the Bose glass and Mott insulator. A challenging problem is how to compute $G_{00}(\omega)$ to obtain the density of state $\rho(\omega)$ from similar arguments, beyond the atomic limit calculation which is trivial. One would then be able to identify the Bose glass from the Mott insulating phase by the standard criterion $\rho(\omega \to 0) \neq 0$ in the Bose glass phase.

5.A Position of the RS/RSB transitions

5.A.1 Zero temperature

For definiteness, let us consider the case $\Delta \lesssim 1$ and $1/2 < \mu < 1$. We have found in section 5.1.6 that the RS to RSB transition occurred at $\mu_c = 1 - \Delta/2 - \delta_s$. Near this point, for small δ defined as $\mu = \mu_c - \delta$, we split the interval for ϵ into a singular $[-\Delta/2, -\Delta/2 + \beta]$ and a regular part $[-\Delta/2 + \beta, \Delta/2]$ with an arbitrary small cutoff β, and change variable to η with $\epsilon = -\Delta/2 + \eta$:

$$\overline{G(\epsilon,\mu)^x} = + \int_{-\Delta/2}^{-\Delta/2+\beta} \mathrm{d}\epsilon G(\epsilon)^x + \int_{-\Delta/2+\beta}^{\Delta/2} \mathrm{d}\epsilon G(\epsilon)^x \tag{5.110}$$

$$= \int_0^\beta \mathrm{d}\eta \left(\frac{2-\delta-\eta}{(\delta+\eta)(1-\delta-\eta)}\right)^x + R \tag{5.111}$$

$$= \int_0^\beta \mathrm{d}\eta \left(\frac{2}{\delta+\eta}\right)^x + R \tag{5.112}$$

$$= R + \begin{cases} 2\ln\left(\frac{\beta+\delta}{\delta}\right) & \text{if } x = 1 \\ \frac{2^x}{1-x}\left((\delta+\beta)^{1-x} - \delta^{1-x}\right) & \text{if } x < 1 \end{cases} \tag{5.113}$$

Clearly, for $\delta \to 0$, $\overline{G^x}$ diverges for $x = 1$ but is finite for any $0 < x < 1$. Thus, there is a threshold δ_s of replica symmetry breaking, such that for $\delta > \delta_s$ the minimum of $f(x)$ is still at $x = 1$ (RS) and for $\delta < \delta_s$ the minimum is at $x < 1$ (RSB).

5.A.2 Finite temperature

In this section, we want to know whether the RSB phase survives at $T > 0$. We will at least manage to a provide lower bound on T_c, which is sufficient to answer positively.

For this purpose, one can extend the previous analysis leading to (5.113) to finite temperatures. For convenience, we restrict the analysis to the regime $\Delta \lesssim 1$ and $1/2 < \mu < 1$ and we use the variable $y = \epsilon - \mu$. The singularity of $G(y)$ from (5.23) is around $y = 1$. Remarking that only the filling numbers $0, 1, 2$ matter for the emergence of a singularity in $G(y)$, we can neglect all others in equation (5.23) for simplicity. Setting $g = e^{-\beta}$, it becomes:

$$G(y = \mu - \epsilon, g) = \frac{1}{y(1-y)} \frac{-2gy + g^y(1+y) + g^{2y}(y-1)}{g + g^y + g^{2y}} \tag{5.114}$$

When $g \to 0$ first (y fixed), we recover the result of zero temperature, because $g^y \gg g \gg g^{2y}$ for $1/2 < y < 1$. On the other hand, for finite temperature, the limit $y \to 1$ is

$$\lim_{y\to 1} G(y = \mu - \epsilon, g) = \frac{1 + 2\beta - e^{-\beta}}{2 + e^{-\beta}} \tag{5.115}$$

The previous $1/(1-y)$ divergence of $G(y)$ which was responsible for the RSB transition in section 5.A.1 is smoothed at finite temperature, thus we need to refine the previous argument. To prove the persistence of the RSB transition, we have to consider an expansion in small temperatures around $y = 1$, conserving terms of order g and g^{2y} at first order :

$$G(y = \mu - \epsilon, g) \sim \frac{1+y}{y(1-y)} + g^{1-y}\frac{-1-3y}{y(1-y)} + g^{y}\frac{-2}{y(1-y)} \tag{5.116}$$

The first term is responsible for the RSB transition at zero temperature, which occurs for $\delta < \delta_s$. This RSB transition occurs when the range of integration of $G^x(y)$ is up to $y = 1-\delta_s$. Therefore, if up to a distance $y = 1 - \delta_s$ of the singularity, $G(\beta) \sim G(\beta = \infty)$, then the RSB transition occurs. This condition reads, comparing the two first terms :

$$\frac{1+y}{y(1-y)} \gg \frac{g}{g^y}\frac{-1-3y}{y(1-y)} \quad \text{for } y = 1-\delta_c \tag{5.117}$$

$$\Leftrightarrow T \ll \frac{\delta_c}{\log(2)} = T_{\text{RSB}} \tag{5.118}$$

The comparison with the second term implies $T \ll U$, which gives no additional constraint. This proves that the RSB phase is preserved at low enough temperature, at least up to T_{RSB}. Of course, this expression is only a lower bound on T_c.

5.A.3 Derivation of the recursion relation for the effective cavity

In this section, we derive the recursion relation (5.26). For convenience, we split the Hamiltonian (5.24) into:

$$\hat{H}_{\text{eff cav}} = \hat{H}_{01} + \hat{H}_{\Psi} \tag{5.119}$$

$$H_{01} = -(\mu+\epsilon_0)\hat{n}_0 + \frac{U}{2}\hat{n}_0(\hat{n}_0-1) - (\mu+\epsilon_1)\hat{n}_1 + \frac{U}{2}\hat{n}_1(\hat{n}_1-1) - J\left(\hat{b}_1\hat{b}_0^\dagger + \hat{b}_1^\dagger\hat{b}_0\right) \tag{5.120}$$

$$H_{\Psi} = -J\left(\hat{b}_1\Psi_1^\dagger + \hat{b}_1^\dagger\Psi_1\right) - J\sum_{i=2,\dots,K}\left(\langle\,\hat{b}_i\,\rangle_{\text{cav i}}\hat{b}_0^\dagger + \langle\,\hat{b}_i^\dagger\,\rangle_{\text{cav i}}\hat{b}_0\right) \tag{5.121}$$

$$= -J\left(\hat{b}_1\Psi_1^\dagger + \hat{b}_1^\dagger\Psi_1\right) - J\left(\hat{b}_0^\dagger + \hat{b}_0\right)\sum_{i=2,\dots,K} JG(\epsilon_i)\Psi_i \tag{5.122}$$

Where we anticipate over the leading order Ψ expansion in the last equality (the J^2 term is expected, see the following). The left-hand part of (5.25) is obviously $\langle b_0\rangle_{\text{cav 0}} = JG(\epsilon_0)\Psi_0$. The right-hand side $\langle b_0\rangle_{\text{eff av}}$ is computed as follows. First, the two-site Hamiltonian without external fields (5.121) is diagonalized, yielding an eigensystem $\{E_n, |E_n\rangle\}$. Then the leading order contribution $\langle\psi|\hat{b}_0|\psi\rangle$ is computed, where $|\,\psi\,\rangle$ is the ground state of $\hat{H}_{\text{eff cav}}$ at linear Ψ order:

$$|\psi\rangle = |E_0\rangle + \sum_{n'}\frac{\langle E_{n'}|\hat{H}_\Psi|E_0\rangle}{E_0 - E_{n'}}|E_{n'}\rangle + \dots \tag{5.123}$$

Since $\hat{H}_{01}$ and $\hat{N}$ commute, we can choose an eigenstate basis $\{E_n, |E_n\rangle\}$ where both $\hat{H}_{01}$ and $\hat{N}$ are diagonal and where $\langle E_n|\hat{b}_0|E_n\rangle = 0$, thus

$$\langle\psi|\hat{b}_0|\psi\rangle = -J^2 \sum_{i=2,\dots,K} G(\epsilon_i)\Psi_i \sum_{n'} \frac{\langle E_{n'}|b_0 + b_0^\dagger|E_0\rangle}{E_0 - E_{n'}} \left(\langle E_0|b_0|E_{n'}\rangle + \langle E_{n'}|b_0|E_0\rangle\right) \tag{5.124}$$

$$- J\Psi_1 \sum_{n'} \frac{\langle E_{n'}|b_1 + b_1^\dagger|E_0\rangle}{E_0 - E_{n'}} \left(\langle E_0|b_0|E_{n'}\rangle + \langle E_{n'}|b_0|E_0\rangle\right)$$

As a consequence, (5.25) implies (5.26) which we write again:

$$\Psi_0 = \sum_{i\neq 1} H^{(a)}(\epsilon_0, \epsilon_1, \epsilon_i)\Psi_i + H^{(b)}(\epsilon_0, \epsilon_1)\Psi_1 \tag{5.125}$$

with

$$H^{(a)}(\epsilon_0, \epsilon_1, \epsilon_i) = -J\frac{G(\epsilon_i)}{G(\epsilon_0)} \sum_{n'} \frac{\langle E_{n'}|b_0 + b_0^\dagger|E_0\rangle}{E_0 - E_{n'}} \langle E_0|b_0 + b_0^\dagger|E_{n'}\rangle \tag{5.126}$$

$$H^{(b)}(\epsilon_0, \epsilon_1, (\epsilon_i)) = -\frac{1}{G(\epsilon_0)} \sum_{n'} \frac{\langle E_{n'}|b_1 + b_1^\dagger|E_0\rangle}{E_0 - E_{n'}} \langle E_0|b_0 + b_0^\dagger|E_{n'}\rangle \tag{5.127}$$

Notice that according to the rule we chose, to chose the site 1 such that $|\epsilon_i - \epsilon_0|$ is smallest for $i = 1$, the second term still depends implicitly on the other ϵ_i's. As a check, we remark that breaking the link $0 \leftrightarrow 1$ in $\hat{H}_{\text{eff cav}}$ yields the cavity mean-field recursion relation like (5.13) between Ψ_0 and other neighboring fields Ψ_i, $i \geq 2$ since (5.126) reduces to $H^{(a)}(\epsilon_0, \epsilon_1, \epsilon_i) = -J\frac{G(\epsilon_i)}{G(\epsilon_0)}(-G(\epsilon_0))$.

5.A.4 Replica solution of the directed polymer problem with several distributions

The solution of the problem with several distributions has been written by Derrida, Cook [231], but in the case when energies $E_\alpha(\epsilon_i)$ only depend on the on-site disorder ϵ_i. They suppose that among the K branches of a node, k_α branches have distribution E_α, with $\sum_\alpha k_\alpha = K$, where $\alpha = 1, \dots, p$. As they show, the replica trick expression of the quenched partition function is:

$$\frac{1}{L}\overline{\ln Z} = \min_x \frac{1}{x} \ln\left(\sum_\alpha k_\alpha \overline{e^{-\beta x E_\alpha}}\right) \tag{5.128}$$

Let us sketch their proof: one can write the replica solution, assuming that the main contribution comes from branches with $p_\alpha L$ links with distribution α, where $\sum_\alpha p_\alpha = 1$, and maximize $\overline{Z^n}$ with respect to the p_α variables.

$$\overline{Z^n} = \max_{\{p_\alpha\}} \left(\frac{L!}{\prod_\alpha (Lp_\alpha)!}\right)^m \left(\prod_\alpha \overline{e^{-\beta E_\alpha n/m}}\right)^{Lm} \tag{5.129}$$

Maximizing with respect to $\{p_\alpha\}$, preserving $\sum_\alpha p_\alpha = 1$, the majority of branches $p_\alpha \sim k_\alpha/K$ do not provide the main contribution, but rather branches with distributions $p_\alpha = \alpha k_\alpha e^{-\beta E_\alpha n/m}$ with α a normalization constant. Then, the result for $\frac{1}{L}\overline{\ln Z}$ follows from the usual $n \to 0$ limit.

5.A.5 Details of implementation for the effective cavity

To compute the matrix elements (5.35) numerically, it is preferable to compute the probability to have ϵ_{i+1} closest to ϵ_i among the K neighbors $P(\epsilon_{i+1}$ closest) and the probability to have one of the given neighbors $\epsilon_{i'+1}$ closer than ϵ_{i+1} and closest than all other $K-1$ neighbors $P(\epsilon_{i'+1}$ closest) (figure 5.10 for the labels). Then we can write:

$$M_{\epsilon_i,\epsilon_{i+1}} = \Delta^{-K} \int \mathrm{d}\{\epsilon'_{i+1}\} \left((H^{(a)}_{i,i+1})^{n/m} \mathbb{I}(\epsilon_{i+1} \text{ closest}) + (H^{(b)}_{i,i+1,i'+1})^{n/m} \mathbb{I}(\epsilon_{i'+1} \text{ closest}) \right) \tag{5.130}$$

$$= \Delta^{-1} \left(P(\epsilon_{i+1} \text{ closest}) (H^{(a)}_{i,i+1})^{n/m} + \int \mathrm{d}\epsilon_{i'+1} P(\epsilon_{i'+1} \text{ closest}) (H^{(b)}_{i,i+1,i'+1})^{n/m} \right) \tag{5.131}$$

The last integral is over the single, closest $\epsilon_{i'+1}$.

$$P(\epsilon_{i+1} \text{ closest}) = \left(1 - \frac{e(\epsilon_{i+1})}{\Delta}\right)^{K-1} \tag{5.132}$$

$$P(\epsilon_{i'+1} \text{ closest}) = \Delta^{-1}(K-1) \left(1 - \frac{e(\epsilon_{i'+1})}{\Delta}\right)^{K-2} \tag{5.133}$$

$$e(\epsilon) = 2\delta(\epsilon) + (\delta'(\epsilon) - \delta(\epsilon))\, \Theta\left(\delta(\epsilon) - \delta'(\epsilon)\right) \tag{5.134}$$

$$\delta(\epsilon) = |\epsilon - \epsilon_i| \qquad \delta'(\epsilon) = \frac{\Delta}{2} - |\epsilon| \tag{5.135}$$

In the previous equations, the function $e(\epsilon)$ is the size of the range of energies closer than ϵ to ϵ_i. This mapping to a one dimensional integral is necessary to integrate numerically the singularities of type $\left(\frac{1}{\epsilon-\epsilon_d}\right)^x$, which are tractable in a one-dimensional integral but not in the previous $K-1$ dimensional integral.

5.B Forward scattering amplitudes

Let us consider a chain with local energy $\hat{H}_0$ and a nearest-neighbor coupling term $\hat{H}_1 = -J\sum_i \hat{b}_i \hat{b}^\dagger_{i+1}$ + h.c.. For definiteness we consider hopping bosons, but the following argument should hold for any degrees of freedom, independently of the form of $\hat{H}_0$ and of the nature of the hopping operator $\hat{b}_i$'s. We want to compute the retarded propagator at distance L, $G^R_L(t) = -i\theta(t)\langle[\hat{b}_L(t), \hat{b}^\dagger_0]\rangle$, at J^Lth order in perturbation theory and at zero temperature. This may be evaluated in a straightforward manner, using for example the unitary operator of evolution

$\hat{U}_{a,b} = Te^{-i\int_a^b \mathrm{d}t\hat{H}(t)}$ and expanding it in interaction representation in $\hat{H}_0$. It is convenient to look at the Fourier transform in time $G_L^R(\omega) = \int \mathrm{d}te^{i\omega t}G_L^R(t)$

$$G_L^R(\omega) = -i\int \mathrm{d}te^{i\omega t}\langle \hat{U}_{t,-\infty}\ \hat{b}_L\ \hat{U}_{0,t}\ \hat{b}_0^\dagger\ \hat{U}_{-\infty,0}\rangle - i\int \mathrm{d}te^{-i\omega t}\langle \hat{U}_{t,-\infty}\ \hat{b}_0^\dagger\ \hat{U}_{0,t}\ \hat{b}_L\ \hat{U}_{-\infty,0}\rangle \quad (5.136)$$

Expanding at order J^L in interaction picture, terms of the form $\mp i(-J)e^{i\hat{H}_0 t}\hat{b}_n\hat{b}_{n+1}^\dagger e^{-i\hat{H}_0 t}$ arise at times $t_{a,i}$, $t_{b,i}$, $t_{c,i}$ (in this order, along the time-contour) respectively when coming from $\hat{U}_{-\infty,0}$, $\hat{U}_{0,t}$ and $\hat{U}_{t,-\infty}$. The $\mp$ term is $-$ for times on the first part of the contour $U_{-\infty,0}$, $U_{0,t}$ and $+$ on the second part $U_{t,-\infty}$, and we call j_- and j_+ the number of such factors. We change variable to positive differences of times $\delta_{a,i} = t_{a,i+1} - t_{a,i} > 0$, $\delta_{b,i} = t_{b,i+1} - t_{b,i} > 0$ and $\delta_{c,i} = -(t_{c,i+1} - t_{c,i}) > 0$ and notice that $t_{i,1} = -\sum_i \delta_{a,i}$, $t = \sum_i \delta_{b,i}$ and that the last time is $t_{L,3} = \sum_i \delta_{b,i} - \sum_j \delta_{c,j}$.

For complete generality [16], we call for the first term and second term in (5.136) respectively:

$$\hat{B}_{-1} = \hat{b}_0^\dagger \text{ (resp. } \hat{b}_L) \quad (5.137)$$

$$\hat{B}_i = \hat{b}_i^\dagger \hat{b}_{i+1} \qquad 0 \le i \le L-1 \quad (5.138)$$

$$\hat{B}_L = \hat{b}_L \text{ (resp. } \hat{b}_0^\dagger) \quad (5.139)$$

We remark that the specific order of the transition sequence is entirely specified by a permutation σ which associate for each rank along path contour $t = \{-1, 0, \ldots, L\}$ a site position $\sigma(t)$ characterizing the operator $B_{\sigma(t)}$ which appears at rank t.

We can now expand both terms in the above expression (5.136)

$$\int \mathrm{d}t\, e^{\pm i\omega t}\langle \hat{U}_{t,-\infty}\ \hat{b}_i\ \hat{U}_{0,t}\ \hat{b}_0^\dagger\ \hat{U}_{-\infty,0}\rangle = (-J)^L(-i)^{j_-}(i)^{j_+}\int_0^\infty \mathrm{d}(\delta_{a/b/c})\langle \hat{B}_{\sigma(L)}\ldots\hat{B}_{\sigma(0)}\hat{B}_{\sigma(-1)}\rangle$$
$$\times e^{-i\sum_j \delta_{a,i}E_{a,i}}e^{-i\sum_j \delta_{b,i}(\mp\omega + E_{b,i})}e^{i\sum_j \delta_{c,i}E_{c,i}} \quad (5.140)$$

where $E_{a/b/c,i} = E_t$ is the bare energy H_0 after the insertion of the operator at time $t_{a/b/c,i}$ and at rank t on the time-contour, minus E_0 the ground state energy. The integration simplifies factors of $\pm i$ and leaves a product of fractions.

$$G_L^R(\omega) = -i(-J)^L\sum_\sigma \prod_{i,j,k}\frac{1}{E_{a,i}}\frac{1}{\mp\omega + E_{b,k}}\frac{1}{E_{c,k}}\langle \hat{B}_{\sigma(L)}\ldots\hat{B}_{\sigma(0)}\hat{B}_{\sigma(-1)}\rangle \quad (5.141)$$

$$= -i(-J)^L\sum_\sigma \prod_{t\in[-1,L]}\frac{1}{\beta_t(\sigma)}\langle \hat{B}_{\sigma(L)}\ldots\hat{B}_{\sigma(0)}\hat{B}_{\sigma(-1)}\rangle \quad (5.142)$$

where we have adopted a condensed notation $\beta_t = (\mp\omega) + E_t$ where $\mp\omega$ should be added only when t is in the section of the time contour $\hat{U}_{0,t}$.

We are going to simplify this sum over all permutation sequences, resuming all terms with equal transition elements $\langle \hat{B}_{\sigma(L)}\ldots\hat{B}_{\sigma(0)}\hat{B}_{\sigma(-1)}\rangle$, that is all terms with the same physical transition sequence T. All permutations belonging to T differ by permutation of ranks that exchange

16. The notation is borrowed from Victor Bapst, whom I would like thank for his notes on the subject.

only *commutative* terms of the sequence $\hat{B}_{\sigma(L)} \dots \hat{B}_{\sigma(0)} \hat{B}_{\sigma(-1)}$. With a given physical sequence T, the simplification which we prove below is

$$F_L^T = \sum_{\sigma/T} \prod_{t\in[-1,L]} \frac{1}{\beta_t(\sigma)} = \prod_{j\in[0,L]} \frac{1}{\mp\omega + E_j} \tag{5.143}$$

where E_j is [17] the local excitation energy at site j (in $\hat{H}_0$) induced in the transition sequence T, and $\mp$ is -1 (resp. $+1$) if $\hat{b}_i \hat{b}_i^\dagger$ (resp. $\hat{b}_i^\dagger \hat{b}_i$) figures in the sequence. Once this simplification is carried out, the J^L contribution to the propagator is given by a sum over all different transition sequences T and then simplified further into

$$G_L^R(\omega) = -i(-J)^L \sum_T \prod_{j\in[0,L]} \frac{1}{\mp\omega + E_j} \langle \hat{B}_{\sigma(L)} \dots \hat{B}_{\sigma(0)} \hat{B}_{\sigma(-1)} \rangle \tag{5.144}$$

$$= -i(-J)^L \prod_{j\in[0,L]} \left(\frac{n_j}{\omega + E_j^-} + \frac{n_j + 1}{-\omega + E_j^+} \right) \tag{5.145}$$

The last step is carried out, considering that each transition sequence is made of a series of step where either $\hat{b}_i \hat{b}_i^\dagger$ or $\hat{b}_i^\dagger \hat{b}_i$ occurs, and the sum over that all the sequences allow for the factorization. Actually, to show that all sequences where a site is filled (F) or emptied (E) first $S = \{FFEEEFEE\}$ are realized, the best is to construct a small algorithm which for any sequence S gives a possible transition sequence T, which is not difficult but requires some attention [18]. In this expression $n_j = \langle \hat{n}_j \rangle_0$, E_j^+, E_j^- are again the atomic limit occupation number, and excited energies.

We show now the statement (5.143) by recursion. Given a transition sequence T, let us call $\alpha_j = (\mp\omega + E_j)$ the denominators in the right-hand side product. We want to prove that the part of the propagator restricted to T obeys $F_L^T = F_{L-1}^T \frac{1}{\alpha_L}$. In terms of permutations, we want

$$F_L^T = \sum_{\sigma\in[-1,L]/T} \prod_{t\in[-1,L]} \frac{1}{\beta_t(\sigma)} = \sum_{\sigma'\in[-1,L-1]/T} \prod_{t\in[-1,L-1]} \frac{1}{\beta_t(\sigma')} \frac{1}{\alpha_L} \tag{5.146}$$

$$= \sum_{\sigma'\in[-1,L-1]/T} \sum_{\sigma_L/T} \prod_{t\in[-1,L]} \frac{1}{\beta_t(\sigma', \sigma_L)} = \sum_{\sigma'\in[-1,L-1]/T} \prod_{t\in[-1,L-1]} \frac{1}{\beta_t(\sigma')} \frac{1}{\alpha_L} \tag{5.147}$$

where we have decomposed the permutation σ into a permutation σ' over $[-1, L-1]$ σ' plus the insertion of an additional element σ_L. This relation will not be hard to prove, thanks to the fact that the equality between the last sums are true term by term within the sum over σ'. In other words, we want to show that

$$\forall \sigma' \qquad \sum_{\sigma_L/T} \prod_{t\in[-1,L]} \frac{1}{\beta_t(\sigma', \sigma_L)} = \prod_{t\in[-1,L-1]} \frac{1}{\beta_t(\sigma')} \frac{1}{\alpha_L} \tag{5.148}$$

17. E_j is not to be confused with E_t

18. For example, one can show what happens for chains of successive EEE and FFF and check that there is a correct algorithm for all boundary conditions.

The proof essentially goes as follows: the time σ_L of insertion of the last site L operator is either before of after the time of insertion $\tilde{t} = \sigma'_{L-1}$ of site $L-1$, yielding two different ordering sequences T, which we should treat separately, but the argument is similar. Assuming that $\sigma_L < \tilde{t}$, a careful examination of the rules of determination of the energy factors E_t in perturbation theory allows one to write that the different factors appearing for all $\sigma_L \in [-1, \tilde{t}-1]$ are

$$\begin{aligned}\sum_{\sigma_L/T} \prod_{t\in[-1,L]} \frac{1}{\beta_t(\sigma',\sigma_L)} &= \frac{1}{\alpha_L} \prod_{t\in[-1,\tilde{t}-1]} \frac{1}{\beta_t+\alpha_L} \prod_{t\in[\tilde{t},L-1]} \frac{1}{\beta_t} \\ &+ \frac{1}{\beta_{-1}} \prod_{t\in[0,\tilde{t}-1]} \frac{1}{\beta_t+\alpha_L} \prod_{t\in[\tilde{t},L-1]} \frac{1}{\beta_t} \\ &+ \frac{1}{\beta_{-1}}\frac{1}{\beta_0} \prod_{t\in[1,\tilde{t}-1]} \frac{1}{\beta_t+\alpha_L} \prod_{t\in[\tilde{t},L-1]} \frac{1}{\beta_t} \\ &+ \ldots + \prod_{t\in[-1,n-1]} \frac{1}{\beta_t} \prod_{t\in[n,\tilde{t}-1]} \frac{1}{\beta_t+\alpha_L} \prod_{t\in[\tilde{t},L-1]} \frac{1}{\beta_t}\end{aligned} \tag{5.149}$$

where the index n in the sum goes from 0 to $\tilde{t}-1$. This sum simplifies telescopically, using

$$\frac{1}{\alpha_L}\frac{1}{\beta+\alpha_L} + \frac{1}{\beta}\frac{1}{\beta+\alpha_L} = \frac{1}{\alpha_L}\frac{1}{\beta} \tag{5.150}$$

successively with $\beta = \beta_{-1}$, $\beta = \beta_0$, etc. This leads immediately to (5.148) and completes the proof of equivalence of (5.143) by recursion since the initialization is satisfied as can be easily checked.

Synopsis

6.1 Chapitre 1 : Introduction aux atomes ultrafroids et à la physique hors-équilibre

Depuis la réalisation d'un condensat de Bose-Einstein [1] à partir de vapeurs atomiques diluées, le domaine des atomes ultrafroids s'est développé dans de nombreuses directions comme la métrologie, la cryptographie et le contrôle logique. Les possibilités offertes par ces dispositifs se multiplient à un rythme rapide, et il est clair que nous ne sommes qu'à l'aube d'une ère qui donnera certainement lieu à de nombreux progrès aussi bien technologiques qu'en recherche fondamentale.

Les systèmes d'atomes froids se révèlent en particulier être de très bons bancs d'étude des propriétés fondamentales de systèmes quantiques à grand nombre d'éléments fortement en interaction [5]. Il est aujourd'hui possible, grâce au vaste effort de recherche qui a été mené en physique atomique, de créer artificiellement une très grande variété de tels systèmes avec un contrôle précis du confinement des atomes et leurs interactions mutuelles en temps réel. Au choix de l'expérimentateur, les assemblées d'atomes peuvent être des bosons ou des fermions, avec ou sans spin, le potentiel de confinement peut être parabolique, ou en forme de réseau, et étendu en une, deux ou trois dimensions.

Une fois le régime des fortes interactions accessible, de nombreux phénomènes habituellement rencontrés en matière condensée ont pu être observés dans les atomes froids, comme la transition de Mott, la superfluidité et la supraconductivité. Parmi les phénomènes nouveaux qui ont été largement étudiés, mentionnons par exemple, dans des systèmes de fermions, la progression depuis un régime superfluide dû à la condensation d'états moléculaires

de fermions à un régime de supraconductivité conventionnel par paires de Cooper [13]. Il est maintenant possible de réaliser une grande variété de transitions de phase quantiques, auxquelles nous allons nous intéresser par la suite.

Les atomes froids sont des systèmes quantiques assez différents des systèmes conventionnels de matière condensée, notamment à cause de leur bonne isolation de l'environnement. Contrairement aux électrons d'un solide, les atomes piégés dans un potentiel périodique ne sont pas couplés à des phonons. D'autre part, un tel réseau est exempt de défauts et donc de tous les effets de diffusion qu'il est impossible d'éliminer totalement dans un solide.

En conséquence, une fois mis hors équilibre, le système est isolé de façon presque complète sur de longues échelles de temps. Se posent alors de nombreuses questions concernant la dynamique unitaire. La question réputée la plus fondamentale concerne la thermalisation, c'est à dire comment et à quelles conditions un système isolé tend vers l'équilibre après une phase de relaxation, et converge ainsi vers un état où les conditions initiales semblent effacées. Des nombreux travaux sur ce sujet, différents scénarios se dessinent selon la nature du système. Dans la limite d'un système chaotique avec une limite semiclassique bien définie, l'hypothèse de "thermalisation des états propres" (eigenstate thermalization hypothesis [45]) semble justifiée et garantit la thermalisation. Dans le cas de systèmes unidimensionnels intégrables, la relaxation vers l'ensemble canonique est impossible et des scénarios de thermalisation partielle sont souvent évoqués [48]. Dans des systèmes sans limite classique et non intégrable, il est pour l'instant impossible d'affirmer en toute généralité s'il y a thermalisation ou si un système peut rester indéfiniment hors-équilibre, en particulier proche de points où la dynamique est intégrable. L'expérience emblématique qui illustre ce problème est l'équivalent quantique du pendule de Newton, par Kinoshita et al. [52], où deux paquets de particules entrent en collision à intervalle régulier, sans relaxation vers l'équilibre sur de longues échelles de temps (figure 1.2).

Il existe bien sûr d'autres problèmes intéressants concernant la dynamique hors-équilibre de systèmes isolés. On peut par exemple se demander ce qui se produit lorsqu'un paramètre est varié afin que le système traverse une transition de phase quantique de manière quasi-adiabatique. Au point critique, où le

temps de réponse du système diverge, le système se retrouve hors-équilibre et les excitations héritent les propriétés du point critique, selon le mécanisme de Kibble-Zurek généralisé au cas quantique [50].

Une autre classe de problèmes intéressants concerne la dynamique d'un système brusquement amené de la phase symétrique à la phase de symétrie brisée. On s'attend de manière générale à ce que la brisure de symétrie locale introduise des défauts, dont la dynamique pourrait avoir des propriétés d'universalité, par analogie à ce qui est connu des systèmes classiques [80].

Un autre effet très général obtenu lors d'une trempe quantique est la propagation de l'information à une vitesse finie, parfois appelé effet cône de lumière. Il existe des résultats exacts, comme la borne de Lieb-Robinson [86], sur la célérité de la vitesse de groupe dans certains systèmes, et cet effet a récemment été observé expérimentalement [53].

De nombreuses autres questions sont aussi explorées, concernant des effets de cohérence aux longs temps, ou encore des relations de fluctuations quantiques, concernant la statistique du travail effectué sur un système, qui sont des extensions directes de résultats classiques. Cette thèse est en partie consacrée à la transition dynamique, un phénomène encore mal connu qui s'apparente peut-être à un phénomène critique hors-équilibre.

6.2 Chapitre 2 : Des atomes ultrafroids au modèle de Bose-Hubbard

Ce chapitre est une revue de la manière dont le modèle de Bose-Hubbard a été réalisé de manière directe dans un système d'atomes froids [5].

Brièvement, le potentiel de confinement et le potentiel périodique sont obtenus à l'aide d'ondes lumineuses stationnaires provenant de lasers. Les atomes sont fortement polarisables, et subissent donc un couplage dipolaire au champ électrique. Lorsque les fréquences respectives du champ électrique et des niveaux résonants de l'atome sont suffisamment éloignées, l'atome subit une force effective due au champ qui l'attire vers les maxima ou les minima du potentiel.

Les interactions entre atomes ont lieu essentiellement dans le canal de l'onde s à faible densité. À l'aide de résonances, qui peuvent être ajustées par un champ magnétique externe, il est possible de modifier la section efficace de diffusion et le signe des interactions. Cet effet est connu sous le nom de résonance de Feshbach [120].

Il est ensuite possible de sonder le système à l'aide de plusieurs méthodes, la plus utilisée étant l'image par temps de vol, où le potentiel confinant est soudainement éteint afin de laisser les atomes se propager librement, ce qui permet de mesurer leur distribution en impulsion.

Lorsqu'un réseau périodique assez fortement confinant est appliqué sur les atomes, il est possible de montrer que l'Hamiltonien effectif du système est celui du modèle de Bose-Hubbard [117], à condition que seule la première bande soit occupée.

Le modèle de Bose-Hubbard (6.151) comprend un terme cinétique, qui correspond à des sauts discrets d'un minimum du réseau à un autre d'amplitude J, et un terme d'interaction U entre paires d'atomes d'un même site.

$$\hat{H} = -J \sum_{\langle ij \rangle} \left(\hat{b}_i^\dagger \hat{b}_j + \text{h.c.} \right) + \frac{U}{2} \sum_i \hat{n}_i (\hat{n}_i - 1) - \mu \sum_i \hat{n}_i \tag{6.151}$$

Donnons à présent une brève description de la transition de phase du modèle de Bose-Hubbard [134, 136]. Dans le cas d'interactions faibles $U \ll J$, le système est superfluide et possède un ordre non-diagonal à longue portée (off-diagonal long range order). Dans la limite opposée des interactions fortes, le système est un isolant de Mott. Dans cet état typique de la physique des interactions fortes, les bosons sont presques localisés, le système est incompressible et il n'existe aucune excitation de basse énergie (existence d'un gap). Les deux phases sont séparées par une transition de phase quantique. Le long de la ligne de transition, on rencontre un point multicritique où la symétrie particule-trous est restaurée, un effet qui trouve une description adéquate dans le cadre de la théorie des champs.

La transition de superfluide à isolant de Mott a pu être observée dans l'expérience célèbre de Greiner et al. [10] et dans celles qui suivirent [147, 148]. Les expériences d'aujourd'hui concernent également la dynamique quantique

hors-équilibre lors de trempes d'une phase à l'autre [90, 156, 131, 155, 53], et des progrès sont attendus dans un avenir proche afin que les conditions des expériences se rapprochent du cadre des prédictions théoriques.

6.3 Chapitre 3 : Dynamique dans les modèles complètement connectés

Ce chapitre aborde la première des deux thématiques générales de cette thèse, la dynamique hors-équilibre d'un système quantique isolé, et en particulier le phénomène nommé transition dynamique.

La première partie de ce travail aborde la dynamique hors-équilibre dans une géométrie très particulière, le réseau de sites complètement connectés. Dans cette géométrie, bien sûr différente des réseaux optiques hypercubiques utilisés dans les expériences, il est possible d'obtenir des équations de champ moyen, qui sont exactes dans la limite de dimension infinie pour certains modèles sur réseau. Nous appliquons cette méthode au modèle de Bose-Hubbard, défini pour un volume $V \gg 1$ (V est le nombre de sites) comme :

$$\hat{H}_{\mathrm{BH}} = -\frac{J}{V}\sum_{i\neq j}\hat{b}_j^\dagger \hat{b}_i + \frac{U}{2}\sum_i \hat{n}_i(\hat{n}_i - 1) \tag{6.152}$$

La méthode développée dans les articles [165, 166] consiste à considérer des fonctions d'ondes symétrique sous toute permutation des sites, une propriété vérifiée par l'état fondamental du système $|\,\Psi_0\,\rangle$, et également par l'état physique après une trempe, car la dynamique unitaire préserve cette symétrie. La fonction d'onde $|\,\Psi(t)\,\rangle$ peut être paramétrée simplement dans les variables de l'espace de Hilbert local, comme l'espace de Fock $|\,n\,\rangle$ pour des bosons. Pour simplifier le propos, nous allons nous restreindre à un cas simplifié où le remplissage d'un site ne dépasse pas $n_b^{\max} = 2$. Dans ce cas, les états sont représentés par la fraction x_i de site contenant i bosons. Comme le nombre de bosons $N = Vn$ est conservé, l'état peut être paramétré par $x_1 = x$ seulement comme $|x\rangle = |1 - x_1 - x_2, x, (n - x_1)/2\rangle$. Il est alors possible d'écrire la dynamique

unitaire comme une équation de Schrödinger sur la fonction d'onde $\Psi_{x,t}$

$$\frac{i}{V}\partial_t \psi_{x,t} = D_x \psi_{x,t} - 2W_x \cosh(2\partial_x/V)\psi_{x,t} \tag{6.153}$$

En constatant que la limite thermodynamique $V \to \infty$ est également la limite classique, il est possible de résoudre la dynamique. En effet, la fonction d'onde $\Psi_{x,t} = \exp(-Vf(x,t))$ prends la forme d'un paquet d'onde étroit dont la position et $x(t)$ et l'impulsion $p(t)$ évoluent selon l'Hamiltonien *classique* :

$$H[x,p] = D(x) - 2W(x)\cos(2p) \tag{6.154}$$

Cette approche permet en définitive de passer d'un problème quantique en interaction fortes et hors-équilibre à une dynamique classique à un faible nombre de variables. Pour le modèle de Bose-Hubbard, il est facile de retrouver la transition de Mott, en reconnaissant que l'état fondamental est le point dans l'espace des phases $\{x(t) = x_0, p(t) = 0\}$ de plus faible énergie. Notons cependant que sur le réseau complètement connecté, la phase superfluide a un gap en énergie, à cause de l'absence de phonons.

Nous avons étudié les différents types de trempes réalisables en supposant que l'état initial est l'état fondamental, et en modifiant instantanément la valeur de l'interaction $U_i \to U_f$. Depuis la phase superfluide $U_i < U_c$ vers la phase d'isolant de Mott $U_f > U_c$, nous retrouvons le phénomène d'effondrement et de restauration du paquet d'onde observé dans l'expérience de Greiner et al. [90]. Dans ce cadre, il est possible de déterminer la période et l'amplitude des oscillations de l'ordre non-diagonal superfluide du système $O(t) = \left\langle \hat{b}_i \hat{b}_j^\dagger \right\rangle$. Il n'est par contre pas possible de prédire le taux d'amortissement de ces oscillations dans l'approximation de champ moyen.

Cette approche permet également d'étudier le phénomène de *transition dynamique*. Cet effet a lieu pour des trempes au sein du régime superfluide. Il peut être identifié comme une variation singulière des valeurs moyennes des observables, au longs temps après une trempe, en fonction de la valeur du paramètre final de la trempe U_f. Par exemple, l'ordre superfluide s'annule avec une singularité logarithmique à la transition dynamique $U_f \sim U_f^d$:

$$\overline{O(t)} \sim -1/\ln(|U_f^d - U_f|) \tag{6.155}$$

Des deux côtés de la transition $U_f \gtrless U_f^d$, les trajectoires appartiennent à des régions différentes de l'espace des phases.

Ce phénomène a d'abord été découvert dans le modèle de Hubbard [62, 159]. Nous avons pu montrer qu'il intervient également dans le modèle de Bose-Hubbard, d'Ising, de Jaynes-Cummings et également dans un modèle sur super-réseau. D'autre part, la transition dynamique semble intrinsèquement reliée à une transition de phase quantique à l'équilibre. En effet, au niveau du champ moyen, la dynamique singulière du paramètre d'ordre à la transition est reliée à celle d'une trempe depuis la phase symétrique vers la phase de symétrie brisée par un renversement du temps.

6.4 Chapitre 4 : Trempes dans le modèle ϕ^4

Pour poursuivre l'étude de la transition dynamique, il est indispensable de comprendre le rôle des corrélations spatiales dans un système sur réseau. Une des questions centrales est de comprendre si la transition est un phénomène critique. Dans le modèle de Bose-Hubbard, la transition de phase spéciale avec symétrie particule-trou est de la classe de symétrie O(2). Une idée naturelle est alors de considérer le problème d'un champ de symétrie O(N), dont la limite des N grands a fait l'objet de beaucoup de travaux et connaît des progrès rapides actuellement, à l'aide du formalisme de Baym-Kadanoff (2-particules irréductible). L'action relativiste que nous considérons porte sur un champ réel ϕ avec interactions quartiques :

$$S[\phi] = \int \mathrm{d}^3x\,\mathrm{d}t \left(\frac{1}{2}\phi_x^n(\Box_x + m_0^2)\phi_x^n + \frac{\lambda}{4!N}(\phi_x^n\phi_x^n)^2 \right) \tag{6.156}$$

Le champ $\phi^n(x,t)$ a n composantes $n \in [1,N]$, il est situé dans un espace à trois dimension de taille finie pour régulariser la théorie. Plus précisément, on suppose que les fonctions de Green sont tronquées pour $p > \Lambda$. Les équations d'évolution du champ $\phi_{\mathbf{x}t} = \langle\hat{\phi}_{\mathbf{x},t}\rangle$ et des corrélations de Keldysh $G_{tt'\mathbf{x}\mathbf{x}'} =$

$\langle\{\hat{\phi}_{\mathbf{x},t}, \hat{\phi}_{\mathbf{x}',t'}\}\rangle - \phi_{\mathbf{x}t}\phi_{\mathbf{x}'t'}$ sont à l'ordre dominant en N :

$$\partial_t^2 \phi_t = -m_t^2 \phi_t \tag{6.157}$$

$$\partial_t^2 G^{nn}_{ptt'} = -\left(p^2 + m_t^2\right) G^{nn}_{ptt'} \tag{6.158}$$

$$m_t^2 = m_0^2 + \frac{\lambda}{6N}\left(\phi_t^2 + \sum_n \frac{1}{2}\int \frac{\mathrm{d}^3 p}{(2\pi)^3} G^{nn}_{ptt'}\right) \tag{6.159}$$

La transition dynamique se signale lors des trempes $(m_0^i)^2 < 0 \to (m_0^f)^2 < 0$ par un changement de régime. Avant la transition $(m_0^f)^2 < (m_0^{f(d)})^2$, le champ ϕ_t oscille et s'amortit vers une valeur finie $\overline{\phi}$ qui diminue en s'approchant de la transition comme $\overline{\phi} \sim \Delta^{1/4}$ où Δ est l'écart relatif entre $(m_0^f)^2$ et $(m_0^{f(d)})^2$. La masse effective $m^2(t)$ tend vers zéro dans ce régime, ce qui signale la divergence des modes transverses, qui sont des modes de Goldstone à l'équilibre.

Après la transition, le champ ϕ_t est lentement amorti vers zéro. En revanche, la masse effective est non nulle et suit une loi d'échelle $\overline{m} \sim \Delta^{1/2}$

Au point exact de transition $(m_0^f)^2 = (m_0^{f(d)})^2$, l'état initial est à champ non nul $\phi(t = 0) > 0$, mais celui-ci évolue sur une trajectoire singulière qui tend exponentiellement vers zéro. Le propagateur $G^{nn}_{ptt'}$ diverge pour des impulsions faibles au temps courts, puis tend vers une expression asymptotique qui suit une loi d'échelle à deux temps :

$$G_{ptt'} \sim \frac{1}{p^2}\left[\cos\left(pt\left(1 - \frac{t'}{t}\right)\right) - \cos\left(pt\left(1 + \frac{t'}{t}\right)\right)\right] \tag{6.160}$$

Dans le contexte d'une théorie des champs stochastique classique, une loi d'échelle en t/t' signale que le système subit un vieillissement. Ici, on parlera plutôt d'un effet ballistique car l'échelle de longueur typique est $x = ct$ ($c = 1$ dans l'action (6.156)). Cet effet de cône de lumière a déjà été rencontré dans le contexte des trempes quantiques, cependant il n'est généralement pas associé à une loi d'échelle. Une autre propriété remarquable qui sous-tend la précédente, est qu'à la transition la masse $m^2(t)$ tend vers zéro plus rapidement que $m^2(t) \lesssim 1/t \ \cos(2\Lambda t)$. Cette absence d'échelle caractéristique permet à une loi d'échelle connue dans des systèmes libres d'émerger dynamiquement

dans un système en interaction arbitrairement forte, uniquement au point de la transition dynamique.

Il est également possible de montrer qu'il existe une échelle de longueur caractéristique qui diverge à la transition dynamique. Celle-ci doit être définie différemment avant et après la transition, mais elle diverge dans les deux cas comme $r(\Delta) \sim 1/\Delta^{1/2}$.

La combinaison des tous ces facteurs, à savoir l'existence d'un comportement d'échelle, d'une échelle de longueur divergente à la transition, et le fait que la trempe à la transition dynamique possède toutes les caractéristiques de la transition de phase statique, porte à croire que nous pouvons qualifier la transition dynamique dans le modèle ϕ^4 comme un phénomène critique hors-équilibre dans un système isolé.

Comme en champ moyen, la transition dynamique est reliée à la dynamique lors d'une trempe de la phase symétrique vers la phase de symétrie brisée. En effet, il se trouve que l'évolution des corrélations aux grands temps est *identique* dans les deux cas et suit la loi d'échelle (6.160).

6.5 Chapitre 5 : Modèle de Bose-Hubbard désordonné

Ce chapitre est consacré à une étude du modèle de Bose-Hubbard avec potentiel chimique aléatoire

$$\hat{H} = \sum_i -\mu\hat{n}_i + \epsilon_i\hat{n}_i + \frac{U}{2}\hat{n}_i(\hat{n}_i - 1) - J\sum_{\langle ij\rangle}\left(\hat{b}_i^\dagger\hat{b}_j + \hat{b}_j^\dagger\hat{b}_i\right) \tag{6.161}$$

où le désordre local ϵ_i a une loi de distribution homogène $P(\epsilon) = \Theta(|\epsilon| - \Delta/2)/\Delta$ et indépendante de site en site.

Pour comprendre ce système, il faut à la fois comprendre l'influence du désordre et des interactions fortes sur les propriétés de cohérence et donc sur l'ordre superfluide. Les premières études sur ce modèle remontent à Fisher et al. [134] où le diagramme des phases a été décrit pour la première fois, ainsi que certaines propriétés critiques. De nombreuses questions restent en suspens malgré des progrès significatifs à l'aide de simulation de type Monte Carlo [206] et de groupe de renormalisation en espace réel [218, 212].

Un nouvel éclairage sur ce problème peut être apporté par la méthode de la cavité, qui a été introduite pour des systèmes quantiques récemment [225, 226]. En particulier, Ioffe et Mézard [228] ont introduit une approximation permettant d'obtenir des résultats analytiques par la méthode des répliques, que nous avons étendu à ce modèle.

Dans méthode de la cavité de champ moyen, l'action des sites voisins sur un site donné i est représentée par un champ Ψ_i :

$$\hat{H}_{\text{cav i}} = -(\mu + \epsilon_i)\hat{n}_i + \frac{U}{2}\hat{n}_i(\hat{n}_i - 1) - J\left(\Psi_i \hat{b}_i^\dagger + \Psi_i^\dagger \hat{b}_i\right) \tag{6.162}$$

En supposant que le réseau est un arbre de Bethe (ou de Cayley), comme montré sur la figure 5.2, le champ obéit à une loi de cohérence en remontant vers la racine de l'arbre :

$$\Psi_0 = \sum_i \langle \hat{b}_i \rangle_{\text{cav i}}(\epsilon_i, \Psi_i) \tag{6.163}$$

Cette relation de récurrence est illustrée sur la figure 5.4. Contrairement à ce que cette présentation superficielle laisse supposer, la méthode de la cavité permet en principe de résoudre exactement un modèle quantique sur un arbre de Bethe [227], mais les champs locaux doivent alors être des fonctions du temps imaginaires $n(\tau)$ et il devient quasiment impossible de traiter un problème avec désordre.

Dans le cadre de l'approximation de la cavité en champ moyen, on peut montrer qu'un faible champ Ψ_b imposé aux bords du système induit par récurrence un champ Ψ_0 à la racine :

$$\Psi_0 = \sum_P \prod_{i \in P} JG(U, \epsilon_i, \mu)\Psi_b \tag{6.164}$$

Cette expression est formellement équivalente à la fonction de partition d'un polymère dirigé, qui peut être calculée exactement [231]

$$\frac{1}{L}\overline{\ln\left(\frac{\Psi_0}{\Psi_b}\right)} = \frac{1}{L}\overline{\ln Z} = \min_{x \in [0,1]} f(x) = -\xi^{-1} \tag{6.165}$$

$$f(x) = \frac{1}{x}\ln\left(K\overline{G(U, \epsilon, \mu)^x}\right) + \ln J \tag{6.166}$$

Il est possible de dériver, à partir de cette expression, de nombreuses propriétés du système. Le diagramme des phases de la figure 5.6 montre la transition de la phase superfluide à la phase isolante (la phase isolante contient en fait la phase d'isolant de Mott et la phase de verre de Bose). Une propriété remarquable de cette méthode est que la transition peut être soit symétrique soit briser la symétrie des répliques. Dans le premier cas, la transition est conventionnelle et l'ordre superfluide Ψ_0 croît en loi de puissance avec l'écart au point critique δJ, alors que dans le second cas (brisure de la symétrie des répliques) la dépendance est exponentielle :

$$\Psi_0 \overset{\text{RS}}{\sim} (\delta J)^{\beta} \tag{6.167}$$

$$\Psi_0 \overset{\text{RSB}}{\sim} \Psi_m \exp\left(-\frac{\mathcal{J}(\mu)}{\delta J}\right) \tag{6.168}$$

Le calcul des exposants critiques à la transition conventionnelle indique également que β varie de façon continue et tend vers l'infini au point de brisure de la symétrie. Il est également intéressant de calculer la susceptibilité superfluide $\chi = \frac{\partial \langle \hat{b} \rangle}{\partial \Psi}$, c'est à dire l'impact sur la valeur de l'ordre non-diagonal d'un champ extérieur infinitésimal $\delta\Psi$ appliqué de façon homogène. Il est possible de montrer que la susceptibilité est infinie au sein de la phase isolante dans certaines régions, qui correspondent au verre de Bose. Les larges queues de la loi de distribution sont en loi de puissance $P(\chi) \sim 1/\chi^{1+\mu}$, et l'exposant μ peut être relié à la fonction $f(x)$ définie en (6.166).

L'avantage de la méthode de la cavité est de permettre de faire des calculs de répliques analytiques, et ainsi de tenir compte de façon exacte des larges contributions des évènements rares, qui ont des effets drastiques sur les transitions de phase.

Epilogue

The work described in this thesis is focused on two topics which can be explored within cold atoms experiments: on the one hand, the nonequilibrium physics of isolated quantum systems, on the other hand, the impact of disorder on strongly correlated systems at equilibrium.

In a first part, we have developed a new mean-field method which applies to a broad range of systems, which maps the off-equilibrium dynamics of a completely connected system onto Newtonian dynamics. This first principles analysis has the advantage of being analytically tractable and to draw a parallel with other known methods such as Gutzwiller Ansatz. The physics of mean-field models is deceptively simple, yet it took a carefully analysis to discover the mean-field dynamical transition in the Hubbard model [236]. Our contribution is to bring indications of the generality of the dynamical transition and of its strong link to the equilibrium critical point, in models where it was left unnoticed despite numerous simulations. The dynamical transition is characterized by a dynamical vanishing of the order parameter on a critical line of quenches within the broken symmetry phase. All time averages of observable have logarithmic singularities around the transition as a function of the quenched interactions. Our formalism, based on symmetry classes under permutation of sites, may be generalized as for example done in [38], to study mean-field models with a first order transition. It could be put to work to study various other problems, as for example the impact of chaos in the classical model on relaxation and thermalization, or to study fluctuation relations in a concrete example.

The second part of our take on off-equilibrium physics is about large N expansions, and the numerical solution of Kadanoff-Baym expansions. This

framework, although not ideal for strongly correlated systems since it is perturbative, allows for the exploration of a broad range of physics. Revisiting the light-cone effect, we find that the velocity of information is always equal to the speed of light c in this relativistic system. Our main result is not only that the dynamical transition is not smoothed out by fluctuations, but also that it has the characteristic features of a critical phenomenon. The two-point correlations have a scaling regime on the dynamical critical point, with aging properties (the scaling function is a ratio of the two times t/t'). This scaling law has a possible interpretation in terms of massless quasiparticles propagation. The critical nature of the transition is also clearly indicated by the presence of a diverging lengthscale and timescale around the transition. Additionally, we draw a parallel between the dynamical transition and the physics of out of equilibrium symmetry breaking, showing that they share the same scaling properties. To extend our results, it would be desirable to assess the robustness of leading order properties against higher order corrections. The next-leading-order equations have been derived in previous studies [186] and in a more general form in this thesis. Solving these equations numerically is possible yet challenging, in particular due to the T^3 computational cost in the total time T. Moreover, in order to analyze the dynamical transition, one has to span over a range of initial conditions with a fine mesh, which is computationally costly. One could also test the robustness of the leading-order scenario for the light-cone effect during quenches to the symmetry breaking phase, which is perhaps easier since only one quench is necessary, yet a good momentum resolution is needed. From a larger perspective, to understand better the dynamics of correlations in finite dimensional systems, perturbative expansions have to be adapted to the physical problem at hand (an off-equilibrium field theory expansion for the Bose-Hubbard model has recently been developed in [110]). On the contrary, perfecting the algorithms to solve Baym-Kadanoff type equations could have a broader impact. Indeed, the state of the art technique is somehow a direct and naive solution, which certainly leaves room for improvement. Among the possible routes, multiscale methods have been used to derive analytical results [188], but could also help to develop efficient solvers. A more physical alternative is the time-dependent renormalization group [109, 110]. It

is well-suited to investigate off-equilibrium criticality, which in my opinion is a topic underdeveloped and full of promises.

The third part of the thesis is dealing with equilibrium aspects of the physics of disordered quantum systems. Like in our previous studies, the disordered Bose-Hubbard model that we consider could be soon investigated in cold atoms experiments. This work is an extension of the powerful method developed by Ioffe, Mézard [228], which is based on the cavity method and on a clever scheme, which allows to extract fine properties of the distribution functions of susceptibility and superfluid order analytically. Our results raise new questions about the Bose glass to superfluid transition. Within the cavity method, we find that the transition is either of infinite disorder, far from the insulating lobes or conventional otherwise, which is a completely unheard of scenario. On the qualitative level, the replica symmetry breaking transition bears similarities with the percolation transition found in real-space renormalization. We also find that the conventional transition has continuously varying critical exponents, which again was not suspected but is not in direct contradiction with any previous study. Finally, we relate all these properties to the large tails of the distribution of susceptibility, which is accessible within various other methods and could be used as a benchmark to compare the cavity results with other approaches. Qualitatively, the approach stresses the consequences of rare realizations of disorder on the transition, an argument that is often evoked about the Mott insulator to Bose glass Griffiths-like transition, but less often about the superfluid to Bose glass transition. Conversely, these predictions about the Bose-Hubbard model can be used as a testing ground for this approximate treatment of the quantum cavity, which has not yet been much compared against other methods. To put our prediction of varying critical exponents and of infinite disorder fixed points to the test, one could for example apply the real-space renormalization group method [212] on different points of the superfluid to insulator transition. We also plan to approach the problem using Migdal-Kadanoff decimation, which yields good approximates for critical exponents on lattices in small dimensions, and thus is a good complement to the Bethe lattice analysis which is valid in the limit of a large number of dimensions [19].

19. M. Tarzia, G. Biroli and B. Sciolla, in preparation.

In the last part of our study, we show that the off-equilibrium cavity method is another way of deriving strong coupling limit expansions for Green's function. Beyond the simple formulas that we obtain, it seems likely that more accurate approximations could be derived along the same lines. Such approximations could, for example, be used within the general framework of Potthoff's self-energy functional [237].

To conclude, let us make some remarks about experimental tests of our predictions. I am quite convinced that future, better experiments on quenches in terms of homogeneity and with more tested quench regimes could bring decisive answers about the existence of the dynamical transition. For example, the onset of Mott insulating regions in a superfluid to superfluid quench is signalled by impeded transport properties [151] and could be visible even in quite inhomogeneous setups. Due to the generality of the dynamical transition, we don't only expect it to be visible in realizations of the Bose-Hubbard model, but also in various other systems where the static quantum phase transition is experimentally accessible. Similarly, the physics of disordered strongly interacting bosons will certainly be accessible soon, but one has to think carefully about signatures of the superfluid to Bose glass transition. In the current experimental conditions, measuring critical exponents will probably be out of reach in forthcoming experiments. However, the infinite disorder fixed point, if present in a finite dimensional lattice system, should be signaled by large tails of the distribution of susceptibility, which is in principle accessible from the space and time-resolved Green's function.

I can not help but conclude with a personal closing remark. From the methodological point of view, it seems to me that there are several complementary ways to do theoretical physics. The first would be the development of clear cut and powerful formalism, as a first principle and natural way to obtain exact or approximate results. The second way is the design and clever use of efficient numerical methods, which leads to unbiased, direct access to physics. Both should perhaps be combined to give a qualitative picture of the physics, providing the incentive and direction of research. I think that our approach borrowed a little from all of these aspects, and that this variety makes me thrilled about physics and doing research.

Bibliography

[1] M H Anderson, J R Ensher, M R Matthews, C E Wieman, and E A Cornell. "Observation of bose-einstein condensation in a dilute atomic vapor." *Science (New York, N.Y.)*, **269(5221)** 198–201 (1995)

[2] T Lahaye, C Menotti, L Santos, M Lewenstein, and T Pfau. "The physics of dipolar bosonic quantum gases". *Reports on Progress in Physics*, **72(12)** 126401 (2009)

[3] M. Saffman, T. Walker, and K. Molmer. "Quantum information with Rydberg atoms". *Reviews of Modern Physics*, **82(3)** 2313–2363 (2010)

[4] Christoph Zipkes, Stefan Palzer, Carlo Sias, and Michael Köhl. "A trapped single ion inside a Bose-Einstein condensate." *Nature*, **464(7287)** 388–91 (2010)

[5] Immanuel Bloch, Wilhelm Zwerger, and Jean Dalibard. "Many-body physics with ultracold gases". *Reviews of Modern Physics*, **80(3)** 885–964 (2008)

[6] M. R. Andrews. "Observation of Interference Between Two Bose Condensates". *Science*, **275(5300)** 637–641 (1997)

[7] M. Matthews, B. Anderson, P. Haljan, D. Hall, C. Wieman, and E. Cornell. "Vortices in a Bose-Einstein Condensate". *Physical Review Letters*, **83(13)** 2498–2501 (1999)

[8] Maciej Lewenstein, Anna Sanpera, Veronica Ahufinger, Bogdan Damski, Aditi Sen(De), and Ujjwal Sen. "Ultracold atomic gases in optical lattices: mimicking condensed matter physics and beyond". *Advances in Physics*, **56(2)** 243–379 (2007)

[9] D. Jaksch, C. Bruder, J. Cirac, C. Gardiner, and P. Zoller. "Cold Bosonic Atoms in Optical Lattices". *Physical Review Letters*, **81(15)** 3108–3111 (1998)

[10] Markus Greiner, Olaf Mandel, Tilman Esslinger, Theodor W Hänsch, and Immanuel Bloch. "Quantum phase transition from a superfluid to a Mott insulator in a gas of ultracold atoms." *Nature*, **415(6867)** 39–44 (2002)

[11] Toshiya Kinoshita, Trevor Wenger, and David S Weiss. "Observation of a one-dimensional Tonks-Girardeau gas." *Science (New York, N.Y.)*, **305(5687)** 1125–8 (2004)

[12] Markus Greiner, Cindy A Regal, and Deborah S Jin. "Emergence of a molecular Bose-Einstein condensate from a Fermi gas." *Nature*, **426(6966)** 537–40 (2003)

[13] Q. Chen, K. Levin, and J. Stajic. "Applying BCS–BEC crossover theory to high-temperature superconductors and ultracold atomic Fermi gases (Review Article)". *Low Temperature Physics*, **32(4)** 406 (2006)

[14] U Schneider, L Hackermüller, S Will, Th Best, I Bloch, T A Costi, R W Helmes, D Rasch, and A Rosch. "Metallic and insulating phases of repulsively interacting fermions in a 3D optical lattice." *Science (New York, N.Y.)*, **322(5907)** 1520–5 (2008)

[15] Robert Jördens, Niels Strohmaier, Kenneth Günter, Henning Moritz, and Tilman Esslinger. "A Mott insulator of fermionic atoms in an optical lattice." *Nature*, **455(7210)** 204–7 (2008)

[16] Jean-Sébastien Bernier, Corinna Kollath, Antoine Georges, Lorenzo De Leo, Fabrice Gerbier, Christophe Salomon, and Michael Köhl. "Cooling fermionic atoms in optical lattices by shaping the confinement". *Physical Review A*, **79(6)** 061601 (2009)

[17] N. Wilkin and J. Gunn. "Condensation of "Composite Bosons" in a Rotating BEC". *Physical Review Letters*, **84(1)** 6–9 (2000)

[18] Vincent Bretin, Sabine Stock, Yannick Seurin, and Jean Dalibard. “Fast Rotation of a Bose-Einstein Condensate”. *Physical Review Letters*, **92(5)** 050403 (2004)

[19] V. Schweikhard, I. Coddington, P. Engels, V. Mogendorff, and E. Cornell. “Rapidly Rotating Bose-Einstein Condensates in and near the Lowest Landau Level”. *Physical Review Letters*, **92(4)** 040404 (2004)

[20] Juliette Billy, Vincent Josse, Zhanchun Zuo, Alain Bernard, Ben Hambrecht, Pierre Lugan, David Clément, Laurent Sanchez-Palencia, Philippe Bouyer, and Alain Aspect. “Direct observation of Anderson localization of matter waves in a controlled disorder.” *Nature*, **453(7197)** 891–4 (2008)

[21] Giacomo Roati, Chiara D’Errico, Leonardo Fallani, Marco Fattori, Chiara Fort, Matteo Zaccanti, Giovanni Modugno, Michele Modugno, and Massimo Inguscio. “Anderson localization of a non-interacting Bose-Einstein condensate.” *Nature*, **453(7197)** 895–8 (2008)

[22] D.M. Basko, I.L. Aleiner, and B.L. Altshuler. “Metal–insulator transition in a weakly interacting many-electron system with localized single-particle states”. *Annals of Physics*, **321(5)** 1126–1205 (2006)

[23] Dario Poletti, Jean-Sébastien Bernier, Antoine Georges, and Corinna Kollath. “Interaction-Induced Impeding of Decoherence and Anomalous Diffusion”. *Physical Review Letters*, **109(4)** 045302 (2012)

[24] Peter Barmettler and Corinna Kollath. “Controllable manipulation and detection of local densities and bipartite entanglement in a quantum gas by a dissipative defect”. *Physical Review A*, **84(4)** 041606 (2011)

[25] Camille Aron, Giulio Biroli, and Leticia F. Cugliandolo. “Driven Quantum Coarsening”. *Physical Review Letters*, **102(5)** 050404 (2009)

[26] Sebastian Diehl, Andrea Tomadin, Andrea Micheli, Rosario Fazio, and Peter Zoller. “Dynamical Phase Transitions and Instabilities in Open Atomic Many-Body Systems”. *Physical Review Letters*, **105(1)** 015702 (2010)

[27] M. Müller, S. Diehl, G. Pupillo, and P. Zoller. "Engineered Open Systems and Quantum Simulations with Atoms and Ions". *arxiv:*1203.6595

[28] Anthony James Leggett. *Quantum Liquids: Bose Condensation and Cooper Pairing in Condensed-Matter Systems (Oxford Graduate Texts)* (Oxford University Press, USA) (2006)

[29] V. Scarola and S. Das Sarma. "Quantum Phases of the Extended Bose-Hubbard Hamiltonian: Possibility of a Supersolid State of Cold Atoms in Optical Lattices". *Physical Review Letters*, **95(3)** 033003 (2005)

[30] F. Cinti, P. Jain, M. Boninsegni, A. Micheli, P. Zoller, and G. Pupillo. "Supersolid Droplet Crystal in a Dipole-Blockaded Gas". *Physical Review Letters*, **105(13)** 135301 (2010)

[31] L Amico, G Mazzarella, S Pasini, and F S Cataliotti. "Hidden order in bosonic gases confined in one-dimensional optical lattices". *New Journal of Physics*, **12(1)** 013002 (2010)

[32] Pasquale Calabrese and John Cardy. "Entanglement entropy and conformal field theory". *Journal of Physics A: Mathematical and Theoretical*, **42(50)** 504005 (2009)

[33] Dmitry Abanin and Eugene Demler. "Measuring Entanglement Entropy of a Generic Many-Body System with a Quantum Switch". *Physical Review Letters*, **109(2)** 020504 (2012)

[34] Marc Mézard and Andrea Montanari. *Information, Physics, and Computation* (Oxford University Press, USA), oxford gra edition (2009)

[35] Fabrizio Altarelli, Remi Monasson, Guilhem Semerjian, and Francesco Zamponi. "A review of the Statistical Mechanics approach to Random Optimization Problems". In *Handbook of Satisfiability* (IOS press) (2008). *arxiv:*0802.1829

[36] B. Apolloni, N. Cesa-Bianchi, and D. de Falco. "Quantum Probability and Infinite Dimensional Analysis". In Habib Ouerdiane and A. Barhoumi, editors, *Proceedings of the 29th Conference, Hammamet, Tunisia, 13-18 October 2008* (World Scientific) (2010)

[37] Thomas Jörg, Florent Krzakala, Guilhem Semerjian, and Francesco Zamponi. "First-Order Transitions and the Performance of Quantum Algorithms in Random Optimization Problems". *Physical Review Letters*, **104(20)** 207206 (2010)

[38] Victor Bapst and Guilhem Semerjian. "On quantum mean-field models and their quantum annealing". *Journal of Statistical Mechanics: Theory and Experiment*, **(06)** P06007 (2012)

[39] Leticia F. Cugliandolo. "Dissipative quantum disordered models". *International Journal of Modern Physics B*, **20** 2795 (2006)

[40] Laura Foini, Guilhem Semerjian, and Francesco Zamponi. "Quantum Biroli-Mézard model: Glass transition and superfluidity in a quantum lattice glass model". *Physical Review B*, **83(9)** 094513 (2011)

[41] L. Perfetti, P. Loukakos, M. Lisowski, U. Bovensiepen, H. Berger, S. Biermann, P. Cornaglia, A. Georges, and M. Wolf. "Time Evolution of the Electronic Structure of 1T-TaS2 through the Insulator-Metal Transition". *Physical Review Letters*, **97(6)** (2006)

[42] L Perfetti, P A Loukakos, M Lisowski, U Bovensiepen, M Wolf, H Berger, S Biermann, and A Georges. "Femtosecond dynamics of electronic states in the Mott insulator 1T-TaS 2 by time resolved photoelectron spectroscopy". *New Journal of Physics*, **10(5)** 053019 (2008)

[43] Nikolai S. Krylov. *Works on the Foundations of Statistical Physics (Princeton Series in Physics)* (Princeton University Press) (1979)

[44] Asher Peres. "Recurrence Phenomena in Quantum Dynamics". *Physical Review Letters*, **49(15)** 1118–1118 (1982)

[45] Mark Srednicki. "Chaos and quantum thermalization". *Physical Review E*, **50(2)** 888–901 (1994)

[46] Marcos Rigol, Vanja Dunjko, and Maxim Olshanii. "Thermalization and its mechanism for generic isolated quantum systems." *Nature*, **452(7189)** 854–8 (2008)

[47] Giulio Biroli, Corinna Kollath, and Andreas Läuchli. "Effect of Rare Fluctuations on the Thermalization of Isolated Quantum Systems". *Physical Review Letters*, **105(25)** 250401 (2010)

[48] Marcos Rigol, Vanja Dunjko, Vladimir Yurovsky, and Maxim Olshanii. "Relaxation in a Completely Integrable Many-Body Quantum System: An Ab Initio Study of the Dynamics of the Highly Excited States of 1D Lattice Hard-Core Bosons". *Physical Review Letters*, **98(5)** 050405 (2007)

[49] M. Cramer, C. Dawson, J. Eisert, and T. Osborne. "Exact Relaxation in a Class of Nonequilibrium Quantum Lattice Systems". *Physical Review Letters*, **100(3)** 030602 (2008)

[50] Anatoli Polkovnikov, Krishnendu Sengupta, Alessandro Silva, and Mukund Vengalattore. "Colloquium: Nonequilibrium dynamics of closed interacting quantum systems". *Reviews of Modern Physics*, **83(3)** 863–883 (2011)

[51] Laura Foini, Leticia F. Cugliandolo, and Andrea Gambassi. "Fluctuation-dissipation relations and critical quenches in the transverse field Ising chain". *Physical Review B*, **84(21)** 212404 (2011)

[52] Toshiya Kinoshita, Trevor Wenger, and David S Weiss. "A quantum Newton's cradle." *Nature*, **440(7086)** 900–3 (2006)

[53] Marc Cheneau, Peter Barmettler, A. Polkovnikov, Manuel Endres, Peter Schauss, Takeshi Fukuhara, Christian Gross, Immanuel Bloch, Corinna Kollath, and Stefan Kuhr. "Light-cone-like spreading of correlations in a quantum many-body system." *Nature*, **481(7382)** 484–7 (2012)

[54] Corinna Kollath, Andreas Läuchli, and Ehud Altman. "Quench Dynamics and Nonequilibrium Phase Diagram of the Bose-Hubbard Model". *Physical Review Letters*, **98(18)** 180601 (2007)

[55] Giuseppe Carleo, Federico Becca, Marco Schiró, and Michele Fabrizio. "Localization and glassy dynamics of many-body quantum systems." *Scientific reports*, **2** 243 (2012)

[56] Denis Ullmo. "Many-body physics and quantum chaos". *Reports on Progress in Physics*, **71(2)** 026001 (2008)

[57] Stéphane Nonnenmacher. "Some open questions in 'wave chaos'". *Nonlinearity*, **21(8)** T113–T121 (2008)

[58] Gilles Montambaux, Didier Poilblanc, Jean Bellissard, and Clément Sire. "Quantum chaos in spin-fermion models". *Physical Review Letters*, **70(4)** 497–500 (1993)

[59] A. R Kolovsky and A Buchleitner. "Quantum chaos in the Bose-Hubbard model". *Europhysics Letters (EPL)*, **68(5)** 632–638 (2004)

[60] Corinna Kollath, Guillaume Roux, Giulio Biroli, and Andreas M Läuchli. "Statistical properties of the spectrum of the extended Bose–Hubbard model". *Journal of Statistical Mechanics: Theory and Experiment*, **(08)** P08011 (2010)

[61] Vladimir Yurovsky and Maxim Olshanii. "Memory of the Initial Conditions in an Incompletely Chaotic Quantum System: Universal Predictions with Application to Cold Atoms". *Physical Review Letters*, **106(2)** 025303 (2011)

[62] Martin Eckstein, Marcus Kollar, and Philipp Werner. "Thermalization after an Interaction Quench in the Hubbard Model". *Physical Review Letters*, **103(5)** 056403 (2009)

[63] Niels Strohmaier, Daniel Greif, Robert Jördens, Leticia Tarruell, Henning Moritz, and Tilman Esslinger. "Observation of Elastic Doublon Decay in the Fermi-Hubbard Model". *Physical Review Letters*, **104(8)** 080401 (2010)

[64] Rajdeep Sensarma, David Pekker, Ehud Altman, Eugene Demler, Niels Strohmaier, Daniel Greif, Robert Jördens, Leticia Tarruell, Henning Moritz, and Tilman Esslinger. "Lifetime of double occupancies in the Fermi-Hubbard model". *Physical Review B*, **82(22)** 224302 (2010)

[65] Jürgen Berges and J. Serreau. "Progress in nonequilibrium quantum field theory II". In *Strong and Electroweak Matter, Helsinki, Finland* (2004). *arxiv:*0410330

[66] Jürgen Berges and Jürgen Cox. "Thermalization of quantum fields from time-reversal invariant evolution equations". *Physics Letters B*, **517(3-4)** 369–374 (2001)

[67] Jürgen Berges. "Controlled nonperturbative dynamics of quantum fields out of equilibrium". *Nuclear Physics A*, **699(3-4)** 847–886 (2002)

[68] S. Juchem, W. Cassing, and C Greiner. "Quantum dynamics and thermalization for out-of-equilibrium $\phi 4$ theory". *Physical Review D*, **69(2)** 0307353 (2004)

[69] T W B Kibble. "Topology of cosmic domains and strings". *Journal of Physics A: Mathematical and General*, **9(8)** 1387–1398 (1976)

[70] W. H. Zurek. "Cosmological experiments in superfluid helium?" *Nature*, **317(6037)** 505–508 (1985)

[71] Wojciech Zurek, Uwe Dorner, and Peter Zoller. "Dynamics of a Quantum Phase Transition". *Physical Review Letters*, **95(10)** 105701 (2005)

[72] Anatoli Polkovnikov. "Universal adiabatic dynamics in the vicinity of a quantum critical point". *Physical Review B*, **72(16)** 161201 (2005)

[73] Diptiman Sen, K. Sengupta, and Shreyoshi Mondal. "Defect Production in Nonlinear Quench across a Quantum Critical Point". *Physical Review Letters*, **101(1)** 016806 (2008)

[74] C. De Grandi, V. Gritsev, and A. Polkovnikov. "Quench dynamics near a quantum critical point". *Physical Review B*, **81(1)** 012303 (2010)

[75] Jacek Dziarmaga. "Dynamics of a quantum phase transition in the random Ising model: Logarithmic dependence of the defect density on the transition rate". *Physical Review B*, **74(6)** 064416 (2006)

[76] Victor Mukherjee, Amit Dutta, and Diptiman Sen. "Defect generation in a spin-12 transverse XY chain under repeated quenching of the transverse field". *Physical Review B*, **77(21)** 214427 (2008)

[77] Chad N. Weiler, Tyler W. Neely, David R. Scherer, Ashton S. Bradley, Matthew J. Davis, and Brian P. Anderson. "Spontaneous vortices in the formation of Bose–Einstein condensates". *Nature*, **455(7215)** 948–951 (2008)

[78] L E Sadler, J M Higbie, S R Leslie, M Vengalattore, and D M Stamper-Kurn. "Spontaneous symmetry breaking in a quenched ferromagnetic spinor Bose-Einstein condensate." *Nature*, **443(7109)** 312–5 (2006)

[79] Giulio Biroli, Leticia F. Cugliandolo, and Alberto Sicilia. "Kibble-Zurek mechanism and infinitely slow annealing through critical points". *Physical Review E*, **81(5)** 050101 (2010)

[80] A.J. Bray. "Theory of phase-ordering kinetics". *Advances in Physics*, **43(3)** 357–459 (1994)

[81] Federico Corberi, Leticia F. Cugliandolo, and Hajime Yoshino. "Growing length scales in aging systems". In L. Cipelletti L. Berthier, G. Biroli, J-P Bouchaud and W. van Saarloos, editors, *Dynamical heterogeneities in glasses, colloids, and granular media* (Oxford University Press, USA) (2010)

[82] Silvio Franz and Guilhem Semerjian. "Analytical approaches to time and length scales in models of glasses". *arxiv:*1009.5248

[83] N Horiguchi, T Oka, and H Aoki. "Non-equilibrium dynamics in Mott-to-superfluid transition in Bose-Einstein condensation in optical lattices". *Journal of Physics: Conference Series*, **150(3)** 032007 (2009)

[84] Jürgen Berges, Alexander Rothkopf, and Jonas Schmidt. "Nonthermal Fixed Points: Effective Weak Coupling for Strongly Correlated Systems Far from Equilibrium". *Physical Review Letters*, **101(4)** 041603 (2008)

[85] Jürgen Berges and Dénes Sexty. "Strong versus weak wave-turbulence in relativistic field theory". *Physical Review D*, **83(8)** 085004 (2011)

[86] Elliott H. Lieb and Derek W. Robinson. "The finite group velocity of quantum spin systems". *Communications in mathematical physics*, **28(3)** 251–257 (1972)

[87] Pasquale Calabrese and John Cardy. "Quantum quenches in extended systems". *Journal of Statistical Mechanics: Theory and Experiment*, **(06)** P06008–P06008 (2007)

[88] Andreas M Läuchli and Corinna Kollath. "Spreading of correlations and entanglement after a quench in the one-dimensional Bose-Hubbard

model". *Journal of Statistical Mechanics: Theory and Experiment*, **(05)** P05018 (2008)

[89] Maxime Ben Dahan, Ekkehard Peik, Jakob Reichel, Yvan Castin, and Christophe Salomon. "Bloch Oscillations of Atoms in an Optical Potential". *Physical Review Letters*, **76(24)** 4508–4511 (1996)

[90] Markus Greiner, Olaf Mandel, Theodor W Hänsch, and Immanuel Bloch. "Collapse and revival of the matter wave field of a Bose-Einstein condensate." *Nature*, **419(6902)** 51–4 (2002)

[91] Jorge Kurchan. "Non-equilibrium work relations". *Journal of Statistical Mechanics: Theory and Experiment*, **(07)** P07005–P07005 (2007)

[92] Satoshi Yukawa. "A Quantum Analogue of the Jarzynski Equality". *Journal of the Physics Society Japan*, **69(8)** 2367–2370 (2000)

[93] Jorge Kurchan. "A Quantum Fluctuation Theorem". *arxiv:*0007360

[94] Michele Campisi, Peter Hänggi, and Peter Talkner. "Colloquium: Quantum fluctuation relations: Foundations and applications". *Reviews of Modern Physics*, **83(3)** 771–791 (2011)

[95] Ross Dorner, John Goold, Cecilia Cormick, Mauro Paternostro, and Vlatko Vedral. "Emergent thermodynamics in a quenched quantum many-body system". *arxiv:*1207.4777

[96] Arnab Das, K. Sengupta, Diptiman Sen, and Bikas Chakrabarti. "Infinite-range Ising ferromagnet in a time-dependent transverse magnetic field: Quench and ac dynamics near the quantum critical point". *Physical Review B*, **74(14)** 144423 (2006)

[97] Patrick Navez and Ralf Schützhold. "Emergence of coherence in the Mott-insulator superfluid quench of the Bose-Hubbard model". *Physical Review A*, **82(6)** 063603 (2010)

[98] Anatoli Polkovnikov, Subir Sachdev, and S. Girvin. "Nonequilibrium Gross-Pitaevskii dynamics of boson lattice models". *Physical Review A*, **66(5)** 053607 (2002)

[99] Qiong-Yi He, Margaret D. Reid, Bogdan Opanchuk, Rodney Polkinghorne, Laura E. C. Rosales-Zárate, and Peter D. Drummond. "Quantum dynamics in ultracold atomic physics". *Frontiers of Physics*, **7(1)** 16–30 (2012)

[100] A. Iucci and M. A. Cazalilla. "Quantum quench dynamics of the Luttinger model". *Physical Review A*, **80(6)** 063619 (2009)

[101] Ferenc Iglói and Heiko Rieger. "Long-Range Correlations in the Nonequilibrium Quantum Relaxation of a Spin Chain". *Physical Review Letters*, **85(15)** 3233–3236 (2000)

[102] Davide Rossini, Alessandro Silva, Giuseppe Mussardo, and Giuseppe Santoro. "Effective Thermal Dynamics Following a Quantum Quench in a Spin Chain". *Physical Review Letters*, **102(12)** 127204 (2009)

[103] P. Calabrese, F. H. L. Essler, and M. Fagotti. "Quantum Quench in the Transverse Field Ising chain I: Time evolution of order parameter correlators". *arxiv:*1204.3911

[104] Pasquale Calabrese, Fabian H. L. Essler, and Maurizio Fagotti. "Quantum Quench in the Transverse Field Ising Chain II: Stationary State Properties". *arxiv:*1205.2211

[105] Alexandre Faribault, Pasquale Calabrese, and Jean-Sébastien Caux. "Quantum quenches from integrability: the fermionic pairing model". *Journal of Statistical Mechanics: Theory and Experiment*, **(03)** P03018 (2009)

[106] Alex Kamenev and Alex Levchenko. "Keldysh technique and non-linear σ-model: basic principles and applications". *Advances in Physics*, **58(3)** 197–319 (2009)

[107] Gordon Baym and Leo Kadanoff. "Conservation Laws and Correlation Functions". *Physical Review*, **124(2)** 287–299 (1961)

[108] Jürgen Berges and J. Serreau. "Progress in Nonequilibrium Quantum Field Theory". In *Proceedings of strong and electroweak matter, Heidelberg, Germany* (2002). *arxiv:*0302210

[109] Aditi Mitra, So Takei, Yong Kim, and A. Millis. "Nonequilibrium Quantum Criticality in Open Electronic Systems". *Physical Review Letters*, **97(23)** 236808 (2006)

[110] Thomas Kloss and Peter Kopietz. "Nonequilibrium time evolution of bosons from the functional renormalization group". *Physical Review B*, **83(20)** 205118 (2011)

[111] Andreas Läuchli, Julien Sudan, and Erik Sø rensen. "Ground-state energy and spin gap of spin-1/2 Kagomé-Heisenberg antiferromagnetic clusters: Large-scale exact diagonalization results". *Physical Review B*, **83(21)** 212401 (2011)

[112] Guifré Vidal. "Efficient Simulation of One-Dimensional Quantum Many-Body Systems". *Physical Review Letters*, **93(4)** 040502 (2004)

[113] A J Daley, C Kollath, U Schollwöck, and G Vidal. "Time-dependent density-matrix renormalization-group using adaptive effective Hilbert spaces". *Journal of Statistical Mechanics: Theory and Experiment*, **(04)** P04005 (2004)

[114] Antoine Georges, Werner Krauth, and Marcelo J. Rozenberg. "Dynamical mean-field theory of strongly correlated fermion systems and the limit of infinite dimensions". *Reviews of Modern Physics*, **68(1)** 13–125 (1996)

[115] M. Eckstein, A. Hackl, S. Kehrein, M. Kollar, M. Moeckel, P. Werner, and F.A. Wolf. "New theoretical approaches for correlated systems in nonequilibrium". *The European Physical Journal Special Topics*, **180(1)** 217–235 (2010)

[116] Emanuel Gull, Andrew Millis, Alexander Lichtenstein, Alexey Rubtsov, Matthias Troyer, and Philipp Werner. "Continuous-time Monte Carlo methods for quantum impurity models". *Reviews of Modern Physics*, **83(2)** 349–404 (2011)

[117] D. Jaksch and P. Zoller. "The cold atom Hubbard toolbox". *Annals of Physics*, **315(1)** 52–79 (2005)

[118] Immanuel Bloch. "Ultracold quantum gases in optical lattices". *Nature Physics*, **1(1)** 23–30 (2005)

[119] C. J. Pethick and H. Smith. "Bose-Einstein condensation in dilute gases"

[120] Cheng Chin, Paul Julienne, and Eite Tiesinga. "Feshbach resonances in ultracold gases". *Reviews of Modern Physics*, **82(2)** 1225–1286 (2010)

[121] P. Fedichev, M. Reynolds, and G. Shlyapnikov. "Three-Body Recombination of Ultracold Atoms to a Weakly Bound s Level". *Physical Review Letters*, **77(14)** 2921–2924 (1996)

[122] Markus Greiner, C. A. Regal, J T Stewart, and D. S. Jin. "Probing Pair-Correlated Fermionic Atoms through Correlations in Atom Shot Noise". *Physical Review Letters*, **94(11)** 110401 (2005)

[123] R. H. Brown and R. Q. Twiss. "Correlation between Photons in two Coherent Beams of Light". *Nature*, **177(4497)** 27–29 (1956)

[124] S Fölling, Fabrice Gerbier, Artur Widera, Olaf Mandel, Tatjana Gericke, and Immanuel Bloch. "Spatial quantum noise interferometry in expanding ultracold atom clouds." *Nature*, **434(7032)** 481–4 (2005)

[125] Ana Rey, Indubala Satija, and Charles Clark. "Quantum coherence of hard-core bosons: Extended, glassy, and Mott phases". *Physical Review A*, **73(6)** 063610 (2006)

[126] J. Ruostekoski, C. Foot, and A. Deb. "Light Scattering for Thermometry of Fermionic Atoms in an Optical Lattice". *Physical Review Letters*, **103(17)** 170404 (2009)

[127] I Carusotto. "Bragg scattering and the spin structure factor of two-component atomic gases". *Journal of Physics B: Atomic, Molecular and Optical Physics*, **39(10)** S211–S219 (2006)

[128] Andrea Damascelli. "Probing the Electronic Structure of Complex Systems by ARPES". *Physica Scripta*, **T109(T109)** 61 (2004)

[129] J T Stewart, J P Gaebler, and D S Jin. "Using photoemission spectroscopy to probe a strongly interacting Fermi gas." *Nature*, **454(7205)** 744–7 (2008)

[130] Christof Weitenberg, Peter Schauß, Takeshi Fukuhara, Marc Cheneau, Manuel Endres, Immanuel Bloch, and Stefan Kuhr. "Coherent Light Scattering from a Two-Dimensional Mott Insulator". *Physical Review Letters*, **106(21)** 215301 (2011)

[131] W S Bakr, A Peng, M E Tai, R Ma, J Simon, J I Gillen, S Fölling, L Pollet, and Markus Greiner. "Probing the superfluid-to-Mott insulator transition at the single-atom level." *Science (New York, N.Y.)*, **329(5991)** 547–50 (2010)

[132] Jacob F Sherson, Christof Weitenberg, Manuel Endres, Marc Cheneau, Immanuel Bloch, and Stefan Kuhr. "Single-atom-resolved fluorescence imaging of an atomic Mott insulator." *Nature*, **467(7311)** 68–72 (2010)

[133] M Endres, M Cheneau, T Fukuhara, C Weitenberg, P Schauss, C Gross, L Mazza, M C Bañuls, L Pollet, Immanuel Bloch, and S Kuhr. "Observation of correlated particle-hole pairs and string order in low-dimensional Mott insulators." *Science (New York, N.Y.)*, **334(6053)** 200–3 (2011)

[134] Matthew Fisher, Peter Weichman, G. Grinstein, and Daniel Fisher. "Boson localization and the superfluid-insulator transition". *Physical Review B*, **40(1)** 546–570 (1989)

[135] Barbara Capogrosso-Sansone, Sebnem Söyler, Nikolay Prokof'ev, and Boris Svistunov. "Monte Carlo study of the two-dimensional Bose-Hubbard model". *Physical Review A*, **77(1)** 015602 (2008)

[136] Subir Sachdev. *Quantum Phase Transitions* (Cambridge University Press) (2000)

[137] T. C. Dorlas and J.-B Bru. "Exact Solution of the Infinite-Range-Hopping Bose–Hubbard Model". *Journal of Statistical Physics*, **113** 177–196 (2003)

[138] J. W. Negele and Henri Orland. *Quantum Many-Particle Systems (Frontiers in Physics)* (Perseus Books (Sd)) (1988)

[139] Peter Weichman. "Dirty bosons: twenty years later". *Modern Physics Letters B*, **22(27)** 2623 (2008)

[140] Konstantin Efetov. *Supersymmetry in Disorder and Chaos* (Cambridge University Press) (1996)

[141] A. Rançon and N. Dupuis. "Quantum criticality of a Bose gas in an optical lattice near the Mott transition". *Physical Review A*, **85(1)** 011602 (2012)

[142] Bogdan Damski and Jakub Zakrzewski. "Mott-insulator phase of the one-dimensional Bose-Hubbard model: A high-order perturbative study". *Physical Review A*, **74(4)** 043609 (2006)

[143] Till Kühner, Steven White, and H. Monien. "One-dimensional Bose-Hubbard model with nearest-neighbor interaction". *Physical Review B*, **61(18)** 12474–12489 (2000)

[144] B. Capogrosso-Sansone, N. Prokof'ev, and B. Svistunov. "Phase diagram and thermodynamics of the three-dimensional Bose-Hubbard model". *Physical Review B*, **75(13)** 134302 (2007)

[145] A. Rançon and N. Dupuis. "Nonperturbative renormalization group approach to strongly correlated lattice bosons". *Physical Review B*, **84(17)** 174513 (2011)

[146] N. Dupuis and A. Rançon. "Infrared behavior of interacting bosons at zero temperature". *Laser Physics*, **21(8)** 1470–1479 (2011)

[147] Thilo Stöferle, Henning Moritz, Christian Schori, Michael Köhl, and Tilman Esslinger. "Transition from a Strongly Interacting 1D Superfluid to a Mott Insulator". *Physical Review Letters*, **92(13)** 130403 (2004)

[148] I. Spielman, W. Phillips, and J. Porto. "Mott-Insulator Transition in a Two-Dimensional Atomic Bose Gas". *Physical Review Letters*, **98(8)** 080404 (2007)

[149] C. Kollath, U. Schollwöck, J. von Delft, and W. Zwerger. "Spatial correlations of trapped one-dimensional bosons in an optical lattice". *Physical Review A*, **69(3)** 031601 (2004)

[150] Nathan Gemelke, Xibo Zhang, Chen-Lung Hung, and Cheng Chin. "In situ observation of incompressible Mott-insulating domains in ultracold atomic gases." *Nature*, **460(7258)** 995–8 (2009)

[151] Jean-Sébastien Bernier, Dario Poletti, Peter Barmettler, Guillaume Roux, and Corinna Kollath. "Slow quench dynamics of Mott-insulating regions in a trapped Bose gas". *Physical Review A*, **85(3)** 033641 (2012)

[152] Nir Friedman, Ariel Kaplan, and Nir Davidson. *Advances In Atomic, Molecular, and Optical Physics Volume 48*, volume 48 of *Advances In Atomic, Molecular, and Optical Physics* (Elsevier) (2002)

[153] T. Meyrath, F. Schreck, J. Hanssen, C.-S. Chuu, and M. Raizen. "Bose-Einstein condensate in a box". *Physical Review A*, **71(4)** 041604 (2005)

[154] Ehud Altman and Assa Auerbach. "Oscillating Superfluidity of Bosons in Optical Lattices". *Physical Review Letters*, **89(25)** 250404 (2002)

[155] David Chen, Matthew White, Cecilia Borries, and Brian DeMarco. "Quantum Quench of an Atomic Mott Insulator". *Physical Review Letters*, **106(23)** 235304 (2011)

[156] A. Tuchman, C. Orzel, A. Polkovnikov, and M. Kasevich. "Nonequilibrium coherence dynamics of a soft boson lattice". *Physical Review A*, **74(5)** 051601 (2006)

[157] C. Kollath, U. Schollwöck, J. von Delft, and W. Zwerger. "One-dimensional density waves of ultracold bosons in an optical lattice". *Physical Review A*, **71(5)** 053606 (2005)

[158] Artur Widera, Michiel Snoek, and Walter Hofstetter. "Lattice-ramp-induced dynamics in an interacting Bose-Bose mixture". *Physical Review A*, **81(4)** 043620 (2010)

[159] Marco Schiró and Michele Fabrizio. "Time-Dependent Mean Field Theory for Quench Dynamics in Correlated Electron Systems". *Physical Review Letters*, **105(7)** 076401 (2010)

[160] Alexander Altland, V. Gurarie, T. Kriecherbauer, and A. Polkovnikov. "Nonadiabaticity and large fluctuations in a many-particle Landau-Zener problem". *Physical Review A*, **79(4)** 042703 (2009)

[161] Jakub Zakrzewski. "Mean-field dynamics of the superfluid-insulator phase transition in a gas of ultracold atoms". *Physical Review A*, **71(4)** 043601 (2005)

[162] Julia Wernsdorfer, Michiel Snoek, and Walter Hofstetter. "Two-dimensional dynamics of ultracold atoms in optical lattices". *Physical Review A*, **76(5)** 051603 (2007)

[163] Stefan Natu, Kaden Hazzard, and Erich Mueller. "Local Versus Global Equilibration near the Bosonic Mott-Insulator–Superfluid Transition". *Physical Review Letters*, **106(12)** 125301 (2011)

[164] F. Wolf, Itay Hen, and Marcos Rigol. "Collapse and revival oscillations as a probe for the tunneling amplitude in an ultracold Bose gas". *Physical Review A*, **82(4)** 043601 (2010)

[165] Bruno Sciolla and Giulio Biroli. "Quantum Quenches and Off-Equilibrium Dynamical Transition in the Infinite-Dimensional Bose-Hubbard Model". *Physical Review Letters*, **105(22)** 220401 (2010)

[166] Bruno Sciolla and Giulio Biroli. "Dynamical transitions and quantum quenches in mean-field models". *Journal of Statistical Mechanics: Theory and Experiment*, **(11)** P11003 (2011)

[167] Kristian Baumann, Christine Guerlin, Ferdinand Brennecke, and Tilman Esslinger. "Dicke quantum phase transition with a superfluid gas in an optical cavity". *Nature*, **464(7293)** 1301–1306 (2010)

[168] Victor Bapst and Guilhem Semerjian. "On quantum mean-field models and their quantum annealing". *arxiv:*1203.6003

[169] M. Snoek. "Rigorous mean-field dynamics of lattice bosons: Quenches from the Mott insulator". *EPL (Europhysics Letters)*, **95(3)** 30006 (2011)

[170] Pierre Gaspard. *Chaos, Scattering and Statistical Mechanics (Cambridge Nonlinear Science Series)* (Cambridge University Press) (1998)

[171] A. Gambassi and P. Calabrese. "Quantum quenches as classical critical films". *EPL (Europhysics Letters)*, **95(6)** 66007 (2011)

[172] Matteo Sandri, Marco Schiro', and Michele Fabrizio. "Linear Ramps of Interaction in the Fermionic Hubbard Model". *arxiv:*1112.5063

[173] Patrice Andre', Marco Schiro', and Michele Fabrizio. "Lattice and surface effects in the out-of-equilibrium dynamics of the Hubbard model"

[174] Alexander Altland and Fritz Haake. "Quantum Chaos and Effective Thermalization". *Physical Review Letters*, **108(7)** 073601 (2012)

[175] Marco Schiró and Michele Fabrizio. "Quantum quenches in the Hubbard model: Time-dependent mean-field theory and the role of quantum fluctuations". *Physical Review B*, **83(16)** 165105 (2011)

[176] Esteban A. Calzetta and Bei-Lok B. Hu. *Nonequilibrium Quantum Field Theory* (Cambridge University Press), cambridge edition (2008)

[177] Michael Bonitz and Karsten Balzer. "Progress in Nonequilibrium Green's Functions IV". *Journal of Physics: Conference Series*, **220(1)** 011001 (2010)

[178] Jø rgen Rammer. *Quantum Field Theory of Non-equilibrium States* (Cambridge University Press) (2007)

[179] E. Calzetta and B. Hu. "Nonequilibrium quantum fields: Closed-time-path effective action, Wigner function, and Boltzmann equation". *Physical Review D*, **37(10)** 2878–2900 (1988)

[180] Gerald D. Mahan. *Many Particle Physics (Physics of Solids and Liquids)* (Springer) (2000)

[181] Alex Kamenev and Alex Levchenko. "Keldysh technique and non-linear sigma-model: basic principles and applications". *arxiv:*0901.3586

[182] John Cornwall, R. Jackiw, and E. Tomboulis. "Effective action for composite operators". *Physical Review D*, **10(8)** 2428–2445 (1974)

[183] Adrian Stan, Nils Erik Dahlen, and Robert van Leeuwen. "Time-propagation of the Kadanoff-Baym equations for inhomogeneous systems". *arxiv:*0906.1704

[184] Yu. B. Ivanov, J. Knoll, and D. N. Voskresensky. "Self-consistent approximations to non-equilibrium many-body theory". *Nuclear Physics A*, **657(4)** 413–445 (1999)

[185] Mark Alford, Jürgen Berges, and Jack Cheyne. "Critical phenomena from the two-particle irreducible 1/N expansion". *Physical Review D*, **70(12)** 125002 (2004)

[186] Gert Aarts, Daria Ahrensmeier, Rudolf Baier, Jürgen Berges, and Julien Serreau. "Far-from-equilibrium dynamics with broken symmetries from the 1/N expansion of the 2PI effective action". *Physical Review D*, **66(4)** 045008 (2002)

[187] Spyros Sotiriadis and John Cardy. "Quantum quench in interacting field theory: A self-consistent approximation". *Physical Review B*, **81(13)** 134305 (2010)

[188] D. Boyanovsky, H. de Vega, R. Holman, and J. Salgado. "Nonequilibrium Bose-Einstein condensates, dynamical scaling, and symmetric evolution in the large N Φ4 theory". *Physical Review D*, **59(12)** 125009 (1999)

[189] D. Boyanovsky, C. Destri, H. de Vega, R. Holman, and J. Salgado. "Asymptotic dynamics in scalar field theory: Anomalous relaxation". *Physical Review D*, **57(12)** 7388–7415 (1998)

[190] Gary Felder and Andrei Linde. "Tachyonic instability and dynamics of spontaneous symmetry breaking". *Physical Review D*, **64(12)** 123517 (2001)

[191] Giuseppe Carleo. *Spectral and dynamical properties of strongly correlated systems*. Ph.D. thesis (2011)

[192] Markus Heyl, Anatoli Polkovnikov, and Stefan Kehrein. "Dynamical Quantum Phase Transitions in the Transverse Field Ising Model". *arxiv:*1206.2505

[193] Aditi Mitra. "Time-evolution and dynamical phase transitions at a critical time in a system of one dimensional bosons after a quantum quench". *arxiv:*1207.3777

[194] R. Stinchcombe, A. Misra, and B. Chakrabarti. "Length and time scale divergences at the magnetization-reversal transition in the Ising model". *Physical Review E*, **59(5)** R4717–R4720 (1999)

[195] P. W. Anderson. "Absence of Diffusion in Certain Random Lattices". *Physical Review*, **109(5)** 1492–1505 (1958)

[196] Elihu Abrahams. *50 Years of Anderson Localization* (World Scientific Publishing Company) (2010)

[197] E. Abrahams. "Scaling Theory of Localization: Absence of Quantum Diffusion in Two Dimensions". *Physical Review Letters*, **42(10)** 673–676 (1979)

[198] Shinobu Hikami. "Anderson localization in a nonlinear-σ-model representation". *Physical Review B*, **24(5)** 2671–2679 (1981)

[199] A Aharony and Y Imry. "The mobility edge as a spin-glass problem". *Journal of Physics C: Solid State Physics*, **10(17)** L487–L492 (1977)

[200] J L Cardy. "Electron localisation in disordered systems and classical solutions in Ginzburg-Landau field theory". *Journal of Physics C: Solid State Physics*, **11(8)** L321–L327 (1978)

[201] D. M. Basko, I. L. Aleiner, and B.L. Altshuler. "On the problem of many-body localization". *arxiv:*0602510

[202] T Giamarchi and H. J Schulz. "Localization and Interaction in One-Dimensional Quantum Fluids". *Europhysics Letters (EPL)*, **3(12)** 1287–1293 (1987)

[203] Anthony Leggett. "Bose-Einstein condensation in the alkali gases: Some fundamental concepts". *Reviews of Modern Physics*, **73(2)** 307–356 (2001)

[204] Richard Scalettar, Ghassan Batrouni, and Gergely Zimanyi. "Localization in interacting, disordered, Bose systems". *Physical Review Letters*, **66(24)** 3144–3147 (1991)

[205] S Rapsch, U Schollwöck, and W Zwerger. "Density matrix renormalization group for disordered bosons in one dimension". *Europhysics Letters (EPL)*, **46(5)** 559–564 (1999)

[206] Nikolay Prokof'ev and Boris Svistunov. "Superfluid-Insulator Transition in Commensurate Disordered Bosonic Systems: Large-Scale Worm Algorithm Simulations". *Physical Review Letters*, **92(1)** (2004)

[207] Juan Carrasquilla, Federico Becca, Andrea Trombettoni, and Michele Fabrizio. "Characterization of the Bose-glass phase in low-dimensional lattices". *Physical Review B*, **81(19)** 195129 (2010)

[208] L. Pollet, N. Prokof'ev, B. Svistunov, and M. Troyer. "Absence of a Direct Superfluid to Mott Insulator Transition in Disordered Bose Systems". *Physical Review Letters*, **103(14)** 140402 (2009)

[209] T. Giamarchi, P. Le Doussal, and E. Orignac. "Competition of random and periodic potentials in interacting fermionic systems and classical equivalents: The Mott glass". *Physical Review B*, **64(24)** 245119 (2001)

[210] A. Brooks Harris. "A Brief History of the Harris Criterion". *Bulletin of the American Physical Society*, **Volume 52,** (2007)

[211] Thomas Vojta. "Rare region effects at classical, quantum and nonequilibrium phase transitions". *Journal of Physics A: Mathematical and General*, **39(22)** R143–R205 (2006)

[212] S. Iyer, D. Pekker, and G. Refael. "Mott glass to superfluid transition for random bosons in two dimensions". *Physical Review B*, **85(9)** 094202 (2012)

[213] T. Senthil and Subir Sachdev. "Higher Dimensional Realizations of Activated Dynamic Scaling at Random Quantum Transitions". *Physical Review Letters*, **77(26)** 5292–5295 (1996)

[214] Luca Dell'Anna and Michele Fabrizio. "How localized bosons manage to become superfluid". *Journal of Statistical Mechanics: Theory and Experiment*, **(08)** P08004 (2011)

[215] Mats Wallin, Erik Sø rensen, S. Girvin, and A. Young. "Superconductor-insulator transition in two-dimensional dirty boson systems". *Physical Review B*, **49(17)** 12115–12139 (1994)

[216] Igor Herbut. "Dual theory of the superfluid-Bose-glass transition in the disordered Bose-Hubbard model in one and two dimensions". *Physical Review B*, **57(21)** 13729–13742 (1998)

[217] Anand Priyadarshee, Shailesh Chandrasekharan, Ji-Woo Lee, and Harold Baranger. "Quantum Phase Transitions of Hard-Core Bosons in Background Potentials". *Physical Review Letters*, **97(11)** 115703 (2006)

[218] Ehud Altman, Yariv Kafri, Anatoli Polkovnikov, and Gil Refael. "Phase Transition in a System of One-Dimensional Bosons with Strong Disorder". *Physical Review Letters*, **93(15)** 150402 (2004)

[219] Ehud Altman, Yariv Kafri, Anatoli Polkovnikov, and Gil Refael. "Insulating Phases and Superfluid-Insulator Transition of Disordered Boson Chains". *Physical Review Letters*, **100(17)** 170402 (2008)

[220] Ehud Altman, Yariv Kafri, Anatoli Polkovnikov, and Gil Refael. "Superfluid-insulator transition of disordered bosons in one dimension". *Physical Review B*, **81(17)** 174528 (2010)

[221] M. Feigel'man, L. Ioffe, and Marc Mézard. "Superconductor-insulator transition and energy localization". *Physical Review B*, **82(18)** 184534 (2010)

[222] U. Bissbort and Walter Hofstetter. "Stochastic mean-field theory for the disordered Bose-Hubbard model". *EPL (Europhysics Letters)*, **86(5)** 50007 (2009)

[223] Hans A. Bethe. "Statistical theory of superlattices". *Proc. Roy. Soc. A*, **150** 552–558 (1935)

[224] M. Mézard and G. Parisi. "The Bethe lattice spin glass revisited". *The European Physical Journal B*, **20(2)** 217–233 (2001)

[225] Florent Krzakala, Alberto Rosso, Guilhem Semerjian, and Francesco Zamponi. "Path-integral representation for quantum spin models: Application to the quantum cavity method and Monte Carlo simulations". *Physical Review B*, **78(13)** 134428 (2008)

[226] C. Laumann, A. Scardicchio, and S. L. Sondhi. "Cavity method for quantum spin glasses on the Bethe lattice". *Physical Review B*, **78(13)** 134424 (2008)

[227] Guilhem Semerjian, Marco Tarzia, and Francesco Zamponi. "Exact solution of the Bose-Hubbard model on the Bethe lattice". *Physical Review B*, **80(1)** 014524 (2009)

[228] L. Ioffe and Marc Mézard. "Disorder-Driven Quantum Phase Transitions in Superconductors and Magnets". *Physical Review Letters*, **105(3)** 037001 (2010)

[229] O Dimitrova and Marc Mézard. "The cavity method for quantum disordered systems: from transverse random field ferromagnets to directed polymers in random media". *Journal of Statistical Mechanics: Theory and Experiment*, **(01)** P01020 (2011)

[230] K V Krutitsky, A Pelster, and R Graham. "Mean-field phase diagram of disordered bosons in a lattice at nonzero temperature". *New Journal of Physics*, **8(9)** 187–187 (2006)

[231] J Cook and B Derrida. "Directed polymers in a random medium: 1/d expansion and the n-tree approximation". *Journal of Physics A: Mathematical and General*, **23(9)** 1523–1554 (1990)

[232] Daniel Fisher. "Random transverse field Ising spin chains". *Physical Review Letters*, **69(3)** 534–537 (1992)

[233] Daniel Fisher. "Random antiferromagnetic quantum spin chains". *Physical Review B*, **50(6)** 3799–3821 (1994)

[234] Markus Mueller. "Giant positive magnetoresistance and localization in bosonic insulators". *arxiv:*1109.0245

[235] J. Cook and B. Derrida. "Lyapunov exponents of large, sparse random matrices and the problem of directed polymers with complex random weights". *Journal of Statistical Physics*, **61(5-6)** 961–986 (1990)

[236] Marco Schiró and Michele Fabrizio. "Time-Dependent Mean Field Theory for Quench Dynamics in correlated electron systems". *arxiv:*1005.0992

[237] Michael Potthoff. "Strongly Correlated Systems". In Adolfo Avella and Ferdinando Mancini, editors, *Theoretical Methods for Strongly Correlated Systems*, volume 171 of *Springer Series in Solid-State Sciences*,

chapter Self-energ, 38 (Springer Berlin Heidelberg, Berlin, Heidelberg) (2012)